New molecular and cellular aspects of mutant calreticulin in Myeloproliferative Neoplasms

MARIA MORLAN-MAIRAL

School of Environment and Life Sciences

University of Salford, UK

Submitted in partial fulfilment of the requirements of the
Degree of Doctor of Philosophy, 2018

To Lorenzo, Marimar and Lucia

Contents

List of Figures

List of Tables

Acknowledgments

Firstly, I would like to express my gratitude to my supervisor Dr. Athar Aziz, for his support and trust throughout this thesis. Thanks for believing in me and for allowing me to do this project. I am equally grateful to my co-supervisor Professor Marija Krstic-Demonacos for her guidance and help during this PhD.

Secondly, I would like to thank Dr Patrick Caswell for his collaboration and for allowing me access to his laboratory to perform the microscopy experiments. To Dr Joseph Hetmanski for his help in microscopy, it was great to have the opportunity to work with you again. To Dr. Farooq A Kiani, for his contribution in the structural analysis and to Dr Petros Papadopoulos, for his collaboration in this project, his support and trust in me in the recent years. Also, I would like to thank the laboratory of Dr Tony Green, for sharing the CALR plasmids and the MARIMO cell line.

I would like to extend my gratitude to my friends in the laboratory for their help over the past three years. To Dr. Laura Brettell, Jess Hall, May Rabaj and Dr. Paz Aranega Bou, it has been great sharing this experience with you. I feel so lucky to have shared the lab and office with you all, thanks for your friendship and continuous support. Special thanks to May for your suggestions and ideas about the calcium experiments. To Basmah Allakari, for providing invaluable help with flow cytometry, it has been essential for me to perform all the FACs analysis. I am also thankful to everyone else in Salford University who gave me advice and support throughout this project, including Jess Kevill, Muna Abubaker, Mathew Jones, Dr. Emyr Baker, Alice Guazzelli and Sangkab Sudsaward.

I would also like to express my gratitude to the University of Salford, for their award of a Pathway to Excellence Studentship which provided me financial support to perform this PhD project.

I would additionally like to thank Inés Mateo and Elena Sánchez for your help and guidance in the laboratory from a distance. Thanks for your useful discussions regarding my project and for your kindness over the years. To Gabriela Pingarrón, your support has been priceless; this

journey would not have been the same without you. To you, and all my friends who provided laugher through difficult times. I could not ask for better friends.

Last, but not least, I would like to thank my family. To my sister, Lucia Morlán, for being my best companion, for all the laughs and for always showing a smile when I needed one. To my mother, Mª del Mar Mairal, for your unconditional love, invaluable support and for teaching me that there is no obstacle in life that cannot be overcome. And finally, to my father, Lorenzo Morlán, who has always believed in me. Thanks for our endless scientific talks, for your advices and for your invaluable help through this project. None of this would have been possible without you.

Declaration

This thesis is presented for the Award of the degree of Doctor of Philosophy by Salford University. The work presented in this thesis has been conducted in approximately three years and a half and has been funded by the Pathway to Excellence Studentship from the University of Salford. No portion of the work referred to in this thesis has been submitted in support of an application for another degree or qualification in this or any other university or other institute of learning.

Although the author has performed most of the experiments, some parts of this thesis were carried out in collaboration with other colleagues. High resolution microscopy shown in sections 5.2.1 and 5.2.2 was performed in collaboration with the laboratory of Dr. Patrick Caswell (The University of Manchester, UK) and microscopy was mostly executed by Dr. Joseph Hetmanski. Moreover, DAMI clones overexpressing *CALR* WT and *CALR* mutations used during this thesis were transduced and established by Dr. Petros Papadopoulos (Hospital Clinico San Carlos, Madrid, Spain).

Abbreviations

[Ca^{2+}$_i$] Intracellular calcium concentration

AM Acetoxymethyl

AML Acute myeloid leukemia

APC Allophycocyanin

BM Bone marrow

Ca^{2+} Calcium

CALR Calreticulin

CCBs Calcium channel blockers

CISH Cytokine inducible SH2

CML Chronic myeloid leukemia

CNX Calnexin

DMS Demarcation membrane system

DTT Ditiotreitol

EDTA Ácido etilendiaminotetraacético

ER Endoplasmic reticulum

ET Essential thrombocythemia

GFP Green fluorescent protein

HSC Haematopoietic stem cell

ID1 Inhibitor of DNA Binding 1

IDP Intrinsically disordered protein

IDPRs   Intrinsically disordered protein regions

IP3-R   Inositol 1,4,5-trisphosphate receptor

I-TASSER   Interactive threading assembly refinement

JAK2   Janus kinase 2

MAPK   Mitogen-activated protein kinase

MDS   Myelodysplastic syndromes

MoRFs   Molecular Recognition Features

MPL   Myeloproliferative leukemia protein

MPNs   Myeloproliferative Neoplasms

mRNA   Messenger RNA

MTS   [3-(4,5-dimethylthiazol-2-yl)-5-(3-carboxymethoxyphenyl)-2-(4-

NMDARs   N-methyl-D-aspartate receptors

PE   Phycoerythrin

Ph   Philadelphia chromosome

pl   Isoelectric point

PI$_3$K   Phosphoinositide 3-kinase

PIM1   Proto-oncogene, serine/threonine kinase

PKC   Protein kinase C

PMA   Phorbol 12-myristate 13-acetate

PMCA   Plasma membrane Ca^{2+} ATPase

PMF   Primary myelofibrosis

PMSF   Fluoruro de fenilmetilsulfonilo

PV   Polycythemia vera

qRT-PCR   Quantitative real-time Polymerase Chain Reaction

SERCA   Sarco/endoplasmic reticulum Ca^{2+} ATPase

SOCE   Store-operated Ca^{2+} entry

SOCS   Suppressor of cytokine signalling

STATs   Signal Transducer And Activator Of Transcription

STIM   Stromal interaction molecule

        sulfophenyl)-2H-tetrazolium, inner salt; MTS]

TG   Thapsigargin

TPO   Thrombopoietin

WHO   World health organization

WT   Wild type

Abstract

Calreticulin (CALR) is an endoplasmic reticulum (ER) protein that plays an important role as a calcium (Ca^{2+}) buffering chaperone. Mutations in *CALR* exon 9 have been identified in essential thrombocythemia and primary myelofibrosis, two myeloproliferative neoplasms (MPNs) characterised by megakaryocyte hyperplasia. Despite the large body of research built around *CALR* mutations, many aspects of the oncogenic mechanisms of CALR in MPNs remain unanswered. This investigation aims to investigate whether *CALR* mutations affect the nature of the C-terminal domain of this protein, its sub-cellular compartmentalisation and its Ca^{2+} buffering activity during megakaryocyte hyperplasia. Additionally, this study establishes a new cellular model to investigate megakaryocyte differentiation in presence of *CALR* mutations.

In silico analysis of the structural characteristics of CALR mutant C-terminal domain revealed that *CALR* mutations lead to changes in its secondary structure, its protein binding properties and changes the acidity of CALR mutant´s C-terminal domain. These physical alterations could affect CALR cellular behaviour by leading to inefficient ER Ca^{2+} buffering activity and lead to a novel oncogenic network of protein interactions.

This study revealed that MARIMO leukemic cell line, which harbours a *CALR* mutation, has *in vitro* megakaryocyte differentiation potential. Importantly, this discovery was useful for further studies aiming to analyse CALR mutant cells during megakaryocyte commitment. Moreover, study of CALR mutant cellular localisation showed that this protein is localised within the ER, but it is also mislocalised within the cytoplasm and cell membrane, where it co-localised with thrombopoietin receptor. Interestingly, CALR cell surface expression increased during megakaryocyte commitment in CALR mutant cells, showing a dynamic process of CALR compartmentalisation during megakaryocyte differentiation.

One of the more significant findings shown in this study is the emergence of intracellular Ca^{2+} concentrations ($[Ca^{2+}_I]$) as an important element during megakaryopoiesis. Importantly, *CALR* mutations impaired the cellular ER Ca^{2+} buffering activity and led to changes in the $[Ca^{2+}_I]$ during the process of megakaryocyte differentiation. In addition, initial experiments revealed

that physical manipulation of [Ca^{2+}$_I$] leads to the emergence of a megakaryocyte phenotype in leukemic cells, showing the relevance of this factor during megakaryocyte commitment.

All together, these findings elucidate novel effects of *CALR* mutations into the physical and functional characteristics of CALR mutant in MPNs, describing new aspects of this driver mutation during the oncogenesis of these diseases. Finally, the current data highlight the importance of studying the effects of *CALR* mutations during the process of megakaryocyte differentiation, as CALR mutant sub-cellular compartmentalisation and ER Ca^{2+} buffering activity variate during the process of megakaryopoiesis.

CHAPTER 1: *General background*

1.1. Overview of normal and malignant megakaryopoiesis

Megakaryocytes are bone marrow cells characterised by a multilobulated or polyploid nucleus and a large cytoplasmic diameter (100-150 μm). These cells are the precursors of platelets, of which approximately $1x10^{11}$ are released daily into the blood stream by a highly dynamic process (Wen et al., 2011). Megakaryocytes are infrequent within the bone marrow, as there are only 1 in 10^3 nucleated cells. Megakaryopoiesis is the complex process of megakaryocyte formation which is highly regulated by external factors such as the bone marrow stroma, cytokines or hormones (Wen et al., 2011; Machlus et al., 2014).

During megakaryopoiesis, megakaryocytes derive from haematopoietic stem cells (HSCs) through several sequential commitment steps. HSCs are a rare population of cells that reside in the bone marrow maintaining the hematopoietic lineage (Ogawa, 1993). These pluripotent embryonic cells can differentiate into hematopoietic progenitor cells (HPCs) which will subsequently commit into either of two different lineages, the common lymphoid progenitors (CLPs) (Kondo et al., 1997) or common myeloid progenitors (CMPs) (Akashi et al., 2000). CLP has the capacity to differentiate into lymphoid cells, whereas CMP leads to the development of the myeloid cell linage. Firstly, CMP differentiate into more differentiated progenitors, known as granulocyte/monocyte progenitors (GMPs) and megakaryocyte/erythroid progenitors (MEPs) (Debili et al., 1996). Finally, MEP generates single lineage progenitor cells which will finally become mature erythroid or megakaryocyte cells (Figure 1). The proportion of each blood cell type is strictly regulated in the bone marrow and therefore, a controlled balance between self-renewal and cell differentiation establishes a healthy blood cell composition.

After megakaryocyte differentiation, cell maturation starts with the expression of platelet specific genes, increase cell size and an increase in cell ploidy (Bianchi et al., 2016; Zimmet and Ravid, 2000). Megakaryocytes ploidy is acquired by a process known as endomitosis, where DNA is replicated but there is a lack of cytoplasmic division. During maturation,

megakaryocytes migrate close to the vasculature within the bone marrow in response to Stromal-derived factor-1α (SDF-1α) (Avecilla et al., 2004). Here, megakaryocytes produce long and branched cytoplasmic projections known as demarcation membrane system (DMS) (Junt et al., 2007; Schulze et al., 2006). These projections are extended into the bone marrow sinusoids lumen and become fragmented, releasing platelets into the circulatory system (Junt et al., 2007) (Figure 1).

Cytokines are produced within the bone marrow microenvironment and these directly support megakaryocyte terminal differentiation (Yu and Cantor, 2012). Thrombopoietin (TPO) is known to be the most important cytokine during megakaryopoiesis. TPO and its receptor myeloproliferative leukemia protein (MPL) are critical for megakaryopoiesis as seen in mouse models where knock down of any of both genes leads to thrombocytopenia (Gurney et al., 1994; Bunting et al., 1997).
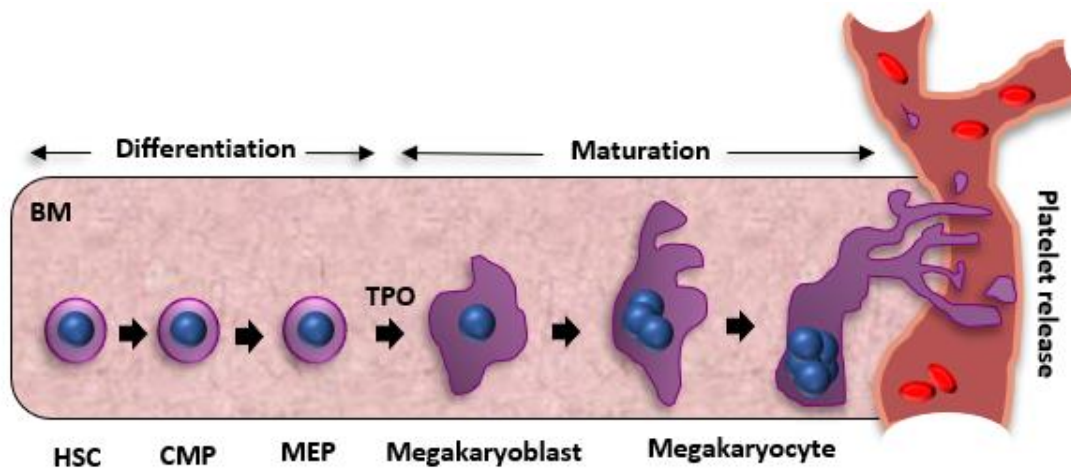
Figure 1. Megakaryopoiesis.
Representative diagram of megakaryocyte formation and platelet release within the bone marrow (BM). HSC: haematopoietic stem cell, CMP: common myeloid progenitor, MEP: megakaryocyte erythrocyte progenitor, TPO: thrombopoietin.

Megakaryocyte proliferation and apoptosis are highly balanced during megakaryopoiesis to reach a tight control of cell production. Nevertheless, when a genetic mutation occurs, this balance might be altered leading to an uncontrolled production of megakaryocytes within the bone marrow. Megakaryocyte hyperplasia can be described in benign diseases such as

idiopathic thrombocytopenia (Ganguly and Cunningham, 2004), however it is mostly associated to malignant or clonal disorders such as chronic myelogenous leukaemia (Carbonell et al., 1982), acute megakaryocytic leukemia (Hahn et al., 2016) or myeloproliferative neoplasms (MPNs).

1.2. Myeloproliferative Neoplasms

Myeloid Neoplasms are a heterogeneous group of stem cell clonal diseases characterised by an overproduction of myeloid cells. The 2016 World Health Organisation (WHO) classification system for haematopoietic tumours establishes three main categories of neoplasms: Acute myeloid leukemia (AML), Myelodysplastic syndromes (MDS) and MPNs (Arber et al., 2016) (Table 1).

AML is a disease characterised by an uncontrolled neoplastic proliferation of myeloid blasts cells in the bone marrow. This production of blast cells leads to a disruption of normal haematopoiesis and consequently haematopoietic insufficiency and bone marrow failure (De Kouchkovsky and Abdul-Hay, 2016). In contrast, MDS are clonal disorders characterised by an ineffective haematopoietic process which could transform into AML. Additionally, cytopenias and dysmorphogenesis of myeloid cells with dysplastic features are hallmarks of MDS (Gangat et al., 2016). On the other hand, MPN display overproduction of functional mature myeloid cells, such as erythrocytes or megakaryocytes, within the bone marrow. Additionally, MPN patients display risk of AML transformation (Tefferi, 2016a).

Nevertheless, this classification is not entirely precise, as patients could display symptoms of MDS and MPNs. This group of patients are assigned to a category of overlap of MDS/MPN. Additionally, the 2016 WHO classification includes myeloid neoplasms associated with eosinophilia and abnormalities of *PDGFRA*, *PDGFRB*, *FGFR1* or *PCM1-JAK2*, mastocytosis and myeloid neoplasms with germ line predisposition as separate categories (Arber et al., 2016).

Table 1. The 2016 WHO classification scheme for Myeloid Neoplasms and subcategorisation of Myeloproliferative Neoplasms (Arber et al., 2016).

MYELOID NEOPLASMS
1) Acute myeloid leukemia (AML) and related neoplasms
2)Myelodysplastic syndromes (MDS)
3) Myeloproliferative Neoplasms (MPN)
i. Chronic myeloid leukemia (CML), BCR-ABL1$^+$
ii. Polycythemia vera (PV)
iii. Essential thrombocythemia (ET)
iv. Primary myelofibrosis (PMF)
PMF, prefibrotic/early stage
PMF, overt fibrotic stage
v. Chronic neutrophilic leukemia (CNL)
vi. Chronic eosinophilic leukemia, not otherwise specified (NOS)
vii. MPNs, unclassifiable
4) MDS/MPN
5) Mastocytosis
5) Myeloid neoplasms associated with eosinophilia and abnormalities of *PDGFRA, PDGFRB*, or *FGFR1*, or with *PCM1-JAK2*
6) Myeloid neoplasms with germ line predisposition

1.2.1. Myeloproliferative neoplasms, the emergence of key clonal markers

The first classification of MPN was registered in 1951 by William Dameshek as myeloproliferative disorders (MPDs), which grouped polycythemia vera (PV), essential thrombocythemia (ET), erythroleukemia, chronic myelogenous leukaemia (CML) and primary myelofibrosis (PMF) based on their clinical and histologic characteristics (Dameshek, 1951). Over the years important discoveries based on the molecular pathology of MPNs have led to a better understanding of the molecular basis of this heterogeneous group of diseases. The latest WHO classification includes seven subcategories in the group of MPNs: CML BCR-ABL1$^+$, Chronic neutrophilic leukaemia (CNL), PV, PMF, ET, Chronic eosinophilic leukaemia (CEL) and MPNs-unclassifiable. This classification is based on the molecular and cellular pathology of the diseases (Table 1) (Arber et al., 2016).

The importance of using molecular markers in the classification of MPNs was firstly confirmed with the discovery of Philadelphia chromosome (*Ph*), characteristic of CML. *Ph* is an aberrant chromosomal translocation, *t(9;22)(q34;q11),* which results in the formation of BCR-ABL fusion protein (Nowell, 2007; Quintas-Cardama and Cortes, 2009). According to molecular

characteristics, ET, PMF and PV are categorised as *Ph*-negative MPN. During recent years, the understanding of the molecular basis of these three diseases has increased greatly.

The discovery in 2005 by four different research groups of a mutation in exon 14 of *Janus Kinase 2* (*JAK2)* gene present in a high proportion of PV, ET and PMF patients opened a new molecular diagnostic approach of *Ph*-negative MPNs (Baxter et al., 2005; James et al., 2005; Kralovics et al., 2005; Levine et al., 2005). The majority of PV patients (up to 95%) carry this mutation, whereas in ET and PMF patients it is found in 50-60% of cases. Further research described a gain-of-function mutation in c-*MPL* gene, which encodes for thrombopoietin receptor, in ET and PMF *JAK2* negative patients (Pikman et al., 2006). These mutations were described as MPN's driver mutations and were included as clonal markers in the 2008 revision of the WHO document for better classification and diagnosis of these diseases (Tefferi and Vardiman, 2008).

Additional studies have described less common mutations including *EZH*2 or *TET2* in MPN patients (Delhommeau et al., 2009; Ernst et al., 2010). Although, these somatic mutations affect only a small fraction of *JAK2* and *c-MPL* negative MPN patients and therefore they are not valuable to use as molecular diagnostic markers of MPNs. However, in 2013 two research groups identified a high incidence mutation in the *Calreticulin* (*CALR*) gene in MPN patients with non-mutated *JAK2* and c-*MPL*, greatly improving the diagnostic approach for these pathologies (Klampfl et al., 2013; Nangalia et al., 2013). The 2016 WHO diagnostic criteria of ET and PMF included the presence of *CALR* mutations as a major criterion for a correct diagnosis of these diseases (Arber et al., 2016) (Table 2).

1.3. Classic Ph-negative MPNs

ET, PV and PMF are considered as stem cell-derived haematological diseases (Beer et al., 2009; Tefferi, 2010). The presence of mutational pathogenic events in *Ph*-negative MPNs occurs in early stages of the hematopoietic process. This has been demonstrated with the identification of *JAK2* and *CALR* somatic mutations in hematopoietic progenitor cells (Kralovics et al., 2005, Nangalia et al., 2013). Interestingly, these two independent driver mutations and c-*MPL* mutations lead to the emergence of three different clinical phenotypes.

However, *CALR* mutations have only been described in ET and PMF, the two MPNs characterised by megakaryocyte neoplasia (Figure 2).
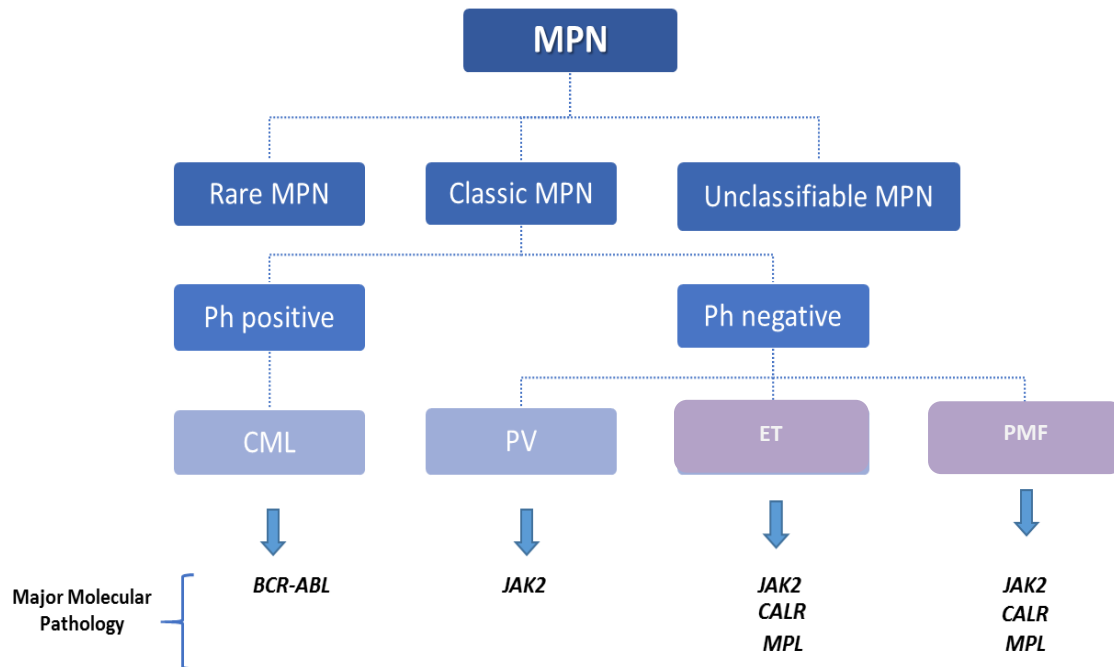
Figure 2. Schematic diagram of MPNs classification.
The 2016 WHO latest classification divides MPNs in three major categories: rare MPN, classic MPN and unclassifiable MPN. Classic MPN are classified as Philadelphia chromosome (Ph) positive or Ph negative. Ph negative includes Polycythemia Vera (PV) which major molecular pathological feature is *JAK2* mutations or Essential thrombocythemia (ET) and primary myelofibrosis (PMF) characterised by *JAK2*, *CALR* of *MPL* mutations. Purple shades identify the MPNs affected by *CALR* mutations.

1.3.1. Essential thrombocythemia

ET is a disease characterised by a neoplastic proliferation of megakaryocytes and platelets within the bone marrow and the blood stream. Platelets characteristic of this disease are functionally and morphologically altered and therefore ET patients display a higher risk of bleeding and thrombosis (Klco et al., 2010; Wilkins et al., 2008).

It is estimated that ET prevalence is about 38-57 per 100,000 individuals (Mehta et al., 2014). Approximately the median age range of ET patients at diagnosis is between 50-60 years old

and the incidence of ET has higher prevalence in females (Aruch and Mascarenhas, 2016). Clinically, ET is characterised by thrombosis, erythromelalgia, transient ischemic attacks and splenomegaly. However, some cases of ET are diagnosed in symptom-free patients during routine blood tests (Sanchez and Ewton, 2006).

The major feature of ET is a platelet count greater than 450,000 x10^9/L, in addition to further diagnostic criteria as listed in Table 2. *JAK2* mutation is the major molecular pathological feature, affecting about 50-60% of ET patients. *CALR* mutation is present in approximately 30%, followed by c-*MPL* mutation which affects 5% of patients (Klampfl et al., 2013). Nevertheless, the molecular pathogeny of the remaining group of patients with non-mutated *JAK2*, *CALR* or c-*MPL* remains elusive.

Evolution of ET to myelofibrosis varies in the disease duration from the onset of diagnosis. In the first decade of diagnosis 3-10% of cases evolve to myelofibrosis and in the second decade it increases greatly, to 6-30%. Additionally, ET could progress to AML in a small percentage of patients, from 1-2.5% during the first decade of the disease, increasing to 5-8% in the next decade (Beer et al., 2011; Sanchez and Ewton, 2006; Wolanskyj et al., 2006). ET patients are considered to be at high risk of thrombotic events. However, it is important to note that recent investigations have shown a differing risk of thrombosis dependent on the driver mutation, as *CALR* mutated patients show a lower risk of thrombosis than *JAK2* and c-*MPL* mutated patients (Rotunno et al., 2014).

Table 2. 2016 Who Diagnostic Criteria for PV, ET and PMF

	PV	ET	prePMF	Overt PMF
Major criteria	**1.** Hgb>16.5 g/dL (men) > 16.0 g/dL (women) Or Hematocrit >49% (men) Hematocrit >48% (women) Or Increased in cell mass	**1.** Platelet count ≥ 450 x 10^9/L	**1.** Megakaryocytic proliferation and atypia, without reticulin fibrosis grade 1, accompanied by increased age-adjusted BM cellularity, granulocytic proliferation, and often decreased erythropoiesis	**1.** Presence of megakaryocytic proliferation and atypia, accompanied by either reticulin and/or collagen fibrosis grades 2 or 3
	2. BM biopsy showing hypercellularity for age with trilineage growth including prominent erythroid, granulocytic, and megakaryocytic proliferation with pleomorphic, mature megakaryocytes (differences in size)	**2.** Megakaryocyte proliferation with large and mature morphology. No significant increase in neutrophil granulopoiesis or erythropoiesis and minor increase in reticulin fibres	**2.** Not meeting WHO criteria for CML, PV, MDS, or other myeloid neoplasm	
	3. Presence of *JAK2V617F* or *JAK2* exon 12 mutation	**3.** Not meeting WHO criteria for CML BCR-ABL$^+$, PV, PMF, MDS, or other myeloid neoplasm **4.** Presence of *JAK2*, *CALR* or c-*MPL* mutation	**3.** Presence of *JAK2*, *CALR* or c-*MPL* mutation or in the absence of these mutations, presence of another clonal marker or absence of minor reactive BM reticulin fibrosis	
Minor criteria	**1.** BM trilineage myeloproliferation **2.** Subnormal serum Epo level **3.** EEC growth	**1.** Presence of a clonal marker or absence of evidence for reactive thrombocytosis	**1.** Leukocytosis ≤11x 10^9/L **2.** Increased serum LDH level **3.** Anemia **4.** Palpable splenomegaly **5.** Leukoerythroblastosis	

1.3.2. Primary myelofibrosis

PMF is a myeloproliferative disorder associated with a neoplastic proliferation of megakaryocytes, abnormal cytokine expression and reactive bone marrow fibrosis (Tefferi, 2016b). Increased bone marrow fibrosis leads to ineffective erythropoiesis and consequently severe anemia. Additional clinical manifestations in PMF include hepatosplenomegaly, thrombosis, bone pain and bleeding, among others (Tefferi and Nagorney, 2000).

The prevalence of PMF is lower than ET, being 4-6 per 100,000 individuals and prevalence of MF post-ET and post-PV varies between 0.5-1.1 and 0.3-0.7 per 100,000 respectively (Mehta et al., 2014). It is estimated that median age at PMF diagnosis is approximately 65 years old and there are not significant differences between sex (Tefferi and Nagorney, 2000).

The revised 2016 WHO criteria distinguished two new subcategories within PMF, known as prefibrotic (prePMF) and overtly fibrotic PMF (Arber et al., 2016). Pre and overt PMF diagnostic criteria are listed in Table 2. Careful diagnosis must be done in prePMF, as it shares a similar mutation profile with ET (60% *JAK2* mutation, 35% *CALR* mutation, 10% c-*MPL* mutation approximately) (Tefferi and Pardanani, 2014). Therefore, cautious analysis of megakaryocyte characteristics is recommended to distinguish between the two diseases (Tefferi, 2016b). PMF has the worst survival rates of *Ph*-negative MPNs and has the higher risk to develop into AML (5-30%) (Mesa et al., 2005; Klco et al., 2010).

1.4. JAK-STAT signalling, a key cellular pathway in megakaryopoiesis and MPNs pathogenesis

The JAK/STAT pathway is a conserved cell signalling cascade involved in development and present in a diverse range of species from flies to humans. This signalling pathway is an important cellular mechanism to transduce cytokine and growth factor signals, being involved in central cellular processes such as cell differentiation and proliferation, as well as playing important roles in the haematopoietic and immune system development (Rawlings et al., 2004).

JAK/STAT signal transduction is mediated by two main protein families: JAKs (JAK1-3 and Tyr) and signal transducer and activator of transcription (STATs) (STAT1-4, STAT5a, STAT5b and STAT6). Intracellular JAK/STAT cascade activation occurs when cytokine ligands bind and stimulate a conformational change of the receptor, inducing the multimerization of the receptor subunits (Rawlings et al., 2004). Receptors involved in JAK/STAT signalling lack intrinsic kinase activity. Receptor dimerization or oligomerization brings JAK kinases associated to the receptor subunits into proximity. This allows the trans-phosphorylation of JAK kinases and consequently an increase in their enzymatic activity (Ihle and Gilliland, 2007). As a result, the active receptor complex recruits dormant cytoplasmic transcription factors, known as STATS. Phosphorylated STAT proteins dimerize and translocate from the cytoplasm to the cellular nucleus. STAT dimers bind to specific DNA regions known as Gamma-interferon activated sequences (GAS) and Interferon-Stimulated Response Element (ISRE), activating or repressing gene transcription (Lim and Cao, 2006). JAK-STAT pathway displays a negative feedback loop in order to control its own signalling. There are three major protein families involved in the negative regulation of this pathway: protein inhibitor of activated stats (PIAS), suppressors of cytokine signalling (SOCS) and protein tyrosine phosphatases (PTPs) (Greenhalgh and Hilton, 2001) (Figure 3).

In theory, JAK/STAT signalling is a simple cellular pathway; however, this cascade cross-talks with more complex signalling pathways such as the mitogen-activated protein kinase (MAPK) pathway (Rawlings et al., 2004). For example, SOCS-3 binds and inhibits RasGAP, a negative regulator of Ras protein, leading to Ras activation (Cacalano et al., 2001). Moreover, MAPK pathway can promote the activation of JAK/STAT pathway by different mechanisms. It has been shown that activation of epidermal growth factor receptor (EGFR) results in an activation of STATs without the interaction of JAK proteins (Park et al., 1996). In addition to MAPK, other signalling pathways have been shown to interact with JAK/STAT signalling, such as phosphoinositide 3-kinase (PI3K) pathway (Abell and Watson, 2005).

The JAK/STAT pathway plays a key role during megakaryopoiesis by transducing signals from TPO, an essential cytokine during this process (Geddis, 2010). Altered TPO signalling is characteristic of PMF, ET and PV. Interestingly, two of the most common driver mutations described in these diseases affect two key components of this pathway, MPL and JAK2, leading to a deregulated JAK/STAT signalling. Thus, strong efforts are being made for the

development of therapies targeting the inhibition of JAK/STAT cascade for the treatment of MPNs. For example, Ruxolitinib is a selective inhibitor of JAK1/2 approved for myelofibrosis treatment (Quintas-Cardama et al., 2010) which shows reductions in myelofibrotic symptoms and improved quality of life in ET and PMF patients (Harrison et al., 2012). Importantly, a previous study revealed a high correlation between the mutation profile in PMF patients and the response rate to Ruxolitinib (Patel et al., 2015). This highlights the importance of enhancing our understanding of the pathology of MPN driver mutations (*JAK2*, *CALR* and c-*MPL*) for a correct treatment of these neoplasms based on the molecular profile of MPN patients.
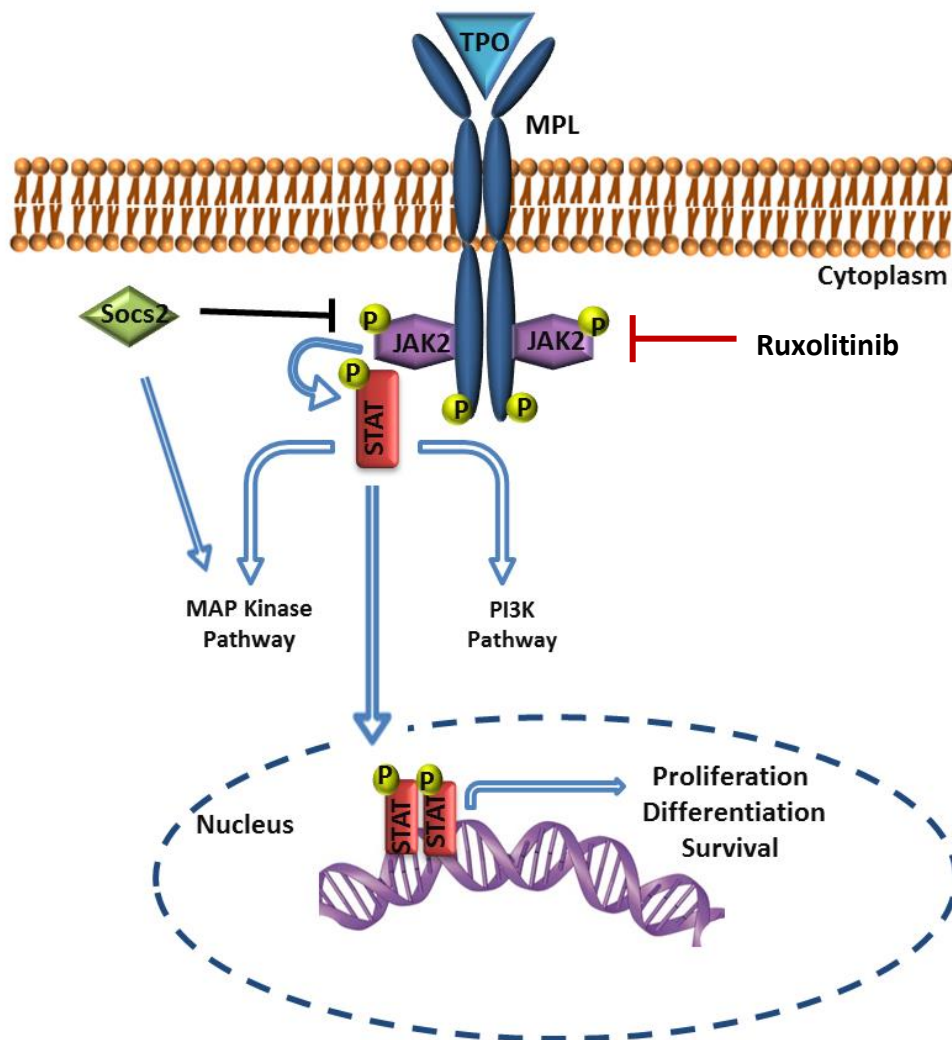
Figure 3. JAK-STAT signalling pathway.
Cytokines ligands bind to the hematopoietin receptors leading to the activation of JAK proteins. These proteins phosphorylate the intracellular domain of the receptor, leading to the formation of docking sites for downstream signalling proteins, such as STATS. Active STATS translocate into the nucleus and active the transcription of target genes. SOCS gene expression is dependent on this signalling pathway and act as a negative feedback loop of this cytokine dependent pathway.

1.5. Classic mutations in *Ph*-negative MPNs

1.5.1. JAK2 mutations

JAK2 protein, member of the JAK family proteins, is a known non-receptor tyrosine kinase involved in signal transduction of JAK-STAT pathway. *JAK2* gene is located in chromosome 9p24 and comprises 25 exons. Oncogenic JAK2^{V617F} mutation is the most frequent mutation in *Ph*-negative MPN patients (Baxter et al., 2005). Additionally, it has been detected in other myeloproliferative diseases, such as CML and AML (Hussein et al., 2008; Kiladjian, 2012). The JAK2^{V617F} somatic mutation found in hematopoietic cells is characterised by a transversion of guanine (G) for thymine (T) leading to a substitution of phenylalanine (F) for valine (V). This mutation leads to a constitutively active JAK2 (Kralovics et al., 2005).

MPN patients carrying JAK2^{V617F} mutations are older than patients negative for these mutations. Additionally, JAK2^{V617F} mutation shows a more aggressive clinical phenotype, with a higher incidence of complications such as haemorrhage, thrombosis and secondary fibrosis (Kralovics et al., 2005).

1.5.2. c-MPL mutations

After the identification of *JAK2* mutations in PV, ET and PMF patients, research was focussed on the identification of the molecular pathology of *JAK2* negative patients. Shortly after the discovery of JAK2^{V617F}, the gain-of-function mutation c*MPL*^{W515L} was described in ET and PMF *JAK2* negative patients (Pikman et al., 2006). c-*MPL* mutation consists in a G to T transition in exon 10, leading to a tryptophan to leucine substitution. This oncogenic event results in constitutive active JAK/STAT, MAPK and PI3K pathways (Chaligne et al., 2008). Presence of c-*MPL* mutation in ET patients is associated with the elderly, low haemoglobin levels, thrombocytosis and microvascular symptoms (Vannucchi et al., 2008).

1.6. Calreticulin, a novel driver mutation in MPNs

After the identification of *JAK2* and c-*MPL* mutations a big subset of MPN patients were considered as c-*MPL* and *JAK2* negative and no driver mutation was known in this group of patients. However, in 2013 two different investigations revealed by using whole-exome sequencing that *CALR* was mutated in this group of MPNs patients (Klampfl et al., 201; Nangalia et al., 2013). *CALR* mutations were described as "indels" within exon 9, generating a +1 bp frameshift. Several types of *CALR* mutations have been identified; all leading to a mutant protein with an altered C-terminal region. The amino acid sequence of CALR mutants described in ET and PMF patients are shown in Table 3, of which two mutations are described as the most common mutation variants: a 52-bp deletion, L367fs*46 (type 1), and a 5 bp insertion, K385fs*47 (type 2) (Nangalia et al., 2013).

CALR mutations were identified in patients with ET and PMF and these mutations were mutually exclusive with *JAK2* and c-*MPL* mutations. *CALR* mutations have been described as the second most common driver mutations after *JAK2* in both diseases. In contrast, no *CALR* mutations were identified in PV patients (Klampfl et al., 2013; Nangalia et al., 2013). However, there is strong evidence supporting that *CALR* and *JAK2* mutated disease phenotypes are different, suggesting two different facets of these diseases based in the molecular pathology (Rumi et al., 2014). *JAK2* and *CALR* mutated ET and PMF are described as distinct disease entities with different clinical outcomes (Rumi et al., 2014; Pietra et al., 2015). Moreover, recent studies have characterised the link between *CALR* mutations subtypes and different clinical phenotype in MPNs (Cabagnols et al., 2015; Pietra et al., 2015). *CALR* type 1 mutations have been mainly associated with a myelofibrotic phenotype and this mutation has been identified in ET with high risk of myelofibrotic progression (Pietra et al., 2015; Cabagnols et al., 2015). In contrast, type 2 mutations are usually associated with ET phenotype. Interestingly, patients with type 2 mutations display higher platelet counts and a lower risk of thrombosis than *JAK2* mutant (Cabagnols et al., 2015; Pietra et al., 2015). Therefore, the studies presented thus far provide evidence that molecular profiling is essential for a correct diagnosis and for a better selection of therapy for each individualised patient.

Table 3. Described CALR mutations in MPN patients.

Mutant sequences are highlighted in grey (Nangalia et al., 2013)

Name	Amino acid sequence
Deletions	
L367fs*46	QDEEQRTRRMMRTKM<u>RMRRMRRTRRKMRRKMSPARPRTSCREACLQGWTEA</u>
E370fs*43	QDEEQRLKEVMRTKM<u>RMRRMRRTRRKMRRKMSPARPRTSCREACLQGWTEA</u>
E370fs*48	QDEEQRLKEQRTRMMRTKM<u>RMRRMRRTRRKMRRKMSPARPRTSCREACLQGWTEA</u>
L367fs*48	QDEEQRQRTRRMMRTKM<u>RMRRMRRTRRKMRRKMSPARPRTSCREACLQGWTEA</u>
L367fs*44	QDEERRMMRTKM<u>RMRRMRRTRRKMRRKMSPARPRTSCREACLQGWTEA</u>
K368fs*51	QDEEQRLRRRQRTRRMMRTKM<u>RMRRMRRTRRKMRRKMSPARPRTSCREACLQGWTEA</u>
L367fs*52	QDEEQRRRRRQRTRRMMRTKM<u>RMRRMRRTRRKMRRKMSPARPRTSCREACLQGWTEA</u>
R366fs*53	QDEEQKRRRRQRTRRMMRTKM<u>RMRRMRRTRRKMRRKMSPARPRTSCREACLQGWTEA</u>
E371fs*49	QDEEQRLKEERQRTRRMMRTKM<u>RMRRMRRTRRKMRRKMSPARPRTSCREACLQGWTEA</u>
K368fs*43	QDEEQRLMMRTKM<u>RMRRMRRTRRKMRRKMSPARPRTSCREACLQGWTEA</u>
E370fs*37	QDEEQRLKE<u>RMRRMRRTRRKMRRKMSPARPRTSCREACLQGWTEA</u>
D373fs*47	QDEEQRLKEEEERTRRMMRTKM<u>RMRRMRRTRRKMRRKMSPARPRTSCREACLQGWTEA</u>
K374fs*53	QDEEQRLKEEEEDKRRRRQRTRRMMRTKM<u>RMRRMRRTRRKMRRKMSPARPRTSCREACLQGWTEA</u>
E371fs*49	QDEEQRLKEERTRRMMRTKM<u>RMRRMRRTRRKMRRKMSPARPRTSCREACLQGWTEA</u>
Insertions	
K385fs*47	QDEEQRLKEEEEDKKRKEEEEAEDNCRRMMRTKM<u>RMRRMRRTRRKMRRKMSPARPRTSCREACLQGWTEA</u>
K385fs*47	QDEEQRLKEEEEDKKRKEEEEAEDLCRRMMRTKM<u>RMRRMRRTRRKMRRKMSPARPRTSCREACLQGWTEA</u>
Complex	
R376fs*55	QDEEQRLKEEEEDKKLCKRRRRQRTRRMMRTKM<u>RMRRMRRTRRKMRRKMSPARPRTSCREACLQGWTEA</u>
K385fs*47	QDEEQRLKEEEEDKKRKEEEEAEDSCRRMMRTKM<u>RMRRMRRTRRKMRRKMSPARPRTSCREACLQGWTEA</u>
E381fs*48	QDEEQRLKEEEEDKKRKEEEDPCRRMMRTKM<u>RMRRMRRTRRKMRRKMSPARPRTSCREACLQGWTEA</u>

Major efforts have been undertaken to improve the molecular diagnosis of MPN patients. Identification of *CALR* mutations in MPN patients is an important step towards a correct categorisation of the disease. Recent investigations have been focussed on the development of efficient techniques for the detection of *CALR* mutations. Importantly, immunohistochemistry to detect the CALR mutant in MPNs patients' samples is highly specific for these mutations, showing that this technique could be very valuable for routine diagnostic tests (Andrici et al., 2016). Furthermore, a novel technique using screening PCR has been proved to be satisfactory when detecting *CALR* mutations in primary bone marrow samples (Jeong et al., 2016). Additionally, recent publication revealed the development of a next generation sequencing assay that could significantly improve the screening of MPN driver mutations during the diagnostic process (Frawley et al., 2018).

In addition to an accurate diagnosis based on the characterisation of the molecular driver mutations of the disease, a deep knowledge of the cellular and molecular basis of these mutations is essential for a correct understanding of MPN's biology. As such, analyses of the CALR cellular functions and the mechanisms of *CALR* mutations oncogenicity are essential to shed light on its contribution to the pathogenesis and prognosis of MPNs.

1.6. Calreticulin: a multifunctional cellular protein

CALR is a chaperone and a Ca^{2+} buffering protein that resides in the lumen of the endoplasmic reticulum (ER). *CALR* gene comprises 5891 bp and is localised on chromosome 19. The obtained protein is formed by 417 amino acids and has three functional and structural domains (Figure 4). The N-terminal domain includes carbohydrate and polypeptide binding sites (Leach et al., 2002). In addition, Zn^{2+} binding sites have been described to be in this domain (Baksh et al., 1995). The proline rich domain also contains carbohydrate and polypeptide binding sites and contains a specific binding region to interact with ER chaperones, such as ERp57 (Frickel et al., 2002). *In vitro* analyses have shown that this region has high binding affinity and low capacity Ca^{2+} binding residues (Baksh and Michalak, 1991).

The CALR C-terminal domain plays an important role in Ca^{2+} buffering as it binds to over 50% of ER Ca^{2+} due to the presence of a high number of negatively charge amino acids (Nakamura et al., 2001b). These residues have low Ca^{2+} binding affinity and high capacity. Finally, CALR C-terminal domain contains the ER retention/retrieval motif, known as KDEL (Lys-Asp-Glu-Leu). This motif ensures the retrieval of this protein from the Golgi apparatus to the ER (Figure 4) (Sonnichsen et al., 1994).
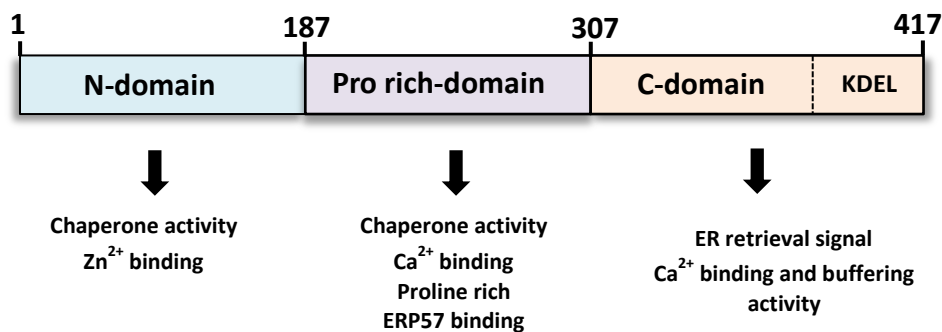
Figure 4. Calreticulin protein and its functional domains.
CALR is formed by 417 amino acids and it comprises three domains: N-terminal domain, Proline-rich domain and C-terminal domain. Each domain is essential for CALR functions within the cell. Importantly, KDEL region (ER retention motif) is located at the end of the C-terminal domain.

1.6.1. CALR chaperone activity

ER is a key cellular organelle essential for protein synthesis and folding. CALR resides mostly within the lumen of the ER where it functions as a chaperone of nascent glycoproteins, ensuring appropriate protein folding (Figure 5). Once glycoprotein chains are synthesised within the ER, two terminal glucose residues are removed in a sequential manner from the oligosaccharide region of these proteins by glucosidase I and II. This ensures the exposure of a $Glc_1Man_9GlcNAc_2$ epitope that is recognised by CALR and calnexin (CNX) (Caramelo and Parodi, 2008). These two lectin chaperones work together to cover a broader range of substrates depending on the topology of the nascent glycoproteins. CNX will bind to proteins next to the ER membrane and CALR will bind to soluble glycans (Hebert et al., 1997).

Intermediated folded glycoproteins interact with CALR/CNX for final protein folding. Then, folded proteins are rapidly deglucosylated and finally are secreted out of the ER. However, glycoproteins for which folding is not complete enter into the "CNX/CALR cycle". Once final deglucosylation is completed they are returned to the cycle by glucosidase I, which adds a glucose residue to the chain. Then, glycan interacts again with CALR/CNX upon correct protein folding (Hebert and Molinari, 2007). CALR depletion leads to a decline of glycoprotein quality control (Molinari et al., 2004).

1.6.2. CALR calcium buffering activity

The ER is the main Ca^{2+} storing organelle within the cell. Reticular Ca^{2+} is essential for a variety of cellular processes, such as gene expression, cell signalling and protein synthesis (Sammels et al., 2010). CALR is one of the most important Ca^{2+} chaperones within the ER, binding to 50% of total ER luminal Ca^{2+} stores (Figure 5). In its C-terminal acidic domain there are high capacity Ca^{2+} binding residues that bind to 25 mole of Ca^{2+} per mole of CALR with low Ca^{2+} binding affinity (K_d= 2 mM) (Baksh and Michalak, 1991, Nakamura et al., 2001b). Mutations affecting this protein domain decrease its Ca^{2+} buffering activity (Breier and Michalak, 1994). Additionally, CALR contains high affinity binding residues (K_d = 10 μM) with low Ca^{2+} binding capacity, equivalent to 1 mole of Ca^{2+} per mole of protein (Baksh and Michalak, 1991; Nakamura et al., 2001b). CALR overexpressing cells show an increase in intracellular Ca^{2+} storage and a reduced amount of Ca^{2+} influx within the ER lumen (Mery et al., 1996). In contrast, cells without CALR show a decrease in Ca^{2+} storage capacity, however, free luminal Ca^{2+} remains the same (Nakamura et al., 2001b).

CALR Ca^{2+} homeostatic activity could have a key role during cardiac development. *CALR null* mice are not viable due to altered cardiac development and *CALR* gene is highly expressed during early stages of cardiac development (Mesaeli et al., 1999). Additionally, mice transiently over-expressing *CALR* leads to arrhythmia and death induced by heart block (Hattori et al., 2007; Nakamura et al., 2001a). These results suggest a critical role of CALR during embryonic heart development and in the pathogenesis of cardiac cycle. Moreover, CALR and its Ca^{2+} homeostasis activity is associated with adipocyte cell differentiation (Szabo

et al., 2008) and osmotic stress in cells within the ascending limb of Henle's loop (Bibi et al., 2011).
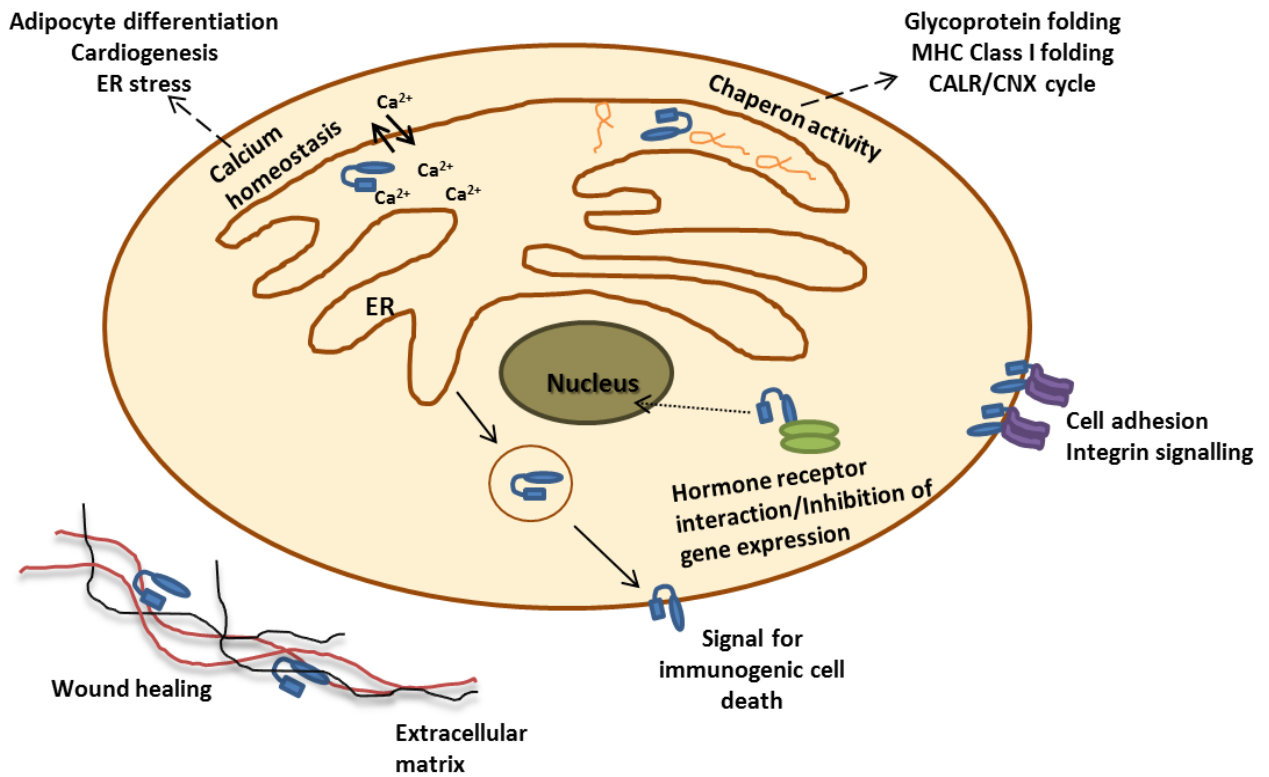
Figure 5. Schematic representation of CALR cellular functions.
CALR is involved in several cellular functions. Within the endoplasmic reticulum (ER) CALR is involved in calcium homeostasis and protein folding. CALR population in the cytoplasm is involved in cell adhesion by integrin interactions and it also interacts with hormone receptors. Within the cell membrane, CALR induces immunogenic cell death and the in extracellular matrix it is involved in wound healing.

1.6.3. CALR functions out of the ER

CALR functions in the cytoplasm

CALR is also compartmentalised in the cytoplasm although the cytoplasmic levels of CALR are minor compared with CALR population in the ER lumen (Shaffer et al., 2005). Here CALR has been associated with several cellular processes, such as cell adhesion (Figure 5). CALR specifically binds to the KXGFFKR sequence of the cytoplasmic tail of α-integrins mediating integrin activation (Coppolino et al., 1997) and transducing Ca^{2+} signalling between integrins and Ca^{2+} channels such as IP_3R (Kwon et al., 2000).

Further studies suggested that CALR interacts with hormone receptors, such as glucocorticoid receptors (GR) (Figure 5). Nuclear hormone receptors contain in their DNA binding domain a homologous protein sequence of the cytoplasmic tail of integrins, KXFFKR. CALR interacts with this sequence and inhibits the direct binding of nuclear hormone receptors to the DNA hormone response elements (Dedhar et al., 1994). Additionally, CALR induces the nuclear export of GR (Holaska et al., 2001). Therefore, CALR directly regulates the transcriptional activity of these receptors.

CALR functions in the cell surface

CALR cell surface expression is a relevant process for immunogenic cell death (Figure 5). CALR exposure on the plasma membrane is induced by anthracyclines, radiotherapy and Ca^{2+} depletion ER stores (Tufi et al., 2008; Wemeau et al., 2010). Apoptotic and cancer cells express CALR within the cell surface and this is recognised by dendritic cells as an "eat me" signal (Wijeyesakere et al., 2016). Inhibition of CALR cell surface expression in anthracycline treated cells leads to depletion of immunogenic cell death (Obeid et al., 2007). Investigations targeting CALR translocation to the cell surface are revealing important information for cancer research. For example, in AML patients, CALR cell surface expression facilitates immunogenic

cell death in response to chemotherapy (Wemeau et al., 2010). However, the molecular mechanisms of cell death driven by CALR cell surface expression remain to be clarified.

CALR functions in the extracellular matrix

Extracellular CALR is involved in wound healing and tissue remodelling (Figure 5). CALR significantly increases wound repair by upregulating the expression of certain growth factors such as transforming growth factor-β3, an important regulator of cutaneous repair (Nanney et al., 2008). Additionally, *in vitro* analyses show that CALR in the extracellular matrix induces cell proliferation and migration of fibroblasts, vascular endothelial cells and keratinocytes (Nanney et al., 2008). The importance of CALR for tissue repair and healing is being investigated for its potential use as a potent therapeutic agent to treat diabetic wound healing and chronic wounds (Greives et al., 2012).

1.7. Oncogenicity of *CALR* mutations in MPNs

Since 2013, several major efforts have been made to increase the understanding of CALR mutant cellular behaviour and its role as a MPN driver mutation. All the *CALR* mutations described in ET and PMF affect a highly conserved amino acid sequence at the end of the C-terminal domain of this protein (Klampfl et al., 2013; Nangalia et al., 2013) (Figure 6). As previously mentioned, this domain plays an important role in the correct functioning of CALR, as it contains the major Ca^{2+} binding sites within the protein. Additionally, CALR C-terminal domain is characteristic of its highly structural instability and it has been proposed that its spatial conformation might be in close relationship with its Ca^{2+} buffering activity and its protein binding functions (Migliaccio and Uversky, 2017). *CALR* mutations are thought to change the nature of this domain, by altering its chemical and physical characteristics (Shivarov et al., 2014; Eder-Azanza et al., 2014), possibly leading to abnormal CALR behaviour within the cell.
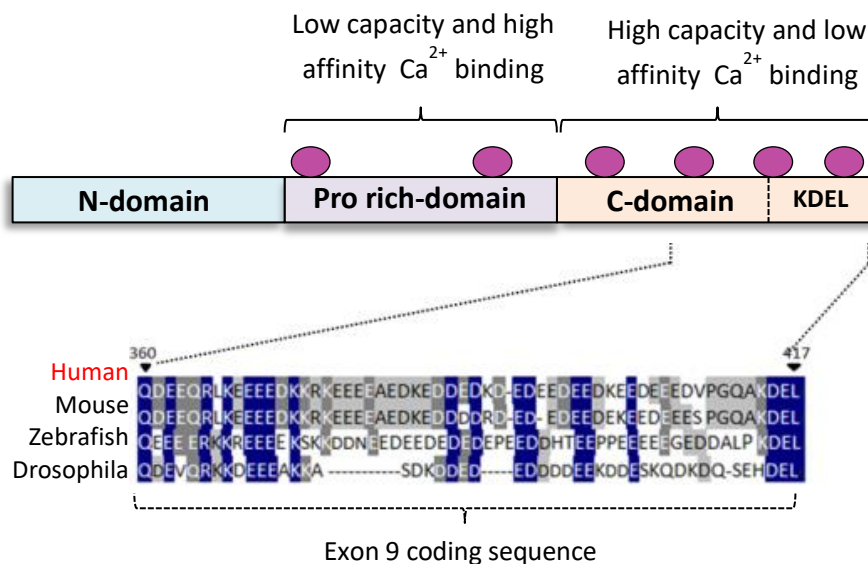
Figure 6. Schematic representation of the CALR conserved sequence affected by mutations found in MPN.
CALR mutations affect a highly conserved sequence within CALR C-terminal domain, which includes high capacity and low affinity Ca^{2+} binding sites and KDEL region. The amino acid conservation rate within the affected C-terminal domain is represented by shading. Blue displaying highly conserved residues and light grey indicates less conserved regions. Purple circles represent Ca^{2+} binding motifs.

When *CALR* was described as a novel MPN driver mutation, there was an initial surprise regarding the finding of an ER chaperone to be involved in the development of ET and PMF. *CALR* mutations did not, apparently, have a direct link with a deregulated JAK/STAT signalling pathway, as previously described in *JAK2* and c-*MPL* mutations. Therefore, investigating the link between *CALR* mutations, deregulated signalling network and MPNs progression has been a continuous concern within the field.

Recent *in vivo* studies have been focused in elucidating the role of mutant CALR in the development of MPN. Retroviral (Marty et al., 2015) and transgenic (Shide et al., 2017) studies demonstrated that *CALR* mutations are sufficient to generate specific MPN phenotype in mice. These studies showed that *CALR* type 1 mutant expressing mice developed high levels of myelofibrosis accompanied with splenomegaly and thrombocytosis (Marty et al., 2015). In contrast *CALR* type 2 mutation expressing mice showed ET-like phenotype. Both mutant mice showed increased platelet counts and an amplified megakaryocyte lineage (Marty et al., 2015; Shide et al., 2017). Moreover, *CALR* mutant mice harbouring a deleted *CALR* exon 9 did not show any disease phenotype, demonstrating that the novel C-terminal domain of CALR mutants is essential for disease induction (Marty et al., 2016).

Further studies have been foccussed on elucidating the direct link between CALR mutation and JAK/STAT signalling pathway. It is now known that MPL receptor is essential for CALR mutant MPN progression, as CALR mutants directly interact with this receptor leading to its activation (Chachoua et al., 2016; Elf et al., 2016; Araki et al., 2016). Activation of MPL receptor by CALR mutant binding is dependent on the N-glycosylation residues located in the extracellular domain of this receptor and the glycan binding site of the N-terminal domain of CALR mutant (Chachoua et al., 2016; Araki et al., 2016). FLAG-tagged CALR mutants used for immunoprecipitation studies showed that mutant CALR physically interacts with MPL receptor and that the positively charged amino acids localised within the novel C-terminal domain are essential for this direct interaction (Elf et al., 2016).

Despite the described interaction between CALR mutants and MPL receptor, the understanding of the consecutive deregulated signalling cascade leading to CALR oncogenicity remains an intense debate within the field. RNA sequencing of Ba/F3 murine cells co-expressing CALR mutant and MPL receptor revealed an enrichment of STAT5/3 gene signatures and additional western blot analysis corroborated the activation of JAK/STAT signalling cascade in these cells (Elf et al., 2016; Marty et al., 2016). Moreover UT-7 cells expressing CALR mutations displayed high levels of JAK2, ERK1/2 and STAT5 phosphorylation in the absence of TPO within the media (Araki et al., 2016). Additionally, the CALR-MPL downstream pathway was blocked by JAK2 inhibitors in these cells (Araki et al., 2016; Elf et al., 2016). On the other hand, a novel study revealed that megakaryopoiesis in CALR driven MPNs might be mediated by MAPK pathway, together with JAK/STAT signalling (Kollmann et al., 2016). Moreover, analysis of ET primary megakaryocytes revealed that STAT5/3 target genes are highly expressed in *JAK2* ET patients, compared with the *CALR* mutant group (Lau et al., 2015). Overall, these studies suggest further complexity in the cellular signalling of CALR mutant MPNs and highlight the need for additional analyses to decipher the molecular pathogenesis of these diseases (Figure 7).

CALR mutations have been described only in MPNs characterised by megakaryocyte hyperplasia. Of note, previous research has linked the presence of CALR mutants with induction of megakaryocyte differentiation. Interestingly, CALR mutants drive the expression

of specific megakaryocytic genes, such as *CD41* and c-*MPL* (Han et al., 2016), however, the molecular mechanism linking *CALR* mutations and the mechanism of induction of megakaryopoiesis remains unclear (Figure 7).

Despite the intense work performed in the last few years characterising CALR mutations in ET and PMF, there are many aspects of this novel mutation that remain to be studied. CALR is a multifunctional protein, which plays important roles within the ER, cytoplasm, cell membrane and ECM. Therefore, mutant CALR might show an alteration in its normal cellular functions during disease. For instance, very little is known about the effects of *CALR* mutations on its Ca^{2+} buffering activity. One recent study demonstrated that CALR mutant primary megakaryocytes displayed an abnormal Ca^{2+} buffering capacity (Pietra et al., 2015). However, further investigation is needed to analyse the consequences of altered Ca^{2+} buffering activity in megakaryocyte hyperplasia during MPNs.

Recent publication revealed that a previously established cell line, known as MARIMO, harbours *CALR* mutation (Kollmann et al., 2015). This cell line was established from a secondary AML patient that evolved from ET treatment (Yoshida et al., 1998). The discovery of *CALR* mutation within a common cultured cell line facilitated the analysis of the pathogenic role of this mutation. However, MARIMO cells are leukemic blast cells and therefore are not committed into the megakaryocytic lineage, hence their differentiation stage is important to bear in mind when using this cell line to analyse the effects of *CALR* mutations in ET and PMF. Interestingly, analysis of JAK/STAT signalling pathway using MARIMO cells revealed that these cells are not dependent on this cascade (Kollmann et al., 2015) and in contrast show an overactivated MAPK pathway (Kollmann et al., 2016).
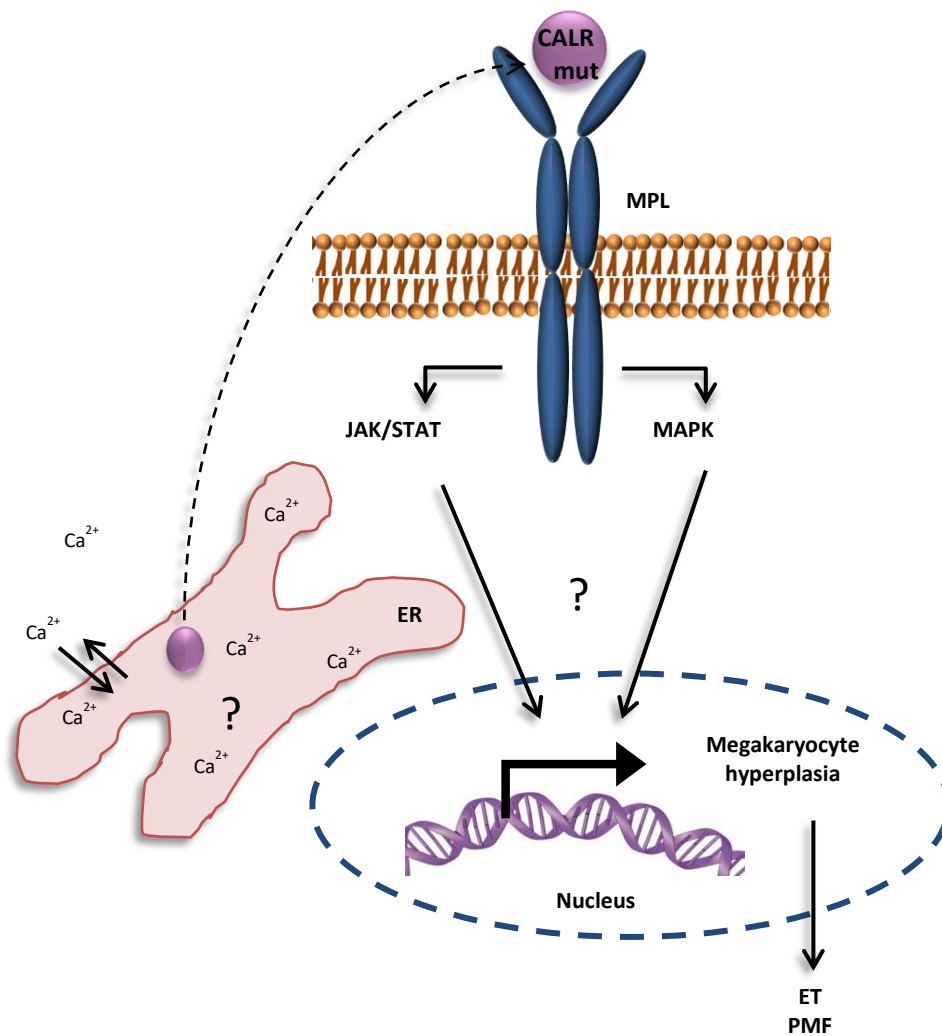
Figure 7. CALR mutant oncogenic activity.

CALR mutant has been shown to interact with MPL receptor, leading to an aberrant cell signalling. However, the exact mechanism of CALR mutant oncogenicity remains unclear. ER: Endoplasmic reticulum, ET: essential thrombocythemia, PMF: primary myelofibrosis

1.8. General hypothesis and aims of this study

Despite the large body of research built around *CALR* mutations in MPNs during recent years, many aspects of its oncogenic mechanisms remain unanswered. This investigation has worked under the hypothesis that *CALR* mutations affect the nature of the C-terminal domain of this protein and this not only leads to deregulated signalling cascades, but there is also a modification of CALR normal cellular behaviour, such as its cellular compartmentalisation and its Ca^{2+} buffering activity.

CALR C-terminal domain is a highly important region for CALR protein binding and Ca^{2+} buffering and its structural and physical properties have been directly linked to its biological functions (Migliaccio and Uversky, 2017). A key question is whether CALR novel C-terminal domain in MPNs leads to changes in the structure of this region, and therefore affects CALR cellular functions. Thus, this thesis seeks to examine the structural properties of CALR mutants' C-terminal domain and identify potential novel protein binding regions within this domain.

CALR mutations lead to the deletion of the KDEL region, an ER retention motif described within the C-terminal domain (Klampfl et al., 2013; Nangalia et al., 2013). Changes in the sub-cellular compartmentalisation of this mutant protein could lead to major effects within the cell. Therefore, the second aim of this study was to investigate the possible changes of CALR mutant sub-cellular localisation.

Differences in the physical characteristics of CALR C-terminal domain and in the compartmentalisation of this protein could lead to alterations in the Ca^{2+} buffering activity of the cell. However, little is known about the importance of Ca^{2+} during megakaryopoiesis in physiological condition and disease (Di Buduo et al., 2016). Therefore, this research aims to characterise the importance of Ca^{2+} during normal megakaryocyte differentiation conditions and the possible effects of *CALR* mutations in the Ca^{2+} buffering activity of CALR mutant cells during megakaryocyte differentiation.

Finally, the limited available cellular models harbouring *CALR* mutations hinder the study of the pathogenic role of *CALR* mutations during megakaryocyte hyperplasia. The recent

characterisation of *CALR* mutation in MARIMO leukemic cell line allowed the study of *CALR* mutation *in vitro* using routine cell culture techniques without the use of transduction or transfection techniques (Kollmann et al., 2015). However, the best cellular model used to study *CALR* mutation would be the use of a cell line committed into the megakaryocyte lineage to mimic ET and PMF pathological cellular conditions. Thus, this investigation aims to analyse the possible megakaryocyte differentiation potential of MARIMO cells which could be useful for the understanding of CALR oncogenicity during megakaryocyte proliferation in ET and PMF harbouring *CALR* mutations.

CHAPTER 2: *Material and Methods*

2.1. Computational methods

2.1.1. Input sequences

The sequence of 417 amino acids of *Homo Sapiens* Calreticulin (CALR) was retrieved from Swiss Prot database (http://www.uniprot.org/uniprot/P27797) (Table 4). CALR mutant sequences of type 1 mutation (L367fs*46) and type 2 mutation (K385fs*47) were obtained from previous literature (Nangalia et al., 2013).

Table 4. CALR amino acid sequences used in this study.
C-terminal domain sequence is in **bold** and mutant sequences are **underlined.**

Name	Amino acid sequence
CALR WT	MLLSVPLLLGLLGLAVAEPAVYFKEQFLDGDGWTSRWIESKHKSDFGKFVLSSGKFYGDEE KDKGLQTSQDARFYALSASFEPFSNKGQTLVVQFTVKHEQNIDCGGGYVKLFPNSLDQTD MHGDSEYNIMFGPDICGPGTKKVHVIFNYKGKNVLINKDIRCKDDEFTHLYTLIVRPDNTYE VKIDNSQVESGSLEDDWDFLPPKKIKDPDASKPEDWDERAKIDDPTDSKPEDWDKPEHIP DPDAKKPEDWDEEMDGEWEPPVIQNPEYKGEWKPRQIDNPDYKGTWIHPEIDNPEYSP DPSIYAYDNFGVLGLDL**WQVKSGTIFDNFLITNDEAYAEEFGNETWGVTKAAEKQMKDK QDEEQRLKEEEEDKKRKEEEEAEDKEDDEDKDEDEEDEEDKEEDEEEDVPGQAKDEL**
CALR type 1 mutation (L367fs*46)	MLLSVPLLLGLLGLAVAEPAVYFKEQFLDGDGWTSRWIESKHKSDFGKFVLSSGKFYGDEE KDKGLQTSQDARFYALSASFEPFSNKGQTLVVQFTVKHEQNIDCGGGYVKLFPNSLDQTD MHGDSEYNIMFGPDICGPGTKKVHVIFNYKGKNVLINKDIRCKDDEFTHLYTLIVRPDNTYE VKIDNSQVESGSLEDDWDFLPPKKIKDPDASKPEDWDERAKIDDPTDSKPEDWDKPEHIP DPDAKKPEDWDEEMDGEWEPPVIQPEYKGEWKPRQIDNPDYKGTWIHPEIDNPEYSPD PSIYAYDNFGVLGLDL**WQVKSGTIFDNFLITNDEAYAEEFGNETWGVTKAAEKQMKDK QDEEQRTRRMMRTKMRMRRMRRTRRKMRRKMSPARPRTSCREACLQGWTEA**
CALR type 2 mutation (K385fs*47)	MLLSVPLLLGLLGLAVAEPAVYFKEQFLDGDGWTSRWIESKHKSDFGKFVLSSGKFYGDEE KDKGLQTSQDARFYALSASFEPFSNKGQTLVVQFTVKHEQNIDCGGGYVKLFPNSLDQTD MHGDSEYNIMFGPDICGPGTKKVHVIFNYKGKNVLINKDIRCKDDEFTHLYTLIVRPDNTYE VKIDNSQVESGSLEDDWDFLPPKKIKDPDASKPEDWDERAKIDDPTDSKPEDWDKPEHIP DPDAKKPEDWDEEMDGEWEPPVIQNPEYKGEWKPRQIDNPDYKGTWIHPEIDNPEYSP DPSIYAYDNFGVLGLDL**WQVKSGTIFDNFLITNDEAYAEEFGNETWGVTKAAEKQMKDK QDEEQRLKEEEEDKKRKEEEEAEDRRMMRTKMRMRRMRRTRRKMRRKMSPARPRTS CREACLQGWTEA**

2.1.2. Computational analysis of the intrinsic disorder predisposition of the C-terminal domain of CALR wt and type1/2 mutants

Evaluation of the residue disorder propensity within the C-terminal domain of CALR wt, type 1 and type 2 mutants were evaluated by using different disorder predictors. From the PONDR family, PONDR$^®$ VLXT and PONDR-FIT (Xue et al., 2010) were used as well as RONN-FIT (Yang et al., 2005), IUPRED (Dosztanyi et al., 2005) and PSIPRED (McGuffin et al., 2000) web servers.

PONDR-FIT is a metapredictor, assembled by combining six different predictors: PONDR$^®$ VLXT/ VSL2/VL3, FoldIndex, IUpred and TopIDP. This predictor shows a relatively improved prediction capacity than each of the components alone and it has been described as one of the best available disorder predictors (Xue et al., 2010; Migliaccio and Uversky, 2017). PONDR$^®$ VLXT was separately used due to its accuracy to predict short sequences disorder propensity associated with molecular recognition features (MoRFs) regions (Dunker et al., 2001). Moreover IUPRED uses an accurate algorithm to predict the disorder propensity of amino acid sequences based in their pair-wise energy (Dosztanyi et al., 2005), whereas PSIPRED and RONN-FIT use neural networks to estimate the coil-coil propensity.

These predictors were used to analyse the primary amino acid sequence of CALR wt, CALR type 1 and type 2 mutants C-terminal domains (highlighted in bold in Table 4) and gave scores for each amino acid of the input sequence showing the individual disorder or structure probability. Finally, the outputs of each individual disorder predictor were averaged, obtaining a consensus to evaluate the CALR C-terminal domain disorder propensity. This approach has been shown to increase the reliability of the results compared to using a single disorder predictor (Fan and Kurgan, 2014; Migliaccio and Uversky, 2017)

2.1.3. Computational analysis of the secondary structure of CALR wt and mutants C-terminal domain

Initial analysis of crystal structure of CALR globular domain was performed by Visual Molecular Dynamics (VMD) using the available CALR PDB code 3O0V (Wijeyesakere et al., 2011) in collaboration with Dr. Farooq A Kiani at IWR, University of Heidelberg (Germany).

In order to predict the secondary structure of CALR C-terminal domain two different servers were used, the Iterative Threading Assembly Refinement (I-TASSER) (Yang et al., 2015) and *S2D* method (Vendrusco Lab- Software, University of Cambridge) (Sormanni et al., 2015). Both online servers were used to perform a comparative analysis between the estimated structure of CALR wt, and CALR type 1 and type 2 mutants.

I-TASSER software matches structure predictions with functional properties. The obtained 3D protein structures are accompanied with C-scores, known as the confidence value to estimate the quality of the predicted model and it ranges between -5 to 2. High C-score values indicate better accuracy of the predicted model. Moreover, S2D method server predicts secondary structure together with intrinsic disorder predisposition of the protein regions. S2D software gave scores for each amino acid of the input sequences (CALR wt and type1 and type 2 mutations) showing the individual amino acid secondary structure population.

2.1.4. Validation of predicted CALR wt and mutants structural models

PROCHECK (Laskowski et al., 1996) was used to validate the best predicted structures of CALR wt, type 1 and type 2 mutations C-terminal domains obtained in the I-TASSER server analysis. PROCHECK analyses the phi (Φ) and psi (Ψ) torsion angles of the predicted models. Obtained plots show a good quality model when 90% of the residues are located in the favoured regions within the obtained Ramachandran plots.

2.1.5. Computational analysis of the presence of MORFs regions within the CALR wt and mutants C-terminal domain

The presence of protein binding sites within disorder protein regions was analysed by MoRFpred (Disfani et al., 2012) and ANCHOR algorithms (Dosztanyi et al., 2009). MoRFpred detects potential Molecular Recognition Features (MoRFs) based in the hallmarks of these regions, such as solvent accessibility or physiochemical characteristics. ANCHOR server uses the pair-wise energy estimation method as previously described by IUPred server (Dosztanyi et al., 2005).

Both predictors were used to analyse the presence of MoRFs within the CALR wt, CALR type 1 and type 2 mutants C-terminal domains and gave scores for each amino acid of the input sequence showing the individual score for MoRFs probability. Finally, the outputs of each individual disorder predictor were averaged, obtaining a consensus to evaluate the CALR C-terminal domain MoRFs propensity.

2.1.6. Analysis of amino acid charge within the CALR wt and mutants C-terminal domain

Isoelectric points (pI) of CALR wt, CALR type 1 and type 2 C-terminal domains were obtained using the Scripps Institute's on-line Protein Calculator v.3.3 (http://www.scripps.edu/Bcdputnam/protcalc.html). Furthermore, visualization of acidic vs basic amino acids within the sequence of interest was performed using the obtained best predictive 3D secondary structures from I-TASSER analysis as scaffolds (see section 2.1.3).

2.2. Laboratory techniques

2.2.1. Cell culture and cell lines

Three myelogenous leukemia cell lines have been used throughout this investigation. K562 cells, originally established from bone marrow blasts cells obtained from a patient with CML in a blast crisis (Lozzio and Lozzio, 1975). MARIMO cell line, established from a patient with secondary AML developed during treatment of ET (Yoshida et al., 1998) and DAMI cells, established from a patient with megakaryoblastic leukemia (Greenberg et al., 1988). Additionally, a human embryonic kidney cell line was used, known as HEK-293T (Graham et al., 1977).

HEK-293T cells were grown in Dulbecco's modified Eagle´s medium (DMEM, Invitrogen) supplemented with 10% Fetal bovine serum (FBS) (Invitrogen), 1% Penicillin and Streptomycin (Gibco), and 1% Sodium pyruvate (Gibco). MARIMO cell line, kindly provided by Dr Hitoshi Kioyi at University of Japan, and K562 cells were grown in Roswell Park Memorial Institute medium 1640 (RPMI, Invitrogen) supplemented with 10% Fetal Calf Serum, 1% Penicillin and Streptomycin and 1% Sodium pyruvate. Clones of DAMI cells overexpressing GFP, CALR wt, CALR type1 and CALR type 2 mutations kindly provided by Dr. Petros Papadopoulos from the Hospital Clinico San Carlos in Madrid, were grown in Iscove's Modified Medium (IMDM, Invitrogen) supplemented with 10% Horse Serum (Invitrogen), 1% Penicillin and Streptomycin, 1% Sodium pyruvate. CALR wt, CALR type 1 and CALR type 2 clones were selected with 2 µg/ml Puromycin (Apollo Scientific).

All cell lines were incubated at 37°C and 5% CO_2 and cells were passed upon confluency every 2-3 days.

2.2.2. Subculture of cell lines

Confluent cells were collected in a sterile 15ml falcon tube and centrifuged at 1200 rpm for 5 minutes in order to pellet the living cells. The supernatant was then discarded and the cell pellet was resuspended in 5 ml of pre-warmed cell culture media. For general subculturing

conditions, 0.5 ml of cells was transferred to a new sterile cell culture flask or plate containing 9.5 ml of fresh media (1:10 dilution from the original culture). Cells were subsequently cultured in optimal conditions.

2.2.3. Freezing and thawing cells

For freezing, cells were centrifuged at 1200 rpm for 5 minutes and cell pellet was resuspended in 1 mL of 10% dimethyl sulfoxide (DMSO) FBS. Cell suspension was transferred into cryovials and stored initially at -80 °C and for long term storage in liquid nitrogen.

For cell thawing, cryovials were thawed in a water bath at 37 °C and cells were rapidly resuspended into 10 ml of pre-warmed media. Then, samples were centrifuged at 1200 rpm for 5 minutes. Supernatant was discarded and the cell pellet was resuspended in 10 ml of fresh media and transferred to a new cell culture flask. Subsequently, cells were cultured in optimal conditions.

2.2.4. Cell counting and trypan blue exclusion

In order to plate the required number of cells during the experiments, viable cells were counted using haemocytometers (Labtech) and the trypan blue exclusion assay was performed. Trypan Blue is used to calculate a dead:viable cell ratio within the cell suspension. Under light microscopy dead cells are recognised due to trypan blue staining being internalised in dead cells. To perform cell counting and trypan blue exclusion assay 10 µl of cell dilution were resuspended in 50 µl of Phosphate buffered saline (PBS) and 40 µl of trypan blue. Then 10 µl of the final solution was loaded into the haemocytometer. Number of living cells in each square corner of the haemocytometer chamber (Figure 8) were counted and averaged. Subsequently, calculations were performed to obtain the number of living cells per µl and the dilutions needed to seed the number of live cells required for following experiments.
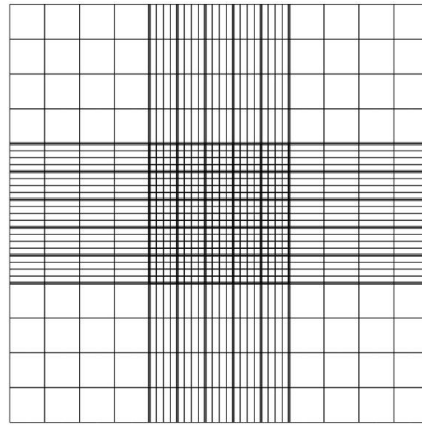
Figure 8. Typical haemocytometer chamber.
10 µl of cell/trypan blue solution were loaded into the chamber. Number of live cells are counted within the 4 square corners using light microscopy.

2.2.5. Extraction of DNA plasmids from Whatman paper

*CALR-WT -FLAG and CALR-K385fs*477Ins-FLAG* plasmids (Table 5) were kindly provided by Dr. Tony Green at Cambridge University (UK) in Whatman® paper. In order to extract the plasmids of interest, the paper containing the DNA was introduced into an eppendorf tube. Then 50 µl of 10 mM Tris (pH: 7.6) was added to the paper, vortexed and subsequently incubated for 15 minutes at room temperature. DNA concentration was measured using NanoDrop 1000 Spectrophotometer (Thermo Scientific) and samples were kept at − 20 ^{0}C until plasmid were finally amplified for further experiments.

2.2.6. Plasmids amplification

For DNA plasmid amplification 1 µg of DNA vector of interest was added to 25 µl of DH5α *E.coli* competent cells (Thermo Fisher Scientific). Cells were gently mixed and were kept on ice for 30 minutes. After incubation, samples were heat-pulsed in a 42^{0}C water bath for 45 seconds and immediately transferred to ice for 2 minutes. 250 µl of sterile Luria-Bertani (LB) media was added to the bacteria and samples were incubated for 1 hour at 37°C whilst shaking. Cells were plated on LB agar plates (100 µg/ml ampicillin) and were incubated aerobically overnight at 37°C for selection of the transformed cells.

The following day, colonies were picked and inoculated into 3 ml of LB (100 µg/ml ampicillin) for selection. Then, samples were incubated overnight at 37°C whilst shaking for further bacteria growth.

Following growth of selective bacteria containing the plasmid of interest, QIApre Spin Midiprep kit (Qiagen) was used as per manufacturer's guidelines to isolate the DNA plasmid. Finally, DNA concentration was measured using NanoDrop Spectrophotometer and samples were kept at –20 ^{0}C until use in further experiments. Amplified plasmids were sequenced by Source Bioscience (Rochdale).

2.2.7. PolyFect transfection

A day before transfection 6 x10^5 of HEK 293T cells per well were plated in 6-well plates (Sigma). The following day 2 µg of the DNA plasmids of interest (Table 5) were diluted in cell growth media containing no serum proteins or antibiotics in a total volume 100 µl in a sterile Eppendorf tube. Afterwards 15 µl of PolyFect Transfection Reagent (Quiagen) were added to the DNA solution. Samples were mixed by vortexing 10 seconds before incubation at room temperature for 10 minutes.

While DNA incubation was taking place, cell growth medium was removed from the plates and cells were washed twice with PBS. Then 1.5 ml of pre-warmed complete cell growth media was added to the cells. Once DNA samples were incubated, 600 µl of growth media were added to the samples. This final solution was added drop by drop over the cell plates.

The following day cell media was removed, and cells were washed twice with PBS in order to avoid cytotoxicity from the PolyFect reagent. Finally, 2 ml of fresh media was added to the cells and were incubated for another 24 hours for further experiments.

Additionally, an empty GFP vector (Table 5) was used in all cell transfection assays as a control for transfection efficiency. GFP expression was detected after 48 hours using fluorescent microscopy.

Table 5. List of plasmids used in this study.

Plasmids used for cell transfection	Source
pLKO-3G-3V-GFP	Gift from Dr Tony Green laboratory (Cambridge University)
pCDNA5_FRT_CALR-NonMutant-FLAG	
pCDNA5_FRT_CALR-K385fs*477Ins -FLAG	
pCDF1-MSC2-EF2- CALR-NonMutant-copGFP	
pCDF1-MSC2-EF2-CALR- K385fs*477Ins-copGFP	
pCMV-10-TPOR-HA	

2.2.8. Immunostaining

Sterile coverslips were washed twice with sterile PBS and incubated with fibronectin (Sigma) (25µg/ml in PBS) to improve cell adhesion and expansion on top of the coverslip surface. Fibronectin was incubated for one hour at room temperature under sterile conditions. Then, coverslips were washed again twice with PBS and placed in 6 well plates.

A day prior to transfection HEK 293T cells were seeded at a concentration of 2×10^5 cells and were plated in 6-well plates containing a previously treated coverslip. The following day cells were subjected to transfection as described in section 2.2.7 with the vectors of interest.

Two days after transfection cells were washed twice with PBS and 4% paraformaldehyde (PFA) was added into the well. After 15 minutes of incubation at room temperature, PFA was removed and cells were washed twice with PBS. Then, cells were incubated with PBS containing 1% triton for 5 minutes at room temperature.

Before blocking, cells were washed twice with PBS. Then cells were incubated with PBS + 1% bovine serum albumin (BSA) for one hour at room temperature. Afterwards, cells were incubated with the primary antibody (1:200 dilution) (see antibodies in Table 6) for 1 hour and then samples were washed three times with PBS for 5 minutes each. Cells were incubated with the secondary antibody (1:200 dilution) for 1 hour at room temperature (see antibodies in Table 6). Finally, samples were washed again three times in PBS and once in dH$_2$O. Then, coverslips were left to air-dry overnight at room temperature.

The following day coverslips were transferred to a glass slide and mounted with mounting media (Vectashield). Slides were stored at 4°C in dark until microscopy.

Table 6. List of antibodies used in this study.

Primary antibodies	Source	Secondary antibodies	Source
Mouse-Flag	Sigma	Anti-mouse 647	Gift from Dr Patrick Caswell laboratory (Manchester University)
Rabbit-Flag		Anti-rabbit Cys3	
Mouse-ERP57		Anti-mouse Cys3	
Mouse-HA	Abcam		

2.2.9. High-resolution imaging

High-resolution imaging was performed in collaboration with the laboratory of Dr Patrick Caswell at The University of Manchester (UK). Fixed cells were imaged using a Leica TCS SP8 STED 3X microscope with an HC PL APO 100X/1.40 oil objective and further 3.0x or 4.0x confocal zoom. A pinhole with 0.7 airy units was used to further improve resolution. White light laser (WLL) was used for imaging captures using the following emission wavelengths: 488, 550 and 653. Then, appropriate acceptance spectrum for GFP, cys3 and far red were used. Z-slide images were taken from the bottom of the cell to the top. Images were deconvolved using Huygens Professional software with default settings and were analysed using LAS X Leica Software.

2.2.10. Lentiviral transduction of DAMI cells

Lentivirus was produced according to previous published protocols (Borg et al., 2010). DAMI cells were transduced in 6 well plates using between 5 to 10 μl of concentrated lentivirus. Puromycin (2 μl/ml final concentration) was added to the cells for selection. At day 7 after transduction, cells were harvested and were used for serial dilution within a 96 well plate to

obtain single clones. pRRLsin.PPTs.hCMV.Wpre vector was used as a backbone for *CALR*-WT, *CALR*-type1 and *CALR*-type2 gene insertion.

2.2.11. Protein extraction

To decrease loss of protein during the extraction protocol, protein extraction was carried out on ice. Cells were pelleted by centrifugation at 1200 rpm for 5 minutes, supernatant was removed and cells were washed twice in ice cold PBS. Then, samples were centrifuged and the cell pellet was resuspended in 500 µl of high salt lysis buffer (HSLB) (45mM HEPES pH 7.5, 400 mM NaCl, 1mM EDTA, 0.5% NP40 (Igepal) 10% Glycerol). 1mM DTT, 1mM PMSF, 5 µl Protease inhibitors (PI), 2 mM Sodium orthovanadate (Na_3VO_4) 10 mM BGP and 5 mM NaPPI were added to activate the lysis buffer before use. Lysates were transferred to a 1.5 ml microcentrifuge tube and were subsequently rotated for 20 minutes at 4 °C and followed by 15 minutes centrifugation at 12000 rpm at 4 °C. The obtained supernatant was transferred to another tube and kept as protein extract. Finally, in order to quantify protein levels within the extracts, the Bradford assay was performed (see section 2.2.12) to ensure the use of equal amounts between samples in subsequent experiments.

2.2.12. Bradford assay

The Bradford assay is a commonly used technique to determinate protein concentration within samples. Initial working solution was prepared diluting 200 µl of Protein assay dye reagent concentrate (Bio-Rad) into 800 µl of distilled water. 2 µl of protein sample was added into 1 ml of working solution in semi-micro cuvettes. As a control, 2 µl of HSLB was used for spectrophotometer calibration. Duplicates of each protein sample were prepared in order to obtain a final average of protein concentration. Using the spectrophotometer cuvettes were read at 595 nm (Lu et al., 2010).

Use of even amounts of protein was necessary for experiments such as Western blotting. Therefore, calculations based on the results obtained from the Bradford assay quantification were performed. A value of 40 µl was given to the sample with the lowest reading of

absorbance (maximal loading volume allowed during electrophoresis). Appropriate relative amount of protein concentration was then calculated for the other samples using the following formula: $\dfrac{\textit{lowest absorbance x } 40}{\textit{absorbance of current sample}}$

Finally, based on previous calculation, appropriate aliquots with the corresponding volume were prepared. Then 3XSDS buffer (see Table 7) was added to the samples (half the volume of the corresponding sample) and samples were kept at – 80 °C until use.

2.2.13. Sodium Dodecyl Sulfate Polyacrylamide Gel Electrophoresis (SDS-PAGE)

10% Ready Gel® Tris-HCl Gel (Bio-Rad) was used for protein electrophoresis. The gel was placed in the running chamber filled with 1XSDS running buffer (see Table 7). Then, protein samples were denatured at 95°C for three minutes and were loaded on the gel alongside Hyperpage protein molecular weight marker (Bio-Rad) using a Hamilton microlitre glass syringe. The gel was set to run at 80 V, which was increased to 110 V once the samples entered the resolving gel.

2.2.14. Western blotting

After SDS electrophoresis, western blot was performed to detect the proteins of interest. Firstly, a polyvinylsise fluoride (PVDF) membrane (Millipore) was activated in 100% methanol for five minutes and washed in 1 X Western Transfer Buffer (see Table 7). Then, transfer cassettes were prepared in the following order: sponge, 2 x filter paper, SDS gel, PVDF membrane, 2 x filter paper and sponge. Finally, cassettes were transferred into a Mini Trans-Blot® Cell (Bio-Rad) filled with 1 x Western Transfer buffer. Transfer was performed at 0.4 mA for 2 hours at 4 °C.

PVDF membrane was washed once with PBS and blocked with skimmed milk (SM) PBS (PBS and 5% SM) for one hour at room temperature. Then, membrane was incubated with the corresponding primary antibodies overnight rotating at 4°C (primary antibodies were diluted in 2.5% SM-PBST following manufacturers guidelines for appropriate concentration). The

following day, using a shaking incubator the membrane was washed three times with PBST for 10 minutes, after which was incubated with the correspondent secondary antibody for 1 hour at room temperature while shaking (secondary antibodies were diluted in 2.5% SM-PBST following manufacturers guidelines for appropriate concentration). After incubation, the membrane was washed again three times with PBST for 10 minutes and finally developed.

The membrane was incubated with SuperSignal West Femto Chemiluminescent Substrate (Thermo Scientific). The working solution of the developer reagent was prepared following manufacture's guidelines. Signal was detected with CL-XPosure™ Film (Life-technologies) in a Photon Ecomax Automatic X-Ray Film Processor.

Antibodies used for western blot were purchased as follows: mouse anti-human CALR (AbCam), anti-mouse (GE Healthcare Life Sciences), rabbit anti-human actin (AbCam), anti-rabbit (GE Healthcare Life Sciences).

Table 7. List of buffers used for western blot analysis.

Buffer name	Composition
0.1% PBS/Tween (PBST)	100ml 1xPBS, 900ml dH2O, 1ml Tween-20
10X SDS Running Buffer	1.9M Glycine, 247.7mM Tris, 35mM SDS
10X Western Transfer Buffer	1.5M Glycine, 272.4mM Tris
1XWestern Transfer Buffer	100 ml 10xWTB, 200 ml Methanol, 700 ml dH2O
3XSDS Loading Buffer	0.01% bromophenol blue, 187mM Tris, 30% Glycerol, 15% 2-mercaptoethanol, 6% SDS,

2.2.15. RNA extraction and cDNA synthesis

Cells were collected and centrifuged at 1200 rpm for 5 minutes. Then, cells were washed twice with ice cold-PBS. After this, RNA of cell pellet was extracted using Isolate II Mini Kit (Bioline) following the manufacturers guidelines. Finally, RNA concentration was determined using NanoDrop spectrophotometer and was stored at - 80°C until use.

Following cell RNA extraction, mRNA was converted into stable complementary DNA (cDNA) by using Tetro cDNA Synthesis Kit (Bioline). To avoid RNA degradation, all reactions were prepared on ice. Samples were prepared as followed: RNA (up to 5 µg), 1 µl of Oligo (dT)$_{18}$, 1 µl of 10 mM dNTP mix, 4 µl of 5x RT Buffer, 1 µl of RiboSafe RNase inhibitor, 1 µl of Tetro Reverse Transcriptase (200 u/µl), dH$_2$O up to 20 µl. Samples were vortexed and incubated at 45°C for 30 minutes before increasing temperature to 85°C for an incubation of 5 minutes. Afterwards samples were incubated on ice until use.

After cDNA synthesis, cDNA concentration was determined using NanoDrop spectrophotometer. Then, cDNA was diluted to an end concentration of 50 ng/ µl and samples were stored at - 20°C until used.

2.2.16. Taq polymerase chain reaction

Optimal temperature of primer annealing was tested by taq PCR. For DNA amplification, DNA Taq polymerase recombinant (Invitrogen) samples were prepared using 2.5 µl of 10x PCR Reaction Buffer, 0.5 µl of 10 mM dNTP mix, 0.2 µl of Taq DNA polymerase, 1 µl of primer mix (10 mM of forward and reverse primers), 2 µl of template cDNA and 18.05 µl of dH$_2$O. Verity 96-well Thermal Cycler was used for the PCR amplification and the samples were subjected to the conditions as described in Table 8.

Table 8. Taq PCR cycles.

Step	Temperature (^{0}C)	Time	Number of cycles
Denature	94	2 minutes	1
Denature	94	45 seconds	35
Anneal	54-60	30 seconds	
Extend	72	20 seconds	
Final Extension	72	10 minutes	1

PCR products were analysed by gel electrophoresis. For gels, 2% agarose (Bioline) was diluted in 1x Tris/Borate/EDTA running buffer (Severn Biotech) containing 1x gel red (Cambridge Bioscience). Samples were mixed with 5x loading buffer (Bioline) and a total volume of 20 μl was loaded into the gel. For reference a 50 bp Hyperladder (Bioline) was loaded into the first well. Electrophoresis was performed at 110 V for 1 hour. Finally, DNA samples were visualised using a Box transilluminator with GeneSnap version 7.12.06 (Syngene).

2.2.17. Quantitative real-time Polymerase Chain Reaction (qRT-PCR)

qRT-PCR is a technique commonly used to analyse and quantify gene expression using fluorescent DNA dyes. In this study SYBR green fluorescent dye was used, which binds specifically to double stranded DNA and emits light upon excitation (VanGuilder et al., 2008).

qRT-PCR samples were performed using the SensiFast SYBR No-Rox mix (Bioline). Samples were prepared on ice as follows: 10 μl of SensiFast SYBR No-Rox mix, 0.75 μl of primer mix of gene of interest (Table 10), 2 μl cDNA and 7.25 μl of dH$_2$o. For every run a non-template control sample was included. During this study, human *GAPDH* gene was used as a housekeeping gene.

Reactions were run on a QIAGEN Rotor-Gene Q Thermocycler. Parameters of the PCR are shown in Table 9. A final dissociation melting curve was performed between 72°C and 95°C at 0.5^{o}C increments with intervals of 5 seconds holds. Fluorescence was acquired in the green channel. Melting curves were performed to corroborate the amplification of a single DNA

product within the samples and to ensure no contamination within the non-template controls.

Table 9. qRT-PCR cycles

Step	Temperature (^{0}C)	Time	Number of cycles
Denature	95	2 minutes	1
Denature	95	5 seconds	
Annealing	59	10 seconds	40
Extend	72	20 seconds	

QIAGEN Rotor-Gene Q Series Analysis Software was used to determinate the Threshold cycle (C_T) values for each sample. Samples were run in triplicate and an average was taken. Only samples with standard deviation of ≤ 1 C_T were used for analysis. Samples were normalised against human *GAPDH* C_T values and subsequently presented relative to the respective controls following comparative C_t method.

Table 10. Primers used in this study.

Gene name	Primer sequence	Reference
GAPDH forward	5'-ATGGGGAAGGTGAAGGTCGG -3'	(Hui et al., 2017)
GAPDH reverse	5'-GACGGTGCCATGGAATTTGC -3'	
CISH forward	5'-AGCCCAGACAGAGAGTGAGC-3'	N/A
CISH reverse	5'-TGACAGCGTGAACAGGTAGC-3'	
ID1 forward	5'-CCAGAACCGCAAGGTGAG-3'	(Tobin et al., 2011)
ID1 reverse	5'-GGTCCCTGATGTAGTCGATGA-3'	
PIM1 forward	5'-CGAGCATGACGAAGAGATCAT-3'	(Kim et al., 2005)
PIM1 reverse	5'-TCGAAGGTTGGCCTATCTGA-3'	
SOCS2 forward	5'-TGCAAGGATAAGCGGACAGG-3'	(Carvalho et al., 2014)
SOCS2 reverse	5'-CAGAGATGCTGCAGAGATGG-3'	
C-MPL forward	5'-GCACTGTGATGCTTTATGCAAC-3'	(Jacquel et al., 2006)
C-MPL reverse	5'-TGAACGGTTTAGAGGATGAGGA-3'	

2.2.18. Comparative C_t method ($2^{-\Delta\Delta CT}$)

In order to present the quantitative gene expression analysis obtained in the qRT-PCR experiment, the $2^{-\Delta\Delta CT}$ method was used (Schmittgen and Livak, 2008). Firstly, ΔC_t was calculated by the subtraction of the average C_t value of the housekeeping gene from the average C_t value of the target gene. This calculation normalises the results to allow comparisons between different samples.

$$\Delta C_{t=} \text{ Ct target gene - Ct Housekeeping gene}$$

Then $\Delta\Delta C_t$ value was calculated by subtracting the ΔC_t of the treated sample from the ΔC_t of the control sample. Finally, fold change was used to calculate the quantitative difference of gene expression from the control.

$$\Delta\Delta C_{t=} \Delta C_t \text{ treated cells - } \Delta C_t \text{ control cells}$$

$$\text{Fold change} = 2^{-\Delta\Delta CT}$$

2.2.19. Propidium Iodide staining and cell cycle analysis

Analysis of cell cycle was performed by Propidium iodide (PI) staining. PI is a fluorescent molecule used to stain DNA, as it intercalates between the DNA bases (Crowley et al., 2016). Cells were collected and centrifuged at 1200 rpm for 5 minutes, followed by two washes in cold PBS. Then, cold 70 % ethanol was added drop by drop into the cell pellet while vortexing and samples were incubated at 4°C for 30 minutes.

After incubation, cells were washed twice with cold PBS. Cell pellet was resuspended in 50 μl of 100 μg/ml Ribonuclease A (RNase A) (Sigma-Aldrich) and incubated at room temperature for 15 minutes. Then, 200 μl of 50 μg/ml PI (Sigma-Aldrich) was added. Cells were incubated at room temperature for 15 minutes and were kept in dark until flow cytometry analysis.

PI fluorescence is directly proportional to the amount of DNA within the cell. Three cell phases of cell cycle (G0/G1, S and G2/M phase) were identified by flow cytometry based on the DNA content of cells (Crowley et al., 2016).

2.2.20. Protein cell surface immunostaining

Cells were collected and centrifuged at 1200 rpm for 5 minutes. After two washes in cold PBS, cells were incubated with the primary antibody diluted in PBS + 1% FBS (1:1000 dilution) for 30 minutes at room temperature (see Table 11). Then cells were washed twice with PBS. When staining was performed with primary antibody containing a fluorescent marker, cells were then resuspended in 500 μl of PBS and were analysed by flow cytometry.

When CALR cell surface staining was performed, cells were subsequently incubated with secondary antibody (see Table 11) diluted in PBS + 1% FBS (1:500 dilution) for 30 minutes at room temperature and were washed twice with PBS. Then, cells were incubated with PE streptavidin (Biolegend) diluted in PBS + 1% FBS (1:500 dilution) for another 30 minutes at room temperature in the dark. Finally, cells were washed twice with PBS and were subjected to flow cytometry analysis.

Table 11. List of antibodies used in this study.

Antibody	Source
Anti-human CALR	AbCam
Anti-human CD235a APC	eBioscience
Anti-human CD41a APC	
Anti-mouse CD41a PE	
Anti-mouse CD117 Alexa Fluor 700	
Anti-human CD110 APC	BD
Anti-mouse Biotinylated	DAKO

2.2.21. Free intracellular calcium staining

Fluo-8 AM (Abcam) chemical intracellular Ca^{2+} indicator was used for staining of intracellular free Ca^{2+}. Fluo-8 AM stock was prepared using pluronic DMSO to improve cell loading efficiency (Hamad et al., 2015).

For Ca^{2+} staining cells were pelleted by centrifugation at 1200 rpm for 5 minutes. Supernatant was removed and cells were washed with PBS and centrifuged again. Cell pellet was resuspended in 1 ml of PBS and 5 µl of Fluo-8 AM (final concentration of 5 µM). After 30 minutes of incubation at room temperature, samples were diluted to a final volume of 10 ml with PBS and were then centrifuged at 1200 rpm for 5 minutes. Then cells were washed with PBS and finally resuspended in 500 µl of PBS. Samples were analysed using flow cytometry.

2.2.22. Flow-cytometry analysis

Samples were analysed using a FACS Verse flow cytometry (BD Bioscience, USA). Forward scatter (FSC) and side scatter (SSC) were used to gate the cell population of interest. Cells were subjected to the detection of specific fluorescent signal using different fluorescent parameters. The following three fluorescent parameters were used during the analysis: phycoerythrin (PE), FITC and allophycocyanin (APC). Data was analysed using FACS Suite software (BD).

2.2.23. ER calcium release assay

ER Ca^{2+} flux into the cytoplasm was quantified in MARIMO, K562 and DAMI cells. Firstly, intracellular Ca^{2+} was stained with Fluo-8-AM as previously described (see section 2.2.22). Then cells were pelleted and were diluted in 1 ml of PBS.

Ca^{2+} cytoplasmic levels were quantified by using flow-cytometry. Samples were recorded each 60 seconds during 18 minutes. Firstly, initial basal intracellular Ca^{2+} levels of the cell population were recorded for two minutes. Afterwards, Thapsigargin (Abcam) was added to the cells in a final concentration of 1 µM. Cells were vortexed and immediately recorded. After Thapsigargin addition, samples were recorded for another 15 minutes each 60 seconds.

Ca^{2+} fluorescent readings were expressed relative to the initial Ca^{2+} cytoplasmic levels. Three independent experiments were performed using cells of different culture passages.

2.2.24. Cell drug treatment

Growing MARIMO, K562 and DAMI cells at a concentration of 3×10^5 cells/ml were treated with the correspondent drug treatment (see Table 12) diluted in complete RPMI medium, unless otherwise stated. Cells were incubated for 72 hours and were subsequently used for further analysis.

Table 12. Drug treatments used in this study.

Drug	Source	Concentration
PMA	Sigma-Aldrich	5 nM
Hemin	Sigma-Aldrich	50 µM
BTP-2	Abcam	50 µM
Fendiline	Alfa Aesar	20 µM
Riluzole	Abcam	100 µM

2.2.25. Mouse bone marrow cells megakaryocyte induction

Bone marrow was harvested from schedule 1 culled C57/Black6 mice from Charles River Laboratories. Freshly isolated bone marrow was aliquoted and frozen down in liquid nitrogen until used.

Cryovials containing bone marrow cells were defrosted as previously described in section 2.2.3. Once the cell pellet was diluted in fresh culture media, 1×10^5 cells per ml were plated in a 12 well plate. In order to induce megakaryocyte formation within the culture, cells were plated in pre-warmed RPMI medium containing 100 ng/ml of mouse thrombopoietin (R&D systems). Cells were subsequently incubated over 10 days at 37°C and 5% CO_2. Samples in day 0, 5 and 10 cells were further stained to detect Ca^{2+} concentration and cell surface markers. Finally, samples were analysed by flow cytometry.

2.2.26. May-Grunwald Giemsa staining

Analysis of MARIMO cell morphology was performed using May-Grunwald Giemsa staining. Undifferentiated MARIMO cells grow in suspension within the culture; therefore cell cytospins were performed in order to obtain a circular monolayer of cells onto a glass slide to further perform cell staining.

MARIMO cells in culture were diluted in PBS at a concentration of $1x10^5$ cells/ml in a microcentrifuge tube. Then, cytofunnel chambers were prepared as follow: cytoclip, glass slide, filter card and cytofunnel, and placed in the cytocentrifuge. 100 μl of cell suspension were loaded into the cytofunnels. Then, samples were centrifuged at 500 rpm for 5 minutes at minimum acceleration. Finally, slides were removed from the centrifuge and left to air dry for 5 minutes.

Sterile coverslips were washed twice in PBS and placed in 6 well plates used for MARIMO cells incubation in PMA. After 72 hrs incubation media was removed from wells and MARIMO differentiated cells were adhered to the coverslips. The cells were then washed twice in PBS.

Cells adhered to the coverslips and within a monolayer in glass slides were fixed by immersion in 100% ethanol and left to air dry for 10 minutes. Then, May-Grunwald Giemsa stain solution (BDH/VWR international limited UK) was diluted to 10% in Giemsa buffer. Giemsa buffer was prepared by diluting one tablet of pH 6.4 (BDH laboratory supplies) in 1 L of dH_2O. The slides and coverslips were covered in Giemsa working solution for 20 minutes at room temperature. After incubation, Giemsa staining was discarded and samples were washed under tap water.

2.2.27. Bright field microscopy

Images of fixed MARIMO cells stained with May-Grunwald Giemsa were captured using a Leica DM 500 compound microscope and 100x oil objective lens (Leica N Plan 1.25).

For live-cell imaging of cells within the culture plates, images were captured using inverted Vert.A1 AXIO (Zeiss) and Zeiss 40X Objective, LD A-Plan (0.5 NA).

2.2.28. Cell proliferation Assay

Cells were plated at 2×10^4 cells per well in a 96-well plate exposed to the relevant drug concentration and incubated for 72 hours. Each drug condition was plated in triplicate. Cell proliferation was measured using CellTiter 96® Aqueous Non-Radioactive Cell Proliferation Assay (Promega) which is composed of two different solutions: [3-(4,5-dimethylthiazol-2-yl)-5-(3-carboxymethoxyphenyl)-2-(4-sulfophenyl)-2H-tetrazolium, inner salt] (MTS) and phenazine methosulfate (PMS), following manufacturers guidelines. MTS working solution was prepared as follows: 100 µl of PMS (0.92 mg/ml) for 2 ml of of MTS (2mg/ml). Then, 20 µl of MTS working solution was added into 100 µl of cells in each well.

Once MTS working solution was added into the wells, cells were incubated for 4 hours at 37 ºC and 5% CO_2. Then, plate absorbance was read on a Thermo Labsystem Multiskan Ascent plate reader at 490 nm and 690 nm. Finally, in order to remove background noise from the readings, the 690 nm values were subtracted from the 490 nm values. Readings were expressed relative to the respective controls. Three independent experiments were performed using cells of different culture passages.

2.2.29. Statistical analyses

Comparisons between groups were carried out using the statistical Student´s t-test. P-values less than 0.05 (*) and 0.01 (**) were considered statistically significant. Microsoft excel program was used to obtain the statistical data and generate graphs.

Chapter 3: *Effects of CALR mutations into the physical characteristics of CALR C-terminal domain in MPNs*

3.1. Introduction

Over the past few decades, structural biologists have intensively characterised protein structures, leading to a large body of knowledge linking amino acid primary sequences with secondary structure. The three-dimensional (3D) structure of a protein and its cellular behaviour are closely related. However, growing evidence suggests that not all the encoded proteins are folded spontaneously into stable structures and instead these proteins can reach dynamic conformations known as intrinsic disorder states (Wright and Dyson, 1999; van der Lee et al., 2014). It is now recognised that the intrinsically disordered proteins (IDPs) or the intrinsically disordered protein regions (IDPRs) stability is determined by the amino acids sequences of the protein (Oldfield and Dunker, 2014). IDPs/IDPRs are characterised by the depletion of specific amino acids. Examples include: Aspartic Acid, Cysteine, Isoleucine, Leucine, Phenylalanine, Tryptophan, Tyrosine and Valine and for the presence of the known disorder promoting residues like Arginine, Glutamine, Glutamic acid, Glycine, Lysine, Proline and Serine (Williams et al., 2001). Correct protein´ order-disorder conformation is essential for their optimal biological activity, as it is now recognised that dysfunctional IDPs are linked with human diseases, such as cancer, neurodegenerative diseases and diabetes (Uversky et al., 2014).

Interestingly, recent studies have shown that IDPs/IDPRs could change to structured regions upon binding with their specific targets (Babu et al., 2011; Migliaccio and Uversky, 2017) and this disorder-to-order transition could be essential for the correct cellular function of the protein. Among long IDPRs it is possible to identify disordered protein binding sites, known as Molecular Recognition Features (MoRFs), which lead to protein folding as consequence of specific binding interaction (Yan et al., 2016).

Recent advances in the field of structural biology have helped to design computational methods to predict IDPs/IDPRs, identify MoRFs within these regions and even build 3D protein structural models. Currently, there are several protein disorder prediction software available, such as PONDR-FIT (Xue et al., 2010) or IUpred (Dosztanyi et al., 2005), which are based on the average of several disorder databases or the protein energy content respectively. Additionally, there are structural and functional protein predictor severs as the interactive threading assembly refinement (I-TASSER) (Yang et al., 2015), which helps to structurally characterise proteins with known sequences and match structure with protein function (Yang et al., 2015). So far, I-TASSER method is one of most accurate server for prediction of protein's secondary structure and during recent years it has been extensively used by many researchers to predict the secondary structure of proteins of interest (Jethra et al., 2012; Manochitra and Parija, 2017). Moreover, a current server known as S2D method (Sormanni et al., 2015) allows an *in silico* study of protein's secondary structure and a simultaneous description on the intrinsic disorder regions using a combined statistical method. Finally, further bioinformatic tools have been designed in order to identify MoRFs within IDPs/IDPRs, such as ANCHOR algorithm (Dosztanyi et al., 2009) or MoRFpred (Disfani et al., 2012).

CALR secondary structure has been an intense focus of study during recent years (Norgaard Toft et al., 2008; Giraldo et al., 2010; Kozlov et al., 2010; Wijeyesakere et al., 2011; Migliaccio and Uversky, 2017). CALR is formed by three structural and functional domains, the N-terminal domain, central P-domain and the C-terminal domain. Previous studies have focused on describing CALR secondary structure and its link with CALR cellular functions (Kozlov et al., 2010). Several investigations based on the structural analysis of CALR attempted to crystallise this protein; however, the intrinsic mobility of the P-domain and the highly disordered C-terminal region affected the crystallisation of CALR. Recent research work by Kozlov and colleagues (2010) depleted the problematic P-domain and C-terminal regions and published the crystal structure of mouse CALR (Kozlov et al., 2010). This primary template of CALR has being useful for further structural CALR studies (Wijeyesakere et al., 2011). However, the precise structure of the C-terminal domain remains unknown.

CALR C-terminal domain is known to be essential for the Ca^{2+} buffering activity of the protein, due to the presence of a high number of negatively charged amino acids within this residue which are known to bind with Ca^{2+} ions (Nakamura et al., 2001). Recent studies showed by

using molecular dynamics simulations and spectroscopic techniques that CALR C-terminal region structure fluctuates depending on Ca^{2+} levels. In low Ca^{2+} concentrations the domain shows a disordered structure, however, in presence of higher Ca^{2+} concentrations, this region becomes compacted and increases the conformational stability of the protein (Giraldo et al., 2010; Migliaccio and Uversky, 2017). Therefore, it appears likely that the nature of the folded structure of this domain is dependent on the Ca^{2+} buffering activity of the protein within the ER.

Interestingly, the recently identified *CALR* mutations in MPNs have been described to produce a novel C-terminal domain of the protein (Klampfl et al., 2013, Nangalia et al., 2013). These mutations are known to change the net charge of the protein from acidic to basic (Shivarov et al., 2014). This suggests that the novel mutant C-terminal domain described in MPNs could have less Ca^{2+} binding affinity within the ER and therefore contribute to the malignancy of these mutations in disease by changing Ca^{2+} dynamics in *CALR* mutant megakaryocytes (Shivarov et al., 2014; Eder-Azanza et al., 2014). A relatively recent bioinformatic analysis identified the presence of a low-complexity region (LCR) within CALR wild-type (wt) C-terminal domain (Eder-Azanza et al., 2014). LCR are known to be protein regions with low amino acid diversity and their position and size are directly linked with the protein binding properties (Coletta et al., 2010). However, CALR mutations lead to changes in the location and length of this LCR (Eder-Azanza et al., 2014). In addition, recent study suggested changes in the MoRFs regions of CALR mutant´s C-terminal domain (Varricchio et al., 2017). Therefore, changes in the LCR together with MoRFs regions within the C-terminal domain could lead to changes in the CALR protein binding affinity during disease. Interestingly, *CALR* type 1 and type 2 mutations have been described to interact with MPL receptor in MPNs and this novel interaction directly dependent on the novel CALR C-terminal domain (Chachoua et al., 2016; Elf et al., 2016), therefore it could be suggested that changes in the protein binding properties within mutant CALR C-terminal domain could be the cause of this novel protein interaction. However, the understanding of the molecular basis of this novel interaction remains unknown.

Additionally, previous bioinformatic analysis using RaptorX, COILS and PAIRCOILS2 secondary structure predictor servers showed that *CALR* type 1 mutation increases the possibility of non-coil regions within the C -terminal domain, possibly leading to a more structured region,

whereas type 2 maintains similar characteristics to CALR wt (Eder-Azanza et al., 2014). Interestingly, previous study using a single disorder predictor known as PONDR-VXLT suggested that CALR mutations affect the disorder profile of the C-terminal domain (Varricchio et al., 2017). Additionally, further *in silico* investigations showed the presence of phosphorylation sites within the new C-terminal domains in CALR type 1 and type 2 mutants. These phosphorylation sites were described to be specific for kinases with important roles in cellular signalling, such as PKC or CDK5 (Eder-Azanza et al., 2014). Therefore, the acquisition of phosphorylation sites within CALR mutants could lead to changes in cellular signalling during disease by establishing new networks of protein interactions.

3.1.1. Aims and hypothesis

Changes in the molecular nature of CALR mutants C-terminal domain could lead to changes in the functionally of CALR and consequently to the oncogenic phenotype of MPNs. Previous bioinformatic studies have suggested that *CALR* mutations described in MPNs could change the disordered status, the secondary structure and the amino acid charge of the novel C-terminal domains. However, further analysis need to corroborate and describe in more detail the specific molecular nature of these mutant proteins and its consequences for CALR functionality. Thus, during this *in silico* study three major aims will be addressed:

I. Comparative study the stability and protein secondary structure of CALR novel C-terminal domain of CALR type 1 and type 2 mutants.

II. Analysis of the impact of *CALR* mutations on the appearance of potential novel protein binding regions within CALR mutants C-terminal domain.

III. Analysis of the effects of *CALR* mutations on the amino acid charge of CALR mutants C-terminal domain.

3.2. Results

3.2.1. Initial analysis of CALR secondary structure

In order to gain a better understanding of the CALR 3D structure, the *in silico* analysis of the available PDB file (3O0V) of mouse CALR (Kozlov et al., 2010) was carried out using VMD software. This structure is depleted with the high motility arm in the P-domain and the IDPR of C-domain (Figure 9 A). As previously described, CALR mutations in MPNs are located in exon 9 (Klampfl et al., 2013; Nangalia et al., 2013). In Figure 9 A, the encoded protein region from exon 9 is highlighted in grey and shows an α-helix structure until the IDPR starts after residue 362. Interestingly, both CALR type 1 and type 2 mutations appear after residues 365 and 381 respectively, within the IDPR. Therefore, this preliminary analysis showed that the available crystallised structure displays the secondary structure of the C-terminal domain until the region where CALR mutations found in MPNs are located; hence these mutations are located within the known IDPR described in CALR wt (Figure 9 B).

Additionally, the distribution of the Ca^{2+} binding motifs within CALR protein was analysed within this model. The location of these amino acids was highlighted in the structure (Figure 9A). Embed in the globular domain Asp^{46} and Asp^{312} (represented in orange) function as high Ca^{2+} binding affinity residues (Ca^{2+} molecule represented in green). Moreover, low affinity and high capacity Ca^{2+} binding residues (represented in yellow) are located in the C-terminal domain. However, only three Ca^{2+} binding residues (Glu^{346}, Asp^{345} and Asp^{342}) are within the last α-helix of the structure. Hence, the rest of Ca^{2+} binding motifs are located within the IDPR of C-terminal domain (Glu^{368}, Glu^{369}, Glu^{370}, Glu^{371}, Asp^{372}, Glu^{377}, Glu^{378}) and are therefore depleted by the *CALR* mutations.

Overall, this analysis shows that *CALR* mutations found in MPN affect the IDPR of CALR C-terminal domain and therefore this region has not been previously crystallised. Moreover, this analysis demonstrates that the IDPR of this C-terminal domain also contains most of the Ca^{2+} binding motifs of CALR. Consequently, the available PDB structure of CALR wt cannot be used as a direct template to build models of the CALR mutants' secondary structure. Therefore, further analysis to investigate mutant CALR C-terminal domains will need to rely on the use of *in silico* secondary structure predictors.

A.

Disordered region

Asp345

Glu346

Asp342

Asp46

Asp311

B.

Disordered region

CALR WT	**DEAYAE EFGNETWGVTKAAEKQMKDKQDEEQRLKEEEEDKKRKEEEEAAEDKEDDEDKDEDEEDEEDKEEDEEEDVPGQAKDEL**
CALR type 1	**DEAYAE EFGNETWGVTKAAEKQMKDK QDEEQRTRRMMRTKMRMRRMRRTRRKMRRKMSPARPRTSCREACLQGWTEA**
CALR type 2	**DEAYAEEFGNETWGVTKAAEKQMKDKQDEEQRLKEEEEDKKRKEEEEAEDRRMMRTKMRMRRMRRTRRKMRRKMSPARPRTS**
	CREACLQGWTEA

Figure 9. Structural characteristics of CALR wt

A) 3D representation of the mouse CALR depleted of P-domain and the unstructured region of the C-terminal domain (PDV 3O0V). Ca^{2+} high binding affinity residues and low binding affinity residues are represented in orange and yellow respectively. Ca^{2+} binding atom is shown in green. Region encoded by exon 9 is shown in grey. **B)** C-terminal domain sequence alignment of CALR WT and CALR type 1 and Type2 mutants with the analysed crystal structure. Grey square represents α-helix structure. Ca^{2+} low binding affinity residues are shown in yellow. Figure based on (Wijeyesakere et al., 2011)

3.2.2. Analysis of CALR mutations effects in the intrinsic disorder state of CALR C-terminal domain

To study whether *CALR* type1 and type2 mutations affect the known disorder state of CALR C-terminal domain, a multiparametric *in silico* analysis of the intrinsic disorder state of the CALR mutants' C-terminal domain was performed by using five different bioinformatic servers: PONDR-VLXT, PONDR-FIT, IUPRED, PSIPRED and RONN-FIT (McGuffin et al., 2000; Dosztanyi et al., 2005; Yang et al., 2005; Xue et al., 2010). The trend to a disorder state of each amino acid was estimated with a score ranging between 0.5 and 1.

Results showed that CALR wt C-terminal domain is highly disordered after residue 353 (Figure 10 A) (estimation based in the average of all the obtained outputs). Interestingly, further analysis of the C-terminal domain of CALR type 1 and type 2 mutants showed an overall decrease in the disorder state in this region (Figure 10 B, C) compared with the CALR wt results. After mutation sequence boundary, all the individual predictors, except PONDER-FIT outputs, showed an overall decrease in the disorder probability of the new mutant C-terminal domain. However, values below the disorder threshold were only observed at the end of the amino acid sequence in both CALR mutations.

Overall, this computational analysis showed a decrease in the disorder probability of CALR C-terminal domain in type 1 and type 2 mutants characteristic of MPNs. This data could suggest that the C-terminal domain of CALR mutants could become a more rigid and defined structure, however further analysis focussing on the structural characteristics of this domain need to be performed in order to reach a better understanding of how *CALR* mutations affect the intrinsic structural characteristics of this novel C-terminal domain.
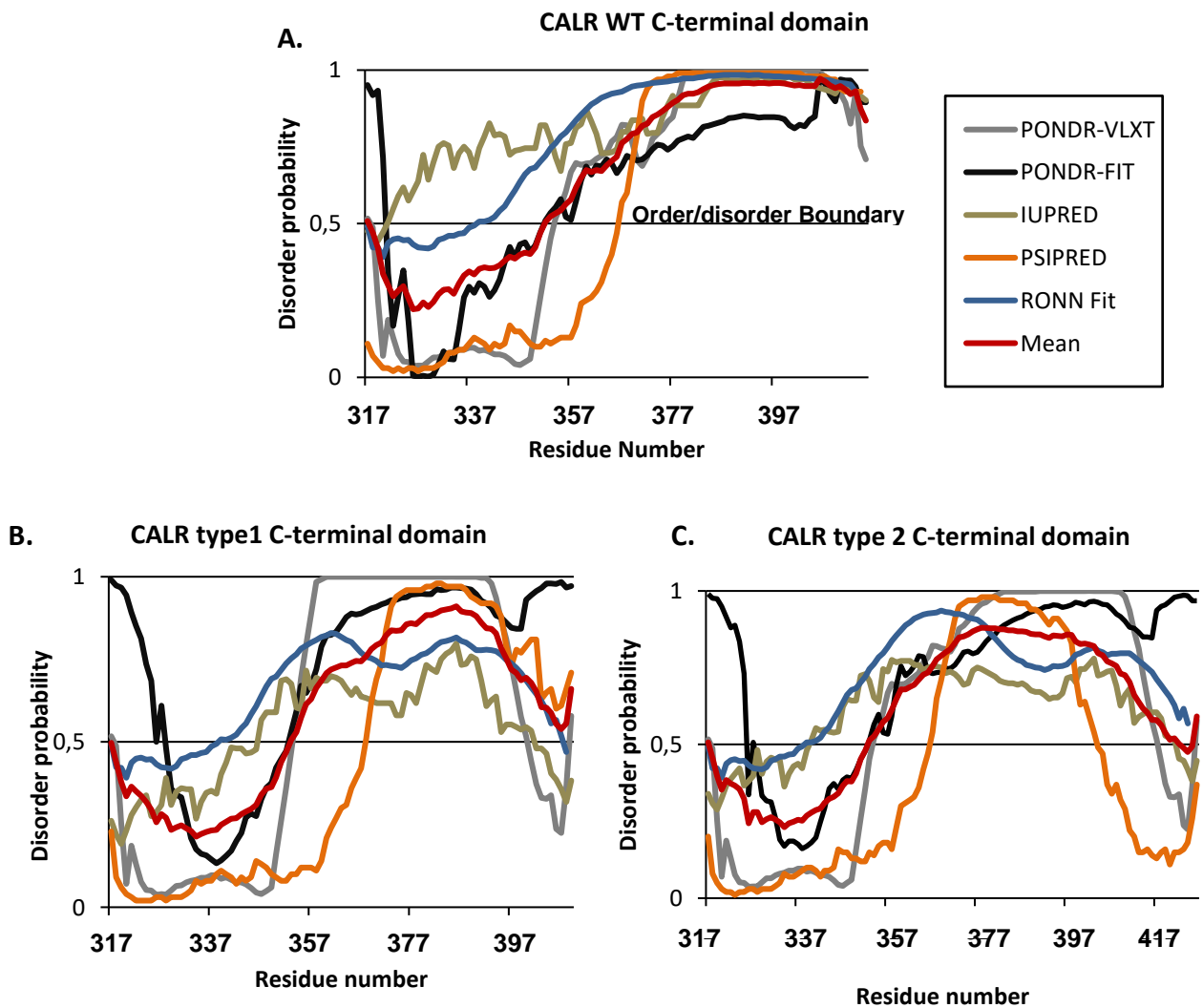
Figure 10. Protein disorder analysis of CALR wt and CALR mutants' C-terminal domain

Results obtained from **(A)** CALR wt sequence**, (B)** type 1 and **(C)** type 2 mutation C-terminal domains using five different disorder predictors : PONDR-VLXT (grey) PONDR-FIT (black), IUPRED (brown), PSIPRED (orange), RONN FIT (blue) and mean (read).

3.2.3. Three-dimensional structural modelling of CALR WT and CALR mutants

After previous results showing a decrease of the disorder probability within the C-terminal domain of CALR mutants, it was questioned whether these physical alterations could lead to changes in the secondary structure of this protein region. As previously described, the experimental characterisation of the secondary structure of CALR wt C-terminal domain is not available yet and therefore the available PDB file cannot be used as a template to characterise and predict CALR mutants C-terminal domain secondary structure. Hence, in order to study the physical properties of CALR mutants C-terminal domain, it is necessary to build a model based on *in silico* comparative analysis. During this *in silico* study, the predicted structural models of CALR wt, CALR type 1 and type 2 mutations were obtained using I-TASSER software (Yang et al., 2015). The obtained results showed the predicted secondary structure of the input sequences. Results were shown as PDB templates and five 3D predicted structures were obtained for each input sequence.

I-TASSER structural modelling starts from identifying structure templates in the PDB library. This analysis showed the PBD templates used for the sequence alignment of the input CALR sequences (Table 13). In this study, CNX (PDB LjhnA), a CALR structural homologue, was used for the alignment. Obtained Z-scored estimates the alignment of the protein sequences. Z-scores >1 indicate higher confident alignment.

Table 13. Rank1 threading templates for query protein sequence.

Input sequence	Structure template	PDB Hit	Z-score
CALR wt			3.87
CALR type 1 mutation	Crystal structure of the luminal domain of Calnexin	ljhnA	2.78
CALR type 2 mutation			2.78

Five predicted 3D structural models of each input sequence were obtained by their alignment with CNX sequence. However, Figure 11 only shows the CALR wt, CALR type 1 and type 2 mutant models considered as the best predicted structures. Obtained C-scores for these

models were -0.3, -0.21 and -1.09 respectively. For this structural analysis the C-terminal region of the proteins was studied in detail. Within the obtained models, the C-terminal domain is represented in orange-red and is pointed by white arrows in Figure 11.

Results showed that after the structured region already predicted to be an α-helix within CALR wt C-terminal domain (Figure 11 A) there is a loop of random coil structural state until the end of the amino acid sequence where a short α-helix is formed (Figure 11 A). Interestingly, *I-TASSER* predicted changes in the secondary structure within the same protein region of CALR mutants. CALR type 1 mutation displayed an α-helix at the beginning of the random coil region and possible another small α-helix after. The α-helix predicted to be at the end of the protein in CALR wt disappears in this mutant region (Figure 11 B). Moreover, CALR type 2 mutant model showed a different structure. CALR type 2 C-terminal domain was formed mostly by random coil, except a short α-helix at the beginning of the region (Figure 11 C).

Overall, the *in silico* analysis of the 3D structure of CALR C-terminal domain using *I-TASSER* software reveals that CALR type 1 and type 2 mutations could lead to changes within the secondary structure of this region. However, further analysis to confirm the fidelity of these structures need to be performed, as *in* silico analysis could have technical limitations.
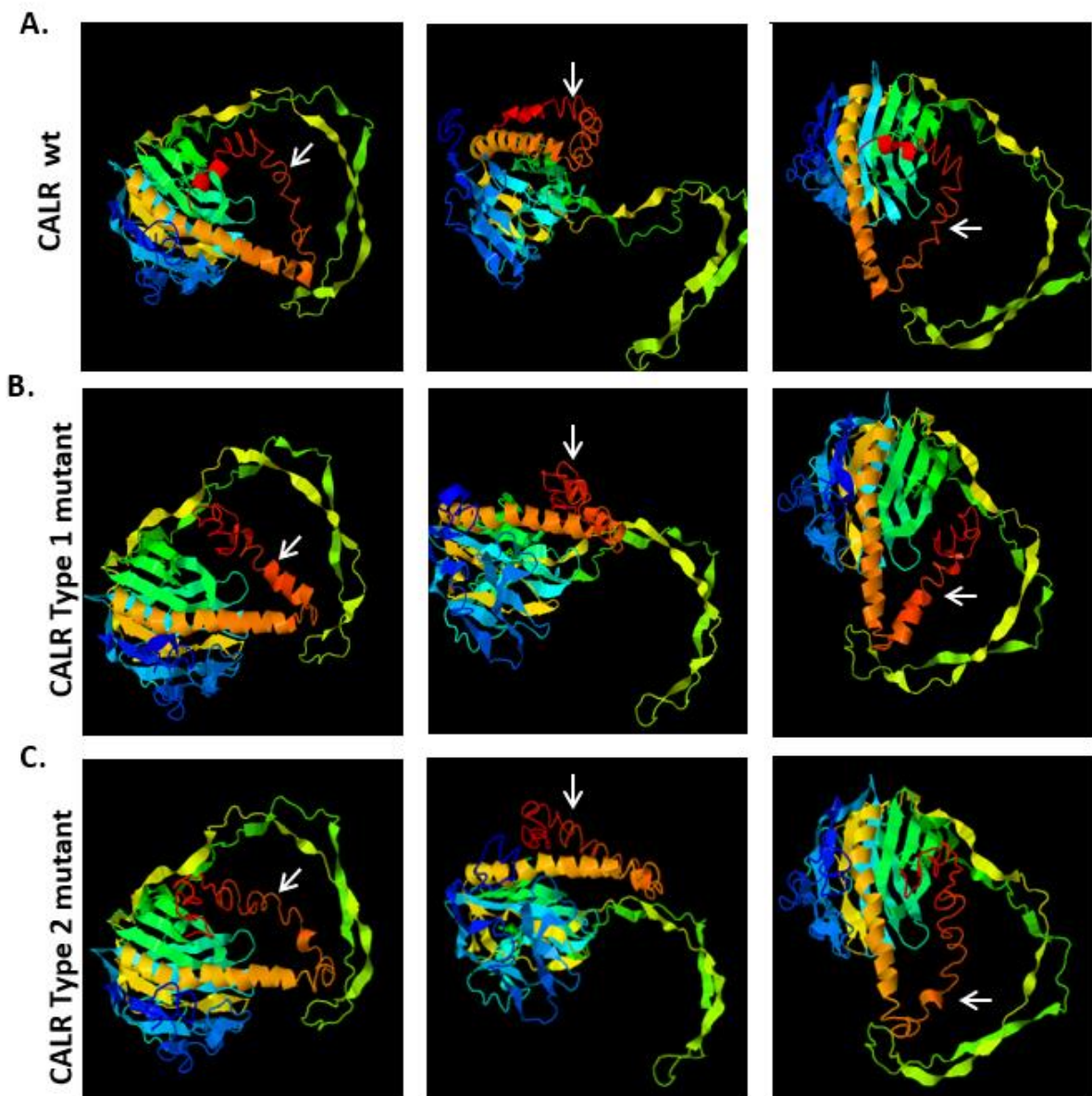
Figure 11. 3D structural modelling of CALR wt, type 1 and type 2 mutants.

Best predicted structural models of **A)** CALR wt, **B)** CALR type 1 and **C)** Type 2 mutation. Image shows three different space orientations of the obtained models by I-TASSER software. White arrows indicate the C-terminal region of the protein.

3.2.4. Assessment of CALR WT and CALR mutants structural predicted models

In order to assess the reliability of the previous structural CALR models the PROCHECK server was used to obtain Psi/Phi Ramachandran plots of the best predicted models by I-TASSER. This analysis was focused on the reliability of the C-terminal domains structural models only.

CALR wt C-terminal domain (residues number 317-417) Psi/Phi Ramachandran plot showed 89.05% residues in the allowed regions, 6% in the generous region and 4.95% in the disallowed region (Appendix 1 A). Overall, 95.05% residues of this model were located in the confidence regions, although residues within the generous region should be investigated more closely.

CALR type 1 C-terminal domain (317-410 residues number) Psi/Phi Ramachandran plot showed 84% residues in the allowed regions, 12% in the generous region and 4% in the disallowed region (Appendix 1 B). Finally, CALR type 2 C-terminal domain (317-428 residues number) showed 87.37% residues in the allowed regions, 9% in the generous region and 3.63% in the disallowed region (Appendix 1 C). Therefore, 96% and 96.37% of the total residues of CALR type 1 and Type 2 mutations C-terminal domain are located within the confidence region of the Ramachandran plots.

PROCHECK results obtained from CALR wt, type 1 and type 2 mutants C-terminal domain Psi/Phi Ramachandran plots suggested a high quality of the predicted models by *I-TASSER*. However, it is important to note that some of the amino acids were within the disallowed region. This suggests that further analysis should be performed to corroborate these models, as less than 90% of the residues were not within the high confidence regions.

3.2.5. Analysis of CALR WT and mutants C-terminal domain secondary structure based on s2D method

As the previous analysis by Ramachandran plots did not show higher than 90% of residues within the high confidence regions of the I-TASSER predicted models, further analyses were performed using other secondary structure predictor. For that, investigations into CALR wt and mutants C-terminal domains by using a novel online server, known as *s2D* method, were

carried out (Sormanni et al., 2015). This method unifies the prediction of the secondary structure population and the disorder probability of each amino acid of the given protein sequence.

CALR wt C-terminal domain analysis showed a general low disorder probability and an increase of α-helix population until amino acid 345. Afterwards the final region of the C-terminal domain showed an exponential increase of random coil (Figure 12 A) reaching values of 0.9 confidence.

Results showed that first α-helix populations predicted in CALR wt remains constant in the two CALR mutations sequences till residue 345. It is important to note that CALR mutations are located after this amino acid sequence, in the IDPR predicted in the previous analysis (Figure 10). CALR type 1 mutation showed an overall decrease in the population of random coil structure and a small population of α-helix at the end of the structure (residues numbers 400-404) (Figure 12 B). Moreover, analysis of CALR type 2 mutant C-terminal domain displayed two decreases in the population of random coil structure and two rises of α-helix populations at the end of the structure (residues numbers 398-403 and 418-423) (Figure 12 C).

Together, these results suggested that *CALR* mutations affecting the C-terminal domain could lead to a more stable conformational state within this protein region as seen previously by I-TASSER and the three disorder predictor servers used in this study. Overall, s2D analysis showed changes in the secondary structure populations within the C-terminal domain of CALR mutants, however the localisation of new α-helix populations did not agree with the I-TASSER predicted models (Figure 11), as this software predicted two small α-helix structures within the mutant region in CALR type 1 mutation and one α-helix in CALR type 2 mutation. However, both servers agreed that *CALR* mutations within this region lead to small changes in the secondary structure and there is an overall decrease in the disorder state of this region.
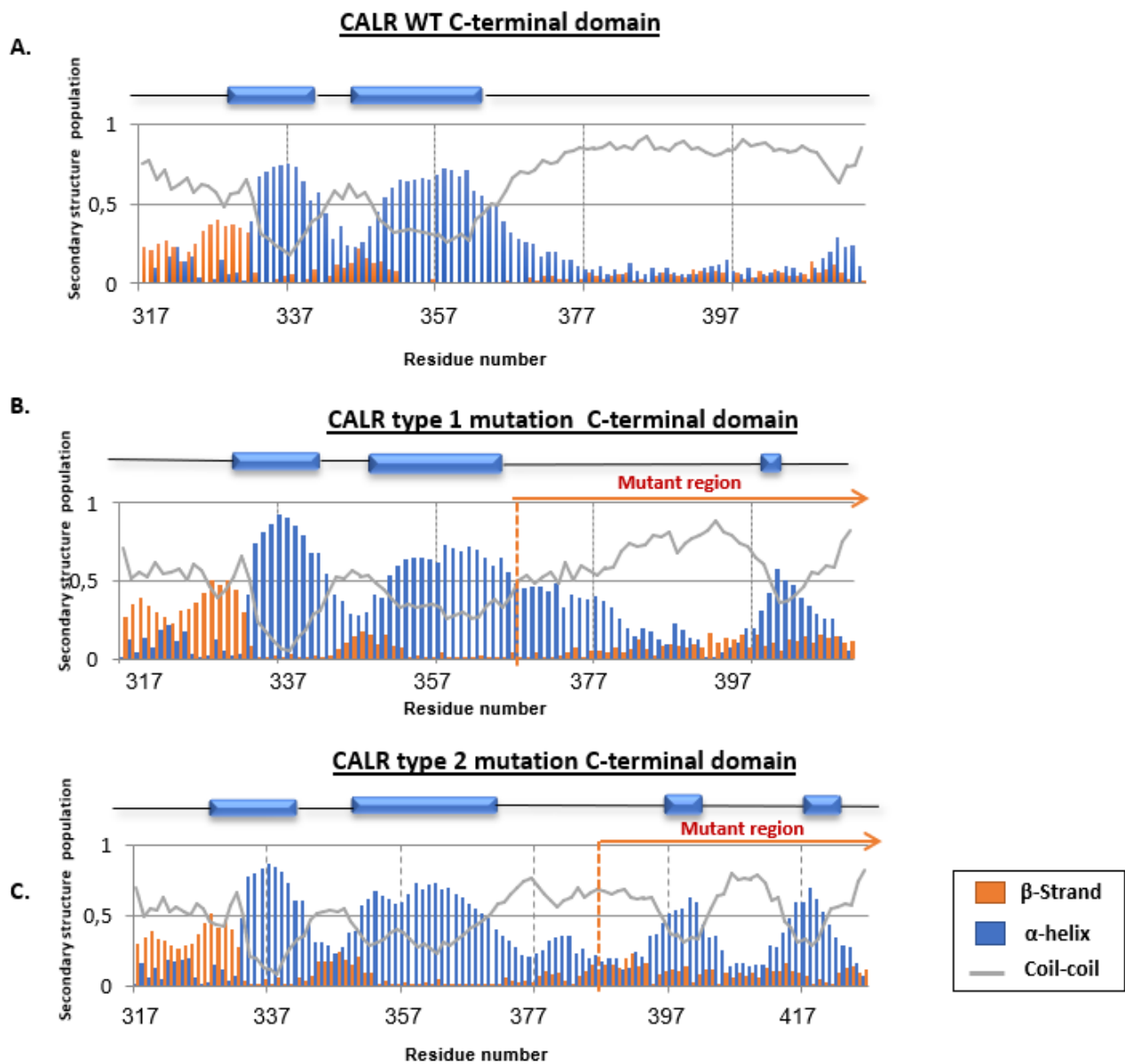
Figure 12. Analysis by S2D method of CALR wt, type 1 and type 2 C-terminal domains.

Representations of **A)** CALR wt, **B)** CALR type 1, **C)** CALR type 2 C-terminal domains analysis performed by S2D server. Graphs show the confidence of α-helix population in blue, β-strands in orange and random coil population in a continuous gray line.

3.2.6. Localisation of disorder-based protein binding sites within the intrinsically disordered CALR WT and CALR mutants C-terminal domain

To further characterise the effects of type 1 and type 2 mutations in the IDPR within CALR C-terminal domain, additional analysis aimed to investigate the presence and characteristics of MoRFs within these mutant regions. For this *in silico* analysis, two different algorithms, ANCHOR (Dosztanyi et al., 2009) and MoRFpred (Disfani et al., 2012) as well as the average of both obtained inputs were used.

Initially, both algorithms identified two MoRFs within the C-terminal domain of CALR wt. Average of both inputs predicted the location of MoRFs within the residues 319-348 and 409-417, which suggested that the IDPR of this C-terminal domain could have the potential for protein binding (Figure 13).

Both *CALR* mutations lead to a reduction of length of the first MoRF identified in this region in CALR wt (29 residues). CALR type 1 showed the location of MoRF in the amino acids 319-333 (15 residues) and CALR type 2 in 319-336 (18 residues). Second MoRF identified at the end of the C-terminal domain within CALR WT (8 residues), increased length in both type 1 and type 2 mutants, 399-411 and 416-428 (13 residues). Changes in length in both MoRFs could lead to changes in the protein binding properties within this region and therefore changes in the disorder-to-order transitions of CALR C-terminal domain (Figure 13).

Surprisingly, MoRFpred identified a potential additional MoRFs within CALR type 1 C-terminal domain, residues 374-382. Interestingly, although this MoRF predicted by MoRFpred was not identified by ANCHOR, this region displayed higher average scores when these were compared with the adjacent amino acids (Figure 13, black arrow). Therefore, this region could have a potential for binding proteins. Moreover, CALR type 2 showed an increase in MoRFs scores within the same region of the protein, predicted by both, ANCHOR and MoRFpred (Figure 13b, black arrow). Hence, ANCHOR and MoRFpred showed that *CALR* mutations found in MPNs change the nature of MoRFs regions within the C-terminal domain and this could potentially affect the range of binding partners of these mutant proteins.
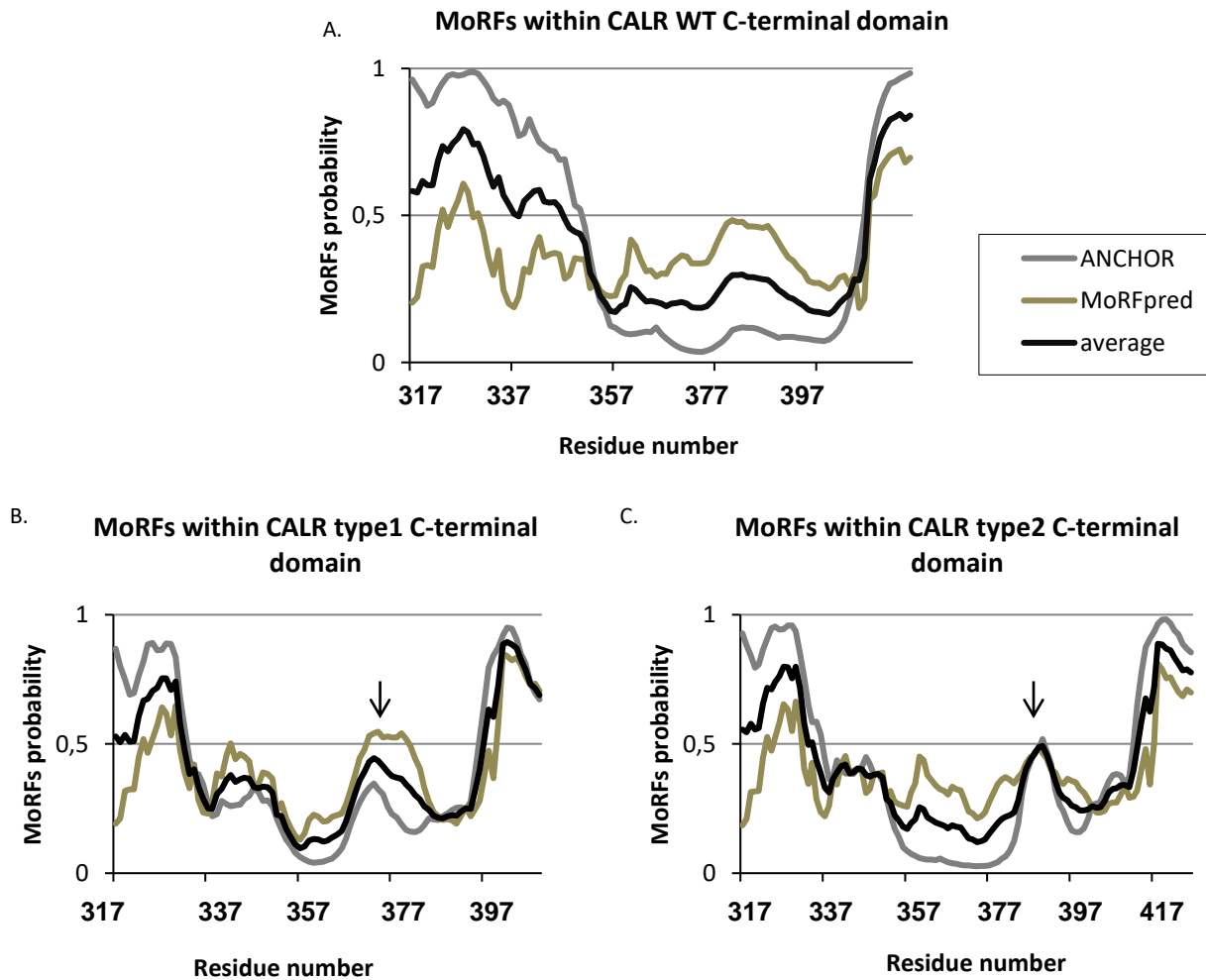
Figure 13. Computational analysis of MoRFs within the C-terminal domain of CALR wt, type 1 and type 2 mutants.

Results obtained from **(A)** CALR wt sequence**, (B)** type 1 mutation and **(C)** type 2 mutation C-terminal domains using two different disorder predictors: ANCHOR (grey) MoRFpred (brown) and mean (black).

3.2.7. Effects of CALR mutations in the amino acid charge within the C-terminal domain

As mentioned previously, CALR C-terminal domain is a highly acidic region and CALR mutations found in MPNs lead to changes in the amino acid sequence, increasing the number of basic residues within this region. Further analysis using the CALR wt, type 1 and type 2 mutations structural models by I-TASSER allowed us to visualise independently the acidic and the basic amino acids within the 3D structure. The CALR C-terminal domain is represented in

red and orange residues, as well as being identified by white arrows. As seen in Figure 14, CALR wt random coil region within the C-terminal domain is mostly formed by acidic amino acids. In contrast, within the same structural region of CALR type 1 and type 2 mutants there is a switch from acidic to basic amino acids (Figure 14).
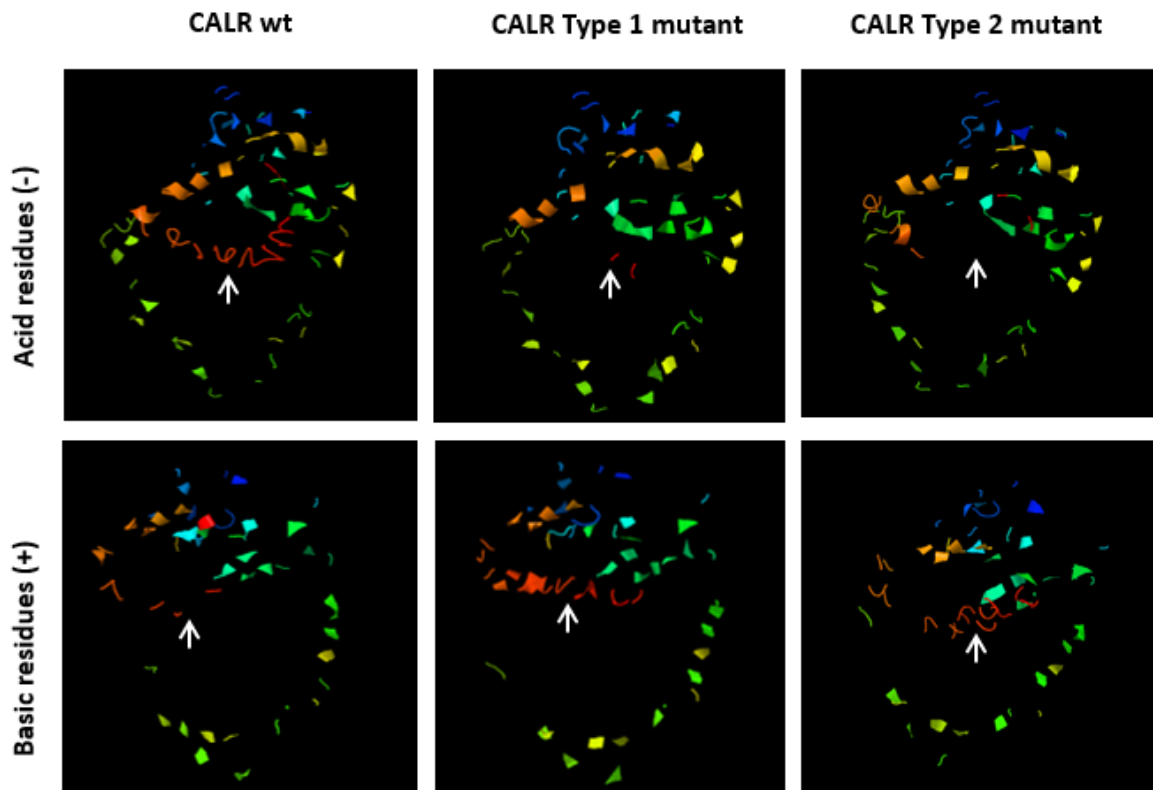
Figure 14. Analysis of acidic and basic residues location within the 3D structural models of CALR WT, type 1 and type 2 mutations.

Visualisation of acid and basic residues within the best predicted structural models of CALR by I-TASSER software. White arrows indicate the C-terminal region of the protein

Moreover, analysis using the Scripps Institute's on-line Protein calculator v.3.3 showed that CALR wt C-terminal domain Isoelectric point (pI) is highly acidic compared with type 1 and type 2 mutants, which are highly basic (Table 14). Therefore, change in amino acid charge

within this region could affect the Ca^{2+} binding capacity of CALR mutants and consequently lead to abnormal ER Ca^{2+} buffering activity.

Table 14. Isoelectric points for WT and mutant CALR peptides used during this study derived from the C-terminus.

Calculations were performed using the Scripps Institute's on-line Protein Calculator v.3.3 (http://www.scripps.edu/Bcdputnam/protcalc.html)

CALR	Sequence	Ip
wt	QDEEQRLKEEEEDKKRKEEEEAEDKEDDEDKDEDEEDEEDKEEDEEEDVPGQAKDEL	3.96
Type 1	QDEE-QRTRRMMRTKMRMRRMRRTRRKMRRKMSPARPRTSCREACLQGWTEA	12
Type2	QDEEQRLKEEEEDKKRKEEEEAEDRRMMRTKMRMRRMRRTRRKMRRKMSPARPRTSCREACLQGWTEA	10.30

3.3. Discussion

CALR C-terminal domain is a functionally important region, as it binds to 50% of ER Ca^{2+} and contains the ER retention motif. Nevertheless, the secondary structural characterisation of this region has not yet been detailed due to its high instability. Novel advances in bioinformatic tools aiming to predict protein secondary structure and stability have recently helped to understand the nature of CALR C-domain (Migliaccio and Uversky, 2017). However, further characterisation of this region could play an important role in deciphering the malignant role of the novel CALR mutant C-terminal domains (Nangalia et al., 2013; Klampfl et al., 2013).

This study reports a deep structural *in silico* based analysis of the C-terminal region of human CALR and the two most common CALR mutations described in MPNs patients. The initial analysis based in the disorder probability of CALR C-terminal domain showed that *CALR* type 1 and type 2 mutations display an intrinsic disorder state in most of the domain, although there are some regions that reach or trend to a more stable status. This multiparametric study corroborates previous published results using single *in silico* predictors (Eder-Azanza et al., 2014, Varricchio et al., 2017). The intrinsic disordered state of CALR wt C-terminal domain could be essential for the functionality of the region as it could provide functional advantages, such as further interface area during protein interactions (Gunasekaran et al., 2003). Also, it has been suggested that IDPR containing high specificity and low affinity binding properties, as seen in CALR C-terminal domain and Ca^{2+} binding sites, allow a rapid and easy dissociation of interactions within these regions (Wright and Dyson, 2009). Therefore, the disordered structural state of CALR C-terminal domain could allow to have more functional efficiency during the Ca^{2+} buffering activity of CALR within the ER and increase interface Ca^{2+} interaction areas. Hence, it could be speculated that *CALR* mutations, which decrease the number of amino acid Ca^{2+} binding sites and also decrease the disorder probability of the C-terminal domain, could lead to an impaired Ca^{2+} buffering activity of CALR mutant proteins.

Additionally, the C-terminal domain of CALR wt is characterised by a coil-coil structure and minimal α-helical content (Migliaccio and Uversky, 2017, Varricchio et al., 2017). However, both CALR mutations analysed in this study showed changes in the structural characteristics of the C-terminal tail, leading to a small change of the α -helical content. These local

conformational changes could impact protein behaviour and may cause abnormal protein-protein interactions. Interestingly, further analysis of MoRFs within the mutant C-terminal tails showed an increased probability of a potential binding site within this region of CALR type 1 and type 2 mutants, as previously described (Varricchio et al., 2017). In addition, these results agree with the described presence of LCR within these protein domains (Eder-Azanza et al., 2014). This data could explain the molecular basis of previous studies which revealed the novel interaction between CALR mutant and MPL receptor, which is dependent on C-terminal domain (Elf et al., 2016; Araki et al., 2016; Chachoua et al., 2016).

However, it is important to bear in mind that the structural models estimated in this study using I-TASSER software do not ensure total accuracy and reliability, as the best predicted models obtained during our study did show residues within the not allowed region in the Ramachandran plots. Given these mutant areas do not have any structural template of a homologous protein that could be used by structural prediction servers to obtain higher reliability models, these results could be considered as a good approximation of CALR mutants' secondary structure. Moreover, in order to gain further details of the secondary structure of these regions of interest an additional predictor was used, known as s2D method, which combines the disorder state and the secondary structure prediction of each amino acid. Results provided further evidence of a decrease in the random coil-coil population within the C-terminal domain in both CALR mutants compared with CALR wt. Furthermore, s2D method showed an increase in α-helix population. However, the α-helix population predicted by s2D server did not agree with the population predicted by I-TASSER. Both servers showed changes in the structural state within these regions but in different amino acid sequences. Therefore, CALR type 1 and type 2 mutations lead to changes in the α-helical content within the C-terminal domain, as previously suggested (Eder-Azanza et al., 2014), however the localisation of this novel structured regions remains unclear.

CALR C-terminal domain contains the basic lysine and arginine residues interspersed in large clusters of acidic residues of aspartic and glutamic acid (Coe and Michalak, 2009). This characteristic amino acid composition leads to the appearance of low affinity and high capacity Ca^{2+} binding residues (Nakamura et al., 2001; Coe and Michalak, 2009). Interestingly, deletion of the interspersed basic amino acids leads to a disruption of Ca^{2+} binding activity of this residue (Breier and Michalak, 1994). Therefore, not only are the acidic regions important

but the complete amino acid sequence of this domain is essential for the correct activity of CALR as a Ca^{2+} buffering protein. In this study, the 3D structural models of CALR wt, type 1 and type 2 mutants obtained using the I-TASSER software were used as templates to visualise the different positions of acidic and basic residues within the novel mutant regions. Both CALR mutations lead to a significant decrease of acidic amino acids and increase in basic residues in both CALR mutants structure. Decrease of acidic residues match with the Ip of each region described here and in previous publications (Shivarov et al., 2014). Importantly, these results suggest that both, changes in the acidity and the amino acid sequence within CALR type 1 and type 2, could impair the Ca^{2+} buffering activity of CALR within the ER.

Overall these results confirm the initial speculations about the effects of CALR C-terminal domain mutations leading to changes in the physical characteristics of the novel mutant regions. *CALR* mutations found in MPN decrease the disorder probability of the C-terminal domain and could lead to the emergence of α-helix structure within this region, as well as changes in the domain´s acidity. These structural changes in CALR C-terminal domain could change CALR cellular behaviour by leading to inefficient Ca^{2+} buffering activity and also promote novel protein-protein interactions.

3.3.2. Conclusion

This *in silico* study describes in detail the structural characteristics of the novel C-terminal domain of CALR type 1 and type 2 mutants and provides more insights into the potential of these regions to establish novel protein interactions. In summary, the major conclusions of this study are:

I.   This multiparametric study shows similar results than the previously obtained using single disorder predictors (Varricchio et al., 2017). *CALR* type 1 and type 2 mutations affect the intrinsic disorder state of the C-terminal domain. Although these regions display an overall disordered status, there is a tendency of decrease towards a stable structure, mostly at the end of the domain.

II.   Both analyses of secondary structure using I-TASSER and S2D servers predict the appearance of an α-helix content within CALR type 1 and type 2 C-terminal domains.

III.   Changes in the molecular properties of type 1 and type2 C-terminal domains lead to the emergence of potential novel MoRFs regions, as previously described (Varricchio et al., 2017).

IV.   CALR mutations change the amino acid charge of the novel C-terminal domains from acidic to basic.

3.3.4. Future work

This preliminary study sets the basis for further experimental analysis of CALR mutants in MPNs. As predictions suggest that *CALR* mutations lead to a decrease in the disorder state of C-terminal domain, it is possible that CALR mutants could be crystallised and analysed further in detail. Additionally, PDB files obtained of each predicted model could be used to perform further molecular dynamics to obtain more reliable models and to estimate Ca^{2+} binding affinity under the simulation of physiological ER conditions.

Additionally, as previously discussed, increase in MoRFs regions within type 1 and type 2 C-terminal domains could increase the binding protein interactions. Binding between mutant CALR and MPL have been described, however it would be of interest to analyse other potential binding partners by using pull-down assay and mass spectrophotometry in order to understand the role of CALR mutant within the aberrant signalling network described in CALR mutant MPNS.

Chapter 4: *MARIMO cell line, a new model to study megakaryopoiesis with CALR mutations*

4.1 Introduction

Hematopoiesis is a complex and highly regulated process in which specific cell-type gene expression signatures lead to the differentiation of pluripotent stem cells into mature blood cells. The study of molecular events during hematopoietic commitment in disease is hindered by the access to purified primary progenitor cells. Thus, the use of leukemic cell lines as models for the study of cell lineage commitment has increased greatly during last two decades (Kang et al., 1996; Smithgall, 1998; Zhang et al., 2007; Hirose et al., 2013; Huang et al., 2014). *In vitro* cellular differentiation using cytokines is a commonly used to study cell commitment under physiological conditions (Syme and Gluck, 2001; Flores-Guzman et al., 2002). However, the use of the pharmacological agents as differentiation inducers is a technique that has shown strong differentiation effects in multiple myeloid leukemia cells (Smithgall, 1998). Classic examples of differentiation inducing agents are phorbol esters or retinoic acids, which have been widely used for the investigation of the differentiation block characteristic of leukemic blasts as well as for the discovery of signalling cascades associated with cellular commitment (Smithgall, 1998; Huo et al., 2006; Hirose et al., 2013; Huang et al., 2014).

Phorbol 12-myristate 13-acetate (PMA) is a phorbol ester commonly used to induce lineage differentiation of several myeloid leukemia cell lines. Previous research demonstrated that the monocytic U-937 and THP-1 and the promyelocitic leukemia HL-60 cell lines differentiate into macrophages under PMA treatment (Huberman and Callaham, 1979; Ways et al., 1987). Also, the erythroleukemia cell lines K562 and HEL differentiate into megakaryocytes in response to PMA induction (Long et al., 1990; Tabilio et al., 1983). PMA megakaryocytic induction is accompanied by the acquisition of the megakaryocyte phenotype, such as

increase cell size and cell adhesion, increase expression of megakaryocyte cell surface antigens (CD41, CD61 and CD110), acquisition of DMS, as well as arrest in cell cycle and endomitosis.

PMA is known to mimic the activity of diacylglycerol. Downstream signalling of this molecule leads to the activation of protein kinase C (PKC) family, which comprises 11 different members. PKC is involved in the intracellular signalling mechanism inducing megakaryocyte commitment (Racke et al., 2001). Previous work demonstrated the cooperation of PKC with GATA-1 during the transcriptional activation of megakaryocyte promoters (Racke et al., 2001). Also, PKC is involved in the activation of Raf-MEK-ERK cascade during megakaryocyte commitment (Ueda et al., 1996; Schonwasser et al., 1998)

The recent finding where a previously established AML-M2 cell line, known as MARIMO (Yoshida et al., 1998), harbors a *CALR* mutation has revealed the importance of this cellular model for the study of the molecular pathogenesis of CALR mutant in MPNs (Kollmann et al., 2015). These cells carry a 61-bp deletion in *CALR* exon 9 (L367fs*43). As all *CALR* mutations found in MPNs, this mutation leads to a +1- bp shift in the reading frame and therefore the formation of a novel C-terminal region. Importantly, *JAK2* and c-*MPL* mutations have not been identified in MARIMO cells (Kollmann et al., 2015).

Since the discovery of *CALR* mutation in MARIMO cells, research using this cell line has been focused in deciphering the signaling profile characteristic of these cells, to shed light in the pathogenesis of CALR mutant MPNs. Interestingly, MARIMO cells' growth do not show dependence on JAK/STAT signaling. These cells are resistant to JAK inhibitors and JAK/STAT downstream JAK2 and STAT5/1/3 proteins show low levels of phosphorylation (Kollmann et al., 2015). This previous publication suggested that *CALR* mutations could induce activation of different signalling cascades other than JAK/STAT signalling during disease (Kollmann et al., 2015). Surprisingly, a recent investigation showed that *CALR* mutant MARIMO cells display a significant dependence on MAPK pathway compared to other myeloid leukemia cell lines (Kollmann et al., 2016). These cells showed high sensitivity to MAPK inhibitors and displayed high phosphorylation levels of downstream components of this cascade such as MEK1 and ERK1 (Kollmann et al., 2016).

Further research analysing the phenotype of these leukemic blasts revealed that MARIMO cells do not express MPL cytokine receptor, neither in mRNA nor protein levels (Kollmann et al., 2016). As previous research demonstrated, CALR mutant protein binds to MPL receptor (Araki et al., 2016; Elf et al., 2016) and this novel protein binding could possibly induce the activation of JAK/STAT pathway during disease (Chachoua et al., 2016; Marty et al., 2016). The fact that MARIMO cells do not express MPL receptor opens the possibility that CALR mutations activate MAPK pathway through other mechanisms in these cells, and that JAK/STAT signalling might not be active due to the absence of expression of this cytokine receptor.

MARIMO cell line was established from a secondary AML patient that evolved from ET treatment (Yoshida et al., 1998). This cell line has been reported to be negative for megakaryocyte (CD61, CD41, CD42) and erythrocyte (CD235a) cell surface markers but positive for CD15 (Kollmann et al., 2015), a marker characteristic of myeloid progenitor cells (Lee et al., 2001). Therefore, this cell surface antigens phenotype suggests a block in differentiation in early stages of the myeloid cell linage in MARIMO cell line.

4.1.1. Aim and hypothesis

As recent data show that the MARIMO leukemic cell line expresses a myeloblast cell surface antigen, lacks any cell surface markers characteristic of cell lineage commitment and does not express MPL, it is therefore possible that these cells could display a block in early stages of myeloid differentiation. Therefore, MARIMO cell line could have the potential to commit into specific cell lineages under the exposure of differentiation inducing agents.

The main aim of this study is to characterise the potential of MARIMO cells to differentiate into the megakaryocyte lineage under PMA treatment, as previously reported with other AML cell lines. The purpose of analysing MARIMO megakaryocyte induction is to establish a cellular model that could be used for the analysis of megakaryopoiesis characteristic of ET and PMF harbouring *CALR* mutations and to study the behaviour of CALR mutant within megakaryocyte differentiated cells. Therefore, in order to assess the megakaryocytic potential of MARIMO cells, four major objectives will be addressed:

I.   Analysis of expression of CD41a megakaryocyte cell surface marker after incubation of MARIMO cells under different PMA concentrations.

II.   Study of the effects of PMA treatment on the cell cycle and replicative potential of MARIMO cells.

III.   Analysis of the emergence of megakaryocyte morphological characteristics, including polyploidy, increase cell size, adhesion and the emergence of DMS.

IV.   Characterisation of JAK/STAT signalling status after PMA treatment.

4.2. Results

4.2.1 Analysis of CD41a expression in MARIMO cells after PMA induction

The potential of *in vitro* megakaryocytic differentiation of MARIMO leukemia cell line was tested by using PMA treatment as a cell commitment inducer. MARIMO cells were seeded at a concentration of 3×10^5 cells/ml and cells were incubated with different PMA concentrations (0 nM, 2 nM, 5 nM, 10 nM, 20 nM). After 72 hours incubation presence of the megakaryocyte cell surface marker CD41a was analysed by immunostaining and flow cytometry.

As previously reported, MARIMO control cells showed no expression of CD41a under normal conditions. However, MARIMO cells under PMA treatment showed an overall increase in CD41a expression within the cell membrane after 72 hours of PMA incubation, suggesting the potential of megakaryocytic differentiation of MARIMO cells. The obtained contour plots of the different PMA treatment showed a major shift in CD41a fluorescence within the cell population under 5 nM PMA treatment (Figure 15). Moreover, 10 nM and 20 nM PMA concentrations did not show a significant increase in CD41a expression compared to 5 nM PMA (Figure 15). Therefore, in order to avoid cellular toxicity under PMA treatment 5 nM PMA was used for further experiments as an optimal concentration for PMA megakaryocytic induced differentiation of MARIMO cells.
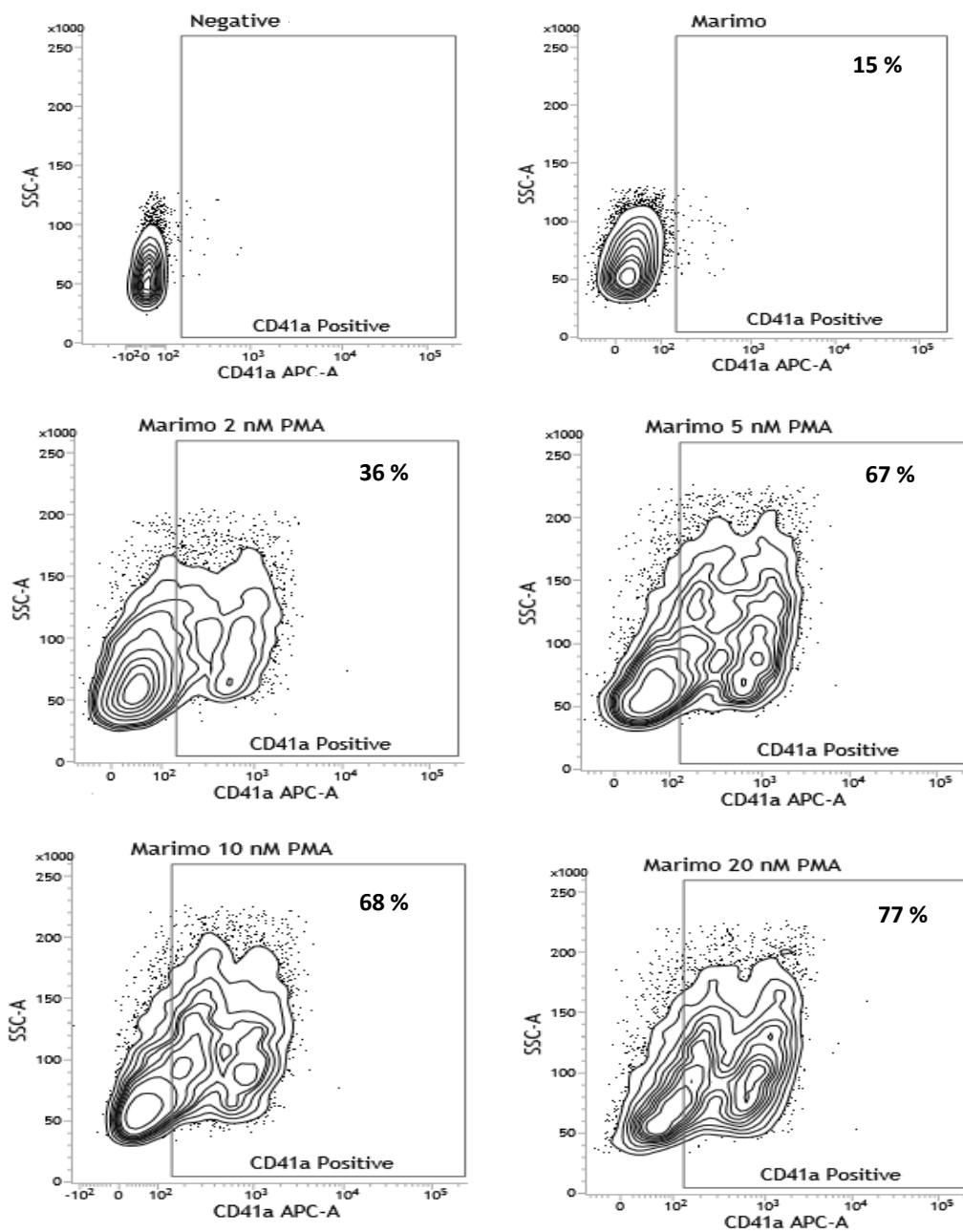
Figure 15. Optimization of MARIMO PMA treatment.

Representative counter plots of flow cytometry analysis measuring CD41a antigen expression in MARIMO cell population after treatment of different concentrations of PMA (2 nM, 5 nM, 10 nM, 20 nM) during 72 hours. Cells were stained with CD41a-APC antibody.

Quantification of CD41a fluorescence of MARIMO cells after 5 nM PMA treatment during 72 hours incubation showed a significant increase in CD41a cell surface expression compared to the control (Figure 16 A, B). Moreover, percentage of cellular events registered to express CD41a antigen within the cell surface increased from 13.41% to 72.8% suggesting that PMA induced megakaryocyte differentiation in the majority of MARIMO cell population (Figure 16 B).

Finally, the toxic effects of 5nM PMA treatment after 72 hours in MARIMO cell line were analysed. Trypan blue was used as an indicator of cell death within the culture. Results showed that PMA induced cell death in about 24% of cells within the culture (Figure 16).

These results demonstrated that PMA treatment induce the expression of a megakaryocytic cell surface marker in MARIMO cells, suggesting a possible differentiation towards the megakaryocytic lineage of this AML-2 cell line.

A.

CD41a expression

B.

%Cells expressing CD41a
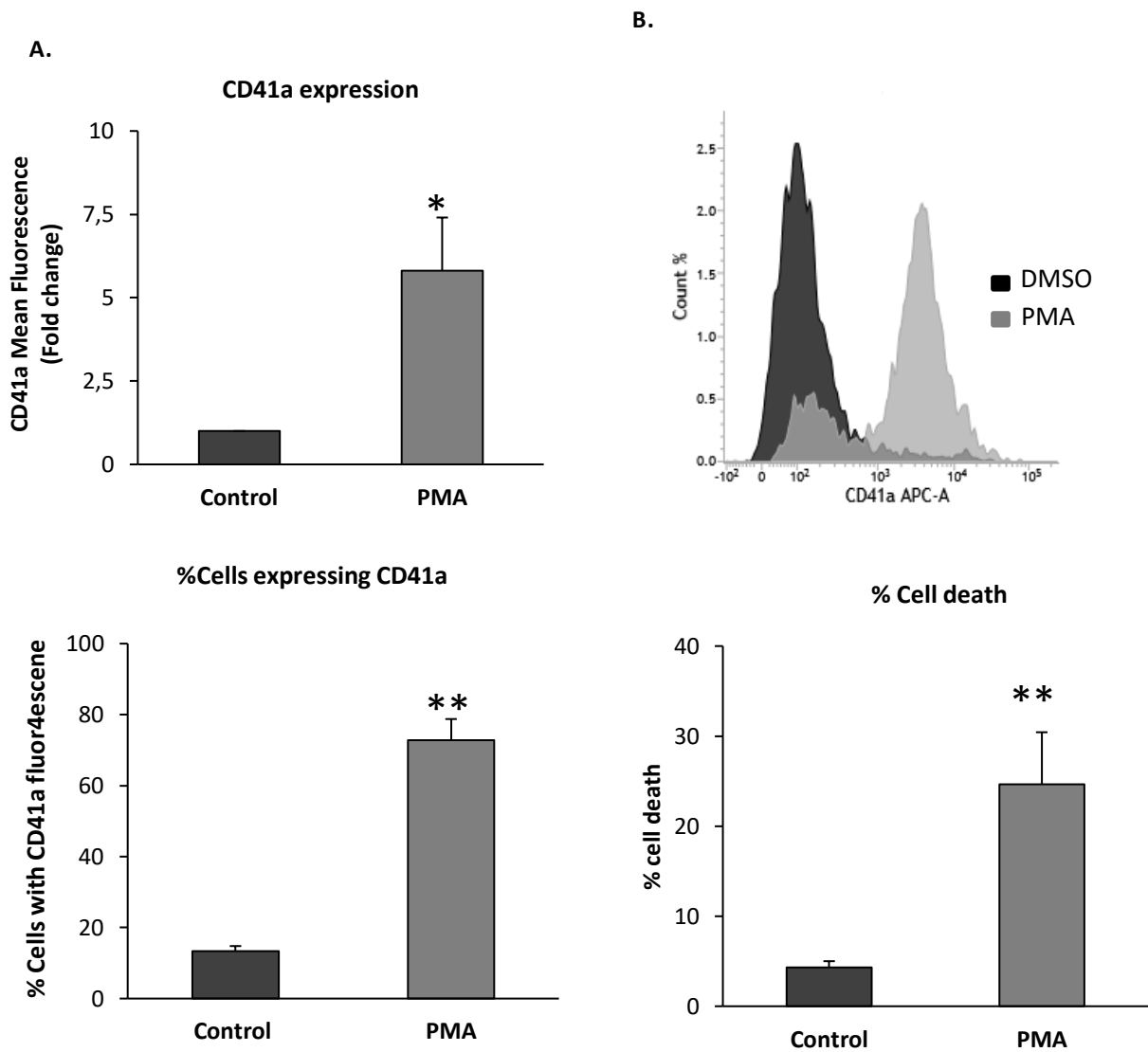
% Cell death

Figure 16. CD41a quantification and cell death induction after MARIMO PMA induction.

A, B) MARIMO cells were subjected to 5 nM PMA treatment during 72 hours and then CD41a expression was analysed and quantified by flow cytometry. **C)** Quantification of CD41a positive cells. **D)** Analysis of cell death after PMA treatment. Values represent mean ± SEM for each group. n=3. **P<0.01, *P<0.05. Student T.test

4.2.2. MARIMO cell cycle analysis after PMA treatment

As MARIMO cells express a megakaryocyte cell surface marker after exposure to PMA, the effects of this inducer in the DNA replication potential of these cells were further examined. In order to study the cellular distribution along the cell cycle, propidium Iodide staining and flow cytometry analysis were used after 72 hours incubation.

Results showed that MARIMO cells under PMA treatment reduced their replication potential (Figure 17). The number of cells found in S phase dropped from 23% in the control group to 6% in the PMA induced cells. Additionally, the number of cells in G2/M also decreased from 15% to 10%. On the contrary, the obtained results displayed an accumulation of cells in G0/G1 phase, increasing from 61% in the control cells to 84% in the PMA treated cells (Figure 17 B). These observations suggested that PMA-megakaryocytic induced differentiation in MARIMO cells leads to an arrest in cell cycle, accumulating cells in G0/G1 phase. The loss of replicative potential is a characteristic of cell terminal differentiation, and therefore these results corroborated the effect of megakaryocytic induction of MARIMO cells under PMA treatment.

Moreover, during megakaryopoiesis cells exhibited increase nuclei size and then enter in endomitosis during final megakaryocyte maturation. Propidium iodide staining showed an increase in 2N and 4N fluorescence intensity, suggesting an initial increase in nuclear size (Figure 17 A). However, no signs of an overall cellular polyploidy (8N, 16N) were found after 72 hours of PMA induction in MARIMO cells
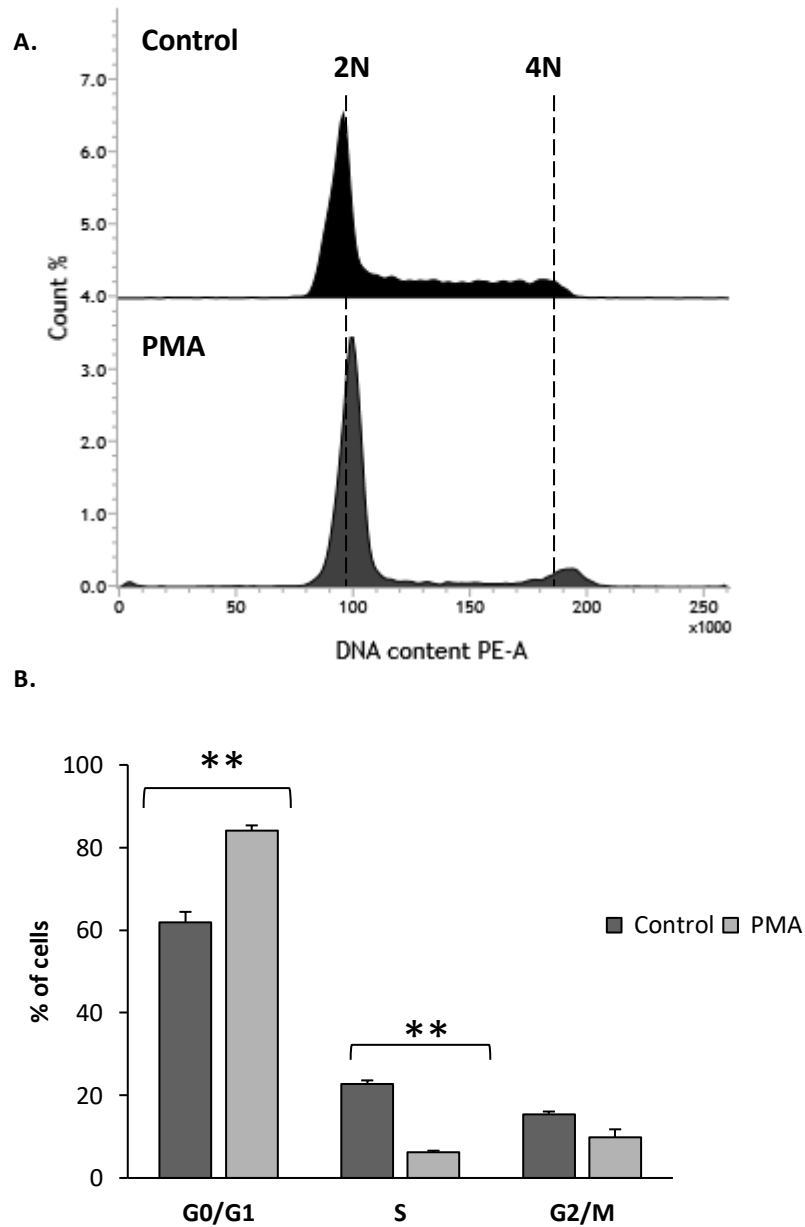
Figure 17. Analysis of cell cycle in PMA induced MARIMO cells.

MARIMO cells were subjected to 5 nM PMA treatment during 72 hours and propidium iodide staining was performed and samples were analysed by flow cytometry. **A)** Representative histogram of cell cycle analysis of MARIMO cells after PMA treatment. **B)** Quantification of number of cells in each cell cycle step. Values represent mean ± SEM for each group. n=3. **P<0.01, *P<0.05. Student T.test

4.2.3. Proliferation assay of MARIMO cells under PMA treatment

A reduction of S phase in MARIMO cells under PMA treatment after 72 hours suggested a decrease in the proliferation capacity of these cells, as expected for induced differentiation cells. To analyse the division capacity of these cells under 5 nM PMA treatment, MTS assay was performed over 72 hours.

Control MARIMO cells increased 4 fold during 3 days of culture (Figure 18). However, PMA induced cells showed a decreased in their rate of proliferation (Figure 18). Inhibition of proliferation after PMA induction was significantly decreased between 24 and 48 hours. After, no further cellular proliferation was detected. These results indicated that 5 nm PMA treated MARIMO cells progressed to only one cycle of cell division before their arrest in cell cycle.
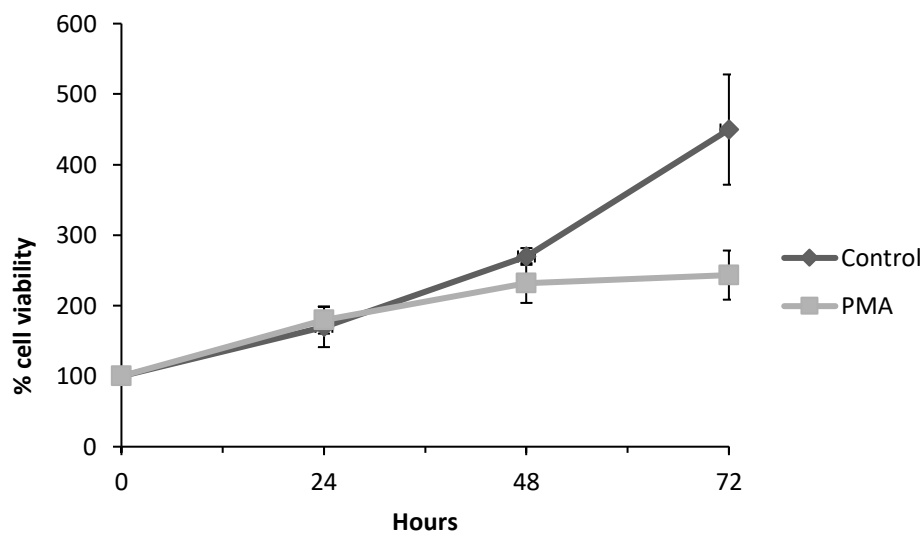
Figure 18. Proliferation analysis during PMA megakaryocytic induction of MARIMO cells.

MARIMO cells were subjected to 5 nM PMA treatment during 0, 24, 48 and 72 hours. Then, MTS assay was performed in order to test cell viability. Values represent mean ± SEM for each group. n=2

4.2.4. Morphological analysis of MARIMO cells under PMA treatment

Megakaryocyte characteristics such as increase cell size or cell adhesion can be easily described in cell cultures under light microscopy (Huang et al., 2014). After describing an increase of CD41a megakaryocyte antigen and an arrest in cell cycle characteristic of cell differentiation, the morphological characteristics of MARIMO cells after PMA induction were analysed.

Initial morphological analysis under light microscopy showed differences between the control and the PMA induced MARIMO cells. In control, cultured MARIMO cells show normal leukemic blast characteristics (Figure 19). MARIMO cells cultured for 72 hours in the presence of 5 nM PMA acquired a megakaryocyte-like phenotype. Overall, MARIMO cells displayed differences in cell morphology after PMA-induced differentiation. Cells show a slight increase in cell size compared to the control group. Also, MARIMO differentiated cells displayed cytoplasmic projections characteristic of DMS for platelet production (Figure 19, black arrows). Moreover, PMA treatment induced an increase in the adhesive capacities of MARIMO cells.

MARIMO control
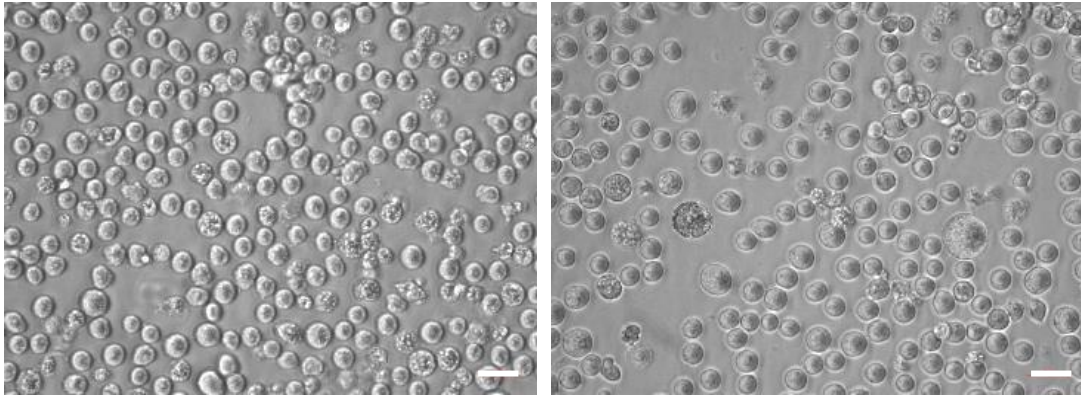
MARIMO 5nM PMA
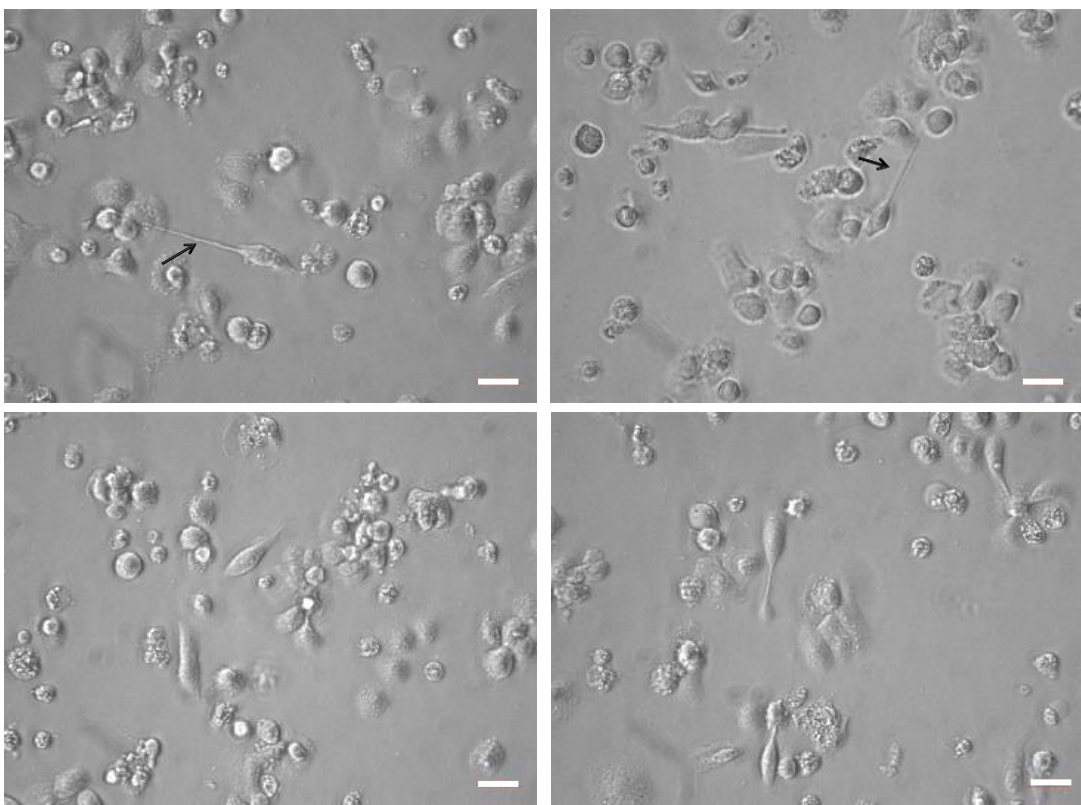
Figure 19. Representative images of MARIMO live cells under PMA treatment.

MARIMO cells were subjected to 5 nM PMA treatment during 72 hours. Then, samples were used for light microscopy. Images were captured using 40x objective. Black arrow: DMS. Scale bars =50μm

MARIMO morphology was analysed in more in detail using Wright-Giemsa staining. In control cells MARIMO displayed a typical basophilic cytoplasm containing abundant lipid vacuoles (Figure 20, black arrows) and rounded nuclei with numerous basophilic nucleoli (Figure 20A, blue arrow). Moreover, cells showed a high nuclear-to-cytoplasm ratio, characteristic of leukemic blasts (Figure 20).

MARIMO cells under PMA megakaryocytic induction showed an overall increase in cell size and fragmented cytoplasm (Figure 20). The cytoplasm was less basophilic, azurophilic granules were occasionally found and extensive DMS were identified (Figure 20 D, orange arrows) as sign of cytoplasm maturation. Moreover, nuclei increased size and displayed oval or kidney shapes, corroborating previous data obtained where there was an increase in 2N and 4N signal in these cells (Figure 20 A). Furthermore, occasional multilobulated nuclear cells were found, suggesting that MARIMO cells undergo endomitosis under PMA treatment after 72 hours. Different cellular stages of megakaryocytic maturation were described according to the number of nuclei and cell size: megakaryoblast with a single oval nucleus and a diameter between 20-30 μM (Figure 20 B), pro-megakaryocyte with 2-4 nuclei (Figure 20 C) and mature megakaryocytes which display 4-16 nuclei and diameter ranges between 30-90 μM (Figure 20 D).

A.

5 nM PMA induction

B.

C.

D.
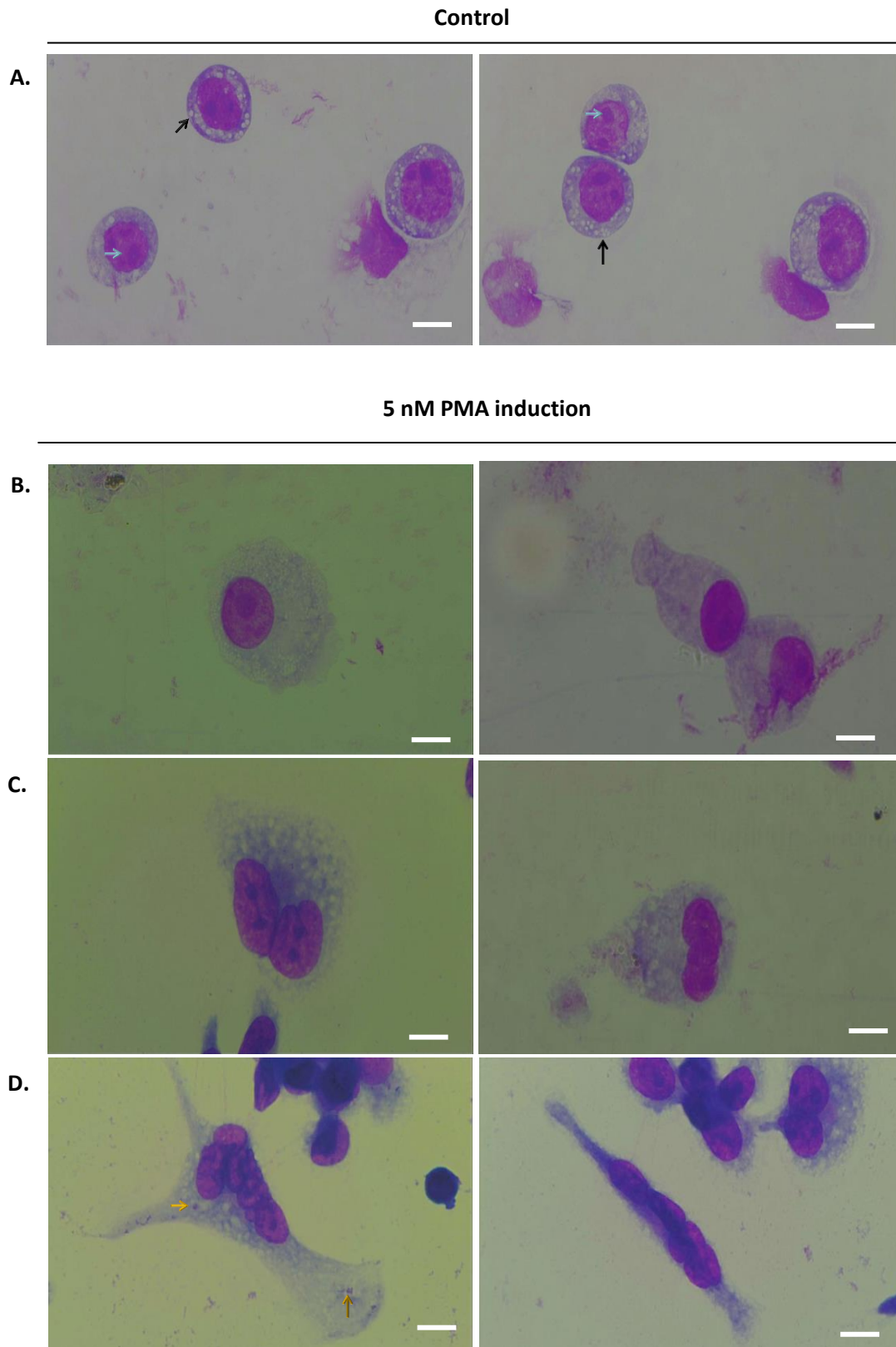
Figure 20. MARIMO cytological changes under PMA treatment.

MARIMO control cells slides were prepared using the Cytospin and cells treated with 5 nM PMA for 72 hours were grown in coverslips. Both groups were subsequently subjected to Wright-Giemmsa staining. Representative images of MARIMO **A)** control and **B, C, D)** PMA treated cytological characteristics are shown. Images were capture using X100 objective. Scale bars = 10 μm.

4.2.5. Analysis of MPL expression in MARIMO cells after PMA treatment

Megakaryocyte maturational process includes the expression and activation of specific proteins and cellular signals. *c-MPL* gene is highly expressed in megakaryocytes and its expression is essential for megakaryocyte formation (Methia et al., 1993, Nagata et al., 1995). Although MARIMO leukemic blasts have been described not to express MPL (Kollmann et al., 2016), the previously described MARIMO megakaryocyte like transformation could lead to an induced expression of *c-MPL.*

To examine the effects of PMA treatment in the expression of MPL, *cMPL* mRNA levels were quantified using qRT-PCR analysis. Results showed a significant upregulation of *c-MPL* gene expression when cells treated with PMA (Figure 21 A). Moreover, MPL protein levels within the cell surface were quantified by flow cytometry and results showed a significant increase of this antigen after PMA induction (Figure 21 B, C). Quantification of MPL positive events estimated that approximately 60% of cells in the culture expressed this receptor within the cell surface (Figure 21 D).

Overall these interesting results showed that PMA megakaryocyte induction in MARIMO cell line leads to an expression of MPL receptor, in both mRNA and protein levels, suggesting a possible activation of JAK/STAT pathway when these cells acquire megakaryocyte characteristics.
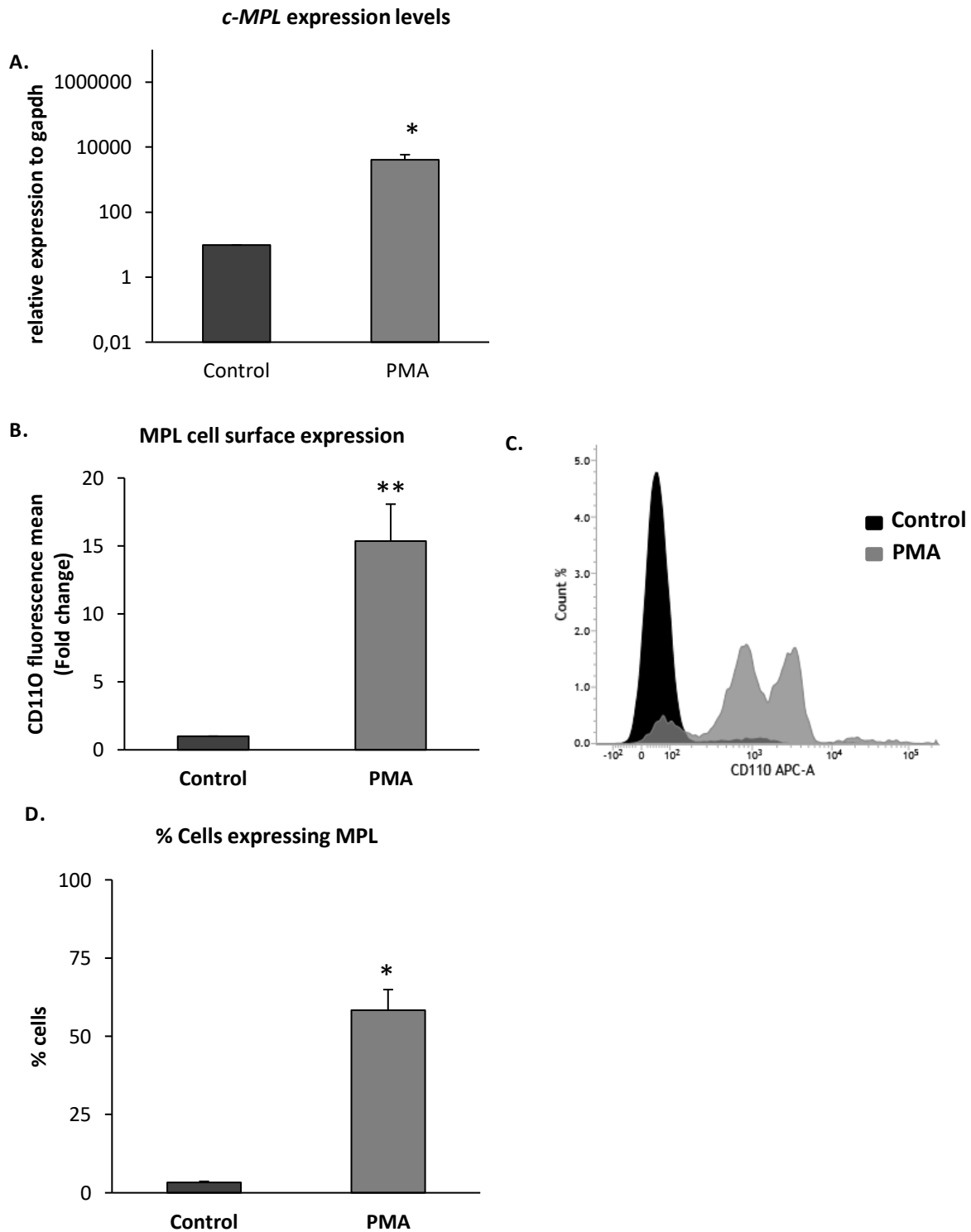
Figure 21. MPL expression in MARIMO cells after PMA megakaryocytic induction.

MARIMO cells were subjected to 5 nM PMA treatment for 72 hours. **A)** mRNA was extracted and converted into cDNA and finally subjected RT-qPCR using primers against *c-MPL.* **B, C)** MPL (CD110) expression was analysed and quantified by flow cytometry. **D)** Quantification of CD41a positive cells. Values represent mean ± SEM for each group. n=3. **P<0.01, *P<0.05. Student T. test.

4.2.6. Study of the expression of STAT5 gene signature in MARIMO cells after PMA treatment.

Detection of JAK/STAT cascade activation by measuring the phosphorylation status of STAT proteins is possible by directly analysing the gene signature of these transcription factors (Sonkin et al., 2015). To study the consequences of the megakaryocyte induction in the signalling signature of MARIMO cells qRT-PCR was used to study the status of STAT5. Four known STAT5 target genes, *PIM1*, *CISH*, *ID1* and *SOCS2,* were selected as targets for this analysis. Previous research reported that this gene signature is highly correlated with the phosphorylation status of STAT5 during haematological malignancies (Sonkin et al., 2015).

qRT-PCR analysis showed that MARIMO PMA induction leads to an overall increase of mRNA expression of the gene signature of STAT5 (Figure 22). Although not statistically significant, mRNA expression of *PIM1* and *ID1,* two oncogenes linked with the development of haematological malignancies (Suh et al., 2008; Brault et al., 2010), showed an overall upregulation in MARIMO PMA treated cells. However, *CISH* and *SOCS2*, which are involved in the negative regulation of JAK/STAT pathway (Quentmeier et al., 2008; Borges et al., 2008), displayed a statistical significant upregulation of mRNA expression compared with the control (Figure 22 C, D) displaying a 6.5 and 9 fold increase respectively.

Thus, MARIMO PMA treatment resulted in a trend for upregulation of the STAT5 gene signature. This, in combination with the previous findings showing an upregulation of MPL expression, suggests an activation of the JAK/STAT signalling within MARIMO PMA treated cells

A. *PIM1 mRNA expression*

B. *ID1 mRNA expression*

C. *CISH mRNA expression*

D. *SOCS2 mRNA expression*
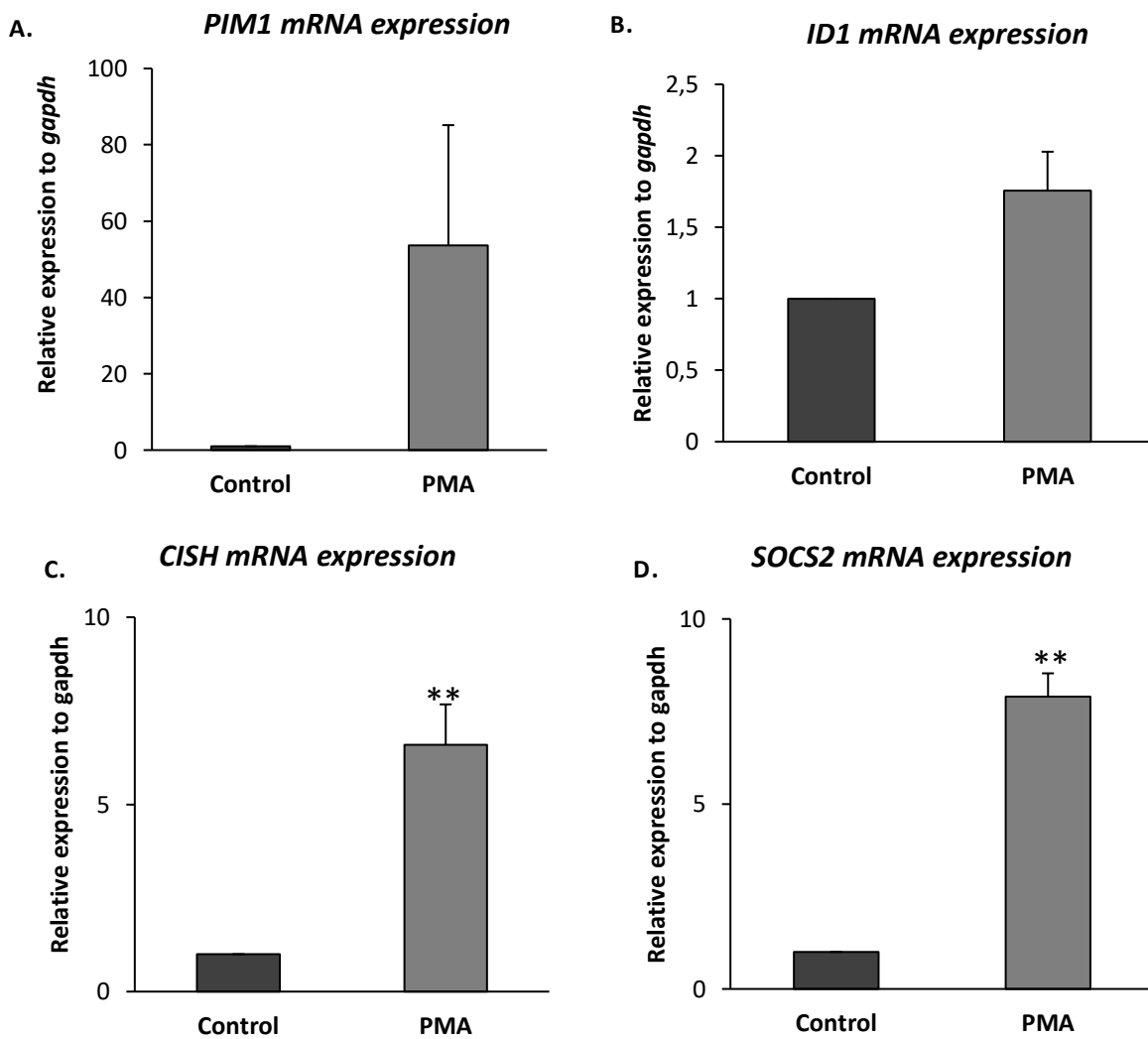
Figure 22. Expression of STAT5 gene signature in MARIMO cells after PMA treatment.

MARIMO cells were subjected to 5 nM PMA treatment during 72 hours. mRNA was extracted, converted into cDNA and finally subjected RT-qPCR using primers against *PIM1*, *CISH*, *ID1* and *SOCS2* genes. Values represent mean ± SEM for each group. n=3. **P<0.01, *P<0.05. Student T.test

4.3. Discussion

CALR mutant MARIMO AML-2 cell line displays a primitive hematopoietic phenotype, expressing an early cell surface myeloblast marker and lacking any cell lineage commitment antigens (Kollmann et al., 2015; Yoshida et al., 1998) (Figure 23). Together with the publication of the establishment of MARIMO cell line, it was reported that these cells only differentiated into granulocytes under all-trans retinoic acid (ATRA) treatment, however, the conditions and results of experiments using phorbol esters were not described (Yoshida et al., 1998). This study demonstrates that the treatment of MARIMO cells with 5 nM of the phorbol ester PMA during 72 hours leads to an induced megakaryocytic lineage commitment of these cells. Analysis of MARIMO cells under PMA treatment revealed that these cells significantly express the megakaryocyte antigen CD41a. Morphologically, PMA induced MARIMO cells showed an increase in cell size as well as cytoplasmic and nuclear megakaryocyte maturation (Figure 23). These structural changes under PMA induction are also accompanied with a cease of cellular proliferation and increase in DNA content.

Detailed morphological analysis of PMA induced MARIMO cells showed a clear increase in cell size and nuclear content, presence of DMS, as well as a decrease in basophilia within the cytoplasm. This phenotype is consistent with the previously described megakaryocyte stages of megakaryoblast and pro-megakaryocyte (Hattori et al., 1987; Long and Williams, 1981). However, a relatively reduced number of mature megakaryocytes was found in the culture, with an extensive DMS and high polyploidy (8N-16N), although no alpha-granules and no cytoplasmic division into platelets were identified in culture. The reduced ability of MARIMO cells to commit into final mature megakaryocytes is not surprising, as *in vitro* terminal differentiation of haematopoietic cell lines commonly fails, such as megakaryocyte and erythrocyte maturation of HEL cells (Long et al., 1990; Papayannopoulou et al., 1987) or HL-60 granulocyte maturation (Collins, 1987). Therefore, these results suggest that either PMA does not entirely induce the final megakaryocyte maturation or that MARIMO cells do not have the capacity to fully differentiate into mature megakaryocytes due to the leukemic transformation of this cell line or the culture conditions.

Endomitosis is a process by which megakaryocytes replicate their DNA without cytoplasmic division, leading to the characteristic polypoid state of these cells. Firstly, megakaryocyte

commitment is accompanied by changes in the cell cycle, reducing the proliferation potential of these cells. Then, megakaryoblasts begin endomitosis reaching 4n-64n DNA content during maturation (Zimmet and Ravid, 2000; Wen et al., 2011). These results show that PMA induced MARIMO cells proliferation potential ceases and cells consequently continue undergoing endomitosis, reaching 2 to 4 times of their baseline DNA content after 72 hours. However, it is possible that increase of PMA incubation time could lead to a continuation of the endomitotic process, reaching higher DNA content in these committed cells. Nevertheless, MARIMO cells displayed a reduction in capacity to synthesise DNA content compared to primary megakaryocytes, as previously seen with other cell lines, such as HEL cells under PMA induction (Long et al., 1990). Although the process of endomitosis is not complete during MARIMO megakaryocyte commitment, the technical problems of studying this process using primary immature megakaryocytes leads to increase interest in using this cell line as a novel model to study the initiation of the endomitotic process.

TPO, the major cytokine regulating megakaryocyte maturation and platelet formation, acts via its MPL receptor. MPL receptor is essential for megakaryopoiesis and its expression is also essential to have a tight control of myeloproliferation (Besancenot et al., 2014). MPL and deregulated JAK/STAT signalling cascade are commonly linked with the pathogenesis of ET and PMF (Kilpivaara and Levine, 2008; Kralovics et al., 2005; Pardanani et al., 2006). CALR mutant MARIMO cell line does not express MPL receptor in its blast stage and consequently JAK/STAT signalling is not activated in these cells (Kollmann et al., 2015; Kollmann et al., 2016). Interestingly, this study has shown that the commitment of MARIMO cells into the megakaryocytic lineage is accompanied by an increased expression of MPL receptor, in mRNA and protein levels. Also, results provided further evidence that STAT5 gene signature (*PIM1*, *CISH*, *ID1* and *SOCS2*) is expressed after MARIMO PMA treatment, suggesting an activation of JAK/STAT pathway in these cells, possibly as a consequence of MPL expression (Figure 23).

MARIMO cells carry L367fs*43 *CALR* mutation which leads to 1+ base pair shift in the reading frame in *CALR* exon 9 fragment. Therefore, *CALR* 61 bp del mutation found in MARIMO cells generates a novel C-terminal domain, as described in the common mutations type 1 and type 2 (Kollmann et al., 2015). Type 1 and type 2 *CALR* mutations have been described to interact with the extracellular domain of MPL receptor leading to its oncogenic activation in ET and PMF (Elf et al., 2016; Araki et al., 2016). However, this interaction has been described using

artificial models, such as retrovirally transduced murine Baf3 and transfected human *HEK-293T* cells. Because MARIMO megakaryocyte like cells increase MPL receptor expression, the interaction of CALR mutant and MPL receptor could be possible in these cells after PMA megakaryocyte induction. Therefore, MARIMO cells could be used as a model to study the binding of the intrinsic CALR mutant and MPL *in vitro*, thus avoiding any artificial effects caused by protein overexpression in specific cellular models.

The JAK/STAT signalling cascade has been linked with cell survival and cancer progression (Kisseleva et al., 2002; Ihle and Gilliland, 2007; Wierenga et al., 2008). Aberrant JAK/STAT signalling pathway in MPNs has accelerated the use of JAK inhibitors for the treatment of this group of diseases, such as Ruxolitinib, a potent JAK1/2 inhibitor used in clinic (Harrison et al., 2012). The understanding of *CALR* mutations and their link with aberrant cellular signalling is a controversial topic. Some studies directly correlate the presence of *CALR* mutations with an overactivated downstream JAK/STAT cascade (Araki et al., 2016; Chachoua et al., 2016; Elf et al., 2016) and other suggests that CALR mutant lead to a deregulated MAPK activation and that this is the major cause of pathogenesis in this group of patients (Kollmann et al., 2016). However, it is important to bear in mind that CALR mutant MPN patients respond well to Ruxolitinib treatment (Harrison et al., 2012; Patel et al., 2015), therefore aberrant JAK1/2 activity is possible in this group of patients. MARIMO cell line was used as a model to demonstrate that CALR mutant cells aberrantly activate MAPK signalling rather than JAK/STAT (Kollmann et al., 2016). However, results in this thesis suggested that the reason why JAK/STAT signalling was not active in this AML-2 cell line was due to a block in the leukemic blast stage. However, further studies are essential to test whether this cascade is active due to a direct interaction of CALR mutant and MPL or other molecular pathologies lead to an activation of this cascade.
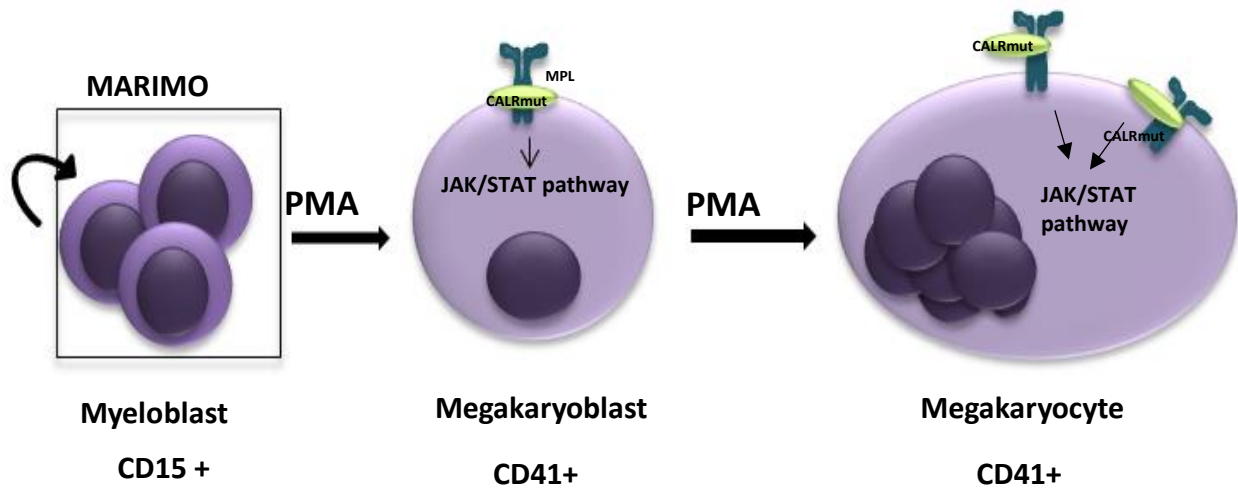
Figure 23. Schematic representation of MARIMO megakaryocyte like cells model based in the results obtained in this study.

Taken together, the current data highlights the importance of MARIMO cell line as a model to study *CALR* mutations. The findings of this investigation reveal a novel cellular model with potential to differentiate into the megakaryocyte lineage and propose its relevance to study *CALR* mutations effects in the physiological process of megakaryocyte formation characteristic of the myeloid neoplasms harboring this driver mutation.

4.3.1. Conclusions

The novel megakaryocyte commitment capacity of MARIMO cells described during this study provides new insights into the biology of this newly characterised CALR mutant cell line. In summary, the major conclusions of this study are:

I.   MARIMO cell line has the potential to commit into the megakaryocytic lineage under 5 nM PMA treatment during 72 hours

II. PMA MARIMO induction leads to the expression of the megakaryocyte antigen CD41a, megakaryocytic-like morphological characteristics, lose the replicative potential and increase nuclear content.

III. MARIMO cells have the capacity to initiate the endomitotic process, although after 72 hr it is mostly incomplete.

IV. PMA treatment decreases the cell proliferation capacity of MARIMO cells after 24 to 48 hours.

V.   MARIMO megakaryocyte committed cells express MPL receptor.

VI. STAT5 gene expression signature (*PIM1*, *CISH*, *ID1* and *SOCS2*) is expressed after MARIMO PMA treatment.

4.3.2. Future directions

Additional studies are needed to further characterise the megakaryocyte commitment potential of MARIMO cells. Analysis of cell surface expression of the megakaryocyte antigen CD41a could be completed with the further study the expression of other megakaryocyte-platelet proteins such as CD61 or CD42. Moreover, a few mature megakaryocytes like cells with clear endomitosis process (8n-16n) were identified. To further understand the complete capacity of MARIMO cells to commit into mature megakaryocytes, analysis of longer incubation of cells with PMA could be essential for the identification of a complete megakaryocyte differentiation process in these cells. Moreover, addition of TPO within the cell media could improve this commitment.

The obtained satisfactory results demonstrating an increase expression of MPL opens the possibility of using this cell line to analyse CALR mutant and MPL binding and the consequently pathogenic downstream signalling. The initial analysis of this novel protein interaction could be addressed by protein pull-down assay and western blot. Additionally, further experiments will be essential to understand which molecular pathogenesis leads to an active status of STAT5 transcription factor, by analysing the quantification of phosphorylated JAK and STATs proteins, as well as downstream MAPK proteins. These molecular analyses will help to shed light into the cellular signalling characteristic of CALR mutant ET and PMF.

CHAPTER 5: Analysis of *CALR mutant sub-cellular localisation*

5.1. Introduction

Ca^{2+} binding protein CALR contains the KDEL region, a C-terminal ER retrieval signal. However, in many occasions this protein has been found to be localised outside the ER (Johnson et al., 2001). Mechanisms by which CALR evades ER retention remain elusive, yet the important role of this protein outside the ER is currently unclear (see section 1.6.3) (Coppolino et al., 1997; Gold et al., 2010; Dedhar et al., 1994; Holaska et al., 2001). Regardless of the essential roles of CALR undertaken outside the ER, the major characterised functions of this protein are carried out within the ER lumen, such as Ca^{2+} homeostasis and chaperone activity (Michalak et al., 2009). Therefore, there is no doubt of the importance of controlled subcellular compartmentalisation of CALR for correct functioning of many cellular processes.

CALR protein can escape from the ER to the Golgi apparatus, where it is recognised by the KDEL-receptors and is subsequently recycled back to the ER (Sonnichsen et al., 1994). Previous study has shown that deletion of the KDEL sequence within the C-terminal domain leads to an increased exit of CALR protein from the ER (Sonnichsen et al., 1994). This escape of proteins from the ER was linked with the inability of the KDEL-receptors to recognise CALR for retrieval (Sonnichsen et al., 1994). Interestingly, CALR mutations described in MPNs delete the KDEL sequence within the C-terminal domain (Klampfl et al., 2013; Nangalia et al., 2013). Although some previous studies have attempted to analyse the cellular localisation of CALR mutant, a full understanding of the effects of KDEL deletion for the subcellular localisation of this mutant protein in megakaryocytes remains elusive. Recent research revealed by fluorescent microscopy that both type 1 and type 2 CALR mutants do not co-localise with the ER marker CNX, therefore suggesting that CALR mutants might not reside within the ER (Chachoua et al., 2016). This study also described that type 1 and type 2 mutants co-localise with the Golgi marker ERGIC53 (Chachoua et al., 2016). Hence, it could be suggested that deletion of KDEL region does not ensure the retrotranslocation of CALR into the ER

(Sonnichsen et al., 1994), and therefore these proteins escape from the ER through the Golgi apparatus, possibly reaching other areas within the cell.

As previously described, CALR mutants directly interact with MPL receptor within the cell surface (Araki et al., 2016; Chachoua et al., 2016; Elf et al., 2016). Therefore, this suggests that CALR mutant cell surface localisation increases upon MPL binding. Previous research aiming to understand the cellular localisation of CALR mutations demonstrated an increase of CALR type 2 mutant protein within the cell membrane using UT-7 cell line (Araki et al., 2016). However, there is no analysis aiming to understand possible differences between the quantification of CALR type1 and CALR type 2 within the cell surface. Interestingly, previous publication agreed that CALR mutants are not retained within the lumen of the ER, although it was published a personal communication from Prof. Tony Green (Cambridge University, UK) who suggested a partial retention of CALR mutants within the ER by an unknown mechanism (Wiersma et al., 2015).

CALR mutants are less stable than CALR wt, and therefore its cellular detection is more complex than long-lived proteins (Han et al., 2016; Kollmann et al., 2016). Their instability has been suggested to be linked with possible changes in protein structure and therefore mutant protein undergo quick proteosomal degradation (Kollmann et al., 2016). Despite CALR mutants are short-lived proteins, these proteins are still able to activate aberrant cellular signalling (Kollmann et al., 2016). It is important to note that the CALR-Flag tagged within the C-terminal domain commonly used in research increases the stability of the protein, possibly increasing artificial effects within the cells (Kollmann et al., 2016). An additional study reported that CALR mutant proteins are secreted to the extracellular medium and more interestingly, there is an increase of CALR mutant protein content when MPL is expressed within the cells (Han et al., 2016). Therefore, this suggests that MPL interaction could decrease the degradation rate of CALR mutant proteins and consequently increase the protein levels of CALR mutant within the cells. Hence, it is possible that CALR mutants' stability and localisation change during megakaryocyte differentiation stages as a result of an increase *c-MPL* expression during megakaryopoiesis.

5.1.1. Aims and hypothesis

Overall the limited available information regarding CALR mutant cellular localisation proposes a sub-cellular mislocalisation of CALR mutants. This study aims to further investigate the localisation of CALR mutants within the cell. Moreover, it is hypothesised that as megakaryocyte maturation entails an increase expression of MPL, it is therefore expected that CALR mutants cell surface localisation could increase after megakaryocyte maturation. Hence, during this investigation three major objectives will be addressed:

I.   Analysis of CALR mutant localisation within the ER and further areas of the cell.

II. Visualisation by immunofluorescence of its interaction with MPL receptor on the cell surface.

III. Analysis of differences of CALR levels on the cell surface between different stages of megakaryocyte maturation.

5.2. Results

5.2.1. Sub-cellular localisation of CALR mutant

To define whether CALR mutations lead to an escape of the protein from the ER and reach a different subcellular localisation of CALR, transfected HEK 293T cells with CALR-wt-GFP and CALR-type2-GFP plasmids were used. Cells were subjected to immunostaining and high resolution confocal microscopy. ERP57, an ER chaperone (Bedard et al., 2005), was used as an ER marker during immunostaining.

Firstly, the cellular localisation of CALR wt was analysed. As expected, results showed a higher expression of CALR wt around the cellular nucleus and this expression co-localised with ERp57 immunostaining (Figure 24 A), suggesting a high expression of CALR wt within the cellular ER. Moreover, some signal was registered within the cell nucleus (Figure 24).

Further analysis of CALR type 2 cellular localisation showed that CALR mutant is around the nucleus co-localising with ERp57, although its expression was also diffused within the cytoplasm (Figure 24 B). CALR type 2 mutant expression was disseminated around the cellular cytoplasm and did not display a clear cellular localisation of expression. Interestingly, its expression was also highly diffused within the cellular nucleus compared with CALR wt (Figure 24 B).
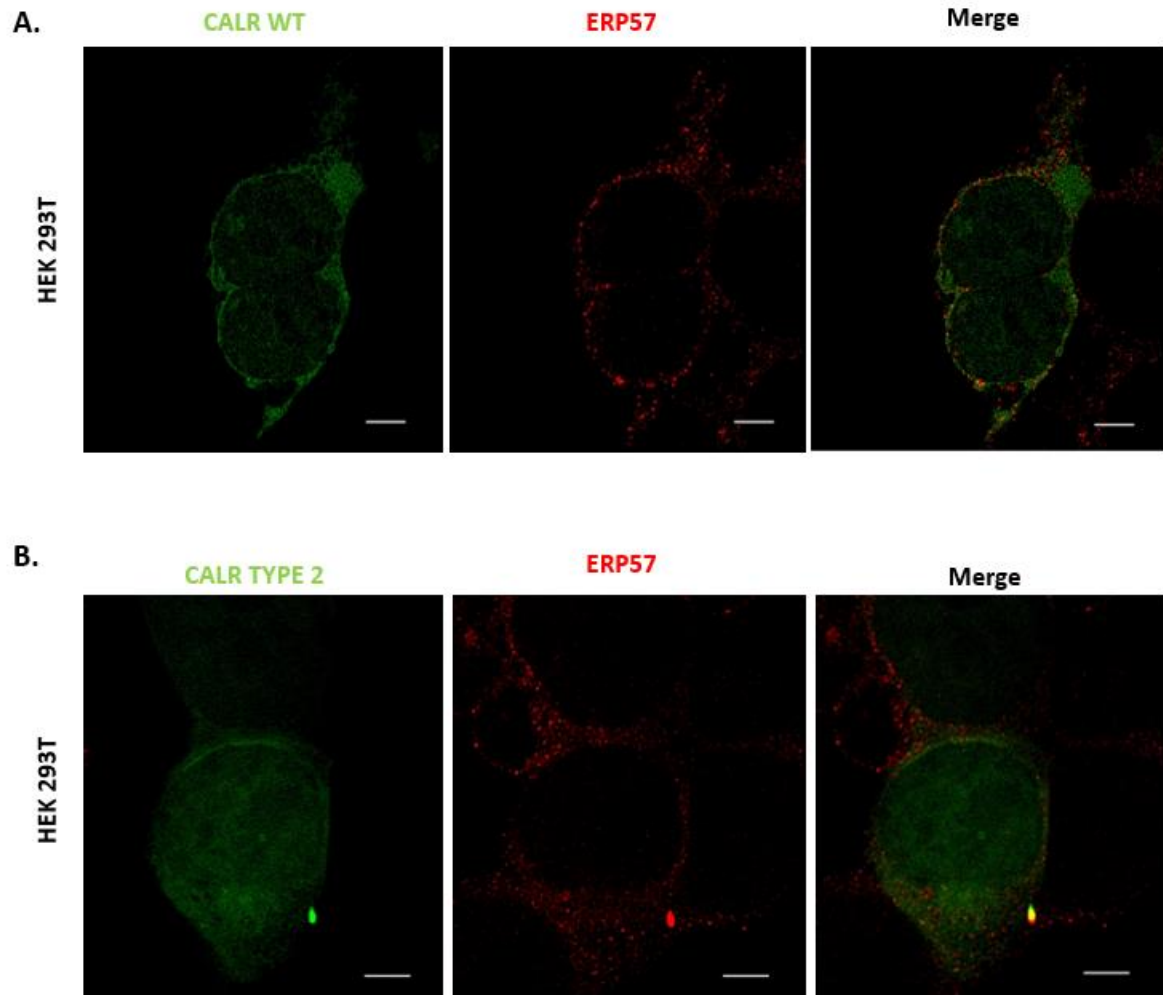
Figure 24. CALR WT and CALR type 2 mutant cellular localisation.

HEK 293T cells were transfected with CALR-WT-GFP and CALR-type 2 mutant-GFP vectors. 48 hr after transfection cells were fixed and were subjected to immunostaining using mouse anti-ERp57 and anti-mouse. **A)** Representative images for CALR WT-GFP co-localization with ERp57 in transfected HEK 293T cells. **B)** Representative images of CALR type 2 mutant –GFP expression in transfected HEK 293T cells. Scale bars = 5 µM

5.2.2. CALR mutant co-localisation with MPL receptor at the cell surface

Recent investigations have examined the contribution of CALR mutants to the development of MPN by studying the direct interaction between CALR and MPL receptor (Araki et al., 2016; Chachoua et al., 2016; Elf et al., 2016). These studies have addressed and analysed this interaction by using co-immunoprecipitation and western blot analyses, however there was no evidence of this interaction when using immunofluorescence and cell microscopy. Here, this issue is addressed by using HEK 293T cells transfected with CALR-Flag and MPL-HA vectors. Cells were subjected to immunofluorescence staining and finally high resolution confocal microscopy.

As seen in the previous analyses, CALR wt is mostly localised around the cellular nucleus. Moreover, this analysis showed MPL receptor expression within the cell membrane and intracellularly. The intracellular fraction corresponds to the ER, as this receptor is synthesised within this cellular organelle. Therefore, it is not surprising to visualise an intracellular co-localisation of CALR WT and MPL; however, there is not a co-localisation of these proteins within the cell membrane (Figure 25 A).

In contrast, CALR type 2 mutant is highly expressed through all the cytoplasmic area and the cell membrane. Results showed co-localisation of MPL and CALR mutant within the cell surface (Figure 25 B). Overall, these results proved an interaction between CALR Type 2 mutant and MPL at the cell membrane and support previous immunohistochemical analyses proving this interaction.
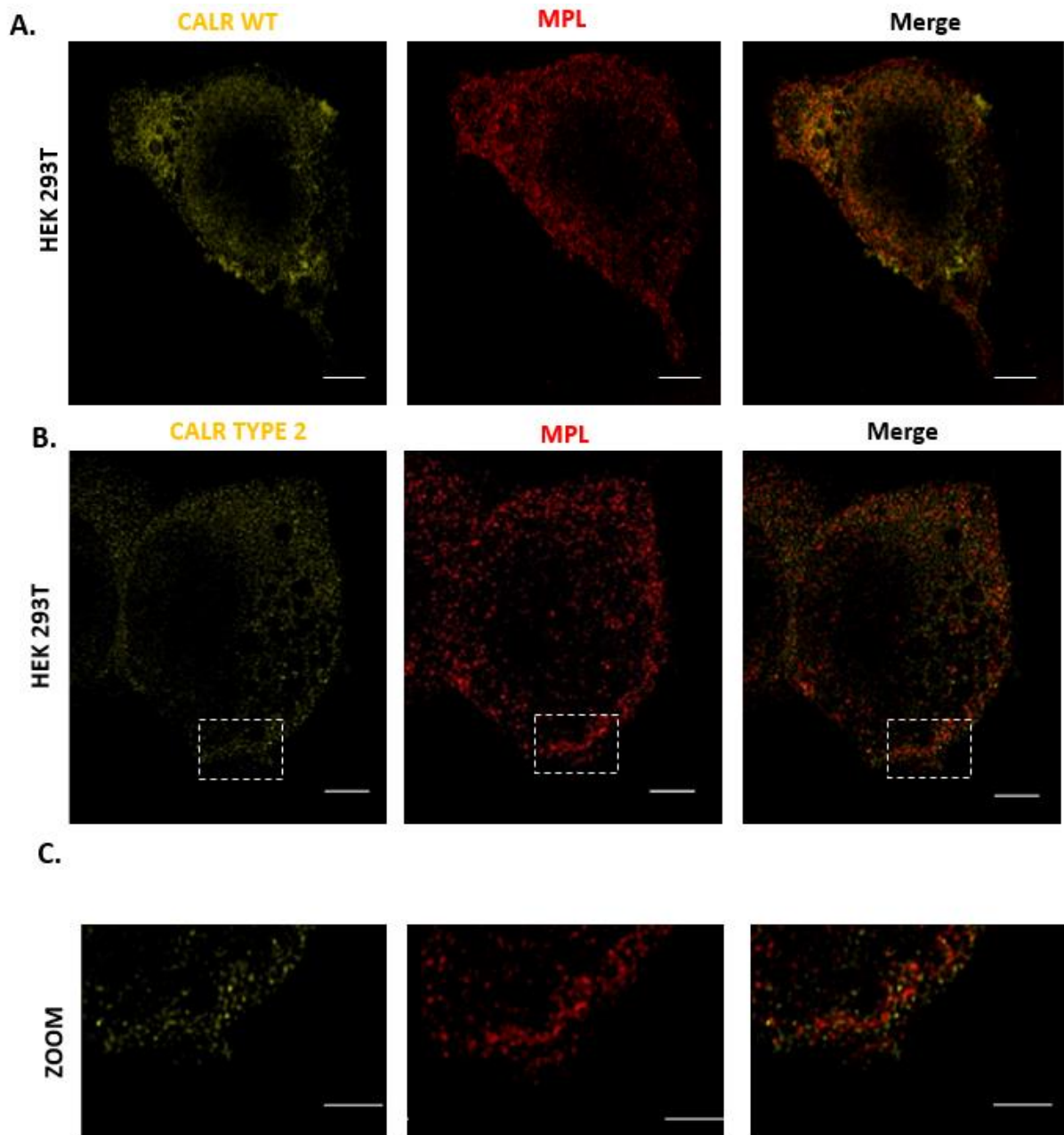
Figure 25. CALR mutant co-localises with MPL within the cell membrane.

HEK 293T cells were transfected with CALR-WT-Flag, CALR-type 2 mutant-Flag and TPO-R-HA vectors. 48 hr after transfection cells were fixed and were subjected to immunostaining using mouse anti-HA, rabbit anti-Flag, anti-rabbit Cys3 and anti-mouse 647. **A)** Representative images for CALR WT-Flag and MPL-HA transfected HEK 293T cells. **B)** Representative images of co-localization of CALR type 2 mutant –Flag and MPL-HA in transfected HEK 293T cells. **C)** Zoomed images showing co-localisation. White squares indicate areas of co-localisation. Scale bars = 5 μM

5.2.3. Analysis of CALR cell surface localisation in leukemic blast cells

Previous study reported that CALR mutations increase its cell surface localisation upon MPL receptor binding (Han et al., 2016). In order to analyse whether increased expression of CALR on the cell surface is totally dependent on this interaction, CALR cell surface levels in MARIMO cell line, which does not express MPL receptor in its leukemic blast stage (Kollmann et al., 2016), were quantified. CALR cell surface analysis was performed by immunostaining and quantified by flow cytometry.

Surprisingly, this study revealed that MARIMO cells displayed a significant increase of CALR cell surface compared with other leukemic cell line negative for *CALR* mutation; K562 cells (Figure 26). Therefore, this result suggests that CALR mutants might be localised into the cell membrane independently of MPL interaction in early stages of megakaryocyte development.
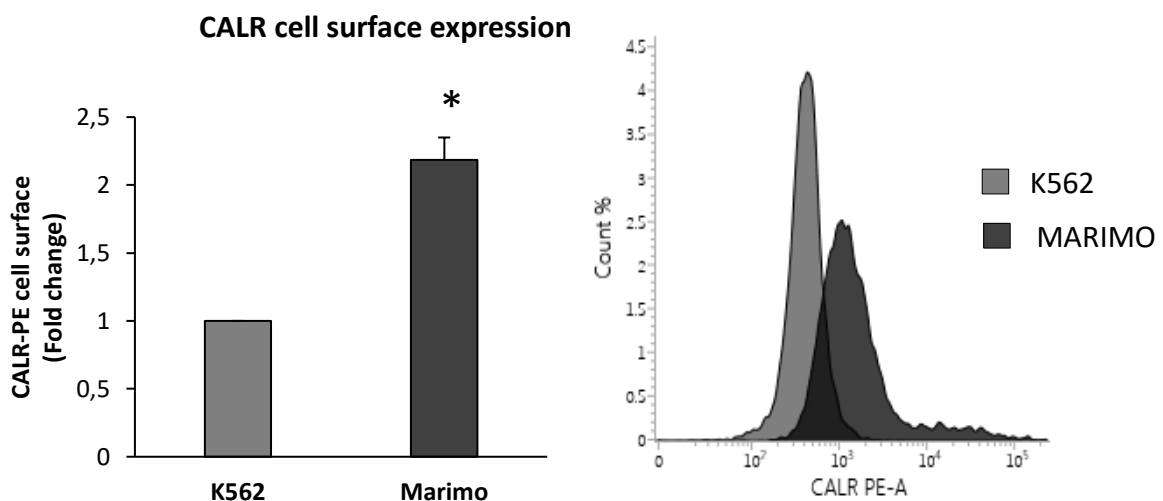
Figure 26. CALR cell surface expression in K562 and MARIMO cells.

Cells were subjected to immunostaining and were further analysed by flow cytometry. **A)** Average quantification of CALR cell surface. **B)** Representative histogram of CALR-PE fluorescence in both samples. Values represent mean ± SEM for each group. n=3. **P<0.01, *P<0.05. Student T.test

To extend the analysis of CALR localisation, CALR cell surface localisation was further quantified in DAMI cells, a megakaryocyte cell line that constitutively express MPL receptor

(Pang et al., 2009; Greenberg et al., 1988). CALR wt, CALR type 1 and CALR type 2 constructs were expressed using a lentiviral vector and transduced into DAMI cells. Empty GFP vector was used as a control for transduction. During the experiment, two clones of each condition were used, and the experiment was performed in triplicates in each clone. Total CALR levels were analysed to ensure equal CALR protein levels and GFP expression of the control group was analysed to ensure transfection efficiency (see Appendix 3).

CALR cell surface quantification using flow cytometry revealed that, CALR type 1 DAMI cells showed a significant increase of CALR expression within the cell surface compared with the control (Figure 27). In contrast, CALR type 2 cells did not show any difference of CALR cell surface expression relative to CALR wt (Figure 27).
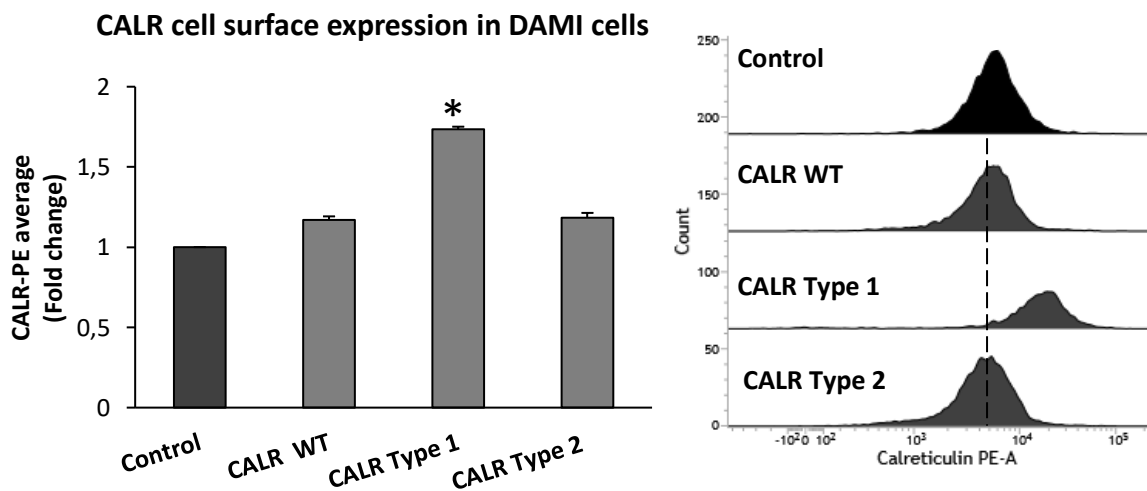
Figure 27. CALR cell surface levels in DAMI cells overexpressing CALR wt, type 1 and type 2 mutations.

Cells were subjected to immunostaining and were further analysed by flow cytometry. **A)** Average quantification of CALR cell surface **B)** Representative histogram of CALR-PE fluorescence. Representative example of fluorescent measurements of a single clone per condition are shown. Values represent mean ± SEM for each group. n=3. **P<0.01, *P<0.05. Student T.test

5.2.4. Analysis of differences of CALR levels within the cell surface between blast and megakaryocyte like cells

Expression of MPL during megakaryocyte differentiation might lead to a consecutive increase of mutant CALR on the cell surface (Han et al., 2016). Therefore, to explore the consequences of megakaryocyte differentiation in CALR cell surface localisation, CALR levels were quantified after megakaryocyte differentiation. This study was performed using DAMI, MARIMO and K562 cellular models. Hence, before analysing CALR cell surface protein levels, the megakaryocyte differentiation potential of these cell lines was tested.

Chemical induction of K562 megakaryocyte differentiation

K562 cells are a known established model used to study megakaryocyte differentiation. In order to analyse CALR protein levels on the cell surface in megakaryocyte like cells, the optimal conditions to induce K562 cell differentiation into the megakaryocyte lineage *in vitro* were established. For this purpose, cells were differentiated into megakaryocytes with 5nM PMA during 72 hours, as shown previously (Koeffler et al., 1981; Huo et al., 2006; Zhang et al., 2007; Huang et al., 2014). To corroborate cell differentiation, expression of the megakaryocyte cell surface marker CD41a was analysed by flow cytometry.

Consistent with previous research, results showed that *in vitro* megakaryopoiesis of K562 cells was induced under 5nM PMA treatment over 72 hours. PMA treatment resulted in a significant increase in CD41a expression and 90% of the cells expressed this marker (Figure 28). Additionally, microscopic examination revealed that cells showed megakaryocyte phenotypic characteristics, such as increase in cell size, adherence and cytoplasmic projections (Figure 28 A).

K562 CD41a expression during megakaryopoiesis

B.

% Cells expressing CD41

K562 Control

C.

K562 5nM PMA
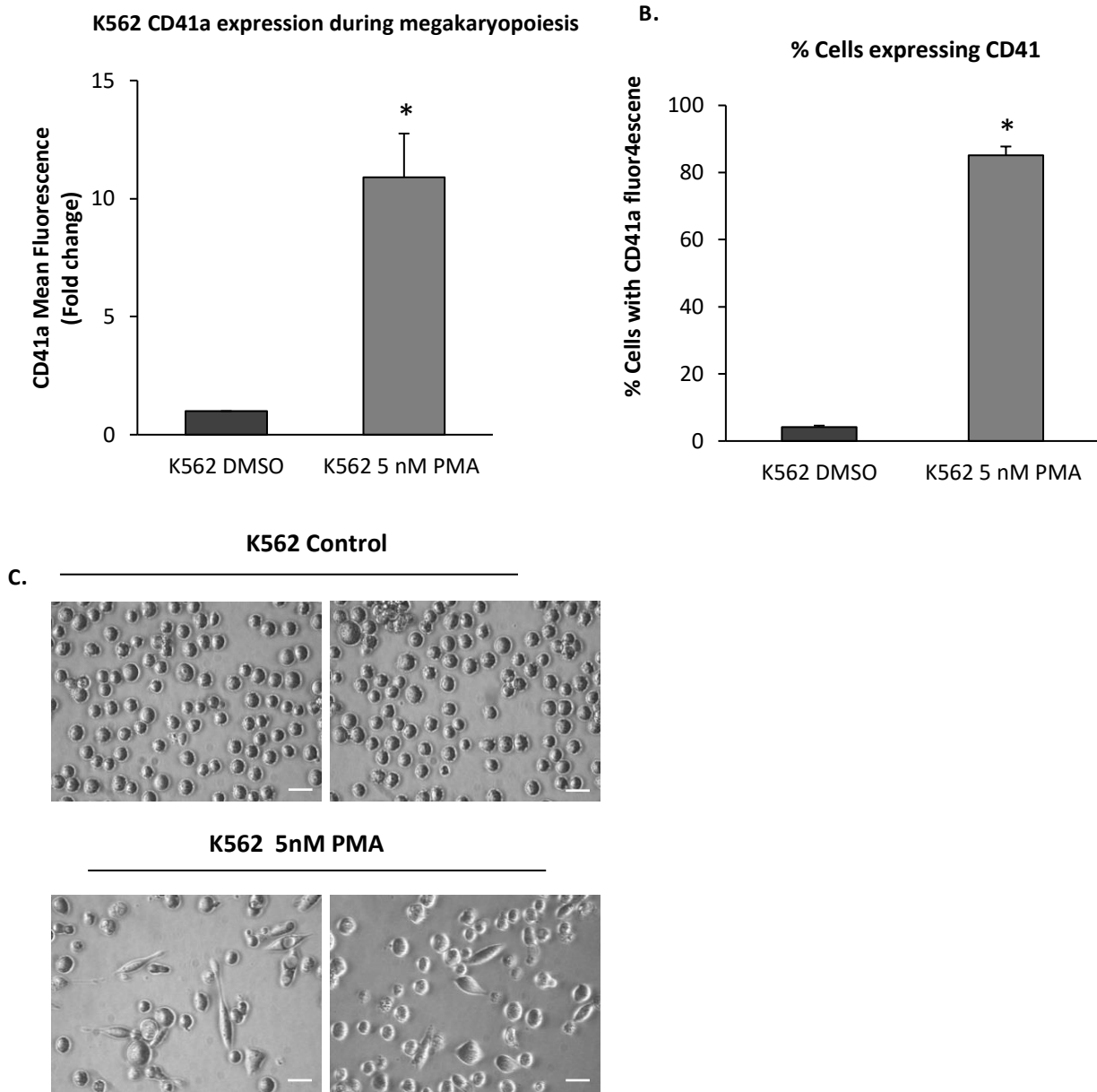
Figure 28. K562 cells under PMA treatment display megakaryocytic characteristics.

A, B) Increase expression of CD41a marker in the cell surface after 72 hr of PMA treatment. **C)** Live cells show changes in cell morphology and increase cell adherence. Images were captured using 40x objective. Values represent mean ± SEM for each group. n=3. **P<0.01, *P<0.05. Student T.test. Error bars = 50μm

Chemical induction of DAMI megakaryocyte differentiation

DAMI cell line is also a model to study megakaryocyte differentiation (Greenberg et al., 1988). DAMI clones overexpressing CALR WT, CALR type 1 and type 2 mutants were differentiated towards mature megakaryocytes to further analyse CALR cell surface population within the cell surface. DAMI cells were incubated under PMA treatment for 72 hours, as previously described in the literature (Greenberg et al., 1988). Then, CD41a expression on the cell surface was analysed by flow cytometry.

Results showed that *in vitro* megakaryocyte formation of the DAMI clones was induced under 5nM PMA treatment over 72 hours. Overall, PMA treatment resulted in a significant increase of CD41a expression in all samples (Figure 29).
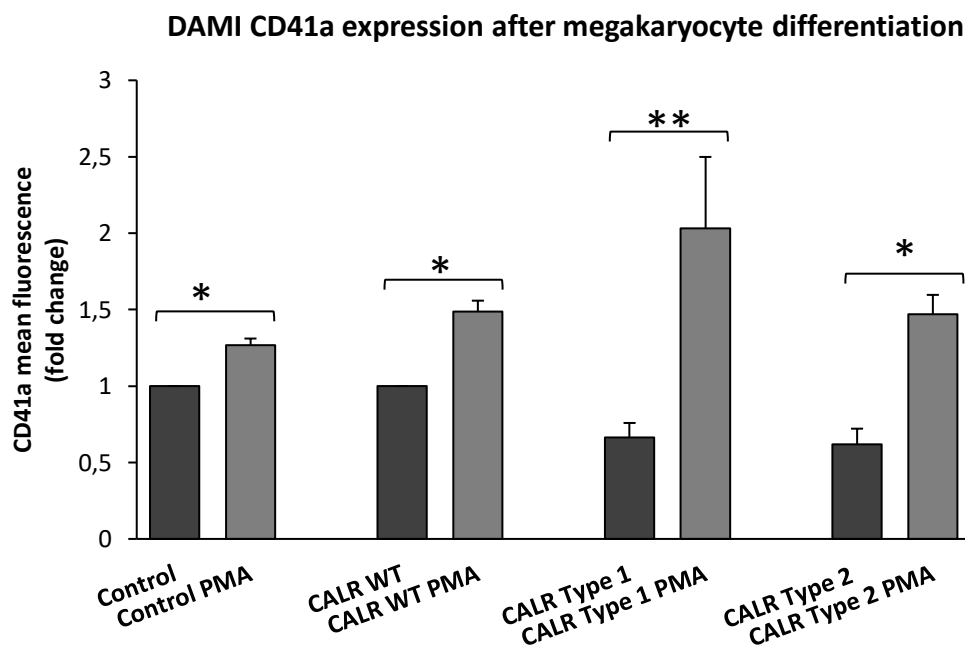
Figure 29. DAMI cells under PMA treatment increase CD41a expression.

Increase expression of CD41a marker in the cell surface after 72 hr of PMA treatment. Results were averaged between three independent experiments. Results were averaged between six independent experiments using two different clones per condition. Values represent mean ± SEM for each group. **P<0.01, *P<0.05. Student T.test.

Finally, phenotypic characterisation revealed that DAMI cells under PMA treatment displayed the morphological characteristics of megakaryocyte maturation (Figure 30). Interestingly, CALR mutant cells showed increased cell adhesion within the culture, and in addition, CALR

type 1 cells after PMA treatment displayed an increased size compared with the controls and CALR type 2 cells.
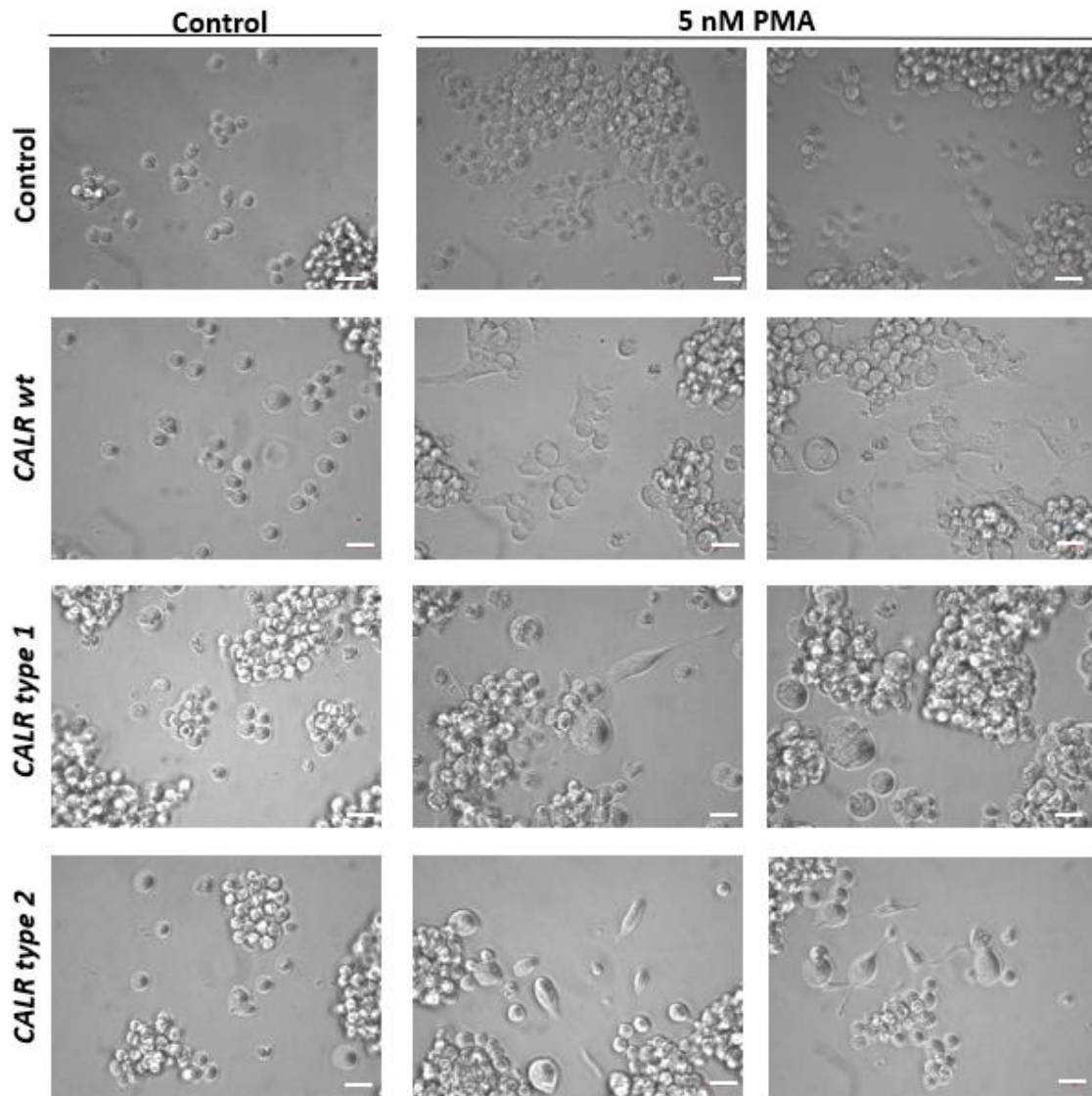
Figure 30. DAMI cells under PMA treatment display megakaryocytic phenotypic characteristics.

DAMI cells were subjected to 5 nM PMA treatment during 72 hours and were subsequently used for light microscopy. Live cells showed changes in cell morphology and increased cell adherence. Images were captured using 40x objective. Error bars = 50µm.

5.2.5. CALR quantification within the cell surface after megakaryocyte differentiation

Once K562, MARIMO and DAMI cells were differentiated towards the megakaryocytic lineage, CALR cell surface expression within these cells was analysed before and after megakaryocyte induction.

Firstly, CALR cell surface expression in K562 and MARIMO cells was quantified in their blast and megakaryocyte stage. K562 and MARIMO cells were differentiated towards megakaryocyte using PMA as previously described. Surprisingly, when K562 cells were differentiated towards mature megakaryocytes, there was a significant increase of CALR on the cell surface compared with its basal levels during the blast stage (Figure 31). Interestingly, when MARIMO cells were induced with PMA, results also showed an increase of CALR on the cell surface compared to its basal control (3.6 fold), however this relative increase was lower than the rise detected in K562 cells (5 fold) (Figure 31). Although the fold increase was smaller in MARIMO cells, the total CALR cell surface quantified in MARIMO megakaryocyte like cells was higher than the control cells. However, this difference was not statistically significant (Figure 31 C).

Next, this study proceeded to analyse CALR cell surface using DAMI cells overexpressing CALR wt, CALR type 1 and CALR type 2. After PMA induction, all samples showed an overall increase of CALR on the cell surface (Figure 32). However, CALR type 1 cells showed a higher increase of cell surface CALR compared with the control (Figure 32). In this case, differences were not statistically significant. CALR type 2 cells showed a similar increase of CALR cell surface after megakaryocyte induction compared with the control cells (Figure 32).
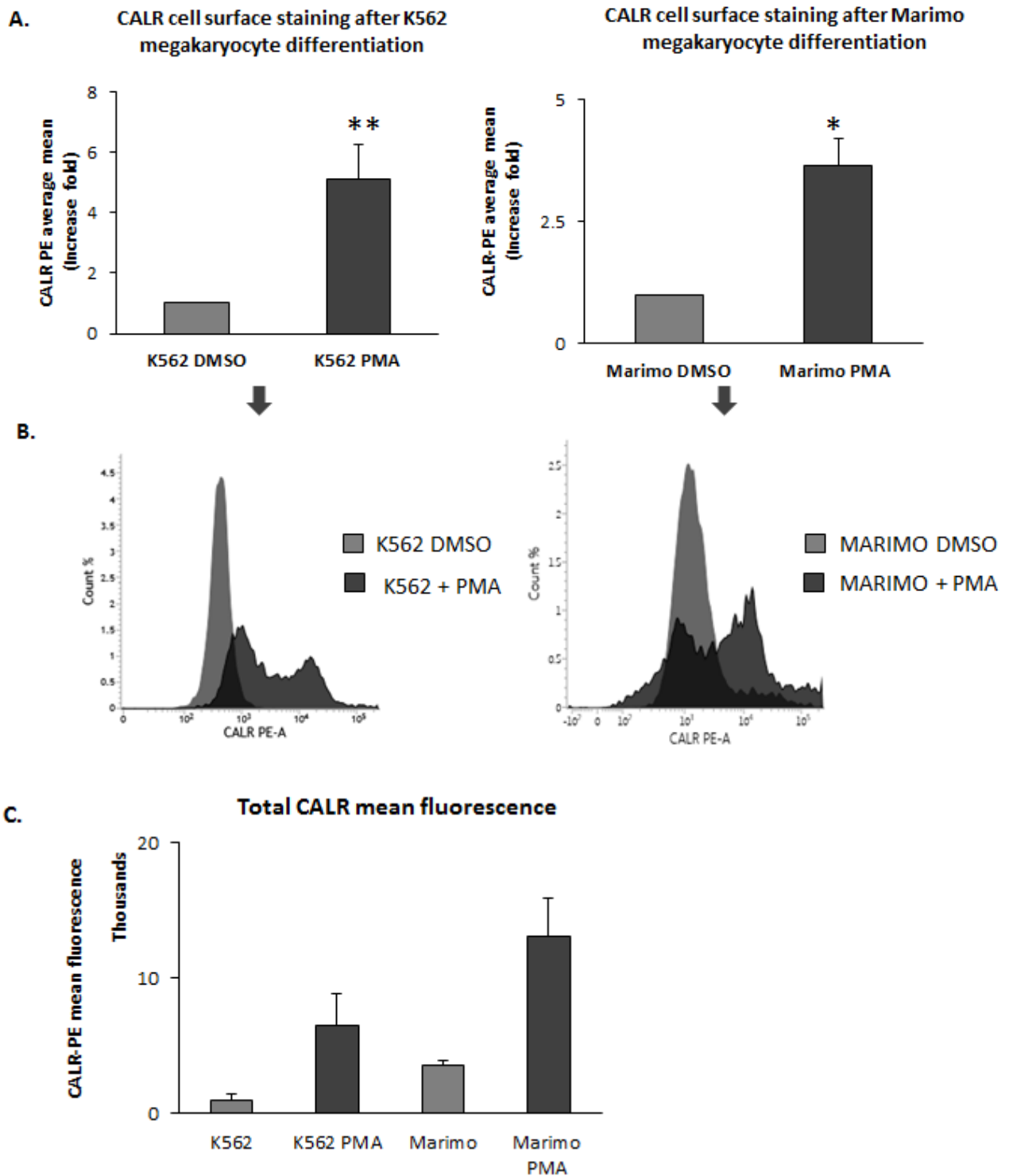
Figure 31. CALR cell surface levels in K562 and MARIMO cells after PMA induction.

Cells were exposed to PMA treatment during 72 hours. Then, cells were used for CALR immunostaining and CALR levels were quantified by flow cytometry. **A)** Average quantification of CALR cell surface. **B)** Representative histogram of CALR-PE fluorescence. **C)** Total CALR-PE fluorescence. Values represent mean ± SEM for each group. n=3. **P<0.01, *P<0.05. Student T.test.
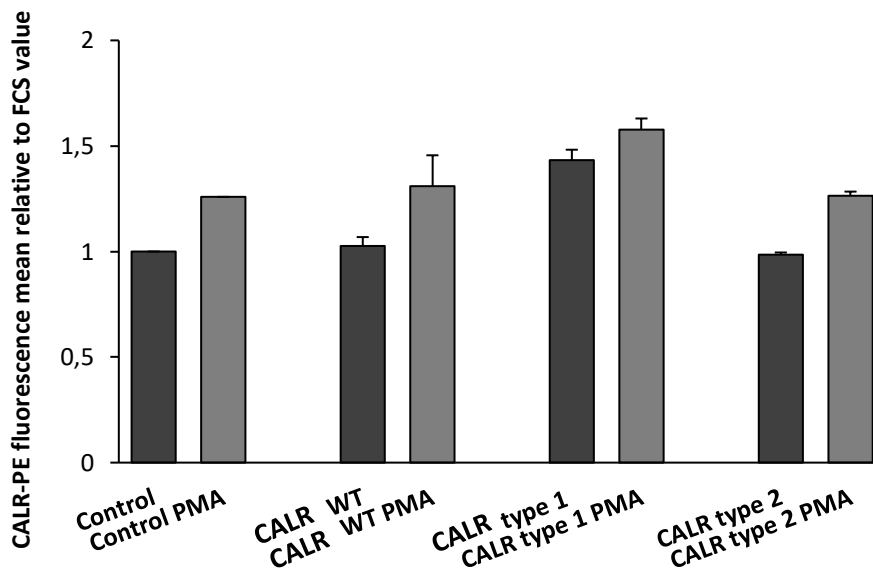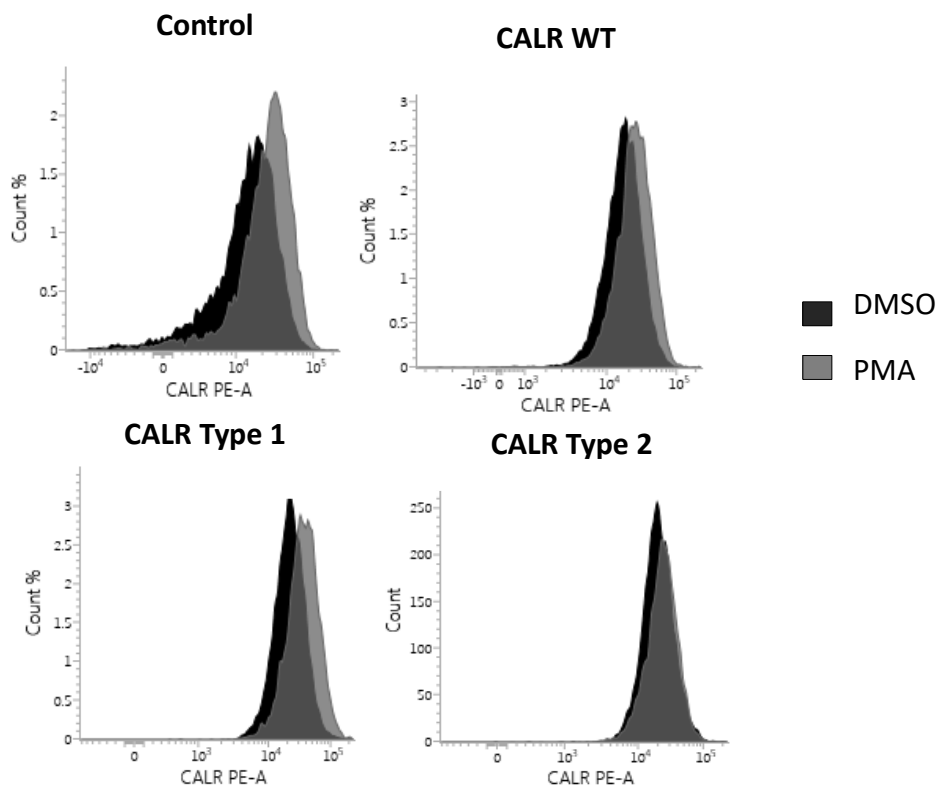
Figure 32. CALR cell surface levels in DAMI cells overexpressing CALR wt, type 1 and type 2 mutations after PMA induction.

DAMI cells were exposed to PMA treatment during 72 hours. Then, cells were used for CALR immunostaining and CALR levels were quantified by flow cytometry. **A)** Average quantification of CALR cell surface. **B)** Representative histogram of CALR-PE fluorescence. Example of fluorescent measurements of a single clone per condition are shown. Results were averaged between six independent experiments using two different clones per condition. Values represent mean ± SEM for each group. **P<0.01, *P<0.05. Student T.test.

5.3. Discussion

CALR protein has been described to be present in multiple localisations inside the cell (Michalak et al., 2009) and therefore alterations of expression levels within different cellular compartments could be key to understand the pathogenesis of CALR driver mutations. This study has demonstrated that CALR mutant proteins characteristic of MPNs display an abnormal cellular localisation and thus, CALR normal cellular functions might be disrupted within these abnormal cells.

The ER is the cellular compartment that contains the major amount of CALR within the cell. The immunofluorescence assay performed in this study suggested that CALR mutant is localised within the ER and its expression is also diffused through the cytoplasm and nucleus. As mentioned in the literature, CALR mutant is present within the Golgi apparatus (Chachoua et al., 2016). Therefore, loss of KDEL region could be the cause of a deregulated retrotranslocation of CALR from the Golgi into the ER, and therefore this mutant protein is transported through the Golgi into different cellular compartments. Of note, CALR has been described to be present within the cellular nucleus in primary megakaryocytes (Iborra and Papadopoulos, 2017) and there have been previous reports about the potential transcriptional activity of CALR (Holaska et al., 2001).

Major interest has been raised by the novel finding of CALR mutant interaction with MPL receptor (Araki et al., 2016; Chachoua et al., 2016; Elf et al., 2016). Therefore, its increase expression within the cell surface is expected. This study shows a co-localisation of CALR type 2 with MPL receptor within the cell surface of HEK 293T cells using microscopy. In addition, DAMI cells overexpressing CALR type 1 and type 2 mutants showed an increase of CALR within the cell surface only in CALR type 1 cells. Although both mutants have been described to directly interact with MPL receptor (Araki et al., 2016), the different quantification levels at the cell surface in DAMI cells between CALR mutant clones described in this study could be linked with the different pathogenic role of both mutations, as CALR type 1 is associated with a more malignant disease phenotype.

One interesting finding is that quantification of CALR cell surface in CALR mutant MARIMO cell line is significantly increased compared with K562 cells. According to previous research

(Kollmann et al., 2016) and this study (see chapter 4), MARIMO cells in their blast stage do not express MPL receptor, and therefore, CALR increase on the cell surface might be caused by independent pathways of the MPL-CALR binding. However, a note of caution is due here as only one leukemic cell line has been used as a control in comparison to MARIMO cell line, and therefore it could be possible that the differences described in this study are due to intrinsic differences between these cell lines. Thus, this study should be completed with the comparison of other leukemic blasts such as HEL, HL-60 or UKE-1.

During megakaryocyte differentiation there is a profound reorganisation of the ER (Ru et al., 2016), towards a complex DMS which is highly dependent on ER activity (Eckly et al., 2014). Therefore, it is possible that there are differences in expression of the ER proteins during megakaryopoiesis. One unanticipated finding in this study was that megakaryocyte differentiation induced by PMA leads to an overall increase of CALR cell surface expression in CALR wt cells. These results are likely to be related to changes within the ER nature during megakaryocyte formation, however this data might be interpreted with caution as megakaryopoiesis was induced in this case by pharmacological treatment and there is no known links between the possible effects of this phorbol treatment into the ER or CALR localisation. In addition, it is interesting to note that CALR mutant cells displayed a higher increase of CALR within the cell surface during megakaryopoiesis, suggesting further abnormal regulation of CALR cellular localisation during megakaryocyte differentiation.

In the current years, an increase in the use of immunotherapy for treatment of neoplastic diseases has been witnessed (Gattinoni et al., 2006). A previous study evaluated the possibility of using CALR mutants within the cell surface of neoplastic cells as targets of immunogenic cell death (Holmstrom et al., 2017). Promising results displayed the possibility of using peptide vaccinations for CALR mutant MPN patients (Holmstrom et al., 2017). Therefore, this novel investigation together with the initial data obtained in this study, where it is demonstrated an increase of CALR within the cell surface during megakaryopoiesis, raise the necessity of further analysis aiming to target this CALR cell surface population as a novel MPN treatment.

The present study makes several noteworthy contributions to the understanding of CALR mutant cellular localisation. It is important to bear in mind that CALR functions are highly

correlated with its cellular compartmentalisation, and therefore an abnormal localisation of this protein could lead to aberrant cell functioning with altered Ca^{2+} buffering activity, change its protein folding capacity or as previously described, lead to changes in cell signalling (Araki et al., 2016; Chachoua et al., 2016; Elf et al., 2016; Han et al., 2016; Kollmann et al., 2016). There is, therefore, a definitive need to further study the link of abnormal CALR mutant sub-cellular localisation and changes in its cellular roles to deeply understand the nature of CALR mutant MPNs.

5.3.1. Conclusions

The data described in this study reveals that mutant CALR is abnormally localised within the cell. Overall, the major conclusions of this study are:

i. CALR mutations known to delete the KDEL region within the C-terminal domain lead to a different localisation of CALR in the cell. Even though CALR mutant is localised within the ER, it is also mislocalised around the cytoplasm.

ii. CALR co-localizes with MPL receptor on the cell surface in CALR mutant expressing cells.

iii. CALR mutant blast cells display an increased expression of mutant CALR at the cell surface, independently of MPL receptor.

iv. Megakaryocyte differentiation leads to an increase of CALR within the cell surface. However, CALR mutant cells display a major increase of this protein in the cell surface during megakaryocyte differentiation.

5.3.2. Future directions

Future research should concentrate on the investigation of CALR mutant protein quantification within the ER, nucleus, Golgi and cytoplasm. This investigation could be carried out by protein purification using different density gradients purification and western blot analysis.

Moreover, the analysis of CALR cell surface increase in MARIMO cells during its blast stage raises new questions of other possible mechanisms of CALR escaping towards the cells surface. It would be of much interest to analyse the possible mechanisms that increase CALR within the cell surface in CALR mutant blast cells to finally understand whether in this case it works as an ER stress marker. However, it would be important to perform this initial experiment using further leukemic cell lines and primary patient samples as control, to avoid intrinsic differences between them.

Chapter 6: *Analysing the importance of calcium during megakariopoiesis and the effects of CALR mutations in calcium homeostasis.*

6.1. Introduction

The Ca^{2+} ion is an essential intracellular molecule required for many cellular functions such as cell proliferation, metabolism, trafficking, apoptosis and differentiation (Berridge et al., 2000; Carafoli, 2002). A tight control of cellular signalling relays on oscillations of the intracellular Ca^{2+} concentration ($[Ca^{2+}_i]$) which are regulated by intracellular and extracellular Ca^{2+} sources. Ca^{2+} channels, Ca^{2+} buffering proteins or Ca^{2+} pumps move this molecule between the ER, the cytosol and the extracellular space in a highly controlled manner to transmit the required cell signals.

6.1.2. Calcium cellular dynamics

In a basal cellular state, the plasma membrane Ca^{2+} ATPase (PMCA) and the sarco/endoplasmic reticulum Ca^{2+} ATPase (SERCA) pumps mostly control the cellular $[Ca^{2+}_i]$. However, when a cell is stimulated and the signal is transmitted, the $[Ca^{2+}_i]$ increases due to mobilisation of intracellular Ca^{2+} storages or Ca^{2+} influx from the extracellular environment into the cytosol (Berridge et al., 2003).

The ER is the major Ca^{2+} store within the cell. However, it has been reported that other organelles such as mitochondria or the Golgi apparatus can contribute to the Ca^{2+} cellular homeostasis (Berridge et al., 2003). Within the ER, Ca^{2+} is buffered by Ca^{2+} binding proteins such as Protein Disulphide Isomerases (PDI), CNX or CALR, which not only act as buffering proteins but also as chaperones and regulators of Ca^{2+} ER channels (Berridge, 2002; Coe and Michalak, 2009). The ER Ca^{2+} is released into the cytoplasm in response to specific intracellular

signals. Activation of the phospholipase-C (PLC) by many cell surface receptors leads to the production of Inositol 1,4,5-trisphosphate (IP$_3$), which will subsequently lead to the activation of Inositol 1,4,5-trisphosphate receptor (IP$_3$-R)/ Ca^{2+} channel. Finally, active IP$_3$-R leads to the ER Ca^{2+} release into the cytosol (Mikoshiba, 2007). In excitable cells, ryanodine receptors (RYRs) are responsible for the Ca^{2+} ER release rather than IP$_3$-R (Lanner et al., 2010).

SERCA is an ER pump that actively transports Ca^{2+} ions from the cytoplasm into the ER lumen, tightly regulating the [Ca^{2+}$_i$] (Periasamy and Kalyanasundaram, 2007). SERCA presence is ubiquitous and it is the only ER Ca^{2+} pump known to maintain the ER Ca^{2+} stores within the cell (Figure 33). *In vitro* inhibition of SERCA pump is a common routine to study cellular ER Ca^{2+} buffering capacity. For that, Thapsigargin, a well-known strong SERCA inhibitor, is commonly used in research (Lytton et al., 1991).

Cells display the store-operated Ca^{2+} entry (SOCE) mechanism to avoid ER Ca^{2+} depletion. SOCE leads to Ca^{2+} influx through the cell membrane and it is activated as a response of ER Ca^{2+} store depletion (Smyth et al., 2010). During this process, Stromal interaction molecule (STIM) proteins, which are located within the ER membrane, act as Ca^{2+} ER sensors (Stathopulos et al., 2008). Upon ER Ca^{2+} decrease, STIM molecules are placed near the cell membrane and then interact with the SOCE channels, formed by the Orai proteins. Next, SOCE channels allow the influx of extracellular Ca^{2+} inside the cell to finally restore the optimal ER Ca^{2+} levels (Figure 33) (Cahalan, 2009; Deng et al., 2009; Schindl et al., 2009).

Extracellular Ca^{2+} enters the cell through the activation of various Ca^{2+} channels and pumps within the cell membrane with widely different characteristics. For example, voltage-operated calcium channels (VOCs), which include L-, P/Q-, N-, R-, and T-type channels, generate fast extracellular Ca^{2+} fluxes in order to modulate rapid intracellular processes (Catterall, 2011). These channels are broadly known to regulate extracellular Ca^{2+} entry in excitable cells like neurons, cardiac and pancreatic-β cells (Yang and Berggren, 2006; Bean, 1991), although L-type channels also have been proved to be relevant in non-excitable cells, such as human T-cells (Stokes et al., 2004). Moreover, further cell membrane Ca^{2+} entry channels regulate the optimal cellular [Ca^{2+}$_i$] within the cell, such as the Second-messenger-operated channels (SMOCs), which are regulated by internal messengers. Additionally, there also are the Receptor-Operated channels (ROCs), including the N-methyl-D-aspartate

receptors (NMDARs) which activate in response to extracellular glutamate (Vyklicky et al., 2014).

6.1.2. Intracellular calcium oscillations

The ability of Ca^{2+} to regulate cell physiological processes relies on the cellular capacity to control $[Ca^{2+}_i]$ in space and time. Oscillations in $[Ca^{2+}_i]$ can be propagated from microseconds to hours and could be described as spontaneous events or derived from downstream cellular cascades. As a consequence of these Ca^{2+} transient oscillations, the course of cellular physiology is determined (Pinto et al., 2016; Putney and Bird, 2008).

The spatial and temporal pattern of Ca^{2+} oscillations can be regulated by internal Ca^{2+} stores, such as ER or Golgi, as well as by the Ca^{2+} channels and pumps within the cell membrane. Moreover, intracellular Ca^{2+} oscillations can be produced as a response of external ligands and can be manipulated *in vitro* by drug treatments (Pinto et al., 2016). Intracellular Ca^{2+} signalling can lead to rapid rise in $[Ca^{2+}_i]$, within microseconds to second ranges, in local areas or promote global increase of $[Ca^{2+}_i]$ levels within the cell. Prolonged Ca^{2+} oscillations that tent to last longer (hours) have been implicated with several cellular processes, such as differentiation (Sun et al., 2007), cytokines production (Uhlen et al., 2000), neuronal growth (Hutchins and Kalil, 2008) and cell migration (Giannone et al., 2002).

Cells are able to interpret changes in the frequency of intracellular Ca^{2+} oscillations using sophisticated systems. For example, PKC and CaMKII have been shown to play pivotal roles in the decoding the frequency of intracellular Ca^{2+} oscillations frequency (Oancea and Meyer, 1998; Dupont et al., 2003).
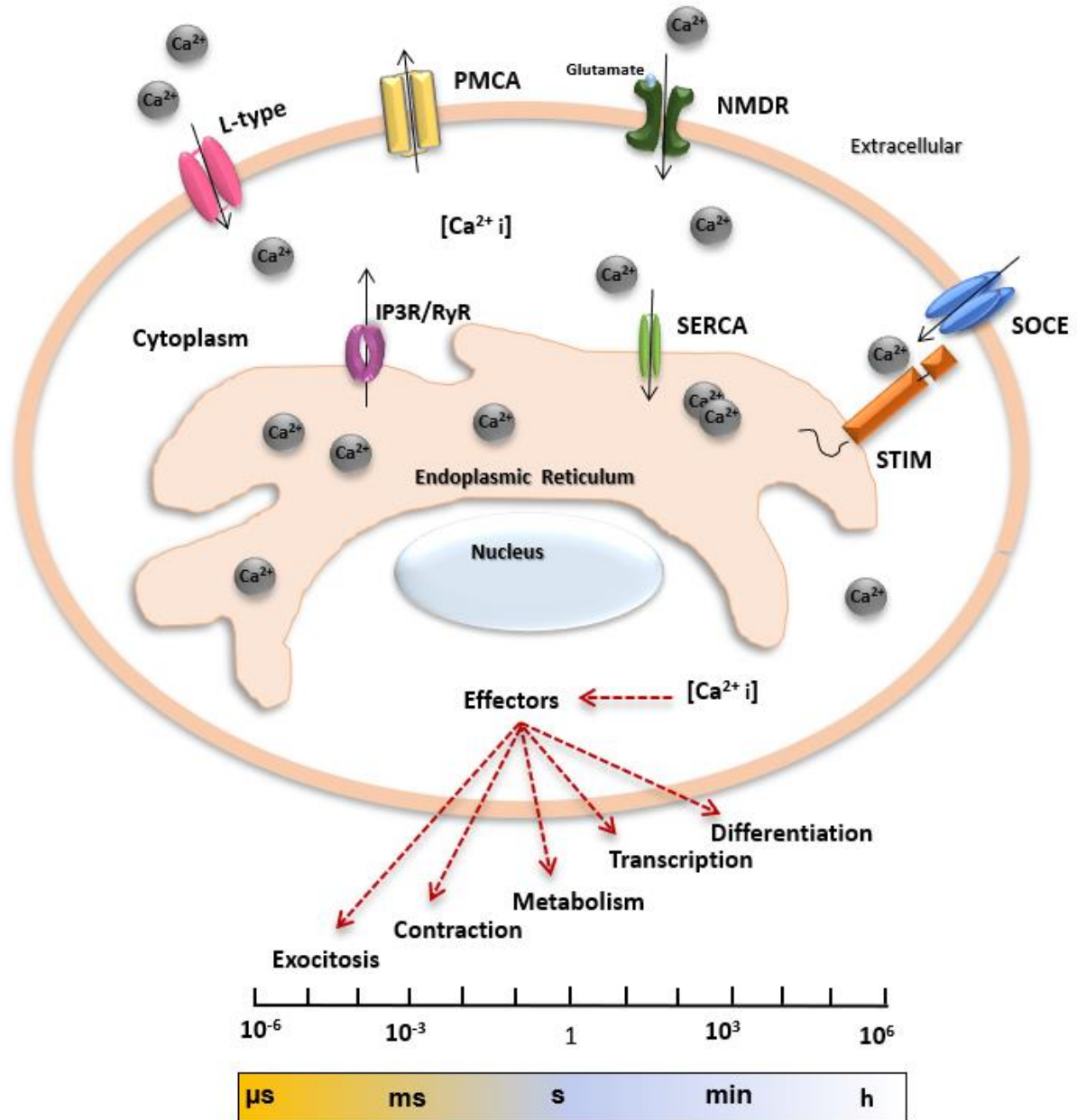
Figure 33. Cellular Ca2+ signalling dynamics.

Cells display a widely specialised protein toolkit to control Ca^{2+} signalling and to maintain specific $[Ca^{2+}_i]$ within the cell. Majority Ca^{2+} is bound to buffering proteins, although a small proportion binds to effectors, leading to the activation of many cellular processes. Black arrows show the direction of movement of Ca^{2+} ions. $[Ca^{2+}i]$: intracellular Ca^{2+} concentrations. SERCA: sarcoendoplasmic reticulum Ca^{2+}-ATPase, IP3R: inositol 1,4,5-triphosphate receptor, PMCA: plasma membrane Ca^{2+} ATPase

6.1.3. Calcium and its role in cellular differentiation

Emergent research has been focused in elucidating the role of intracellular Ca^{2+} signalling during cell differentiation. A recent systematic literature review suggested that stem cell differentiation is triggered by transient oscillations of $[Ca^{2+}_i]$, and the different nature of these oscillations could determinate specific cell fates (Pinto et al., 2016). This statement was based in previous published data where it was demonstrated that erythrocyte, neurons and muscles cells differentiation are initiated by global increases of $[Ca^{2+}_i]$ (Gu et al., 1994; Miller et al., 1988; Miller et al., 1989). Moreover, it has been observed that physical manipulation of intracellular Ca^{2+} oscillations of mesenchymal cells (MSC) can lead to cell commitment into the osteoblast lineage (Sun et al., 2007). Therefore, there is a growing body of literature that recognises the importance of intracellular Ca^{2+} oscillations during the initiation of cell commitment into specific cell fates.

Intracellular Ca^{2+} oscillations play a critical role in the control of gene expression. Previous studies have demonstrated a direct link between activation of Ca^{2+} signalling pathways and activity of specific transcription factors (Dolmetsch, 2003; West et al., 2002). Changes in amplitude, spatial and temporal features of $[Ca^{2+}_i]$ could lead to the activation of different transcriptional signatures (Dolmetsch et al., 1997; Dolmetsch et al., 1998). Although growing evidences prove the importance of $[Ca^{2+}_i]$, the link between intracellular Ca^{2+} oscillations and gene transcription during cell differentiation is still poorly understood. However, a previous research reported a link between Ca^{2+} signalling and gene expression during neural differentiation (Chang and Spitzer, 2009). Therefore, there is a growing need of shedding light into this area of investigation to unravel the complex mechanisms of cellular differentiation.

6.1.4. Megakaryocytes and calcium

During early megakaryocyte maturation stages, cells display few undeveloped membranous organelles, such as the Golgi apparatus and ER. However, it is characteristic of megakaryocyte maturation an increase of the cytoplasmic area, which is accompanied by an expansion of ER, essential for the DMS (Eckly et al., 2014; Ru et al., 2016). During this process there is profound reorganisation of ER Ca^{2+} pumps and channels that lead to a tight control of $[Ca^{2+}_i]$ during megakaryopoiesis (Lacabaratz-Porret et al., 2000; Nurden et al., 2006). Previous research demonstrated that SERCA3 expression increases in the latest stages of megakaryocyte differentiation, as well as IP3RI/II (Lacabaratz-Porret et al., 2000). Further evidence suggests the important role of Ca^{2+} during this process. For example, TPO signalling leads to a change of cellular Ca^{2+} in megakaryocytes (den Dekker et al., 2001). Thus, reorganisation of Ca^{2+} ER storage and Ca^{2+} signalling could be key elements to maintain a tight control of megakaryopoiesis.

Of note, NMDARs have been described to be highly expressed in megakaryocytes (Genever et al., 1999) and also, these receptors could have a pivotal role in regulating megakaryocyte functions (Hitchcock et al., 2003). A recent publication demonstrated that leukemic blasts treated with NMDARs antagonist such as Nemamtine or Riluzole, reduced proliferation and increased megakaryocyte-like characteristics, such as polyploidy and cell morphology (Kamal et al., 2015). Hence, it is possible that changes in the $[Ca^{2+}_i]$ caused by NMDARs inhibition could activate megakaryocyte commitment, as previously described with other cell types (Sun et al., 2007).

Although much research has been focused in the understanding of the role of intracellular Ca^{2+} during megakaryocyte differentiation, a recent publication revealed that Ca^{2+} is also essential for the regulation of megakaryocyte physiological functions (Di Buduo et al., 2014). This previous investigation demonstrated that Ca^{2+} mobilisation from the ER and extracellular Ca^{2+} entry by SOCE machinery in human megakaryocytes directly regulate important cellular functions, such as megakaryocyte adhesion to the extracellular matrix, megakaryocyte motility and proplatelet formation (Di Buduo et al., 2014). However, further investigation is needed to help to understand the complex functions of Ca^{2+} during megakaryocyte differentiation, survival and correct cellular functions.

6.1.5. Calcium and pathological megakaryocyte production

Megakaryocyte hyperplasia has been previously linked with abnormal Ca^{2+} homeostatic regulation (Di Buduo et al., 2016). Interestingly, mice expressing an activated form of STIM1 which results in an increase of $[Ca^{2+}{}_i]$, displayed megakaryocyte hyperplasia (Grosse et al., 2007). Noteworthy, after 6 months, these mice showed bone marrow fibrosis and splenomegaly, both pathological characteristics of PMF (Grosse et al., 2007). Therefore, a tight control of $[Ca^{2+}{}_i]$ by cell membrane Ca^{2+} channels and the ER in megakaryocytes could be a key element to maintain a tight balance of megakaryocyte production. However, to which extent Ca^{2+} homeostasis contributes to MPNs development remains to be clarified.

Based on the current information about the role of intracellular Ca^{2+} in megakaryocytes, previous publication hypothesised that rise in $[Ca^{2+}{}_i]$ could promote megakaryocyte proliferation, motility and increased platelet production (Di Buduo et al., 2016) (Figure 34). Coincidently these characteristics are pathological features in ET and PMF.

CALR mutations described in PMF and ET are thought to influence Ca^{2+} buffering capacity of this protein during megakaryocyte hyperplasia. To this regard, previous research using primary mature megakaryocytes harbouring *CALR* type 1 and type 2 mutations demonstrated that these mutations enhanced ER Ca^{2+} release under cyclopiazonic acid (CPA) treatment. Of note, CALR type 1 showed significant higher ER Ca^{2+} release values than CALR type 2 mutant cells (Pietra et al., 2015). Interestingly, *CALR* type 1 is associated with worst disease prognosis than type 2 (Cabagnols et al., 2015). To this extent it could be possible that differences in Ca^{2+} homeostasis caused by these mutations could lead to the different disease phenotype, although more data is essential to understand the link between abnormal Ca^{2+} homeostasis and the different subtypes of *CALR* mutations. Moreover, analysis of MARIMO cells in response to thapsigargin have also showed deregulated ER Ca^{2+} buffering activity (Kollmann et al., 2015). However, the registered ER Ca^{2+} homeostasis shown in this previous study was opposite to the results published in primary megakaryocytes (Pietra et al., 2015), therefore showing discrepancies in our understanding of CALR mutant ER Ca^{2+} buffering activity.
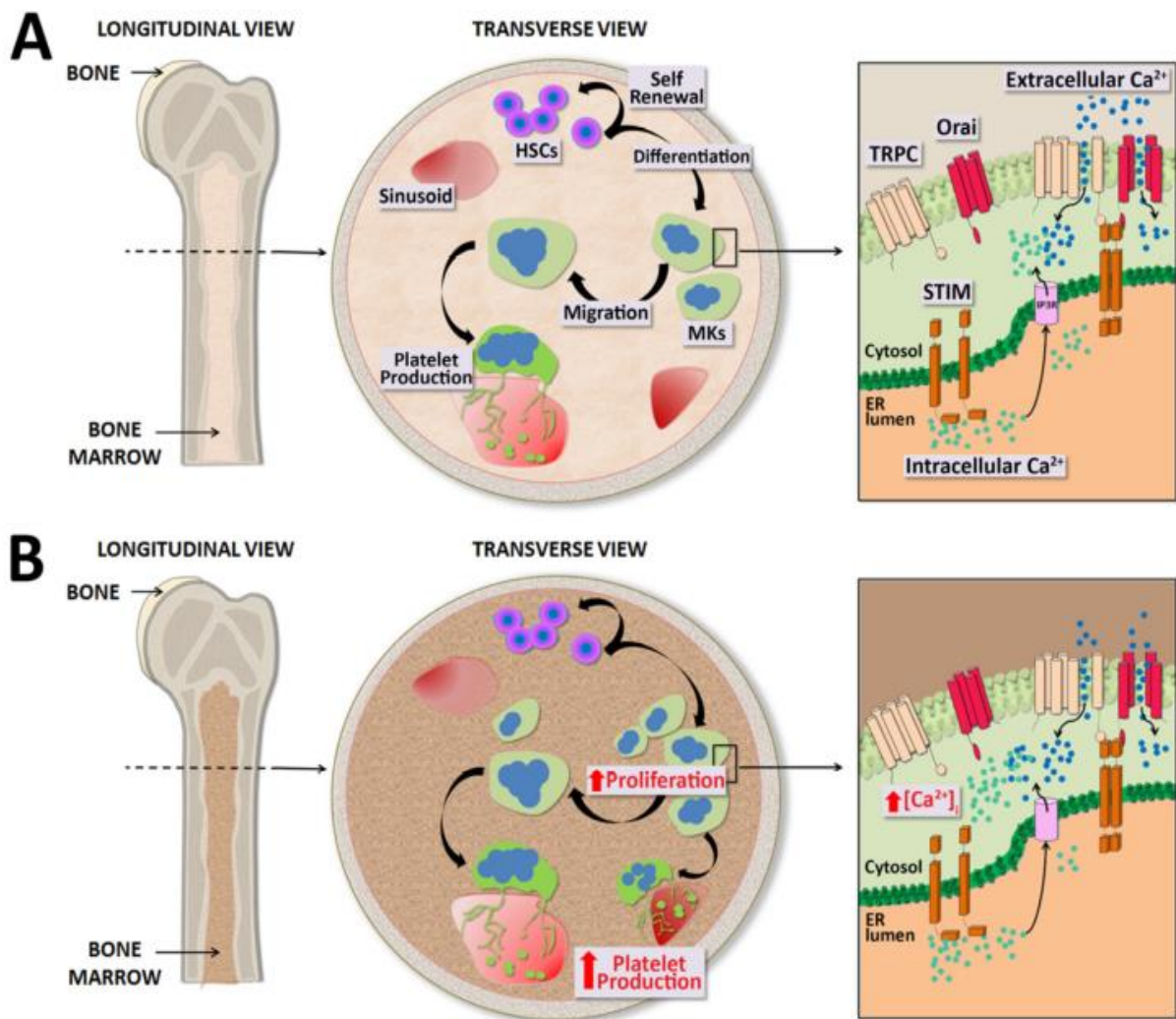
Figure 34. Proposed model of megakaryocyte hyperplasia induced by increase [Ca2+I].

A) Physiological megakaryocyte formation. **B)** Pathological megakaryocyte formation occasioned by abnormal Ca^{2+} homeostasis during the differentiation of megakaryocytes. Previous data showed the relevance of SOCE machinery during MPNs development, however further analysis need to be completed to fit the role of CALR mutant within this model. Figure reproduced from (Di Buduo et al., 2016).

6.1.6. Methods to study intracellular calcium

Considering the relevance of Ca^{2+} signalling for many cellular processes, the development of techniques to measure intracellular Ca^{2+} levels has been a major focus of research for many years. Nowadays, the use of fluorescent Ca^{2+} indicators is a common and successful technique to study intracellular Ca^{2+} processes (Paredes et al., 2008). Currently, there are two different types of Ca^{2+} indicators: genetically modified proteins or chemically engineered fluorophores.

However, chemical indicators offer major advantages, such as their easy manipulation, the availability of many well established loading protocols (Takahashi et al., 1999; Paredes et al., 2008) and importantly, these dyes do not require to be transfected or overexpressed within cells.

Chemical intracellular Ca^{2+} indicators are classified in three different groups according with their chemical forms: salts, dextran conjugates or acetoxymethyl (AM) esters (Paredes et al., 2008). The salt Ca^{2+} indicators require invasive cell loading techniques, such as microinjections, due to their membrane impermeability characteristic. Also, once these indicators cross the membrane could be compartmentalised in vacuoles within the cytosol and are consequently degraded within 30 minutes to an hour. Dextran conjugates show no compartmentalisation issues although they still require invasive cell loading procedures (Paredes et al., 2008). Finally, AM indicators offer easier cell loading methods, as AM dyes are membrane permeable and can cross the cellular membrane passively. Once the dye reaches the cytoplasm, cellular esterases cleave the AM group and the fluorescent dye is trapped inside the cell (Paredes et al., 2008; Tsien, 1981).

Once optimal Ca^{2+} indicators are selected for the experimentation, multiples techniques are used to study the Ca^{2+} buffering capacity and Ca^{2+} dynamics within the cell. Ca^{2+}channel blockers (CCBs) are widely used to manipulate *in vitro* the cellular Ca^{2+} dynamics. Therefore, CCBs could be widely used to analyse the effects of inhibiting specific Ca^{2+} channels within the cell. Although a variety of CCBs are commonly used in clinic to treat many different disorders, such as vascular diseases or migraines, (Olson et al., 2005) these drugs are extremely useful in research. For example, BTP-2 and Riluzole, inhibitors of SOCE and NMDR receptors respectively, were used in previous research to demonstrate the role of both Ca^{2+} channels in megakaryocytes (Di Buduo et al., 2014; Kamal et al., 2015). As well as Fendiline, an L-Type Ca^{2+} channel and calmodulin antagonist, which has been used to prove the importance of Ca^{2+} dynamics on platelet aggregation (Luckhoff et al., 1991)

6.1.7. Aims of the study

The existing body of research suggests a central role of $[Ca^{2+}_i]$ during cell fate differentiation. However, the link between $[Ca^{2+}_i]$ and megakaryocyte differentiation remains poorly understood. Intriguingly, *CALR* mutations described in MPNs raise new questions about the importance of this ion during abnormal megakaryocyte maturation in ET and PMF. Therefore, the analysis of Ca^{2+} dynamics during megakaryocyte formation is a major step that will lead to a better understanding of megakaryocyte cell fate differentiation in physiological conditions and disease. Thus, during this investigation, three major aims were addressed:

I.   Determine the existence of $[Ca^{2+}_i]$ oscillations during megakaryocyte cell commitment in physiological conditions.

II. Characterisation of the effects of *CALR* mutations in Ca^{2+} dynamics by analysing $[Ca^{2+}_I]$, cellular ER Ca^{2+} buffering activity and quantification of the stored ER Ca^{2+} in different megakaryocyte differentiation stages.

III. Study the effects of physical manipulation of $[Ca^{2+}_i]$ by using different CCBs as inductors of megakaryocyte like phenotype in leukemic blasts.

6.2. Results

6.2.1. Building a model of [Ca$^{2+}_i$] oscillations during megakaryocyte differentiation.

[Ca$^{2+}_i$] oscillations have been described to be essential in many cell fate differentiation (Sun et al., 2007; Gu et al., 1994). One purpose of this study was to analyse whether there are transient oscillations of [Ca$^{2+}_i$] that could determinate the nature of megakaryocyte cell fate in physiological conditions. For that, [Ca$^{2+}_i$] was measured during megakaryopoiesis using three different cellular models, two leukemic cell lines with potential to differentiate into megakaryocytes, K562 and DAMI cells, as well as primary mouse bone marrow cells. To measure [Ca$^{2+}_i$] an intracellular Ca^{2+} indicator known as Fluo-8-AM was used during this study. Fluorescence intensity was quantified with flow cytometry at different time points during megakaryocyte maturation.

Analysis of [Ca$^{2+}_i$] oscillations during K562 induced megakaryopoiesis

K562 cells are characterised as highly undifferentiated cells. However, as previously described; these cells differentiate into megakaryocytes after 72 hours of 5 nM PMA incubation (See section 5.2.4) (Kang et al., 1996; Hirose et al., 2013; Huang et al., 2014). Analysis of [Ca$^{2+}_i$] during the *in vitro* megakaryopoiesis of K562 cells could allow to determine [Ca$^{2+}_i$] levels, since early differentiation stages until megakaryocyte like cells.

Results showed that during the first stages of megakaryocyte commitment [Ca$^{2+}_i$] raised significantly in a 6 ~ fold ratio compared with the control during the first 24 hours. Afterwards, [Ca$^{2+}_i$] showed a gradual decrease over time (Figure 35). 72 hours after PMA megakaryocyte induction, mature cells displayed a significant increase of [Ca$^{2+}_i$] of 3 ~ fold compared with the initial K562 cells (Figure 35 A).

Overall, these results showed that [Ca$^{2+}_i$] oscillate over time, in hours scale, during megakaryocyte cell fate differentiation of K562 cells. Additionally, it showed a significant increase in [Ca$^{2+}_i$] which could be required for the commitment into the megakaryocyte lineage.

A)

[Ca²⁺]I during K562 megakaryopoiesis

B)
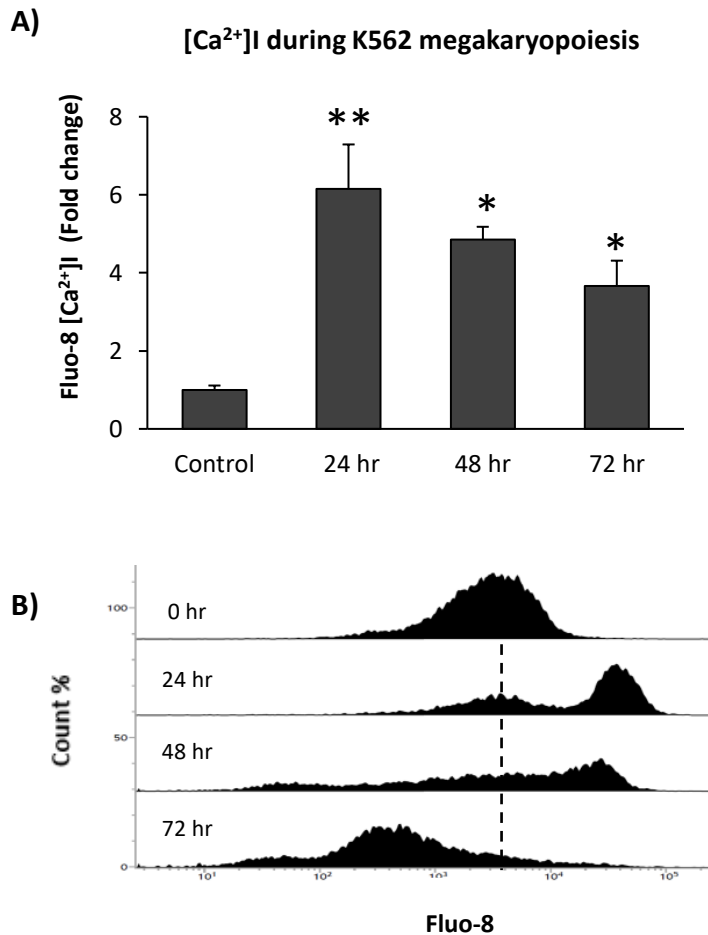
Figure 35. [Ca2+i] oscillations during K562 megakaryocyte formation.

K562 cells were subjected to 5 nM PMA treatment for 72 hours and then Fluo-8 fluorescence was quantified by flow cytometry **A)** Average quantification of [Ca²⁺ᵢ] over time during K562 megakaryopoiesis. **B)** Representative histogram of [Ca²⁺ᵢ] oscillations over 72 hours. Results were averaged between three independent experiments. Values represent mean ± SEM for each group. n=3. **P<0.01, *P<0.05. Student T.test

Analysis of [Ca²⁺ᵢ] oscillations in mouse bone marrow cells during in vitro megakaryopoiesis

Further analysis aiming to study [Ca²⁺ᵢ] oscillations during megakaryocyte formation were performed. Mouse bone marrow cells were induced to differentiate toward the megakaryocyte lineage and [Ca²⁺ᵢ] was subsequently analysed in different maturation stages. To induce differentiation, bone marrow cells were incubated with TPO (10 µg/ml) over 10 days. To select three different populations with different maturation status along the megakaryocyte lineage, CD117 (cKIT) and CD41a cell surface markers were used for the flow cytometry gating strategy based on previous publication (Hunt et al., 1992). HSC/Early

progenitors (CD117$^+$, CD41a$^-$), megakaryocyte progenitors/early mature megakaryocyte (CD117$^+$, CD41a$^+$) and mature megakaryocytes (CD117$^-$, CD41a$^+$) were gated in order to analyse the [Ca$^{2+}_i$] levels within these three different populations (Figure 36). The [Ca$^{2+}_i$] of each cellular population was measured using Fluo-8-AM staining together with CD117 and CD41a markers. Measurements were taken at day 1, day 5 and day 10 during this process.

Optimal gating of the three cellular populations of interest was firstly established. Then, further analysis to decipher the [Ca$^{2+}_i$] of these populations was carried out. As expected, over the 10 days since the exposure of cells to TPO, the fluorescent intensity of CD117 decreased and CD41a increased gradually, together with changes in the number of HSC/progenitors, megakaryocyte progenitors and mature megakaryocytes (Figure 36). First day after TPO treatment, HSC/progenitors population had a significant higher number of events compared to the following 10 days (Figure 36 C). At day 5, the number of megakaryocyte progenitors increased (Figure 36 D) and finally, after 10 days, the events of mature megakaryocytes increased significantly (Figure 36 E). Therefore, changes in the number of events of each cell population suggested an efficient cell differentiation towards the megakaryocyte lineage within the culture.

Once it was corroborated that megakaryopoiesis was taking place within the culture, the [Ca$^{2+}_i$] of these three cellular populations was analysed to obtain levels of [Ca$^{2+}_i$] during dynamic conditions of differentiation, rather than in static cellular differentiation stages within the culture. Results showed significant differences of [Ca$^{2+}_i$] between the different stages of maturation. Interestingly, HSC/early progenitors showed significant lower levels of [Ca$^{2+}_i$] compared with megakaryocyte progenitors and mature megakaryocytes. Early megakaryocyte progenitors rise [Ca$^{2+}_i$] compared with HSC/progenitors population and finally, mature megakaryocytes displayed a reduction of [Ca$^{2+}_i$] compared with megakaryocyte progenitors (Figure 37).

Figure 36. In vitro megakaryopoiesis of mouse bone marrow cells.

Purified mouse bone marrow cells were incubated with TPO (10 µg/ml) for 10 days. **A)** Changes in cell populations within the 10 days. **B)** CD117 and CD41 fluorescent fluctuations during 10 days of treatment. **C)** Quantification of number of events within each population during the 10 days of incubation. Values represent mean ± SEM for each group. n=3

Therefore, different megakaryocyte maturation stages display differences in $[Ca^{2+}_i]$ which could be directly linked with the functionality of these cells. $[Ca^{2+}_i]$ levels of primary

HSC/progenitors, megakaryocyte progenitors and megakaryocytes agreed with the previously oscillations described during K562 megakaryocyte induction. Overall, megakaryocyte commitment displays an increase in [Ca^{2+}_i] which is maintained in early megakaryocyte progenitors. Then during final maturation this [Ca^{2+}_i] decreases until reaching the required levels for mature megakaryocytes.
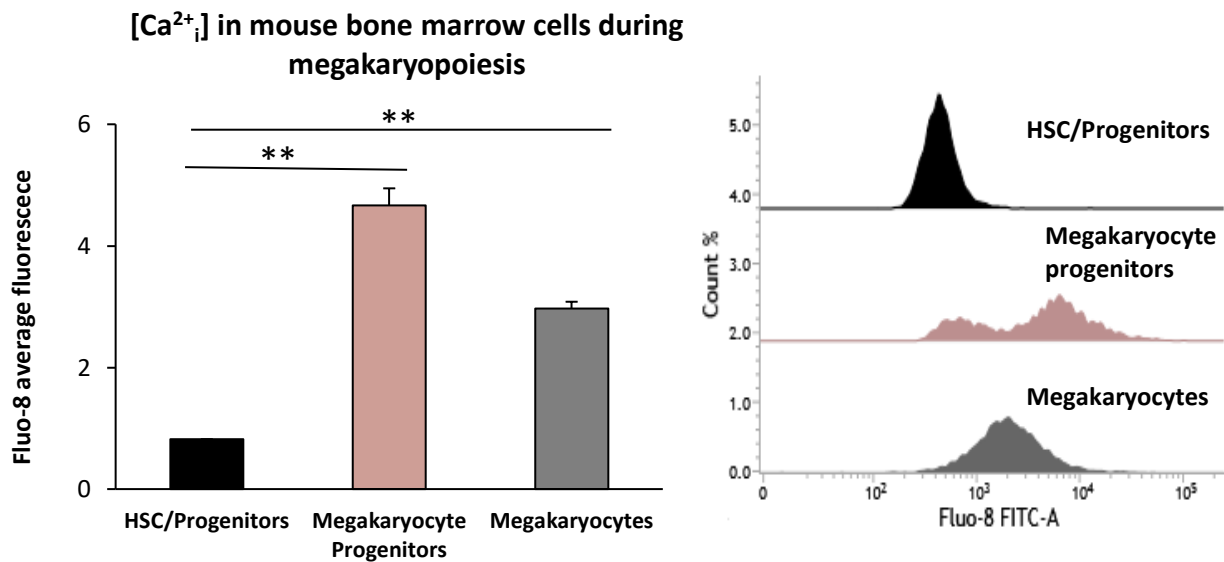
Figure 37. [Ca^{2+}_i] levels of HSC/Progenitors, megakaryocyte progenitors and megakaryocytes during in vitro megakaryopoiesis of mouse bone marrow cells.
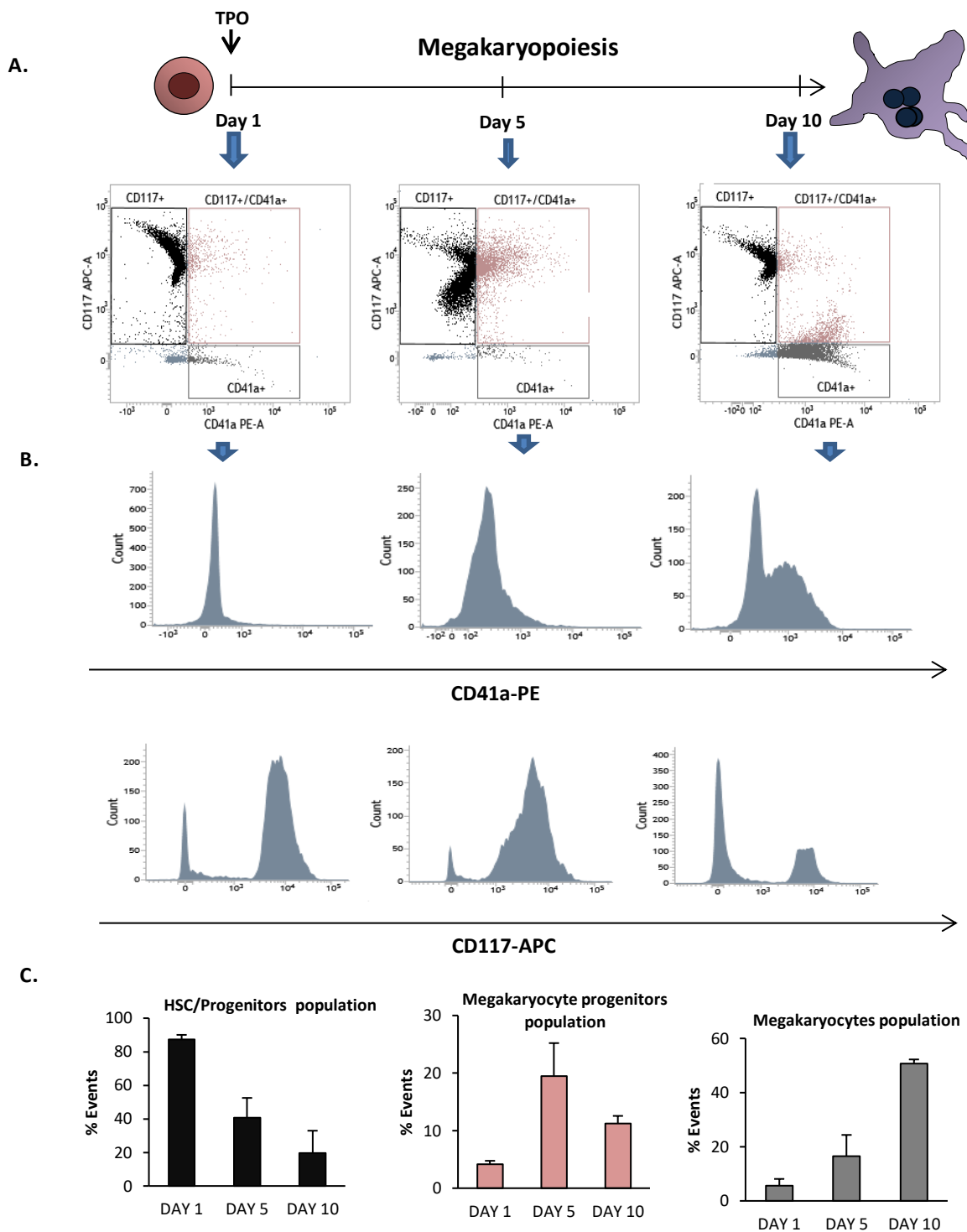
Purified mouse bone marrow cells were incubated with TPO (10 μg/ml) for 10 days and [Ca^{2+}_i] levels of selected cellular populations were analysed using Fluo-8 staining and flow cytometry. Figure shows average quantification of [Ca^{2+}_i] levels of HSC/Progenitors, megakaryocyte progenitors and megakaryocytes and a representative histogram of [Ca^{2+}_i] oscillations. Values represent mean ± SEM for each group. n=3. **$P<0.01$, *$P<0.05$. Student T.test

Analysis of [Ca^{2+}_i] oscillations in DAMI cells during induced megakaryopoiesis

Final analysis aiming to investigate the link between the last stage of megakaryocyte maturation and decrease of [Ca^{2+}_i] was performed. DAMI cell line, which is known to differentiate from megakaryoblast to megakaryocyte, when exposed to PMA, was used for this experiment (Greenberg et al., 1988). (See section 5.2.4). [Ca^{2+}_i] was quantified after the maturation of DAMI cells into mature megakaryocytes to verify the decrease of [Ca^{2+}_i] during this last stage of megakaryocyte differentiation.

As expected, megakaryocyte maturation of DAMI cells showed a decrease in $[Ca^{2+}_i]$ after PMA treatment (Figure 38). DAMI mature megakaryocytes displayed a decrease of 0.6 ~ fold compared to the control (Figure 38). Therefore, these results agreed and validated the previous statement where it is proposed a decrease in $[Ca^{2+}_i]$ during final mature megakaryocyte differentiation.

$[Ca^{2+}_i]$ during DAMI megakaryopoiesis
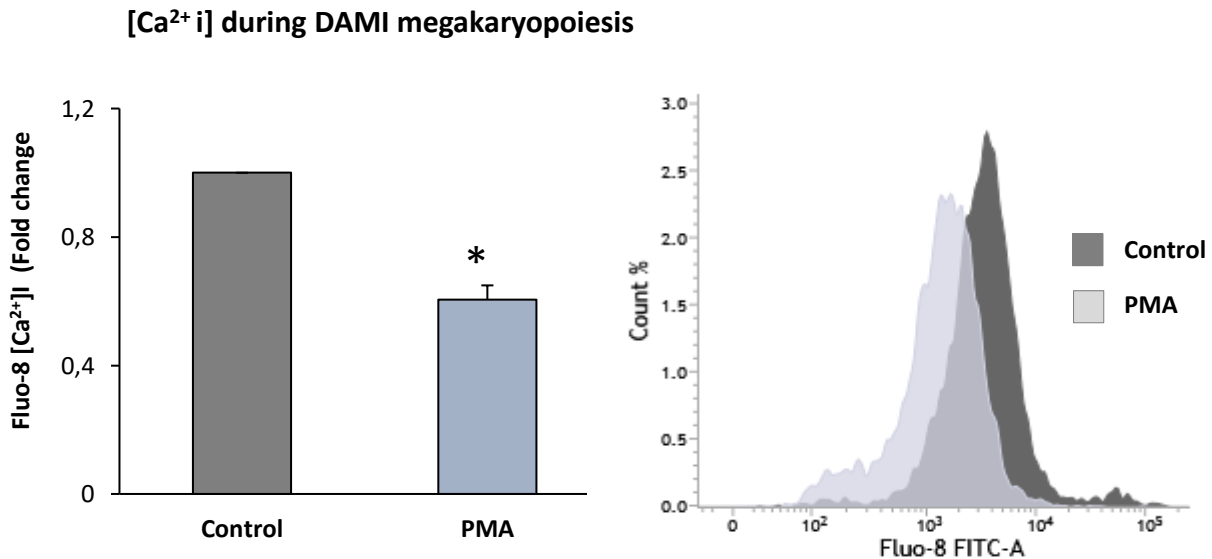
Figure 38. [Ca2+i] oscillations during DAMI megakaryocyte formation.

DAMI cells were subjected to 5 nM PMA treatment for 72 hours and then Fluo-8 fluorescence was quantified by flow cytometry **A)** Average quantification of $[Ca^{2+}_i]$ over time during DAMI megakaryocypoiesis. **B)** Representative histogram of $[Ca^{2+}_i]$ oscillations. Results were averaged between three independent experiments. Values represent mean ± SEM for each group. n=3. **P<0.01, *P<0.05. Student T.test

Overall these experiments showed a rather remarkable result. Analysis of $[Ca^{2+}_i]$ during megakaryocyte formation of three different cellular models revealed novel insights of Ca^{2+} dynamics during megakaryopoiesis. Together, these results demonstrate that there are intracellular Ca^{2+} oscillations during megakaryocyte cell fate differentiation. The model described here showed that initial megakaryocyte commitment displays an increase of $[Ca^{2+}_i]$ followed by a decrease of this ion within the cytoplasm during the last stages of megakaryocyte maturation (Figure 39). These intracellular changes could be essential for initial megakaryocyte commitment and further functionality of mature megakaryocytes and platelets.
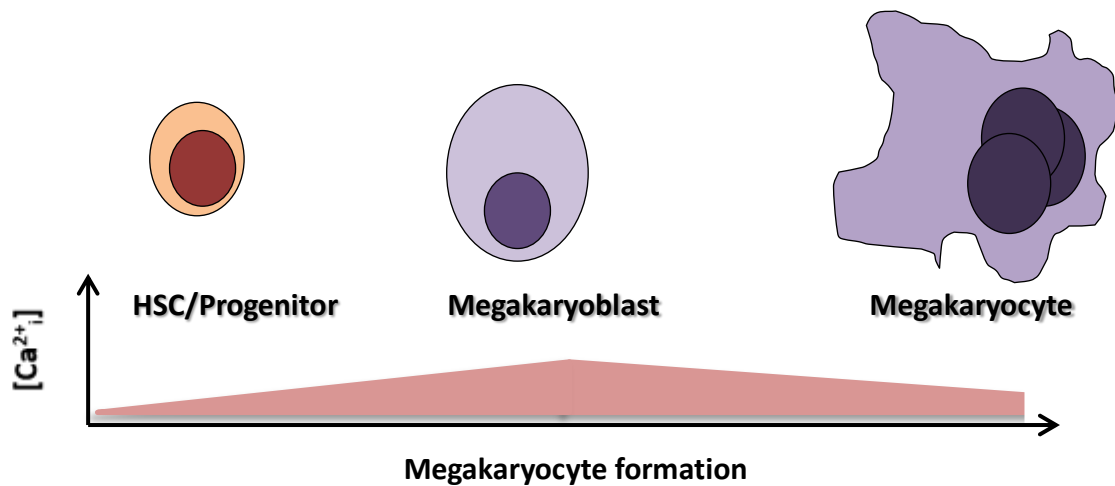
Figure 39. Model proposed in this study of [Ca^{2+}$_i$] oscillations during megakaryocyte formation in physiological conditions

6.2.2. Analysis of the specificity of [Ca^{2+}$_i$] oscillations during cell differentiation of different blood lineages

The previous experiments do not determinate whether the established model of [Ca^{2+}$_i$] oscillations is only characteristic for megakaryocyte differentiation or it is common during cell fate determination in the haematopoietic lineage. Therefore, to unravel the pattern of [Ca^{2+}$_i$] oscillations during different cell fate commitment, this investigation further analysed [Ca^{2+}$_i$] during erythropoiesis.

K562 cells are a known established model to study megakaryocyte and erythrocyte formation (Huo et al., 2006). Therefore, K562 cells were selected as a model to analyse the differences of [Ca^{2+}$_i$] oscillations between erythropoiesis and megakaryopoiesis. Hence, optimal conditions for K562 erythrocyte commitment *in vitro* were stablished. [Ca^{2+}$_i$] levels were measured and consequently compared with K562 megakaryopoiesis [Ca^{2+}$_i$] data.

K562 erythropoiesis was induced with 50 µM Hemin treatment for 72 hours and erythrocyte induction was tested using CD235 erythrocyte cell surface marker and flow cytometry. K562 50 µM Hemin treatment resulted in a significant increase in CD235a expression within the cell surface in almost 80% of these cells (Figure 40 A, B). Moreover, haemoglobin production was visualised by an increased red cell pellet compared with the control (Figure 40 C), as

previously described (Zhang et al., 2007). Cell death assay showed that Hemin treatment induced ~30% cell death (Figure 40 D).
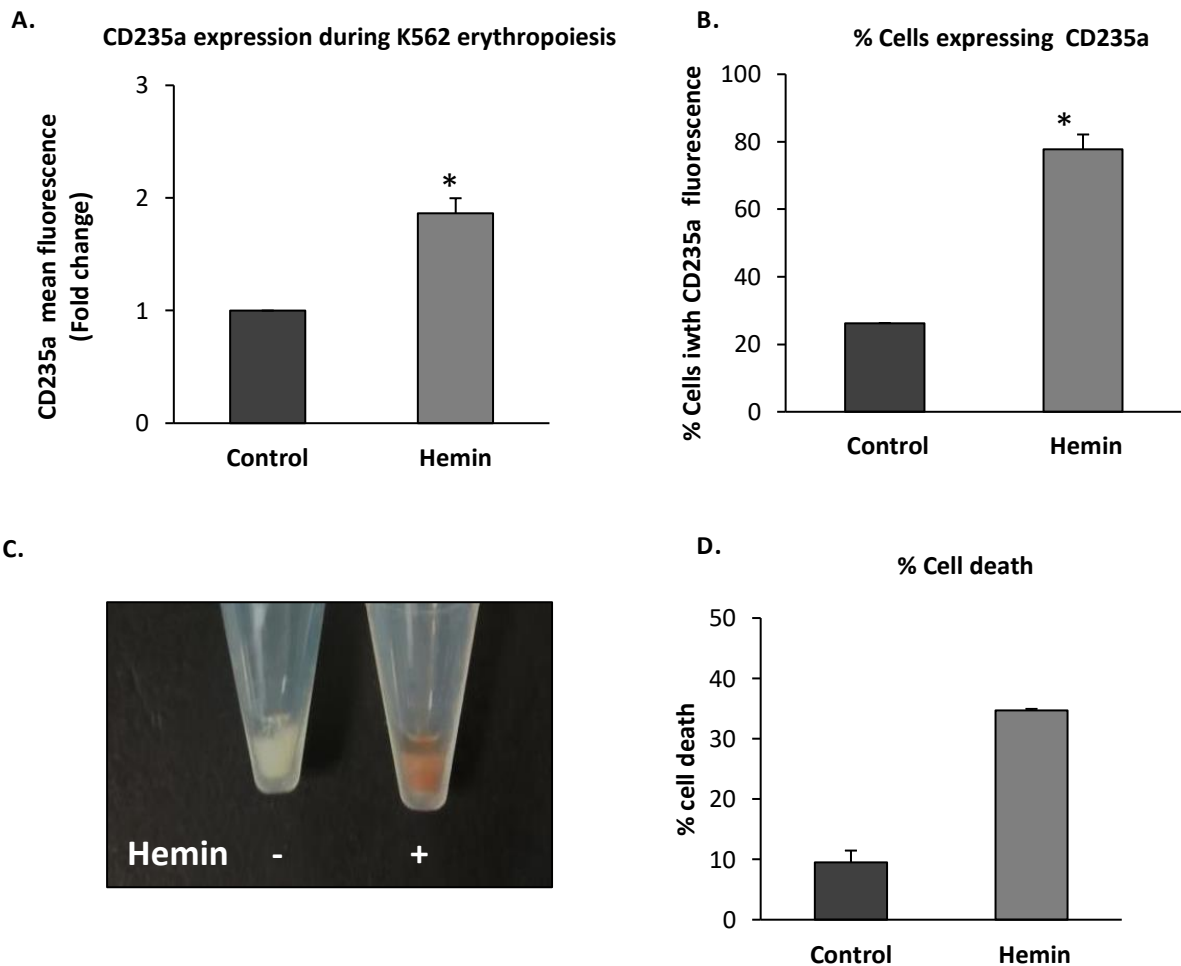
Figure 40. K562 cells under Hemin treatment display erythrocyte characteristics.

A, B) Increase expression of CD235 marker in the cell surface after 72 hr of Hemin treatment.**C)** Change of color after Hemin treatment. Results were averaged between three independent experiments. Values represent mean ± SEM for each group. n=3. **P<0.01, *P<0.05. Student T.test

Once K562 erythropoiesis was confirmed, $[Ca^{2+}_i]$ was analysed during this process. Surprisingly, K562 treatment with Hemin and PMA led to a significant difference in $[Ca^{2+}_i]$ oscillations during cell fate differentiation (Figure 41). K562 incubated with Hemin displayed a gradual increase of $[Ca^{2+}_i]$, reaching a significant increase of 3 ~ fold compared with the control at 72 hours incubation (Figure 41).
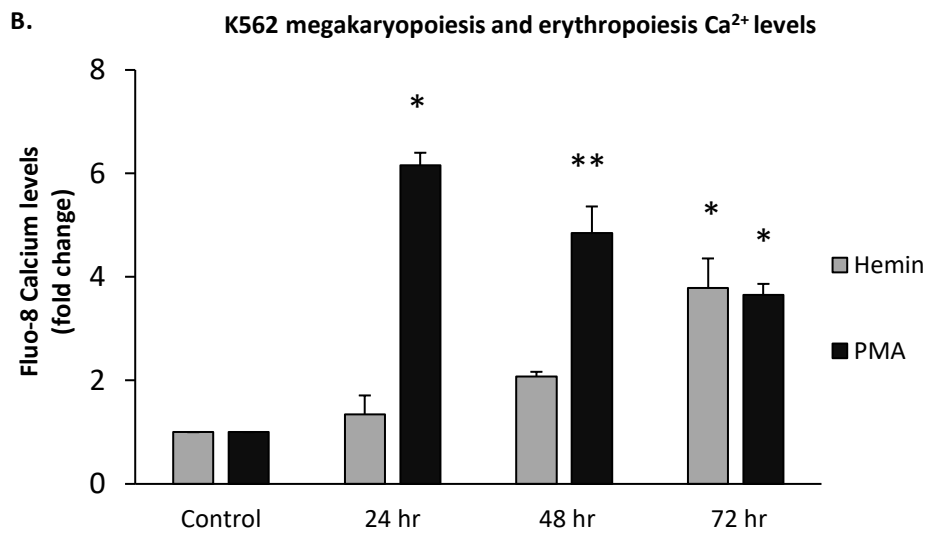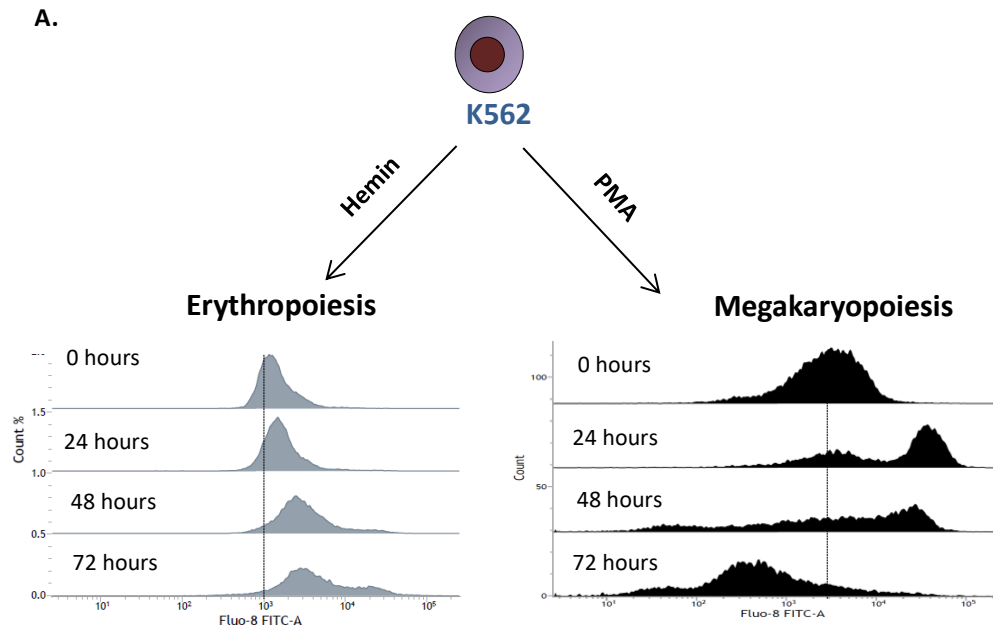
Figure 41. [Ca2+i] fluctuations during K562 erythropoiesis and megakaryopoiesis.

A) Representative histogram showing the difference of basal calcium over time during K562 erythropoiesis and megakaryopoiesis. **B)** Results were averaged between three independent experiments. Values represent mean ± SEM for each group. n=3. **P<0.01, *P<0.05. Student T.test

Taken together, the data emerged from this study show a specific pattern of Ca^{2+} oscillation on a temporal scale during cell differentiation, therefore, suggesting an important role of this molecule during the haematopoietic commitment.

6.2.3. Ca^{2+} dynamics in CALR mutant cells: an integrative analysis of different megakaryocyte differentiation stages.

CALR mutations lead to a deletion of the majority of Ca^{2+} binding sites and reduce the acidity of this C-terminal domain. Therefore, CALR mutations described in MPNs might affect the intracellular Ca^{2+} dynamics during megakaryocyte hyperplasia. This study aimed to analyse the Ca^{2+} dynamics in CALR mutant cells in two different stages of megakaryocyte differentiation: early blast stage and mature megakaryocytes. In order to analyse Ca^{2+} dynamics within these cells the [Ca$^{2+}_i$], the ER Ca^{2+} buffering activity and the amount of Ca^{2+} stored within the ER were analysed.

6.2.3.1. Basal [Ca$^{2+}_i$] of leukemia blasts harbouring CALR mutations

To understand how CALR mutations affect Ca^{2+} dynamics within the cell, initial experiments were focussed on analysing [Ca$^{2+}_i$] in CALR mutant cells during early stages of cell differentiation.

Firstly, [Ca$^{2+}_i$] of MARIMO cells were analysed and compared to K562 [Ca$^{2+}_i$]. Interestingly, results showed a significant difference of [Ca$^{2+}_i$] between the two cell lines (Figure 42). MARIMO cells displayed a decrease in [Ca$^{2+}_i$] compared with K562 level (Figure 42). These results suggested that CALR mutation L367fs*43 could affect Ca^{2+} homeostasis of CALR mutant cells.

Next, further analysis of basal [Ca$^{2+}_i$] within the megakaryoblast stage were performed. DAMI cells overexpressing CALR wt, CALR type 1 and CALR type 2 were used for this experiment. Results showed a significant decrease in [Ca$^{2+}_i$] in CALR type 2 cells compared with the control (Figure 43). Additionally, a small decrease in the [Ca$^{2+}_i$] of CALR type 1 cells was described, although results were not significant (Figure 43). These results demonstrated that CALR mutations lead to an overall decrease in [Ca$^{2+}_i$] during early stages of differentiation and this could have an impact in the Ca^{2+} signalling during initial megakaryopoiesis in ET and PMF.

A.
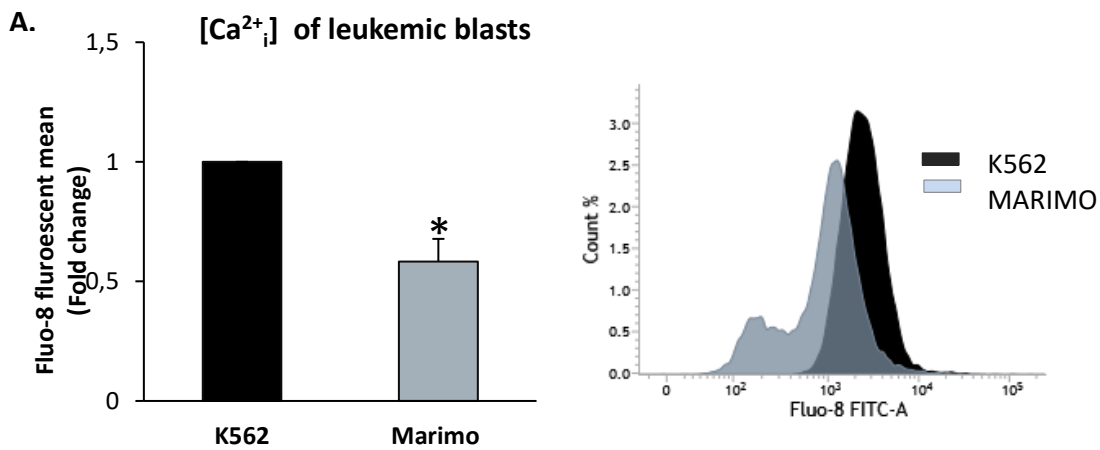
Figure 42. [Ca^{2+}$_i$] levels in leukemic blasts.

Cells were stained using FLUO-8-AM and basal intracellular Ca^{2+} levels were quantified by flow cytometry. Results were averaged between three independent experiments. Values represent mean ± SEM for each group. n=3. **P<0.01, *P<0.05. Student T.test

A.
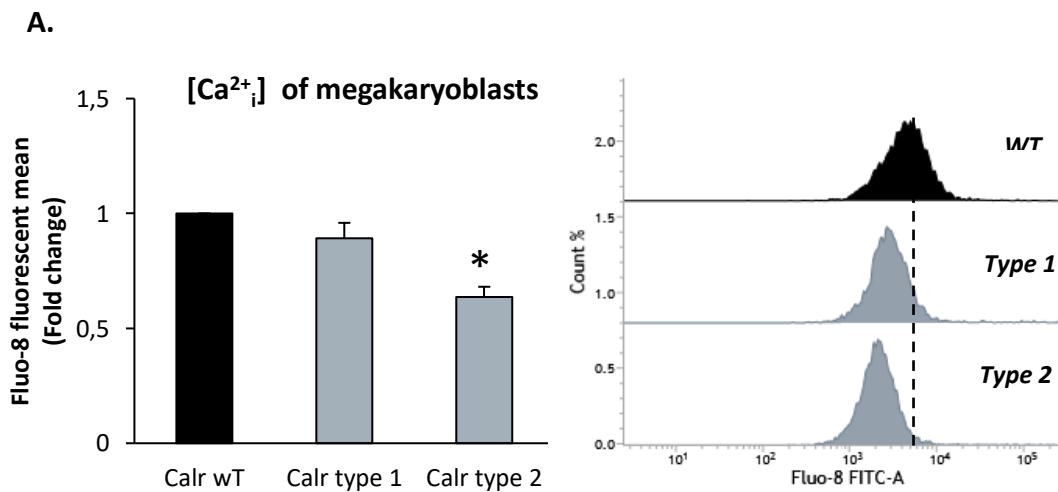
Figure 43. [Ca^{2+}$_i$] levels in DAMI cells overexpressing CALR wt, type 1 and type 2 mutations.

Cells were stained using FLUO-8-AM and basal intracellular Ca^{2+} levels were quantified by flow cytometry. Results were averaged between six independent experiments. Values represent mean ± SEM for each group. **P<0.01, *P<0.05. Student T.test.

6.2.3.2. ER Ca²⁺ buffering activity of leukemic blasts harbouring CALR mutations

CALR mutations are described to be present from early stages of cellular differentiation. As previously described, CALR mutant cells in blast stages display lower $[Ca^{2+}_i]$. Cellular $[Ca^{2+}_i]$ is highly regulated by the ER Ca^{2+} buffering activity. Therefore, to further characterise the effects of *CALR* mutations, the ER Ca^{2+} buffering activity of cells in early stages of differentiation were analysed. To evaluate cytoplasmic Ca^{2+} mobilisation from the ER, cells were exposed to thapsigargin (1 µM). Thapsigargin is a SERCA inhibitor which treatment results in an increase of $[Ca^{2+}_i]$ as a consequence of preventing ER Ca^{2+} sequestration and finally leading to ER Ca^{2+} depletion. This technique is commonly used to study the ER Ca^{2+} levels within the cells. During this experiment cells were stained with Fluo-8-AM and $[Ca^{2+}_i]$ were registered up to 15 minutes after thapsigargin treatment using flow cytometry.

Initial analysis was carried out using MARIMO and K562 cell lines. As expected, thapsigargin ER Ca^{2+} depletion induced an increase of $[Ca^{2+}_i]$ due to passive release of the ER Ca^{2+} storage into the cytoplasm (Figure 44 A). Afterwards, $[Ca^{2+}_i]$ decreased to the baselines levels of Ca^{2+} registered in both cell lines (Figure 44 A) as the cellular membrane Ca^{2+} channels extruded to the extracellular medium this excess of Ca^{2+}.

Analysis of ER Ca^{2+} buffering activity in MARIMO leukemic blasts, showed a slower release of Ca^{2+} upon thapsigargin treatment, compared with the control (Figure 44 A). Moreover, quantification of the total ER Ca^{2+} released during ER depletion revealed that MARIMO cells displayed a significant lower amount of stored ER Ca^{2+} compared with K562 cells (Figure 44 B).

ER Ca²⁺flow induced by Thapsigargin in leukaemic blasts

A.

Ca²⁺ release from the ER

B.
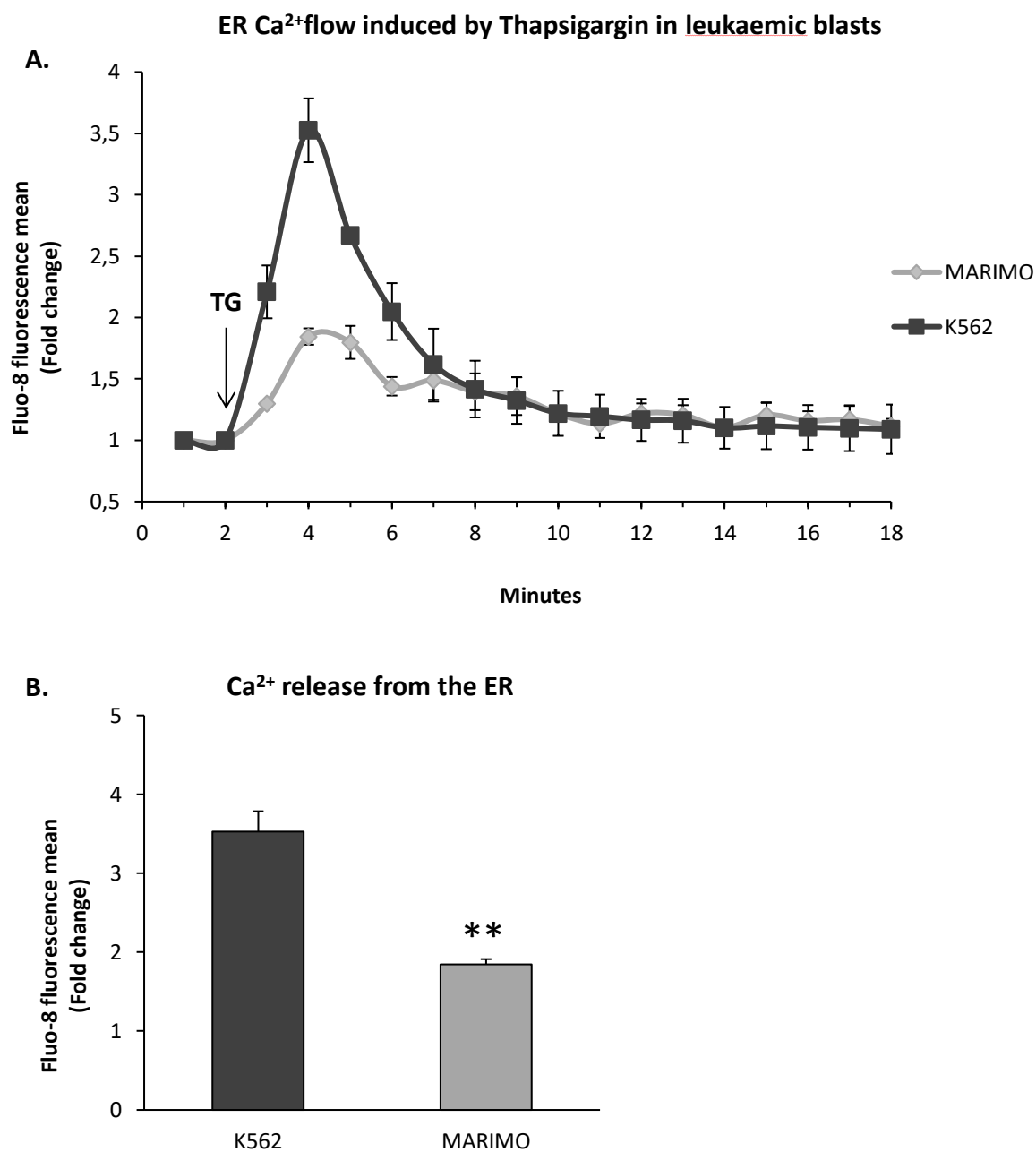
Figure 44. Fluorescence-based analysis of ER Ca2+ flow in K562 and MARIMO cells.

A) Cells were stained using Fluo-8-AM and were subsequently resuspended in PBS. Once 1 µM thapsigargin was added to the cells, fluorescence measurements were registered using flow cytometry for 15 minutes. **B)** Measurements of ER Ca^{2+} release in K562 and MARIMO cells. Values represent mean ± SEM for each group. n=3. **P<0.01, *P<0.05. Student T.test

Following the same experimental procedure, the cytoplasmic Ca^{2+} mobilisation from the ER of DAMI cells overexpressing *CALR* wt, *CALR* type 1 and type 2 mutants upon thapsigargin treatment was analysed. The experiment was performed using two different DAMI clones of each condition in triplicates.

Results showed that DAMI cells exposed to thapsigargin displayed ER Ca^{2+} depletion following the same dynamics as described with MARIMO and K562 cells (Figure 45). Interestingly, DAMI cells harbouring both *CALR* mutations, type 1 and type 2, showed a decrease of cytosolic Ca^{2+} oscillation after thapsigargin treatment (Figure 45 A). A slightly decrease in the rate of ER Ca^{2+} release was found in both mutants compared with the control (Figure 45 A). Additionally, *CALR* mutant cells showed a significant lower amount of stored ER Ca^{2+} compared with *CALR* wt DAMI cells (Figure 45 B).

Overall, there results prove that the three *CALR* mutations used during this study type 1 and type 2 together with L367fs*43 affect cytoplasmic Ca^{2+} mobilisation from the ER in cells blocked in early stages of megakaryocyte differentiation. *CALR* mutations, indistinctively of the *CALR* type of mutation, lead to a significant decrease of ER Ca^{2+} storage as well as decrease of Ca^{2+} mobilisation the cytoplasm from the ER in leukemic blasts.

ER Ca²⁺flow induced by thapsigargin in megakaryoblasts

A.

B.

Ca²⁺ release from the ER
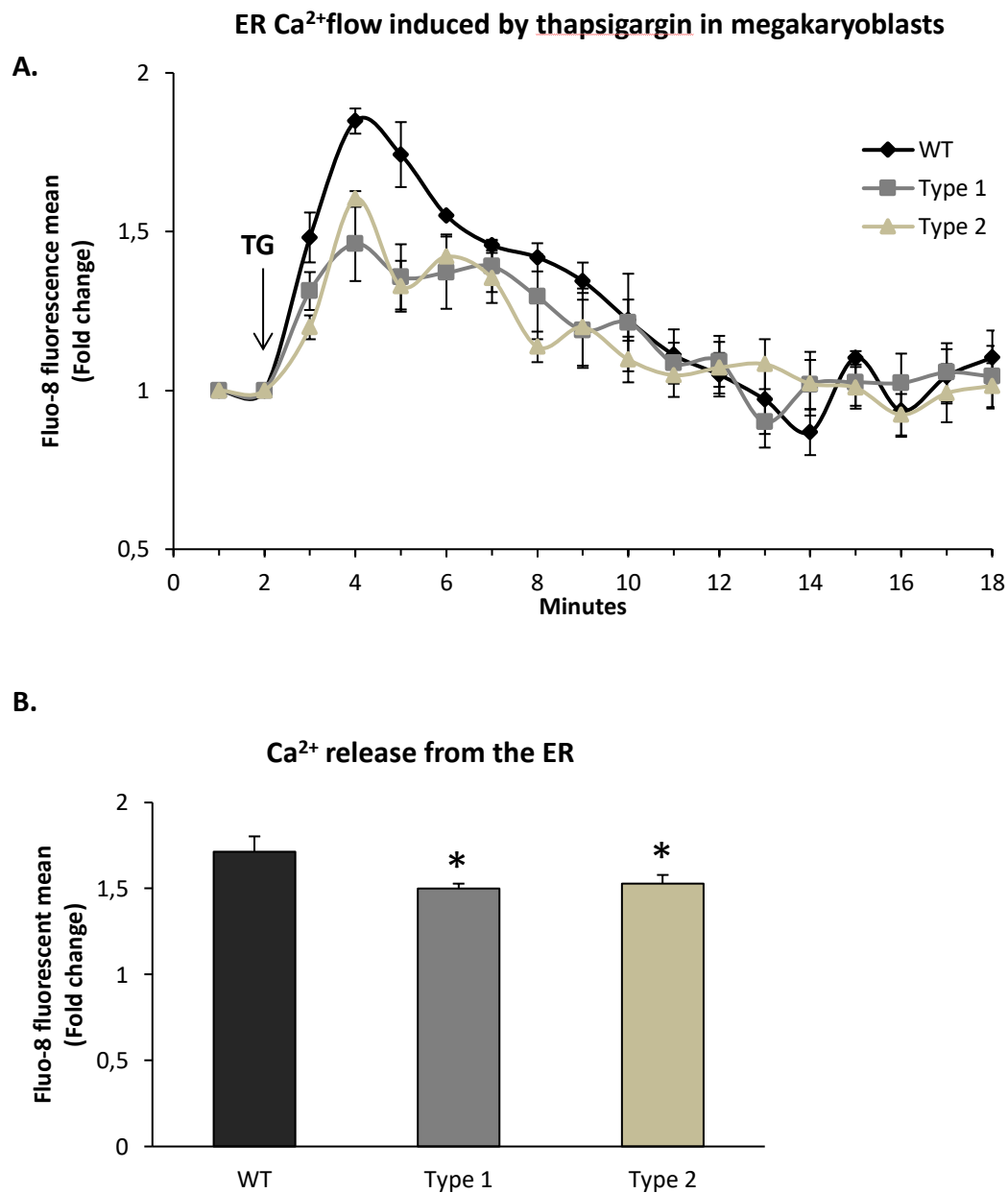
Figure 45. Fluorescence-based analysis of ER Ca2+ flow in DAMI cells overexpressing CALR WT, type 1 and type 2 mutations.

A) Cells were stained using Fluo-8-AM and were subsequently resuspended in PBS. Once 1 μM thapsigargin was added to the cells, fluorescence measurements were registered using flow cytometry for 15 minutes. Representative example of fluorescent measurements of a single clone per condition are shown. **B)** Measurements of ER Ca²⁺ release in DAMI cells. Results were averaged between six independent experiments using two different clones per condition. Values represent mean ± SEM for each group. n=3. **P<0.01, *P<0.05. Student T.test

6.2.3.3. Analysis of $[Ca^{2+}{}_i]$ in megakaryocyte like cells harbouring CALR mutations

To further explore the effects of *CALR* mutations in the Ca^{2+} dynamics during megakaryocyte maturation, basal $[Ca^{2+}{}_i]$ in DAMI cells overexpressing CALR wt, type1 and type 2 cells after PMA megakaryocyte induction were analysed. Experiments were performed in triplicates using two different clones for each condition.

As previously described, DAMI cells significantly decreased their $[Ca^{2+}{}_i]$ from the megakaryoblast to the mature megakaryocyte stages after PMA induction. Interestingly, none of the PMA-megakaryocyte induced CALR mutant DAMI cells showed a significant decrease of $[Ca^{2+}{}_i]$. Surprisingly, *CALR* type 1 cells showed a slight increase in $[Ca^{2+}{}_i]$ compared with its correspondent basal control, although this difference was not statistically significant (Figure 46). Moreover, DAMI *CALR* type 2 did not show any difference in $[Ca^{2+}{}_i]$ after PMA megakaryocyte induction (Figure 46).

Overall, these results proved that *CALR* mutations affect the $[Ca^{2+}{}_i]$ during the last stages of megakaryocyte commitment. Surprisingly, analysis of the $[Ca^{2+}{}_i]$ of the matured megakaryocytes showed significant differences between CALR wt and CALR mutant cells. Both mutants displayed a significant increase in $[Ca^{2+}{}_i]$ at the final mature megakaryocyte stage, compared with CALR wt (Figure 46 B). Interestingly, *CALR* type 1 megakaryocytes displayed higher $[Ca^{2+}{}_i]$ levels compared with CALR type 2 megakaryocytes (Figure 46 B).

A. Ca²⁺ levels during DAMI megakaryopoiesis
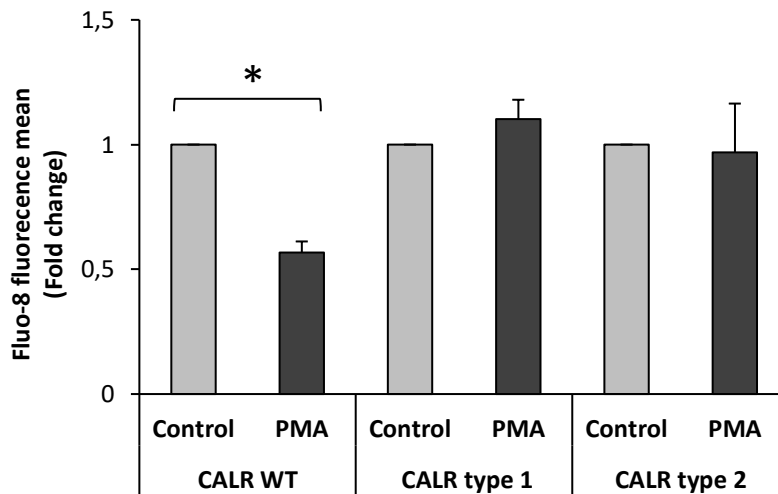
B. Ca²⁺ levels of DAMI mature megakaryocytes
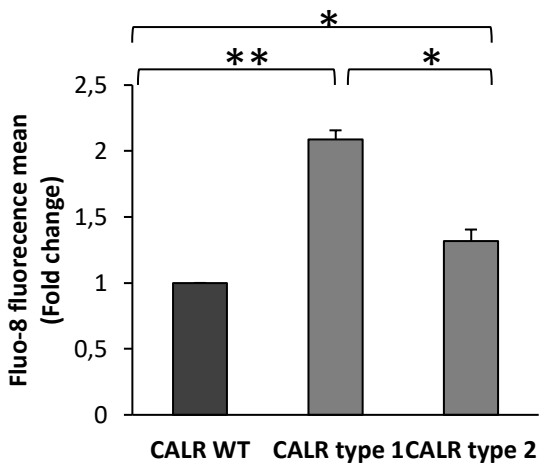
C.
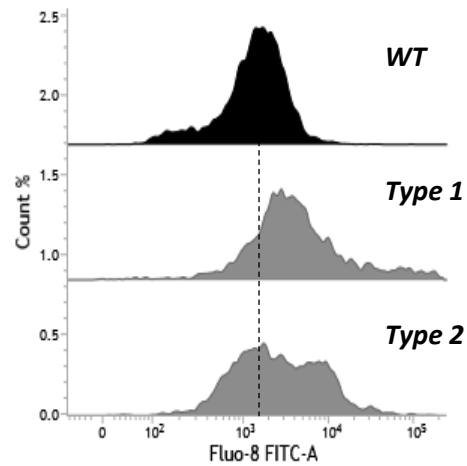
Figure 46. [Ca²⁺ᵢ] levels in DAMI cells overexpressing CALR wt, type 1 and type 2 mutations after PMA induction.

DAMI cells were exposed to PMA treatment for 72 hours. Cells were stained using FLUO-8-AM and basal intracellular Ca^{2+} levels and quantified by flow cytometry. **A)** [Ca^{2+}_i] before and after DAMI megakaryocyte induction. **B)** [Ca^{2+}_i] of DAMI megakaryocyte cells. **C)** Representative histogram of the [Ca^{2+}_i] of one clone per condition. Results were averaged between six independent experiments using two different clones per condition. Values represent mean ± SEM for each group. **P<0.01, *P<0.05. Student T.test

6.2.3.4. ER Ca^{2+} buffering activity of megakaryocyte like cells harbouring CALR mutations

Previous analyses demonstrated that *CALR* mutations lead to a decrease of basal [Ca$^{2+}_i$], drop cytoplasmic Ca^{2+} mobilisation from the ER as well as decrease the ER Ca^{2+} storage during early stages of megakaryocyte differentiation (blast and megakaryoblast stages). However, *CALR* type 1 and type 2 mutations seem to lead to a final increase in the basal [Ca$^{2+}_i$] in DAMI mature megakaryocytes. Therefore, to further understand the effects of *CALR* mutations in the Ca^{2+} dynamics of mature megakaryocytes, this study further analysed whether *CALR* mutations affect the cytoplasmic Ca^{2+} mobilisation from the ER at this differentiation stage. For this, DAMI cells overexpressing *CALR* wt, *CALR* type 1 and *CALR* type 2 were treated with PMA during 72 hours. Then, Fluo-8 stained megakaryocytes were treated with thapsigargin, and intracellular Ca^{2+} levels were recorded as previous experiments.

DAMI PMA induced cells exposed to thapsigargin displayed ER Ca^{2+} depletion (Figure 47). Interestingly, DAMI cells harbouring both *CALR* mutations, type 1 and type 2, showed an increase of cytosolic Ca^{2+} oscillation after thapsigargin treatment compared to the control (Figure 47 A). Additionally, a slightly increase in the rate of ER Ca^{2+} release was found in both mutants (Figure 47 B). Finally, both mutants showed an increase of ER Ca^{2+} storage, although differences were not statistically significant (Figure 47 B).

Comparison of the ER Ca^{2+} mobilisation between CALR mutant DAMI cells in their megakaryoblast and megakaryocyte stage showed surprising results. Both *CALR* mutations increase the rate of Ca^{2+} release after megakaryocyte maturation (Figure 48 B, C). Furthermore, megakaryocyte differentiation in both mutants leads to a significant increase of ER Ca^{2+} storage (Figure 49). In contrast CALR wt DAMI cells did not show any differences between both differentiation stages.
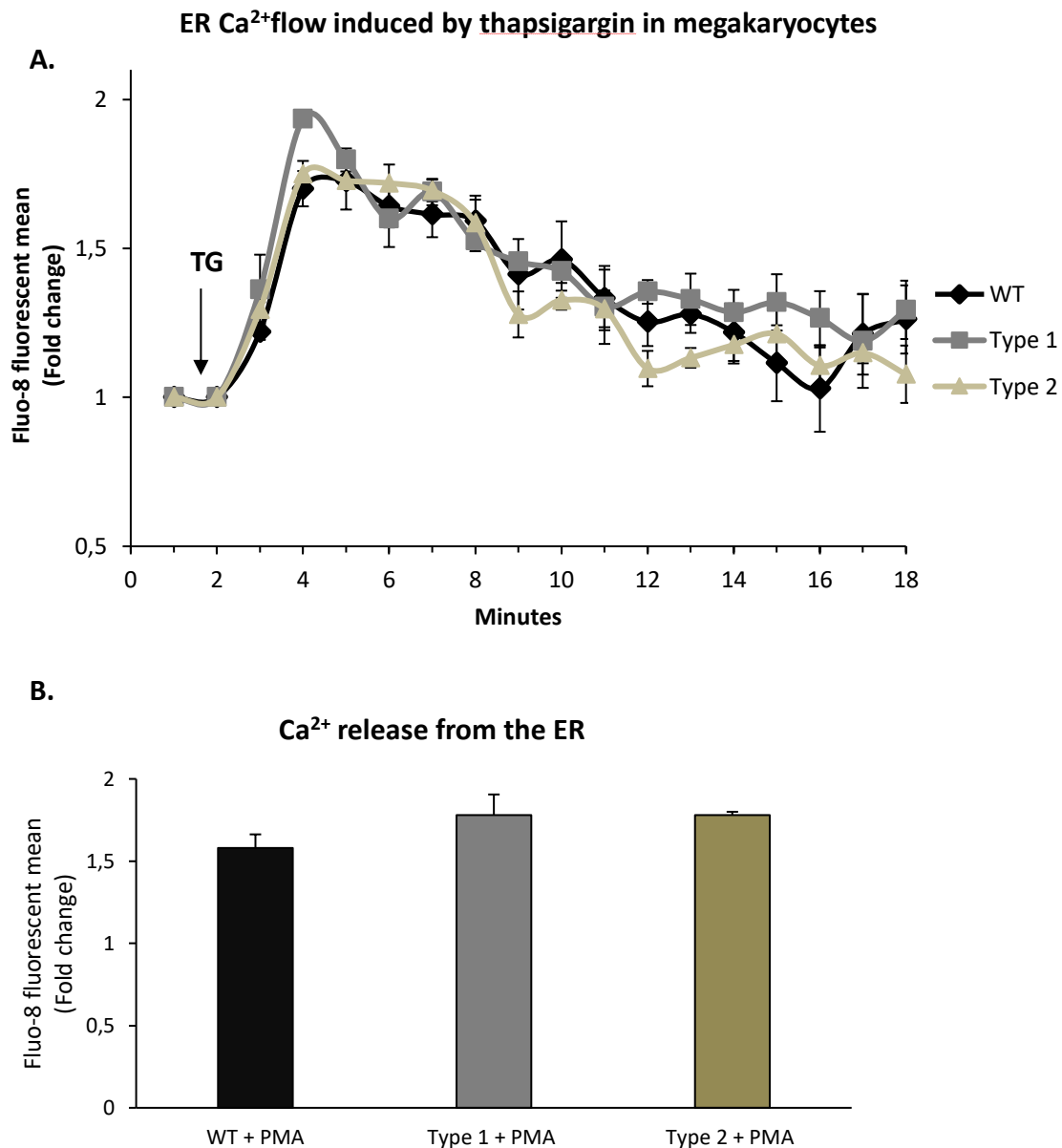
Figure 47. Fluorescence-based analysis of ER Ca2+ flow in DAMI PMA induced cells overexpressing CALR WT, type 1 and type 2 mutations.

A) DAMI cells were differentiated into megakaryocytes under PMA treatment for 72 hours. Then, cells were stained using Fluo-8-AM and were subsequently resuspended in PBS. Once 1 µM thapsigargin was added to the cells, fluorescence measurements were registered using flow cytometry for 15 minutes. Representative example of fluorescent measurements of a single clone per condition are shown. **B)** Measurements of ER Ca^{2+} release in DAMI megakaryocyte cells. Results were averaged between six independent experiments using two different clones per condition. Values represent mean ± SEM for each group. n=3. **P<0.01, *P<0.05. Student T.test

A.

ER Ca²⁺ flow in DAMI *CALR WT*

B.

ER Ca²⁺ flow in DAMI *CALR* type 1

C.

ER Ca²⁺ flow in DAMI *CALR* type 2
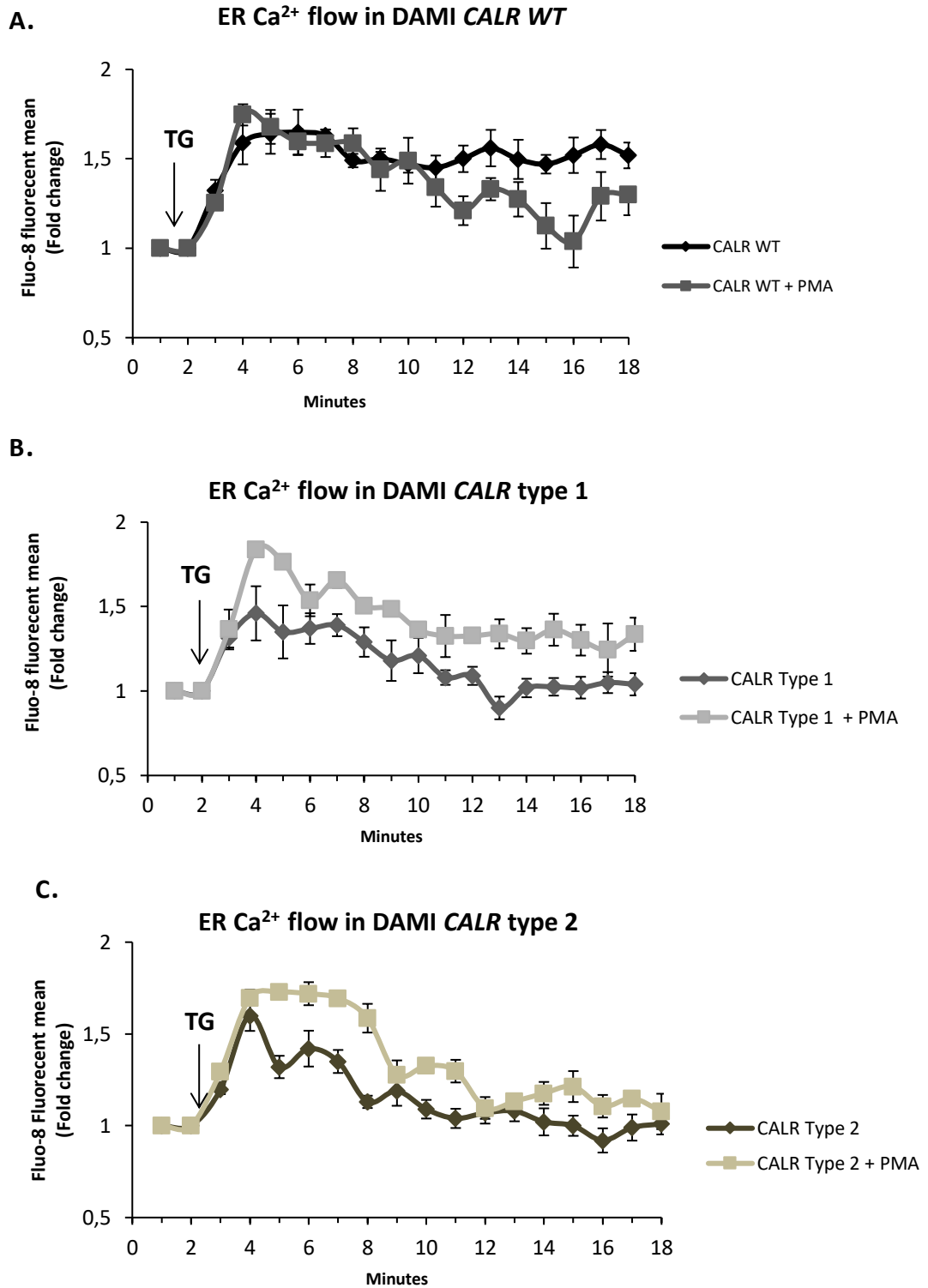
Figure 48. Comparison of the fluorescence-based analysis of ER Ca2+ flow between DAMI cells overexpressing CALR wt, type 1 and type 2 mutations before and after PMA megakaryocyte induction.

Representative example of fluorescent measurements of a single clone per condition are shown. Values represent mean ± SEM for each group.

Ca²⁺ release from the ER
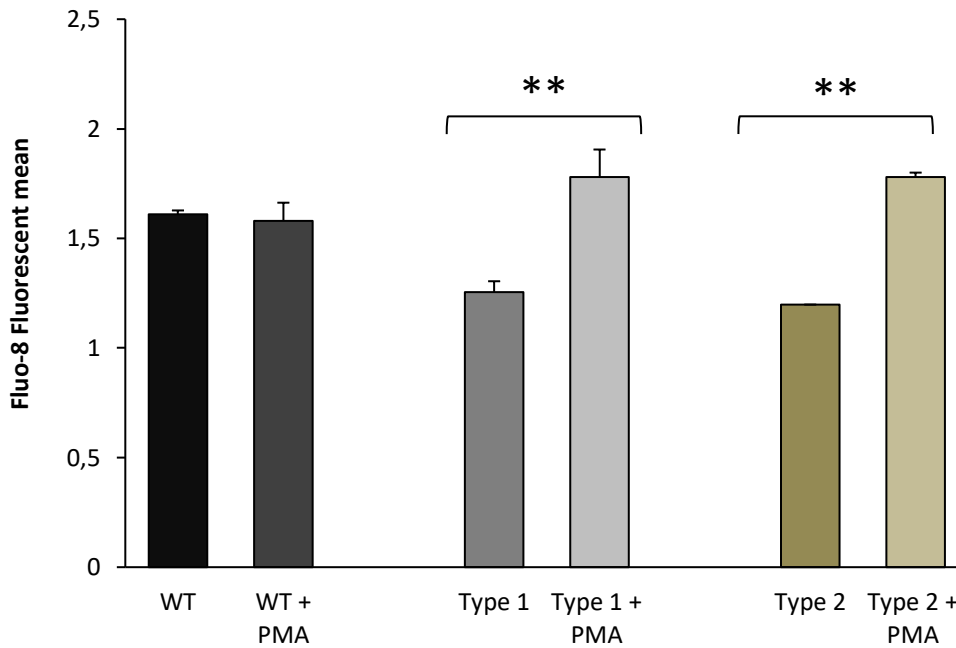
Figure 49. Comparison of the ER Ca2+ release between DAMI cells overexpressing CALR wt, type 1 and type 2 mutations before and after PMA megakaryocyte induction.

Results were averaged between six independent experiments using two different clones per condition. Values represent mean ± SEM for each group. **P<0.01, *P<0.05. Student T.test

Together these results provide novel insights into the nature of *CALR* mutations. CALR mutant cells display abnormal Ca^{2+} dynamics through the megakaryocyte maturational process. These cells show different patterns of ER Ca^{2+} release during different stages of megakaryocyte differentiation. In contrast CALR wt cells do not show any alteration of this activity during megakaryopoiesis.

6.2.4. Ca2+ channel blockers as inducers of megakaryocytic differentiation

Physical manipulation of intracellular Ca^{2+} has shown to induce differentiation of specific cellular lineages (Sun et al., 2007; Pinto et al., 2016). This study has demonstrated that $[Ca^{2+}_i]$ could play an essential role during megakaryocyte formation. Additionally, *CALR* mutations characteristic of megakaryocytic neoplastic cells change the Ca^{2+} dynamics during megakaryocyte differentiation. All these results together with the recent published study showing that treatment with Riluzole, a CCB specific of NMDAR, induces megakaryocytic characteristics in leukemic blast (Kamal et al., 2015), suggest that changes in Ca^{2+} dynamics within the cells could induce megakaryocyte cell fate. To evaluate whether physical manipulation of $[Ca^{2+}_i]$ could induce megakaryocyte characteristics, we exposed leukemic blast cells were exposed to three CCBs. BTP-2 is an inhibitor of SOCE machinery and Fendiline an inhibitor of L-type channels. Furthermore, Riluzole treatment was also used to test further megakaryocyte characteristics under its treatment than the previously published data (Kamal et al., 2015).

CD41a expression under BTP-2 and Fendiline treatment

CD41a cell surface marker was used to test the induction of megakaryocytic differentiation under BTP-2 and Fendiline treatment. Firstly, K562 and MARIMO cells were incubated with BTP-2 under different concentrations (0, 20, 25, 50 µM) over 72 hours and cell surface expression of CD41a marker was analysed. Results showed an increase in CD41a expression in a BTP-2 dose dependant manner (Figures 50 and 51). The major shift in CD41a fluorescence in both cell lines, was found with 50 µM BTP-2 treatment after 72 hours. Then, cells were incubated with 50 µM BTP-2 and CD41a cell surface expression was recorder every 24 hours over 72 hours. Results showed the major increase in cell surface expression after 72 hours (Figures 50 and 51). Therefore, 50 µM BTP-2 treatment over 72 hours was selected as optimal condition for further experiments.

Figure 50. Analysis of CD41a cell surface marker expression in K562 cells after BTP-2 treatment.

Representative counter plots of flow cytometry analysis measuring CD41a antigen expression in K562 cell population after treatment of different concentrations of BTP-2 (20, 25, 50 μM) and times of incubation (24, 48 and 72 hours). Cells were stained with CD41a-APC antibody.
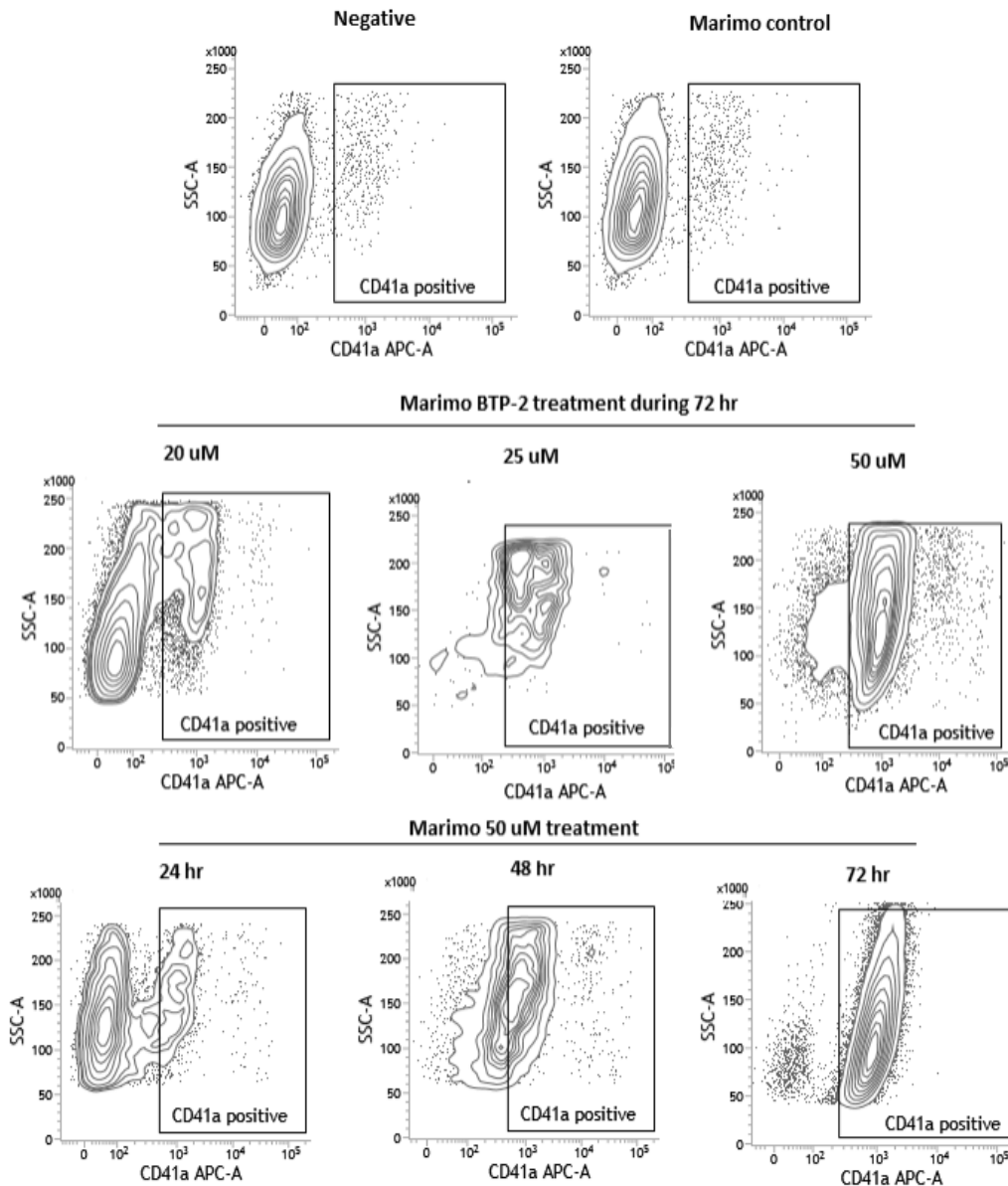
Figure 51. Analysis of CD41a cell surface marker expression in MARIMO cells after BTP-2 treatment.

Representative counter plots of flow cytometry analysis measuring CD41a antigen expression in MARIMO cell population after treatment of varying concentrations of BTP-2 (20, 25, 50 µM) and different times of incubation (24, 48 and 72 hours). Cells were stained with CD41a-APC antibody.

CD41a fluorescence was quantified in both cell lines after 50 µM BTP-2 treatment for 72 hours. K562 and MARIMO cells showed a significant increase in CD41a marker compared with the untreated control, suggesting an induction of megakaryocyte characteristics under these

conditions (Figure 52 A, B). Almost 100% of events displayed CD41a expression in both cell lines (Figure 52 C).

Figure 52. CD41a quantification and cell death induction after 50 μM BTP-2 treatment.

A, B) K562 and MARIMO cells were subjected to 50 μM BTP-2 treatment for 72 hours and CD41a expression was analysed and quantified by flow cytometry. **C)** Quantification of CD41a positive cells. Values represent mean ± SEM for each group. n=3. **P<0.01, *P<0.05. Student T.test

After SOCE machinery inhibition, the effects of non-voltage-gated L-type channels inhibition was analysed by using Fendiline treatment. K562 and MARIMO cells CD41a cell surface expression was analysed after cell incubation with different Fendiline concentrations (0, 5, 10, 20 µM) over 72 hours. Results showed a shift in CD41a fluorescence under 20 µM concentration in both cell lines (Figures 53 and 54). Moreover, measurements every 24 hours under 20 µM showed that cells under this treatment display CD41a within the cell surface after 72 hours (Figures 53 and 54)
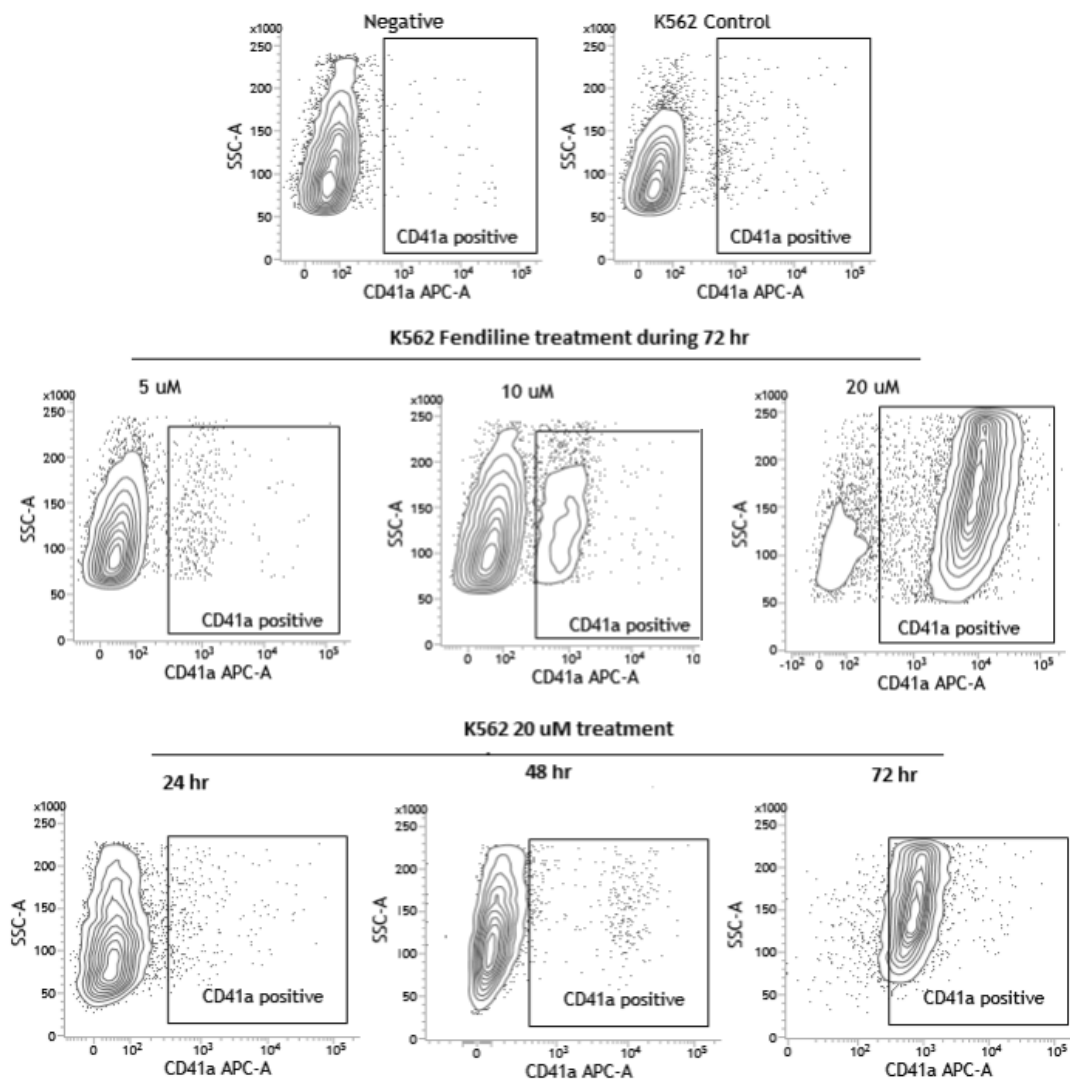
Figure 53. Analysis of CD41a cell surface marker expression in K562 cells after Fendiline treatment.

Representative counter plots of flow cytometry analysis measuring CD41a antigen expression in K562 cell population after treatment of different concentrations of Fendiline (5, 10, 20 µM) and different times of incubation (24, 48 and 72 hours). Cells were stained with CD41a-APC antibody.
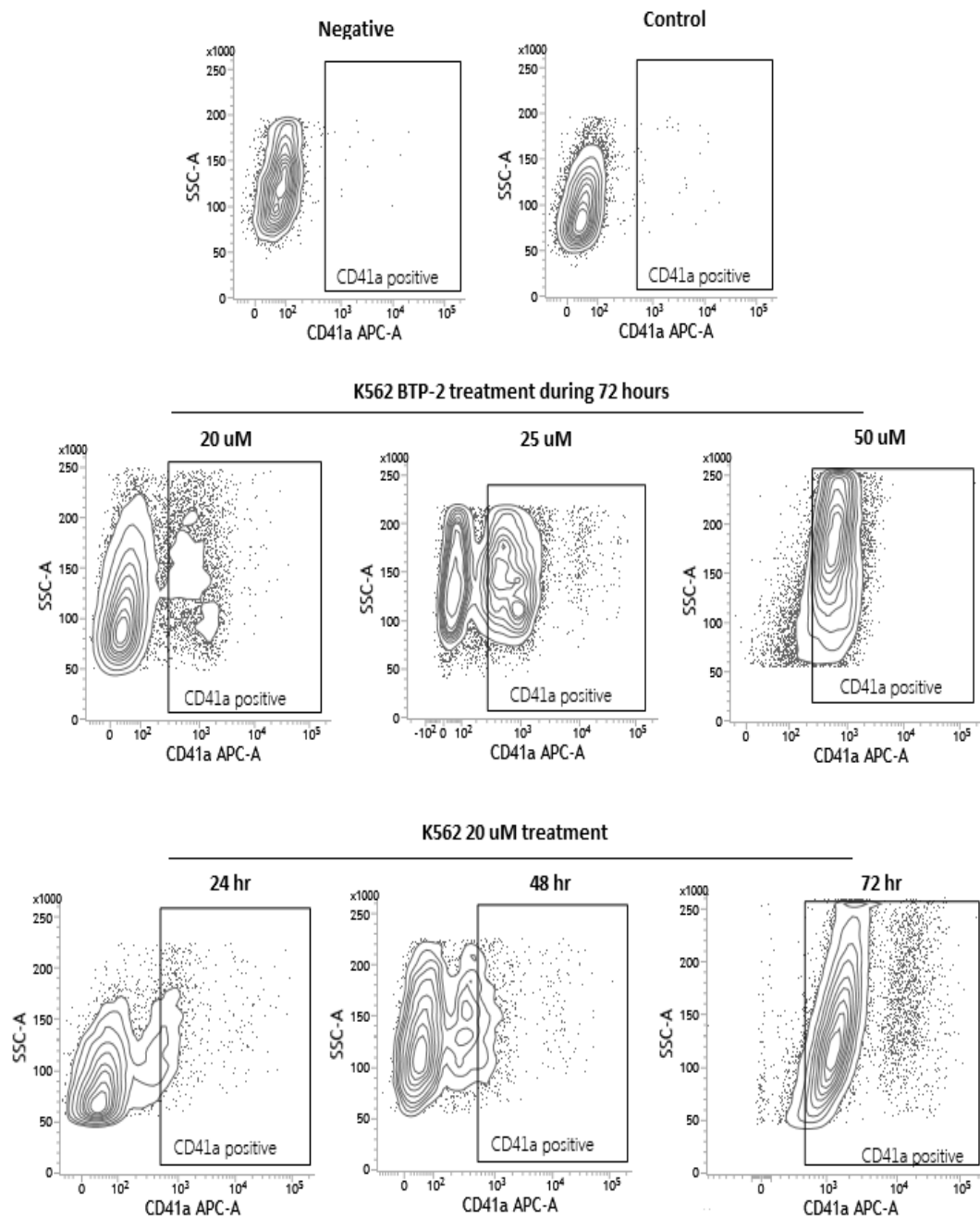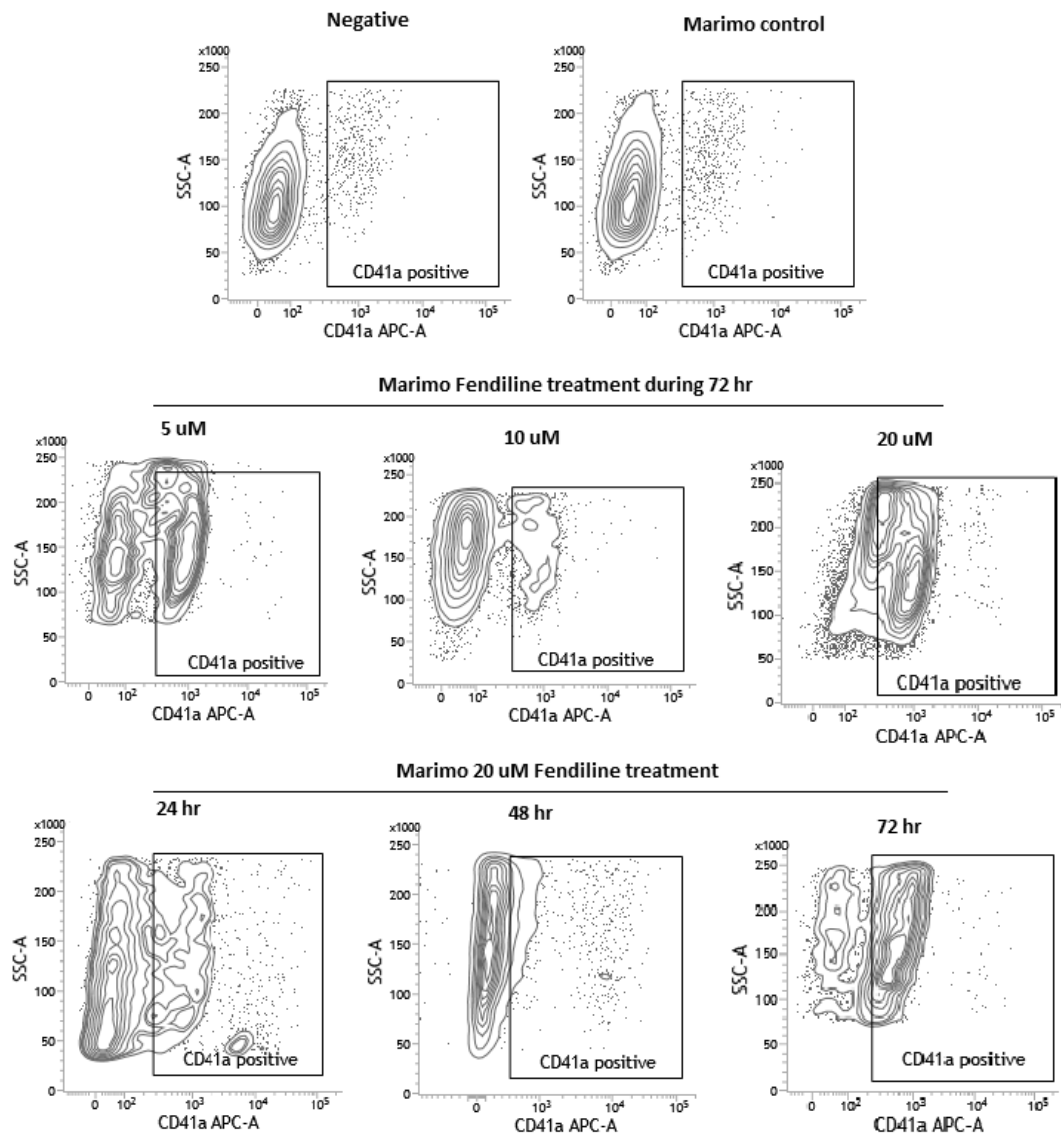
Figure 54. Analysis of CD41a cell surface marker expression in MARIMO cells after Fendiline treatment.

Representative counter plots of flow cytometry analysis measuring CD41a antigen expression in MARIMO cell population after treatment of different concentrations of Fendiline (5, 10, 20 μM) and different times of incubation (24, 48 and 72 hours). Cells were stained with CD41a-APC antibody

Finally, CD41a fluorescence was quantified in K562 and MARIMO after 20 μM Fendiline treatment for 72 hours. Both cell lines showed an increase in CD41a expression compared with control (Figure 55 A, B). Moreover, almost 100% of events displayed CD41a expression in K562 and 80 % in MARIMO cells (Figure 55 C).
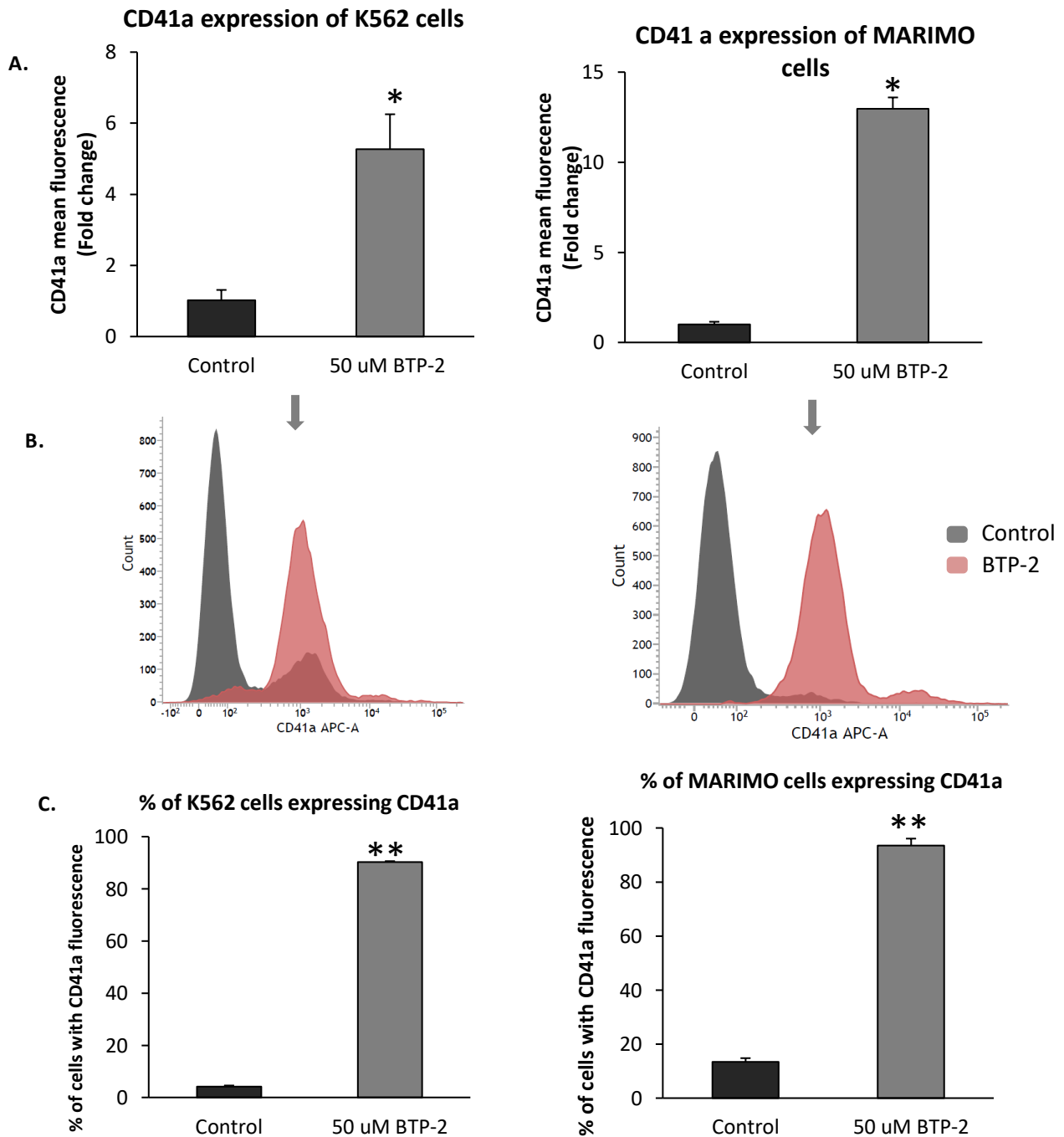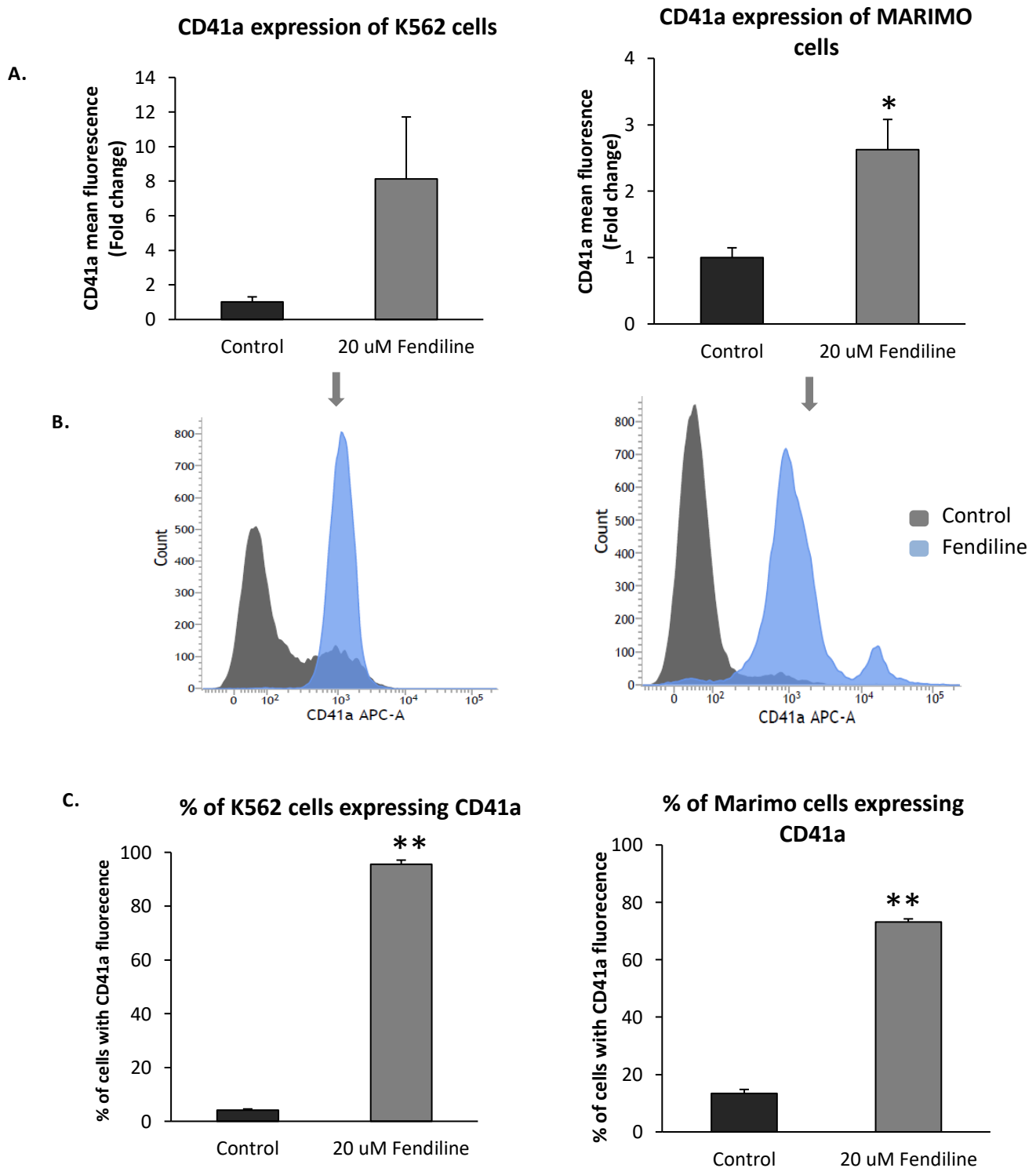
Figure 55. CD41a quantification and cell death induction after 20 μM Fendiline treatment.

A, B) K562 and MARIMO cells were subjected to 20 μM Fendiline for 72 hours and then CD41a expression was analysed and quantified by flow cytometry. **C)** Quantification of CD41a positive cells. Values represent mean ± SEM for each group. n=3. **P<0.01, *P<0.05. Student T.test

MTS analysis after BTP-2 and Fendiline treatment

Cell exposure to CCBs could induce high cytotoxicity within the cell culture. Therefore, before carrying out further molecular analysis using BTP-2 and Fendiline treatment the cytotoxic effect of these CCBs were investigated by MTS assay. Cells were cultured under different drug concentrations (0, 5, 10, 20, 50, 100 µM) for 72 hours.

MTS results showed that BTP-2 and Fendiline treatment provided a strong decrease of cell growth in both cell lines in a dose dependent manner (Figure 56 A). 50 µM of BTP-2 treatment, the optimal concentration where CD41a was expressed in both cell lines, reduced K562 cell number to 62 ± 10 % (Figure 56 A). Moreover, MARIMO cells were more sensitive to the exposure to this CCB, as cell viability was reduced to 48 ± 13 % (Figure 56 A).

Fendiline showed a higher inhibitory effect compared with BTP-2. MARIMO cells exposed to 20 µM Fendiline displayed a decrease in cell viability to 34.19 ± 2.3 % (Figure 56 B). K562 showed a slightly higher sensitivity under these conditions, and their cell growth rate decrease to 26.36 ± 8.7 % (Figure 56 B).

Overall, MTS results showed that optimal BTP-2 and Fendiline concentrations for induction of megakaryocyte like characteristics chosen above provided a strong decrease of cell growth in both, K562 and MARIMO cell lines.
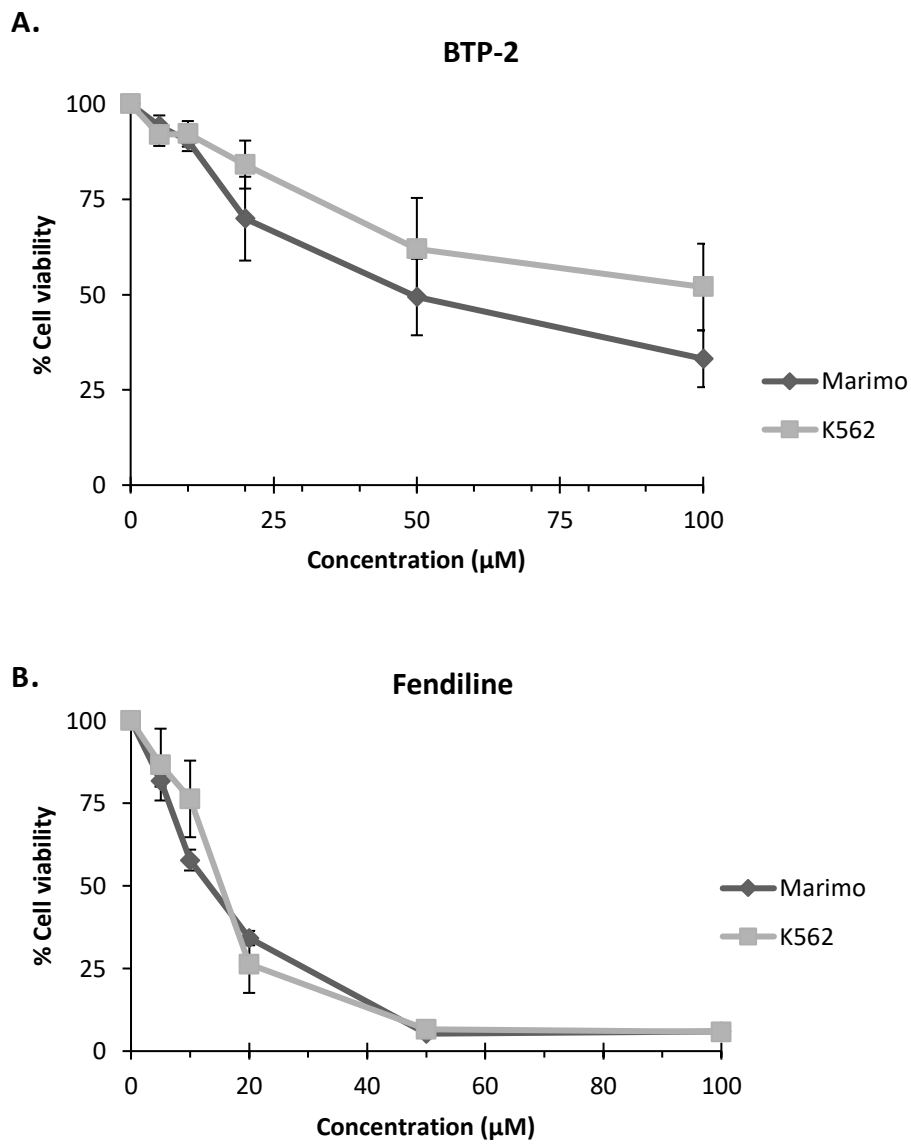
Figure 56. Cell proliferation analysis of MARIMO and K562 cells exposed to BTP-2 and Fendiline treatment.

MARIMO and K562 cells were subjected to 0, 5, 10, 20, 50, 100 µM treatment of **A)** BTP-2 and **B)** Fendiline for 72 hours. Then, MTS assay performed to test cell viability. Values represent mean ± SEM for each group. n=3.

MPL expression under BTP-2, Fendiline and Riluzole treatment.

During megakaryocyte formation, the expression of *c-MPL* is essential for a correct cellular function. In order to study whether intracellular Ca^{2+} manipulation can induce highly important events such as *c-MPL* expression, MARIMO cells, which have been shown to be negative for this receptor (Kollmann et al., 2016) were exposed to BTP-2, Fendiline and Riluzole during 72 hours.

Initially, *c-MPL* mRNA levels were tested using qRT-PCR analysis. Surprisingly, results showed a significant upregulation of *c-MPL* gene expression after treatment with the three CCBs (Figure 57). Additionally, flow cytometry analysis revealed a significant increase of MPL protein levels within the cell surface of MARIMO cells after BTP-2, Fendiline and Riluzole treatment (Figure 57). Quantification of MPL positive events estimated about 100% of cells under Riluzole and BTP-2 treatment and 75% of cells treated with Fendiline to express this protein within the cell surface.

Therefore, physical intracellular Ca^{2+} manipulation by blocking NMDR, SOCE or L-type channels independently by using CCBs led to a significant expression of MPL receptor, in both mRNA and protein levels.

A.

c-MPL mRNA levels

B. **MPL cell surface expression**

C.

D. **% Cells expressing MPL**

Figure 57. MPL expression in MARIMO cells after Riluzole, BTP-2 and Fendiline treatment.

MARIMO cells were subjected to 100 µM Riluzole, 50 µM BTP-2 or 20µM Fendiline treatment for 72 hours. **A)** RNA was extracted and converted into cDNA and finally subjected qRT-PCR using primers against *c-MPL.* **B, C)** MPL (CD110) expression was analysed and quantified by flow cytometry. **D)** Quantification of CD41a positive cells. Values represent mean ± SEM for each group. n=3. **P<0.01, *P<0.05. Student T. test.

Expression of STAT5 target genes after BTP-2, Fendiline and Riluzole treatment

Previous results clearly stated an important role of intracellular Ca^{2+} during megakaryocyte formation. However, there is no previous evidence suggesting whether Ca^{2+} signalling has any directly link with JAK/STAT cascade, which is known to be essential for correct megakaryopoiesis. For that reason, the activation status of STAT5 after exposure to Riluzole, Fendiline and BTP-2 was further studied. MARIMO cells were used in this experiment, as this cell line has been previously reported to display an inactive JAK/STAT cascade (Kollmann et al., 2016; Kollmann et al., 2015). Expression of four known STAT5 target genes *PIM1, CISH, ID1* and *SOCS2* (Sonkin et al., 2015) was analysed after 72 hours of drug incubation.

Interestingly, qRT-PCR analysis showed that MARIMO cells exposed to CCB display a significant increase of mRNA of the four gene signature of STAT5 (Figure 58). Although some samples did not show a statistically significant increase due to higher variability between the experiments, an overall increase of expression was found. Thus, MARIMO cells exposed to CCBs resulted in a trend for upregulation of the mRNA expression of the STAT5 gene signature. These results together with the previous findings showing an upregulation of MPL expression after intracellular Ca^{2+} manipulation by using CCBs, suggested a direct link between Ca^{2+} dynamics and JAK/STAT signalling.

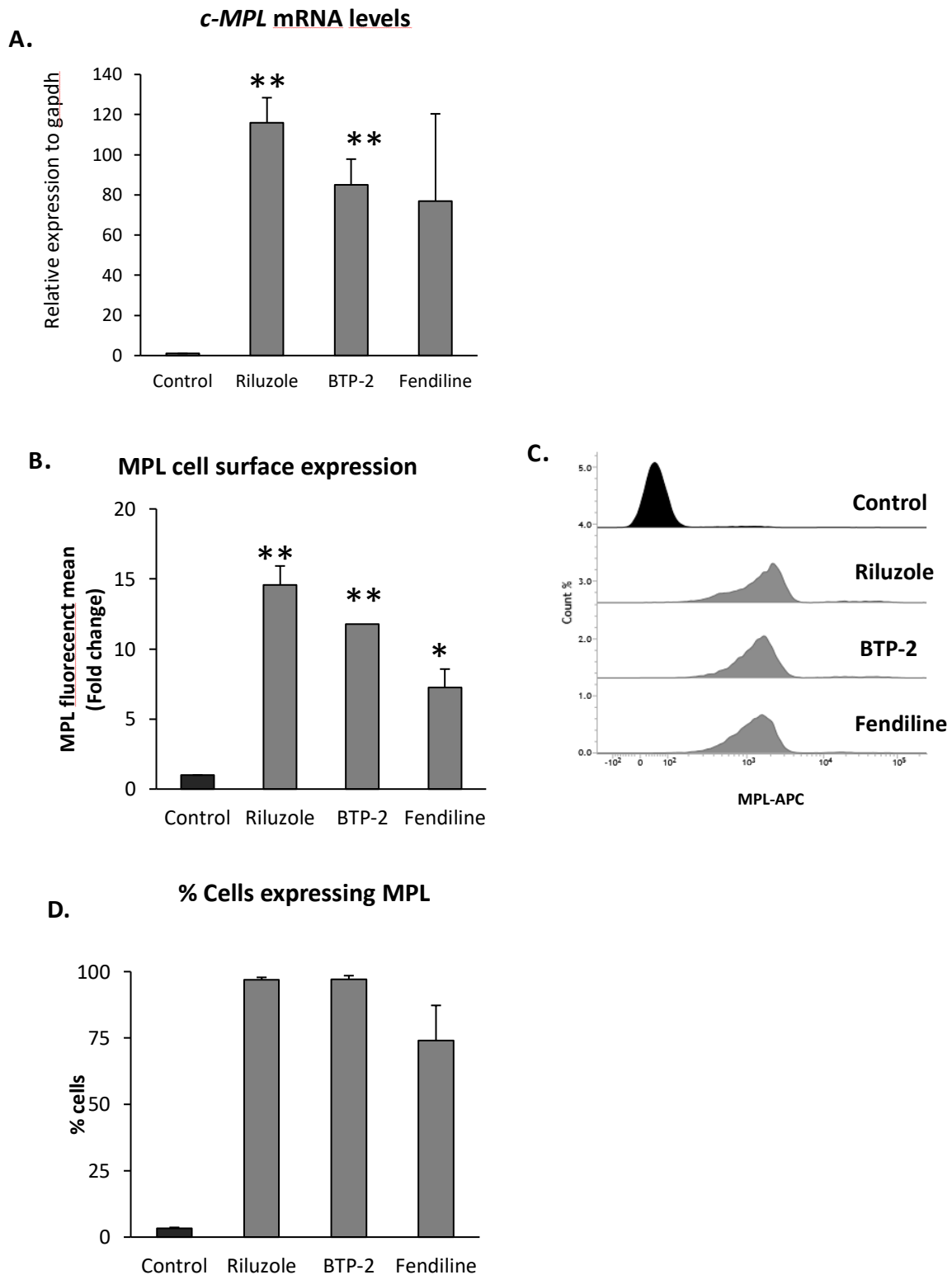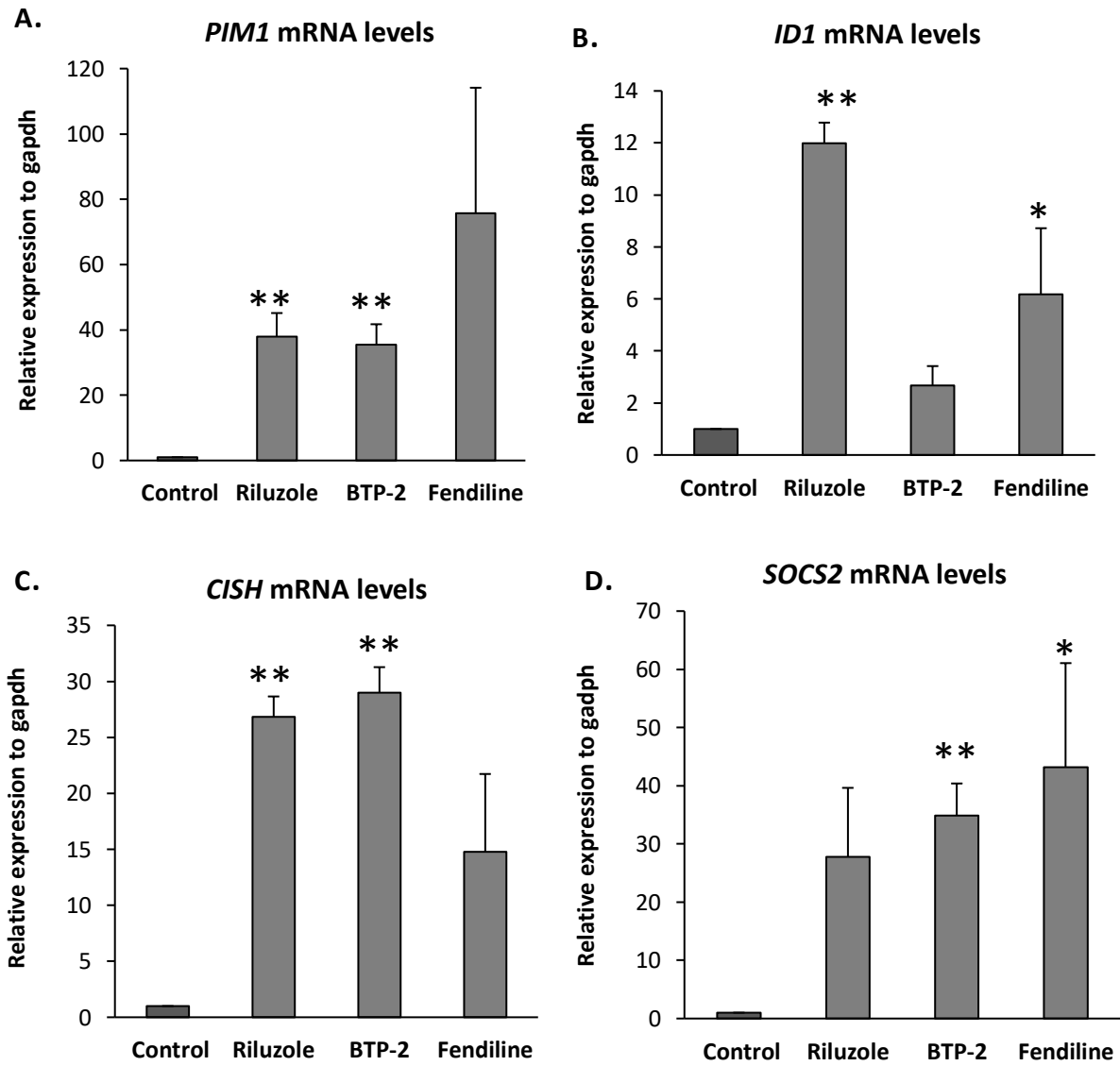**Figure 58. Expression of STAT5 gene signature in MARIMO cells after Riluzole, BTP-2 and Fendiline treatment.**

MARIMO cells were subjected to 100 µM Riluzole, 50 µM BTP-2 or 20µM Fendiline treatment for 72 hours. RNA was extracted and converted into cDNA and finally subjected RT-qPCR using primers against *PIM1*, *CISH*, *ID1* and *SOCS2* genes. Values represent mean ± SEM for each group. n=3. **P<0.01, *P<0.05. Student T.test

6.3. Discussion

Cell differentiation is directly controlled by long term transient oscillations of $[Ca^{2+}_i]$ (Pinto et al., 2016). A strong relationship between $[Ca^{2+}_i]$ oscillations and specific cell differentiation lineages has been previously established. However, although Ca^{2+} dynamics seem to play a pivotal role in megakaryocyte differentiation and functions, the temporal changes of $[Ca^{2+}_i]$ during the differentiation of this lineage have not been described. This study demonstrates that $[Ca^{2+}_i]$ oscillate between different megakaryocyte maturational stages in a highly controlled manner during megakaryocyte commitment. In this investigation, three *in vitro* cellular models showed that megakaryocyte commitment is accompanied by highly regulated transient Ca^{2+} oscillations in hours scale.

During the analysis of $[Ca^{2+}_i]$ oscillations, two different megakaryocyte inducers where used, PMA and TPO. Hence, the $[Ca^{2+}_i]$ oscillations observed in this study were not an artificial product based on a specific drug treatment. Interestingly, previous research aiming to decipher the role of mitochondrial function during megakaryocyte commitment, described the same Ca^{2+} oscillations during K562 megakaryopoiesis, and they considered this transient Ca^{2+} changes to be consequence of transitional changes in reactive oxygen species (ROS) during cell differentiation (Huang et al., 2014). However further evidence is needed to understand the molecular basis of these specific $[Ca^{2+}_i]$ oscillations and their repercussions during megakaryocyte commitment.

Erythrocyte cell differentiation is highly dependent on $[Ca^{2+}_i]$ (Schaefer et al., 1997). Previous analysis demonstrated that EPO induces increases of $[Ca^{2+}_i]$ (Miller et al., 1989). Thus, $[Ca^{2+}_i]$ is suggested to be an important intracellular signal during erythrocyte differentiation. Results measuring the $[Ca^{2+}_i]$ of K562 under Hemin erythrocyte induction displays an increase of $[Ca^{2+}_i]$ over time. Therefore, the Ca^{2+} oscillations during K562 erythropoiesis described here agrees with previous statements suggesting an increase of $[Ca^{2+}_i]$ during erythrocyte cell commitment (Miller et al., 1988; Miller et al., 1989). These results, together with previous studies that reported a rise in $[Ca^{2+}_i]$ for neurons and muscles cells differentiation, suggest that increase in $[Ca^{2+}_i]$ is an initiating event for cellular differentiation. Interestingly, K562 Ca^{2+} oscillations differ in space and time depending on erythrocyte/megakaryocyte

commitment. Hence, the frequency of these transient $[Ca^{2+}_i]$ oscillations could be a key signal for cell differentiation fate during haematopoiesis.

Cytosolic Ca^{2+} dynamics directly depends on the ER Ca^{2+} and its constant flow towards the cytoplasm. Previous investigations targeting the analysis of intracellular Ca^{2+} dynamics in *CALR* mutant cells showed contradictory results regarding the ER Ca^{2+} release capacity of these cells. Interestingly, the ER Ca^{2+} release of MARIMO cells in response to thapsigargin treatment shows a decreased capacity of ER Ca^{2+} release (Kollmann et al., 2015). On the contrary, primary megakaryocytes from MPN patients harbouring *CALR* type 1 and type 2 mutations treated with CPA displayed a significant increase of ER Ca^{2+} release compared with *JAK2* mutants or healthy subjects (Pietra et al., 2015). Initially, results using MARIMO and DAMI cells overexpressing *CALR* type 1 and type 2 cells in their blast stage showed a decrease capacity of ER Ca^{2+} release in response to thapsigargin compared to the control, as previously described (Kollmann et al., 2015). Unexpectedly, when DAMI cells were differentiated towards megakaryocyte under PMA treatment, both CALR mutant cells increased their ER Ca^{2+} release rate, as seen in primary megakaryocytes (Pietra et al., 2015). Therefore, this study demonstrates that the previously registered discrepancies are due to differences in the differentiation stage of the cellular models used in these studies. DAMI *CALR* type 1 showed a tendency to a slightly higher increase rate of ER Ca^{2+} release compared with *CALR* type 2. These observations are consistent with previous studies where primary patient megakaryocytes *CALR* type 1 subjects displayed a significant higher capacity of ER Ca^{2+} release (Pietra et al., 2015), which is known to have more pronounce pathological effects than *CALR* type 2.

However, not only the ER Ca^{2+} release capacity fluctuates in CALR mutant cells, but the basal $[Ca^{2+}_i]$ differ as well during different stages of differentiation within these cells. MARIMO cells and DAMI cells overexpressing *CALR* mutations displayed a significant decrease of $[Ca^{2+}_i]$ in their blast stage compared with *CALR* wt cells. However, when cells were differentiated towards mature megakaryocytes, the basal $[Ca^{2+}_i]$ raised, reaching a significant difference compared with the control. Importantly, Ca^{2+} has been proved to be a key element for normal megakaryocyte and platelet function (Di Buduo et al., 2014, Di Buduo et al., 2016), hence changes in $[Ca^{2+}_i]$ could directly affect megakaryocyte functions during disease.

CALR mutations affect intracellular Ca^{2+} in a cell differentiation stage manner during megakaryopoiesis, and it is possible that transient changes of Ca^{2+} buffering activity contribute to the pathogenesis of megakaryocyte hyperplasia. Of note, a recent publication suggested that there are quantitative changes at the protein level of CALR mutants during megakaryopoiesis (Iborra and Papadopoulos, 2017). CALR mutant proteins undergo rapid degradation when overexpressed in DAMI and HEL cell lines (Kollmann et al., 2016). In contrast, significantly higher CALR mutant protein levels were described in platelets from MPN patients (Kollmann et al., 2016). Therefore, it has been proposed that during early stages of megakaryocyte maturation cells undergo a process of readjustment of CALR mutant protein levels to achieve cell survival (Iborra and Papadopoulos, 2017). Changes in ER Ca^{2+} buffering activity and basal $[Ca^{2+}_i]$ during megakaryocyte differentiation described in this study could be directly linked with the protein levels of CALR mutants within the cell during the different megakaryocyte maturational stages. However, further analysis is needed to corroborate the transitions of CALR mutant protein levels within the megakaryocyte lineage in order to link this with changes of the Ca^{2+} buffering activity within CALR mutant cells during megakaryopoiesis.

Increase of $[Ca^{2+}_i]$ in megakaryocytes has been previously linked with the development of megakaryocyte hyperplasia in mice expressing an activated form of STIM protein (Grosse et al., 2007). According to the results showed in this study, *CALR* mutations, which are restricted to MPNs displaying megakaryocyte hyperplasia, lead to an increase of $[Ca^{2+}_i]$ in mature megakaryocyte cells. Therefore, it could be suggested that changes in the $[Ca^{2+}_i]$ caused by CALR mutants could be the driving force of megakaryocyte hyperplasia during ET and PMF, together with an active JAK/STAT and MAPK pathway. Therefore, this study extends our knowledge of the effects of *CALR* mutations into megakaryocytes and it increases the possible oncogenic roles of this mutation in MPNs.

Furthermore, this study reveals that leukemic cell lines with potential to commit into the megakaryocytic lineage express megakaryocyte like molecular characteristics when exposed to different CCBs. NMDARs, SOCE and L-type channels facilitate extracellular Ca^{2+} flow into the cytoplasm, helping to maintain high $[Ca^{2+}_i]$ in response to specific stimuli. This study demonstrates that the following NMDARs, SOCE and L-type antagonist known as Riluzole, BTP-2 and Fendiline respectively, increase the expression of CD41a and MPL megakaryocyte

cell surface markers, as well as induction of STAT5 transcriptional activity. To our knowledge, this is the first study to report that inhibition of overall extracellular Ca^{2+} entry in leukemic cells induces megakaryocyte features, suggesting that physical manipulation of intracellular Ca^{2+} facilitates megakaryocyte differentiation as previously reported in other cell types (Sun et al., 2007).

NMDARs have been previously described to be active in human platelets (Kalev-Zylinska et al., 2014) as well as to regulate megakaryocyte formation *in vitro* (Hitchcock et al., 2003). Moreover, it was shown that NMDARs inhibition leads to expression of CD41a, CD61 and induce polyploidy in leukemic blasts (Kamal et al., 2015). This thesis supports this previous study by adding novel data proving that NMDARs inhibition increases MPL cell surface expression and induces expression of *PIM1*, *CISH*, *SOCS2* and *ID1* genes, showing the relevance of NMDAR for megakaryocyte maturation. Moreover, SOCE machinery actively regulates human megakaryocyte functions (Di Buduo et al., 2014). This investigation demonstrates that SOCE machinery could regulate, together with NMDARs receptors, Ca^{2+} homeostasis during megakaryopoiesis, as BTP-2 treatment leads to expression of the same megakaryocytic characteristics as Riluzole treatment (Kamal et al., 2015). In contrast L-type channels have not been shown to have any direct link with megakaryocyte formation. However, this study indicates that the use of antagonists of these channels leads to induction of megakaryocytic characteristics. Though, further studies regarding the expression of L-type channels and their activity in these cells is necessary to fully understand their functional role in megakaryocyte formation.

Additionally, it is important to note the high cytotoxicity of the described optimal concentrations of Fendiline and BTP-2 for the induction of megakaryocyte characteristics in comparison to the previously reported Riluzole (Kamal et al., 2015). Consequently, characterisation of cell morphology of the live cells within the culture was not doable and therefore further analysis of megakaryocyte characteristics were not completed, such as analysis of polyploidy. Therefore, the test of other SOCE inhibitors, such as CRAC or 2-APB and L-type channel inhibitors like A5605 and A7232 will be essential to identify optimal drug treatment to reduce cytotoxicity and induce megakaryocyte characteristics in leukemic blasts.

Leukaemia cells are characterised by a blockage in early stages of differentiation and fail to differentiate into fully mature cells (Sell, 2005). Differentiation therapy has shown promising results in the treatment of acute promyelocytic leukaemia (APL) by using the differentiation agent ATRA (Degos and Wang, 2001). ATRA treatment has improved greatly the prognosis of APL patients, therefore much of today's research is focussed on the identification of further differentiating agents for the treatment of myeloid leukaemia's. These findings provide further depth to the current understanding of the relevance of intracellular Ca^{2+} in cell differentiation and open the possibility that Ca^{2+} might be an important target for the development of novel differentiation inducing agents for leukemic differentiation therapy.

In summary, this investigation reveals that Ca^{2+} oscillations could be the driving force of megakaryocyte differentiation. *CALR* mutations lead to changes in Ca^{2+} dynamics during the process of megakaryocyte formation, and therefore these changes could favour the megakaryocyte cell differentiation during the process of hyperplasia in disease and consequently alter megakaryocyte and platelet functions in ET and PMF.

6.3.1. Conclusions

The novel data presented in this study showing the correlation between Ca^{2+} and megakaryocyte formation in physiological conditions and disease reveals new insights into the important role of Ca^{2+} dynamics and megakaryocyte cell commitment. The major conclusions of this study are:

I. Megakaryocyte differentiation displays a characteristic pattern of $[Ca^{2+}_i]$ oscillations in hours scale, which could induce specific signalling necessary for the initiation of megakaryocyte differentiation.

II. Differentiation towards megakaryocyte or erythrocyte cell commitment show differential frequency of $[Ca^{2+}_i]$ oscillations, suggesting a direct correlation between $[Ca^{2+}_i]$ and cell commitment during haematopoiesis.

III. Presence of *CALR* mutations in early stages of megakaryocyte commitment leads to a decrease of basal $[Ca^{2+}_i]$ as well as decreased ER Ca^{2+} flow towards the cytoplasm and total ER Ca^{2+} stored.

IV. Mature megakaryocytes harbouring *CALR* mutations display higher $[Ca^{2+}_i]$ in their megakaryocyte stage compared with CALR wt cells. Moreover, megakaryocyte commitment in these mutant cells lead to an increase of ER Ca^{2+} flow towards the cytoplasm and total ER Ca^{2+} stored.

V. Intracellular Ca^{2+} manipulation by CCB treatment leads to the appearance of megakaryocyte like characteristics in leukemic cells, such as CD41a, MPL expression or activation of STAT5 transcriptional activity.

6.3.2. Future directions

To obtain more results regarding human megakaryocyte Ca^{2+} physiology in health and disease, further analysis using the same experimental procedures used during this study will be required using human megakaryocyte cultures from CD34+ progenitor cells of healthy subjects and *CALR* mutant MPN patients. It will be of much interest the analysis of the effects of a decrease of $[Ca^{2+}_i]$ during early stages of development and an increase of $[Ca^{2+}_i]$ in final mature megakaryocytes and its effect for the correct physiology of these cells and final platelet production rate and function. Moreover, analysis of CALR protein levels during megakaryopoiesis by western blot analysis could help to shed light into the different effects of CALR mutants during this process.

Analysis of physical manipulation of $[Ca^{2+}_i]$ as a driving force for megakaryocyte differentiation provided highly interesting results. The use of CCBs for inhibition of SOCE, L-type and NMDR receptors, showed the capacity of these drugs to induce megakaryocyte differentiation, although with high cytotoxicity. Therefore, investigation of the use of other L-type and SOCE antagonist to reduce cytotoxicity could help to understand the role of Ca^{2+} during megakaryopoiesis in more reliable cell conditions. Additionally, analysis of inhibition of other Ca^{2+} channels within the membrane, such as Na^+/Ca^{2+} exchangers or PMCA pump, could provide more data to reach a broader knowledge of the important role of the membrane Ca^{2+} channels and megakaryocyte formation.

Moreover, this study hinted that L-type channels could have a key role for megakaryocyte formation. However, the role of L-Type channels has not been clearly described in megakaryocytes; therefore, further studies targeting the understanding of these channels within these cells could reveal important information of the Ca^{2+} dynamics of megakaryocytes.

CHAPTER 7: *General Discussion*

7.1. Discussion

ET, PV and PMF are rare myeloproliferative malignancies characterised by a neoplastic proliferation of mature myeloid cells (Rumi and Cazzola, 2017). These diseases are associated with an increased risk of mortality and a decrease quality of life in these patients (Mesa et al., 2016). Identification of the MPNs driver mutations in *JAK2*, *c-MPL* and *CALR* genes has led to an advance in our knowledge about the development of these malignancies. However, there is a clear need for a better understanding of the molecular and cellular pathology of these mutations to further improve individual patient outcome.

The discovery of *CALR* mutations in ET and PMF has opened a new paradigm in the biology of MPNs (Klampfl et al., 2013; Nangalia et al., 2013). Constitutive activation of MPL receptor driven by CALR mutant proteins is a novel mechanism of oncogenic transformation in MPNs (Araki et al., 2016; Chachoua et al., 2016; Elf et al., 2016). Despite the large body of research aiming to decipher the oncogenicity of CALR mutant proteins, very little is known about the effects of these mutations on the multiple CALR cellular functions. Therefore, this investigation has worked under the hypothesis that *CALR* mutations alter the physical characteristics of CALR C-terminal domain, and this not only leads to deregulated signalling cascades, but there is also a modification of CALR normal cellular behaviour, such as changes in its cellular compartmentalisation and its intracellular Ca^{2+} buffering activity during megakaryocyte hyperplasia.

Structural analyses have been used to predict the molecular pathogenesis of mutations in disease (Khan and Vihinen, 2007). Minor variations in the amino acid sequence within a protein can result in major consequences, including modifying or preventing the cellular function of the protein (Choi et al., 2012). To understand the molecular pathogenesis of MPNs, a particular focus has been placed on the analysis of the physical alterations within CALR C-terminal domain caused by *CALR* type 1 and type 2 mutations. Chapter 3 described in detail an *in silico* structural analysis of the C-terminal region of CALR wt, CALR type 1 and type 2 mutants. This study has shown that *CALR* mutations lead to i) a decrease in the disorder

state, hence increasing the stability of C-terminal region, ii) an increase in the α-helix content, which are known to be interactive regions in other proteins, iii) an appearance of potential novel MoRFs regions, thus potentially modifying the function or interactions of CALR and iv) changes in the pI within C-terminal domain. The current data highlight the need to understand the changes in the structure-function relationship within these mutant proteins in order to decipher the genotype-phenotype correlation in ET and PMF.

Sub-cellular mislocalisation of proteins can lead to their loss of function, deregulation of their activity or lead to a damaging activity within the wrong cellular compartment. Hence, abnormalities in the sub-cellular compartmentalisation of specific proteins can cause diseases that involve aberrant cell signalling or protein aggregation (Hung and Link, 2011). Several cancer types have been linked with abnormal protein localisation, such as breast (Xia et al., 2004) and colon (Ogino et al., 2009) cancer, however in the pathogenesis of MPNs no driver mutations were known to lead to an oncogenic phenotype due to protein sub-cellular mislocalisation until *CALR* was found to be mutated in this type of myeloid neoplasms. CALR is a multi-compartment protein and the localisation of it highly correlates with its cellular functions (Michalak et al., 2009). Results within Chapter 5 suggested an escape of CALR from the ER and described an increase of CALR protein within the cell surface in CALR mutant cells. This change in localisation leads to a gain of function phenotype, as microscopy analyses revealed a co-localisation of CALR and MPL within the cell membrane, in accordance with previous publications (Araki et al., 2016; Chachoua et al., 2016; Elf et al., 2016). These results led to the hypothesis that the described structural changes and the emergence of potential MoRFs regions within CALR C-terminal domain could be the direct cause of CALR-MPL binding, as this protein interaction is dependent only on this domain (Elf et al., 2016). Also, these structural and localisation alterations caused by *CALR* mutations could lead to a novel network of protein interactions, such as the previously proposed interactions with cellular kinases, including PKC, PKA or CDK5 (Eder-Azanza et al., 2014), which activation could potentially contribute to ET and PMF phenotype.

Therapeutic treatment targeting protein mislocalisation has been proposed as a promising strategy in many human disorders, such as cancer or neurodegenerative diseases (Hung and Link, 2011). Identification of CALR mutant in MPNs as a mislocalised protein with gain of function within the wrong cellular compartment is a novel example of how deregulated

protein localisation can lead to an oncogenic transformation. Understanding whether therapeutic treatment could reverse this mislocalisation and therefore its oncogenic interaction network could be a potent area of investigation to improve the treatment of CALR mutant ET and PMF. However, it is important to analyse further effects of *CALR* mutations on the functional roles of this protein, such as its Ca^{2+} buffering activity, to gain a broader understanding of the pathogenesis of *CALR* mutations for the development of novel therapeutic agents.

During recent years there has been a growing interest of how deregulated components of Ca^{2+} signalling pathways contribute to an oncogenic transformation (Roderick and Cook, 2008). However, whether the abnormal Ca^{2+} homeostasis is needed to sustain the oncogenic process remains to be established. There is very little published data about the effects of *CALR* mutations on the Ca^{2+} homeostasis in megakaryocyte cells during MPNs progression (Pietra et al., 2015). The present study makes several noteworthy contributions regarding *CALR* mutations and Ca^{2+}. Chapter 6 describes an overall abnormal ER Ca^{2+} buffering activity and changes in $[Ca^{2+}_i]$ in *CALR* mutant cells. It can thus be suggested that changes in the pI of CALR C-terminal domain and changes in the localisation of CALR mutant could be the direct cause of deregulated Ca^{2+} homeostasis during ET and PMF oncogenesis. Interestingly, differences in CALR expression levels have been linked with the development of many cancer types (Lu et al., 2015). For example, increased *CALR* expression enhances cell migration in bladder cancer cells (Lu et al., 2011) and squamous cell carcinoma (Chiang et al., 2013) by unknown mechanisms. However, this study shows evidences that deregulation CALR Ca^{2+} buffering activity could be a novel oncogenic mechanism of CALR during disease. Moreover, results shown in this thesis contribute to the hypothesis that changes in $[Ca^{2+}_i]$ are associated with pathological thrombopoiesis as previously described (Grosse et al., 2007). However, to develop a full picture of the role of CALR mutants and abnormal Ca^{2+} homeostasis in megakaryocyte hyperplasia, further work within this thesis aimed to gain a broader picture about the importance of $[Ca^{2+}_i]$ during physiological megakaryocyte differentiation.

Studies demonstrating an essential role of $[Ca^{2+}_i]$ oscillations during erythrocyte, neuronal, osteocyte cell fate differentiation showed the relevance of Ca^{2+} homeostasis for a correct developmental process (Miller et al., 1988; Bikle et al., 2004; Sun et al., 2007; Gu et al., 1994). Several components of the regulatory network of Ca^{2+} signalling have proven to be necessary

for megakaryopoiesis and megakaryocyte function (Hitchcock et al., 2003, Di Buduo et al., 2014, Kamal et al., 2015). However, there is no previous knowledge about the spatial and temporal dynamics of $[Ca^{2+}_i]$ during megakaryocyte differentiation. Chapter 6 revealed a specific temporal pattern of $[Ca^{2+}_i]$ oscillations during megakaryopoiesis. This study is pioneer in the description of Ca^{2+} dynamics during the megakaryocyte differentiation process; however, the molecular mechanism that leads to these $[Ca^{2+}_i]$ oscillations remains unknown. Interestingly, alterations in the regulation of $[Ca^{2+}_i]$ by ER Ca^{2+} proteins have been linked with a carcinogenic phenotype, such as altered IP_3R expression (Mound et al., 2017; Singh et al., 2017). Therefore, a tight control of $[Ca^{2+}_i]$ by ER Ca^{2+} proteins during megakaryopoiesis could be key to suppress megakaryocyte hyperplasia.

Understanding the regulatory mechanisms of Ca^{2+} dynamics is a major step to further improve our knowledge of the remodelling of Ca^{2+} during oncogenesis of CALR mutant MPNs. Intracellular Ca^{2+} regulation during megakaryopoiesis seems to be rather complex (Di Buduo et al., 2016). SOCE machinery, NMDAR and L-type channels have been described to be key cell membrane Ca^{2+} channels involved in megakaryocyte and platelet function (Di Buduo et al., 2014; Kamal et al., 2015; Hitchcock et al., 2003; Luckhoff et al., 1991). This study demonstrates that the use of CCBs targeting these three main channels leads to the emergence of megakaryocyte like characteristics in leukemic cells, such as expression of CD41a marker and upregulation of megakaryocyte like genes. Therefore, this investigation suggests that several Ca^{2+} entry pathways are involved in the regulation of megakaryocytic differentiation. In addition, these results propose that SOCE, NMDAR and L-type channel's activity could support the leukemic phenotype, as their inhibition leads to an unblock of the blast undifferentiated phenotype. This hypothesis is supported by recent reports where Ca^{2+} signalling has been shown to play key roles in carcinogenesis (Prevarskaya et al., 2014; Wen et al., 2016), in addition to the previous data linking abnormal Ca^{2+} dynamics in CALR mutant cells. Therefore, this study could have future clinical implications, suggesting the Ca^{2+} regulatory components as potential therapeutic targets in megakaryocytic pathologies.

Analysis of megakaryocyte differentiation in ET and PMF is a major challenge in the understanding of MPNs pathologies (Balduini et al., 2011; Mondet et al., 2015). Previous investigations have studied the role of *CALR* mutations in megakaryocyte like cells (Pietra et al., 2015; Kollmann et al., 2016); however, there are no previous analysis of megakaryocyte

maturation in ET and PMF harbouring *CALR* mutation. This work has demonstrated the importance of studying the process of megakaryopoiesis in presence of *CALR* mutations, as the results presented here revealed that CALR mutant functions could differ between different megakaryocyte stages. This study has identified an overall increase of CALR cell surface population during induced megakaryocyte differentiation, suggesting that CALR cellular distribution might vary during megakaryopoiesis. Thus, as CALR mutant sub-cellular mislocalisation significantly differs between different stages of development, its functional role could also be altered following the megakaryocyte maturation process, such as its Ca^{2+} buffering activity. Moreover, this study demonstrated that Ca^{2+} dynamics significantly differ between different megakaryocyte differentiation stages in CALR mutant cells. Therefore, this investigation highlights the need of studying MPN driver mutations in the dynamic process of megakaryocyte differentiation in order to reach a better understanding of megakaryocyte hyperplasia and the defects of megakaryocyte maturation characteristic of ET and PMF positive for *CALR* mutations (Balduini et al., 2011; Loghavi et al., 2016).

Myeloid leukemic cell lines have been widely used for the understanding of megakaryocyte differentiation (Tan et al., 2010; Datta and Long, 2002; Wang et al., 2016). However, there has been a lack of cellular models harbouring *CALR* driver mutations with capacity to differentiate into the megakaryocyte lineage that could be used to study megakaryocyte maturation in MPNs. Importantly; in this study MARIMO cell line has been proposed as a novel megakaryocyte differentiation model, which harbours CALR mutation (Kollmann et al., 2015). MARIMO cells, in response to PMA treatment displayed megakaryocyte like characteristics, such as increase in size, cell adherence, polyploidy and expression of megakaryocytic genes. This finding opens the possibility of studying the process of megakaryocyte differentiation under the presence of CALR mutations using basic cell culture techniques.

The results of this thesis targeting the analysis of CALR mutant localisation and Ca^{2+} dynamics have been performed using cell lines with megakaryocyte-like characteristics or during the process of megakaryocyte differentiation. Additionally, this study is pioneer in using MARIMO cell line as a model of megakaryocyte differentiation in the study of *CALR* mutations. However, the use of cell lines has disadvantages when extrapolating the results to the MPN disease pathology (Iborra and Papadopoulos, 2017). Therefore, future work analysing the

effects of *CALR* mutations presented in this thesis should be cautious, as the studies displayed here need to be continued with human primary megakaryocytes from ET and PMF patients.

7.2. Concluding remarks

Structural characteristics of CALR C-terminal domain are affected by *CALR* exon 9 mutations found in MPNs. Changes in the physical properties of this mutant domain, together with the abnormal CALR mutant sub-cellular localisation described in this study, could be the base for the molecular and cellular understanding of novel protein interactions, such as MPL binding, and abnormal Ca^{2+} buffering activity during megakaryocyte hyperplasia.

Intracellular Ca^{2+} regulation is highly important for megakaryocytic differentiation in physiological conditions and disease. *CALR* mutations affect this highly controlled regulation during megakaryocyte formation, by altering $[Ca^{2+}_i]$ and ER Ca^{2+} buffering activity, suggesting that intracellular Ca^{2+} homeostasis plays an important role during the pathogenesis of MPNs harbouring *CALR* mutations.

Establishment of MARIMO cell line as a novel model to study megakaryopoiesis in presence of *CALR* mutations opens the possibility of an easy accessible cellular model to study the pathogenesis of CALR mutant cellular functions during the process of megakaryocyte formation characteristic of ET and PMF. These results, together with the data shown in this thesis revealing the importance of analysing the different effects of *CALR* mutations during the process of megakaryocyte formation, lead to an innovative approach to study the pathogenic role of these driver mutations described in MPNs.

Overall, these findings shed light into the effects of *CALR* mutations in the physical and functional characteristics of CALR in MPNs, describing new aspects of the oncogenic capacity of this driver mutation. This thesis helps to complete our understanding of CALR mutant cellular pathogenesis, which will be essential to reach a full interpretation of the clinical manifestations of ET and PMF patients harbouring *CALR* mutations.

7.3. Research limitations

Although this study has achieved its aims, there were some technical limitations and shortcomings that should be highlighted. The study was conducted using several cell lines and therefore, the extrapolation of the obtained results to primary human megakaryocytes would be important for a correct interpretation of the effects shown in this study.

The laboratory techniques used during this investigation displayed some limitations that should be taken into consideration. Cellular Ca^{2+} quantification was performed using flow cytometry. This technique is valid and has been used for this purpose (Kollmann et al., 2015), however, the use of fluorescent microscopy to register Ca^{2+} fluctuations in a continuous time frame could provide more detailed results than flow cytometry. During this project, several attempts were performed to use microscopy to measure the Ca^{2+} fluctuations in response to thapsigargin treatment; however the use of this technique was not successful due to limitations of the equipment.

SYBR green, used for RT-QPCR, is reported to give background signal and false positives. However, during this study we carefully analysed and optimised primer efficiency as well as melting curves to ensure the amplification of a single product (see appendix 2).

The use of bioinformatic tools to analyse the secondary structure of mutant CALR C-terminal domain displayed some imprecisions between different prediction servers. Although the obtained models showed good predictive ratios, the discrepancies described between different predictor tools confirmed the limitations of using *in silico* techniques. Thus, the models described here should be taken as preliminary models which should be used to perform further structure modelling analyses, possibly adding further variants that could affect its structure, such as physiological Ca^{2+} concentrations. Such models should be confirmed using X-ray diffraction and NMR spectroscopy analysis which were beyond the scope of the current study.

Finally, extrapolation of the experimental results obtained during this study into a phenomenon *in vivo*, such as animal or clinical models, is an important point that required consideration. This will be essential to understand the importance of single molecular effect in a more complex model.

References

Abell, K. & Watson, C. J. 2005. The Jak/Stat pathway: a novel way to regulate PI3K activity. *Cell Cycle,* 4, 897-900.

Akashi, K., Traver, D., Miyamoto, T. & Weissman, I. L. 2000. A clonogenic common myeloid progenitor that gives rise to all myeloid lineages. *Nature,* 404, 193-197.

Andrici, J., Farzin, M., Clarkson, A., Sioson, L., Sheen, A., Watson, N., Toon, C. W., Koleth, M., Stevenson, W. & GILL, A. J. 2016. Mutation specific immunohistochemistry is highly specific for the presence of calreticulin mutations in myeloproliferative neoplasms. *Pathology,* 48, 319-24.

Araki, M., Yang, Y., MAsubuchi, N., Hironaka, Y., Takei, H., Morishita, S., Mizukami, Y., Kan, S., Shirane, S., Edahiro, Y., Sunami, Y., Ohsaka, A. & Komatsu, N. 2016. Activation of the thrombopoietin receptor by mutant calreticulin in CALR-mutant myeloproliferative neoplasms. *Blood,* 127**,** 1307-16.

Arber, D. A., Orazi, A., Hasserjian, R., Thiele, J., Borowitz, M. J., Le Beau, M. M., Bloomfield, C. D., Cazzola, M. & Vardiman, J. W. 2016. The 2016 revision to the World Health Organization classification of myeloid neoplasms and acute leukemia. *Blood,* 127, 2391-405.

Aruch, D. & Mascarenhas, J. 2016. Contemporary approach to essential thrombocythemia and polycythemia vera. *Curr Opin Hematol,* 23, 150-160.

Avecilla, S. T., Hattori, K., Heissig, B., Tejada, R., Liao, F., Shido, K., Jin, D. K., Dias, S., Zhang, F., Hartman, T. E., Hackett, N. R., Crystal, R. G., Witte, L., Hicklin, D. J., Bohlen, P., Eaton, D., Lyden, D., De Sauvage, F. & Rafii, S. 2004. Chemokine-mediated interaction of hematopoietic progenitors with the bone marrow vascular niche is required for thrombopoiesis. *Nat Med,* 10, 64-71.

Babu, M. M., Van Der Lee, R., De Groot, N. S. & Gsponer, J. 2011. Intrinsically disordered proteins: regulation and disease. *Curr Opin Struct Biol,* 21, 432-40.

Baksh, S. & Michalak, M. 1991. Expression of calreticulin in Escherichia coli and identification of its Ca2+ binding domains. *J Biol Chem,* 266, 21458-65.

Baksh, S., Spamer, C., Heilmann, C. & MIchalak, M. 1995. Identification of the Zn2+ binding region in calreticulin. *FEBS Lett,* 376, 53-7.

Balduini, A., Badalucco, S., Pugliano, M. T., Baev, D., De Silvestri, A., Cattaneo, M., Rosti, V. & Barosi, G. 2011. In vitro megakaryocyte differentiation and proplatelet formation in Ph-negative classical myeloproliferative neoplasms: distinct patterns in the different clinical phenotypes. *PLoS One,* 6, e21015.

Baxter, E. J., Scott, L. M., CampbelL, P. J., East, C., Fourouclas, N., Swanton, S., Vassiliou, G. S., Bench, A. J., Boyd, E. M., Curtin, N., Scott, M. A., Erber, W. N., & Green, A. R. 2005. Acquired mutation of the tyrosine kinase JAK2 in human myeloproliferative disorders. *Lancet,* 365, 1054-61.

Bean, B. P. 1991. Pharmacology of calcium channels in cardiac muscle, vascular muscle, and neurons. *Am J Hypertens,* 4, 406S-411S.

Bedard, K., Szabo, E., Michalak, M. & Opas, M. 2005. Cellular functions of endoplasmic reticulum chaperones calreticulin, calnexin, and ERp57. *Int Rev Cytol,* 245, 91-121.

Beer, P. A., Erber, W. N., Campbell, P. J. & Green, A. R. 2011. How I treat essential thrombocythemia. *Blood,* 117, 1472-1482.

Beer, P. A., Jones, A. V., Bench, A. J., Goday-Fernandez, A., Boyd, E. M., Vaghela, K. J., Erber, W. N., Odeh, B., Wright, C., Mcmullin, M. F., Cullis, J., Huntly, B. J., Harrison, C. N.,

Cross, N. C. & Green, A. R. 2009. Clonal diversity in the myeloproliferative neoplasms: independent origins of genetically distinct clones. *Br J Haematol,* 144, 904-8.

Berridge, M. J. 2002. The endoplasmic reticulum: a multifunctional signaling organelle. *Cell Calcium,* 32, 235-49.

Berridge, M. J., Bootman, M. D. & Roderick, H. L. 2003. Calcium signalling: dynamics, homeostasis and remodelling. *Nat Rev Mol Cell Biol,* 4, 517-29.

Berridge, M. J., Lipp, P. & Bootman, M. D. 2000. The versatility and universality of calcium signalling. *Nature Reviews Molecular Cell Biology,* 1, 11-21.

Besancenot, R., Roos-Weil, D., Tonetti, C., Abdelouahab, H., Lacout, C., Pasquier, F., Willekens, C., Rameau, P., Lecluse, Y., Micol, J. B., Constantinescu, S. N., Vainchenker, W., Solary, E. & Giraudier, S. 2014. JAK2 and MPL protein levels determine TPO-induced megakaryocyte proliferation vs differentiation. *Blood,* 124, 2104-15.

Bianchi, E., Norfo, R., Pennucci, V., Zini, R. & Manfredini, R. 2016. Genomic landscape of megakaryopoiesis and platelet function defects. *Blood,* 127, 1249-59.

Bibi, A., AgarwaL, N. K., Dihazi, G. H., Eltoweissy, M., Nguyen, P. V., Mueller, G. A. & Dihazi, H. 2011. Calreticulin is crucial for calcium homeostasis mediated adaptation and survival of thick ascending limb of Henle's loop cells under osmotic stress. *International Journal of Biochemistry & Cell Biology,* 43, 1187-1197.

Bikle, D. D., Oda, Y. & Xie, Z. 2004. Calcium and 1,25(OH)2D: interacting drivers of epidermal differentiation. *J Steroid Biochem Mol Biol,* 89-90, 355-60.

Borg, J., Papadopoulos, P., Georgitsi, M., Gutierrez, L., Grech, G., Fanis, P., PhylactideS, M., Verkerk, A. J., Van Der Spek, P. J., ScerrI, C. A., Cassar, W., Galdies, R., Van Ijcken, W., Ozgur, Z., Gillemans, N., Hou, J., Bugeja, M., Grosveld, F. G., Von Lindern, M., Felice, A. E., Patrinos, G. P. & Philipsen, S. 2010. Haploinsufficiency for the erythroid

transcription factor KLF1 causes hereditary persistence of fetal hemoglobin. *Nat Genet,* 42, 801-5.

Borges, S., Moudilou, E., Vouyovitch, C., Chiesa, J., Lobie, P., Mertani, H. & Raccurt, M. 2008. Involvement of a JAK/STAT pathway inhibitor: cytokine inducible SH2 containing protein in breast cancer. *Adv Exp Med Biol,* 617, 321-9.

Brault, L., Gasser, C., Bracher, F., Huber, K., Knapp, S. & Schwaller, J. 2010. PIM serine/threonine kinases in the pathogenesis and therapy of hematologic malignancies and solid cancers. *Haematologica-the Hematology Journal,* 95, 1004-1015.

Breier, A. & Michalak, M. 1994. 2,4,6-Trinitrobenzenesulfonic acid modification of the carboxyl-terminal region (C-domain) of calreticulin. *Mol Cell Biochem,* 130, 19-28.

Bunting, S., Widmer, R., Lipari, T., Rangell, L., steinmetz, H., Carver-moore, K., Moore, M. W., Keller, G. A. & De Sauvage, F. J. 1997. Normal platelets and megakaryocytes are produced in vivo in the absence of thrombopoietin. *Blood,* 90, 3423-9.

Cabagnols, X., Defour, J. P., Ugo, V., Ianotto, J. C., Mossuz, P., Mondet, J., Girodon, F., Alexandre, J. H., Mansier, O., Viallard, J. F., Lippert, E., Murati, A., Mozziconacci, M. J., Saussoy, P., Vekemans, M. C., Knoops, L., Pasquier, F., Ribrag, V., Solary, E., Plo, I., Constantinescu, S. N., Casadevall, N., Vainchenker, W., Marzac, C. & Bluteau, O. 2015. Differential association of calreticulin type 1 and type 2 mutations with myelofibrosis and essential thrombocytemia: relevance for disease evolution. *Leukemia,* 29, 249-52.

Cacalano, N. A., Sanden, D. & Johnston, J. A. 2001. Tyrosine-phosphorylated SOCS-3 inhibits STAT activation but binds to p120 RasGAP and activates Ras. *Nat Cell Biol,* 3, 460-5.

Cahalan, M. D. 2009. STIMulating store-operated Ca(2+) entry. *Nat Cell Biol,* 11, 669-77.

Carafoli, E. 2002. Calcium signaling: A tale for all seasons. *Proceedings of the National Academy of Sciences of the United States of America,* 99, 1115-1122.

Caramelo, J. J. & Parodi, A. J. 2008. Getting in and out from calnexin/calreticulin cycles. *J Biol Chem,* 283, 10221-5.

Carbonell, F., Hoelzer, D., Thiel, E. & Bartl, R. 1982. Ph1 -positive CML associated with megakaryocytic hyperplasia and thrombocythemia and an abnormality of chromosome no. 3. *Cancer Genet Cytogenet,* 6, 153-61.

Catterall, W. A. 2011. Voltage-gated calcium channels. *Cold Spring Harb Perspect Biol,* 3, a003947.

Chachoua, I., Pecquet, C., El-Khoury, M., Nivarthi, H., Albu, R. I., Marty, C., Gryshkova, V., Defour, J. P., Vertenoeil, G., Ngo, A., Koay, A., Raslova, H., Courtoy, P. J., Choong, M. L., Plo, I., Vainchenker, W., Kralovics, R. & Constantinescu, S. N. 2016. Thrombopoietin receptor activation by myeloproliferative neoplasm associated calreticulin mutants. *Blood,* 127, 1325-35.

Chaligne, R., Tonetti, C., Besancenot, R., Roy, L., Marty, C., Mossuz, P., Kiladjian, J. J., Socie, G., Bordessoule, D., Le Bousse-Kerdiles, M. C., Vainchenker, W. & Giraudier, S. 2008. New mutations of MPL in primitive myelofibrosis: only the MPL W515 mutations promote a G1/S-phase transition. *Leukemia,* 22, 1557-66.

Chang, L. W. & Spitzer, N. C. 2009. Spontaneous calcium spike activity in embryonic spinal neurons is regulated by developmental expression of the Na+, K+-ATPase beta3 subunit. *J Neurosci,* 29, 7877-85.

Chiang, W. F., Hwang, T. Z., Hour, T. C., Wang, L. H., Chiu, C. C., Chen, H. R., Wu, Y. J., Wang, C. C., Wang, L. F., Chien, C. Y., Chen, J. H., Hsu, C. T. & Chen, J. Y. 2013. Calreticulin, an endoplasmic reticulum-resident protein, is highly expressed and essential for cell proliferation and migration in oral squamous cell carcinoma. *Oral Oncol,* 49, 534-41.

Choi, Y., Sims, G. E., Murphy, S., Miller, J. R. & Chan, A. P. 2012. Predicting the functional effect of amino acid substitutions and indels. *PLoS One,* 7, e46688.

Coe, H. & Michalak, M. 2009. Calcium binding chaperones of the endoplasmic reticulum. *General Physiology and Biophysics,* 28, F96-F103.

Coletta, A., Pinney, J. W., Solis, D. Y. W., Marsh, J., Pettifer, S. R. & Attwood, T. K. 2010. Low-complexity regions within protein sequences have position-dependent roles. *Bmc Systems Biology,* 4.

Collins, S. J. 1987. The HL-60 promyelocytic leukemia cell line: proliferation, differentiation, and cellular oncogene expression. *Blood,* 70, 1233-44.

Coppolino, M. G., Woodside, M. J., Demaurex, N., Grinstein, S., Starnaud, R. & Dedhar, S. 1997. Calreticulin is essential for integrin-mediated calcium signalling and cell adhesion. *Nature,* 386, 843-847.

Crowley, L. C., Chojnowski, G. & Waterhouse, N. J. 2016. Measuring the DNA Content of Cells in Apoptosis and at Different Cell-Cycle Stages by Propidium Iodide Staining and Flow Cytometry. *Cold Spring Harb Protoc,* 2016, pdb prot087247.

Dameshek, W. 1951. Some Speculations on the Myeloproliferative Syndromes. *Blood,* 6, 372-375.

Datta, N. S. & Long, M. W. 2002. Modulation of MDM2/p53 and cyclin-activating kinase during the megakaryocyte differentiation of human erythroleukemia cells. *Exp Hematol,* 30, 158-65.

DE KOUCHKOVSKY, I. & ABDUL-HAY, M. 2016. Acute myeloid leukemia: a comprehensive review and 2016 update. *Blood Cancer Journal,* 6.

Debili, N., Coulombel, L., Croisille, L., Katz, A., Guichard, J., Breton-Gorius, J. & Vainchenker, W. 1996. Characterization of a bipotent erythro-megakaryocytic progenitor in human bone marrow. *Blood,* 88, 1284-96.

Dedhar, S., Rennie, P. S., Shago, M., Hagesteijn, C. Y., Yang, H., Filmus, J., Hawley, R. G., Bruchovsky, N., Cheng, H., Matusik, R. J. & et al. 1994. Inhibition of nuclear hormone receptor activity by calreticulin. *Nature,* 367, 480-3.

Degos, L. & Wang, Z. Y. 2001. All trans retinoic acid in acute promyelocytic leukemia. *Oncogene,* 20, 7140-7145.

Delhommeau, F., Dupont, S., Della Valle, V., James, C., Trannoy, S., Masse, A., Kosmider, O., Le Couedic, J. P., Robert, F., Alberdi, A., Lecluse, Y., Plo, I., Dreyfus, F. J., Marzac, C., Casadevall, N., Lacombe, C., Romana, S. P., Dessen, P., Soulier, J., Viguie, F., Fontenay, M., Vainchenker, W. & Bernard, O. A. 2009. Mutation in TET2 in myeloid cancers. *N Engl J Med,* 360, 2289-301.

Den Dekker, E., Gorter, G., Van Der Vuurst, H., Heemskerk, J. W. & Akkerman, J. W. 2001. Biogenesis of G-protein mediated calcium signaling in human megakaryocytes. *Thromb Haemost,* 86, 1106-13.

Deng, X., Wang, Y., Zhou, Y., Soboloff, J. & Gill, D. L. 2009. STIM and Orai: dynamic intermembrane coupling to control cellular calcium signals. *J Biol Chem,* 284, 22501-5.

Di Buduo, C. A., Balduini, A. & Moccia, F. 2016. Pathophysiological Significance of Store-Operated Calcium Entry in Megakaryocyte Function: Opening New Paths for Understanding the Role of Calcium in Thrombopoiesis. *Int J Mol Sci,* 17.

Disfani, F. M., Hsu, W. L., Mizianty, M. J., Oldfield, C. J., Xue, B., Dunker, A. K., Uversky, V. N. & Kurgan, L. 2012. MoRFpred, a computational tool for sequence-based prediction

and characterization of short disorder-to-order transitioning binding regions in proteins. *Bioinformatics,* 28, i75-83.

Dolmetsch, R. 2003. Excitation-transcription coupling: signaling by ion channels to the nucleus. *Sci STKE,* 2003, PE4.

Dolmetsch, R. E., Lewis, R. S., Goodnow, C. C. & Healy, J. I. 1997. Differential activation of transcription factors induced by Ca2+ response amplitude and duration. *Nature,* 386, 855-8.

Dolmetsch, R. E., Xu, K. & Lewis, R. S. 1998. Calcium oscillations increase the efficiency and specificity of gene expression. *Nature,* 392, 933-6.

Dosztanyi, Z., Csizmok, V., Tompa, P. & Simon, I. 2005. IUPred: web server for the prediction of intrinsically unstructured regions of proteins based on estimated energy content. *Bioinformatics,* 21, 3433-4.

Dosztanyi, Z., Meszaros, B. & Simon, I. 2009. ANCHOR: web server for predicting protein binding regions in disordered proteins. *Bioinformatics,* 25, 2745-6.

Dunker, A. K., Lawson, J. D., Brown, C. J., Williams, R. M., Romero, P., Oh, J. S., Oldfield, C. J., Campen, A. M., Ratliff, C. M., Hipps, K. W., Ausio, J., Nissen, M. S., Reeves, R., Kang, C., Kissinger, C. R., Bailey, R. W., Griswold, M. D., Chiu, W., Garner, E. C. & Obradovic, Z. 2001. Intrinsically disordered protein. *J Mol Graph Model,* 19, 26-59.

Dupont, G., Houart, G. & De Koninck, P. 2003. Sensitivity of CaM kinase II to the frequency of Ca2+ oscillations: a simple model. *Cell Calcium,* 34, 485-497.

Eckly, A., Heijnen, H., Pertuy, F., Geerts, W., Proamer, F., Rinckel, J. Y., Leon, C., Lanza, F. & Gachet, C. 2014. Biogenesis of the demarcation membrane system (DMS) in megakaryocytes. *Blood,* 123, 921-30.

Eckly, A., Heijnen, H., Pertuy, F., Geerts, W., Proamer, F., Rinckel, J. Y., Leon, C., Lanza, F. & Gachet, C. 2014. Biogenesis of the demarcation membrane system (DMS) in megakaryocytes. *Blood,* 123, 921-30.

Eder-Azanza, L., Navarro, D., Aranaz, P., Novo, F. J., Cross, N. C. & Vizmanos, J. L. 2014. Bioinformatic analyses of CALR mutations in myeloproliferative neoplasms support a role in signaling. *Leukemia,* 28, 2106-9.

Elf, S., Abdelfattah, N. S., Chen, E., Perales-Paton, J., Rosen, E. A., Ko, A., Peisker, F., Florescu, N., Giannini, S., Wolach, O., Morgan, E. A., Tothova, Z., Losman, J. A., Schneider, R. K., Al-Shahrour, F. & Mullally, A. 2016. Mutant Calreticulin Requires Both Its Mutant C-terminus and the Thrombopoietin Receptor for Oncogenic Transformation. *Cancer Discov,* 6, 368-81.

Ernst, T., Chase, A. J., Score, J., Hidalgo-Curtis, C. E., Bryant, C., Jones, A. V., Waghorn, K., Zoi, K., Ross, F. M., Reiter, A., Hochhaus, A., Drexler, H. G., Duncombe, A., Cervantes, F., Oscier, D., Boultwood, J., Grand, F. H. & Cross, N. C. 2010. Inactivating mutations of the histone methyltransferase gene EZH2 in myeloid disorders. *Nat Genet,* 42, 722-6.

Fan, X. & Kurgan, L. 2014. Accurate prediction of disorder in protein chains with a comprehensive and empirically designed consensus. *J Biomol Struct Dyn,* 32, 448-64.

Flores-Guzman, P., Gutierrez-Rodriguez, M. & Mayani, H. 2002. In vitro proliferation, expansion, and differentiation of a CD34+ cell-enriched hematopoietic cell population from human umbilical cord blood in response to recombinant cytokines. *Arch Med Res,* 33, 107-14.

Frawley, T., O'brien, C. P., Conneally, E., Vandenberghe, E., Percy, M., Langabeer, S. E. & Haslam, K. 2018. Development of a Targeted Next-Generation Sequencing Assay to Detect Diagnostically Relevant Mutations of JAK2, CALR, and MPL in Myeloproliferative Neoplasms. *Genet Test Mol Biomarkers*.

Frickel, E. M., Riek, R., Jelesarov, I., Helenius, A., Wuthrich, K. & Ellgaard, L. 2002. TROSY-NMR reveals interaction between ERp57 and the tip of the calreticulin P-domain. *Proceedings of the National Academy of Sciences of the United States of America,* 99, 1954-1959.

Gangat, N., Patnaik, M. M. & Tefferi, A. 2016. Myelodysplastic syndromes: Contemporary review and how we treat. *American Journal of Hematology,* 91, 76-89.

Ganguly, S. & Cunningham, M. T. 2004. Idiopathic thrombocytopenic purpura associated with bone marrow sea-blue histiocytosis. *Am J Hematol,* 77, 405-6.

Gattinoni, L., Powell, D. J., Jr., Rosenberg, S. A. & Restifo, N. P. 2006. Adoptive immunotherapy for cancer: building on success. *Nat Rev Immunol,* 6, 383-93.

Geddis, A. E. 2010. Megakaryopoiesis. *Semin Hematol,* 47, 212-9.

Genever, P. G., Wilkinson, D. J., Patton, A. J., Peet, N. M., Hong, Y., Mathur, A., Erusalimsky, J. D. & Skerry, T. M. 1999. Expression of a functional N-methyl-D-aspartate-type glutamate receptor by bone marrow megakaryocytes. *Blood,* 93, 2876-83.

Giannone, G., Ronde, P., Gaire, M., Haiech, J. & Takeda, K. 2002. Calcium oscillations trigger focal adhesion disassembly in human U87 astrocytoma cells. *J Biol Chem,* 277, 26364-71.

Giraldo, A. M. V., Medus, M. L., Lebrero, M. G., Pagano, R. S., Labriola, C. A., Landolfo, L., Delfino, J. M., Parodi, A. J. & Caramelo, J. J. 2010. The Structure of Calreticulin C-terminal Domain Is Modulated by Physiological Variations of Calcium Concentration. *Journal of Biological Chemistry,* 285, 4544-4553.

Gold, L. I., Eggleton, P., Sweetwyne, M. T., Van Duyn, L. B., Greives, M. R., Naylor, S. M., Michalak, M. & Murphy-Ullrich, J. E. 2010. Calreticulin: non-endoplasmic reticulum functions in physiology and disease. *FASEB J,* 24, 665-83.

204

Graham, F. L., Smiley, J., Russell, W. C. & Nairn, R. 1977. Characteristics of a human cell line transformed by DNA from human adenovirus type 5. *J Gen Virol,* 36, 59-74.

Greenberg, S. M., Rosenthal, D. S., Greeley, T. A., Tantravahi, R. & Handin, R. I. 1988. Characterization of a new megakaryocytic cell line: the Dami cell. *Blood,* 72, 1968-77.

Greenhalgh, C. J. & Hilton, D. J. 2001. Negative regulation of cytokine signaling. *J Leukoc Biol,* 70, 348-56.

Greives, M. R., Samra, F., Pavlides, S. C., Blechman, K. M., Naylor, S. M., Woodrell, C. D., Cadacio, C., Levine, J. P., Bancroft, T. A., Michalak, M., Warren, S. M. & Gold, L. I. 2012. Exogenous calreticulin improves diabetic wound healing. *Wound Repair Regen,* 20, 715-30.

Grosse, J., Braun, A., Varga-Szabo, D., Beyersdorf, N., Schneider, B., Zeitlmann, L., Hanke, P., Schropp, P., Muhlstedt, S., Zorn, C., Huber, M., Schmittwolf, C., Jagla, W., Yu, P., Kerkau, T., Schulze, H., Nehls, M. & Nieswandt, B. 2007. An EF hand mutation in Stim1 causes premature platelet activation and bleeding in mice. *J Clin Invest,* 117, 3540-50.

GU, X. N., OLSON, E. C. & SPITZER, N. C. 1994. Spontaneous Neuronal Calcium Spikes and Waves during Early Differentiation. *Journal of Neuroscience,* 14, 6325-6335.

GUNASEKARAN, K., TSAI, C. J., KUMAR, S., ZANUY, D. & NUSSINOV, R. 2003. Extended disordered proteins: targeting function with less scaffold. *Trends Biochem Sci,* 28, 81-5.

GURNEY, A. L., CARVER-MOORE, K., DE SAUVAGE, F. J. & MOORE, M. W. 1994. Thrombocytopenia in c-mpl-deficient mice. *Science,* 265, 1445-7.

HAHN, A. W., LI, B., PROUET, P., GIRI, S., PATHAK, R. & MARTIN, M. G. 2016. Acute megakaryocytic leukemia: What have we learned. *Blood Reviews,* 30, 49-53.

Hamad, M. I., Krause, M. & Wahle, P. 2015. Improving AM ester calcium dye loading efficiency. *J Neurosci Methods,* 240, 48-60.

Han, L., Schubert, C., Kohler, J., Schemionek, M., Isfort, S., Brummendorf, T. H., Koschmieder, S. & Chatain, N. 2016. Calreticulin-mutant proteins induce megakaryocytic signaling to transform hematopoietic cells and undergo accelerated degradation and Golgi-mediated secretion. *J Hematol Oncol,* 9, 45.

Harrison, C., Kiladjian, J. J., Al-Ali, H. K., Gisslinger, H., Waltzman, R., Stalbovskaya, V., Mcquitty, M., Hunter, D. S., Levy, R., Knoops, L., Cervantes, F., Vannucchi, A. M., Barbui, T. & Barosi, G. 2012. JAK inhibition with ruxolitinib versus best available therapy for myelofibrosis. *N Engl J Med,* 366, 787-98.

Hattori, A., Koike, T., Soga, N., Shibata, A. & Ihzumi, T. 1987. The morphology of megakaryocytes. *Rinsho Byori,* 71, 34-48.

Hattori, K., Nakamura, K., Hisatomi, Y., Matsumoto, S., Suzuki, M., Harvey, R. P., Kurihara, H., Hattori, S., Yamamoto, T., Michalak, M. & Endo, F. 2007. Arrhythmia induced by spatiotemporal overexpression of calreticulin in the heart. *Molecular Genetics and Metabolism,* 91, 285-293.

Hebert, D. N. & Molinari, M. 2007. In and out of the ER: protein folding, quality control, degradation, and related human diseases. *Physiol Rev,* 87, 1377-408.

Hebert, D. N., Zhang, J. X., Chen, W., Foellmer, B. & Helenius, A. 1997. The number and location of glycans on influenza hemagglutinin determine folding and association with calnexin and calreticulin. *J Cell Biol,* 139, 613-23.

Hirose, K., Monzen, S., Sato, H., Sato, M., Aoki, M., Hatayama, Y., Kawaguchi, H., Narita, Y., Takai, Y. & Kashiwakura, I. 2013. Megakaryocytic differentiation in human chronic myelogenous leukemia K562 cells induced by ionizing radiation in combination with phorbol 12-myristate 13-acetate. *J Radiat Res,* 54, 438-46.

Hitchcock, I. S., Skerry, T. M., Howard, M. R. & Genever, P. G. 2003. NMDA receptor-mediated regulation of human megakaryocytopoiesis. *Blood,* 102, 1254-9.

Holaska, J. M., Black, B. E., Love, D. C., Hanover, J. A., Leszyk, J. & Paschal, B. M. 2001. Calreticulin is a receptor for nuclear export. *Journal of Cell Biology,* 152, 127-140.

Holmstrom, M. O., Martinenaite, E., Ahmad, S. M., Met, O., Friese, C., Kjaer, L., Riley, C. H., Thor Straten, P., Svane, I. M., Hasselbalch, H. C. & Andersen, M. H. 2017. The calreticulin (CALR) exon 9 mutations are promising targets for cancer immune therapy. *Leukemia*. 32, 429-437.

Huang, R., Zhao, L., Chen, H., Yin, R. H., Li, C. Y., Zhan, Y. Q., Zhang, J. H., Ge, C. H., Yu, M. & Yang, X. M. 2014. Megakaryocytic differentiation of K562 cells induced by PMA reduced the activity of respiratory chain complex IV. *PLoS One,* 9, e96246.

Huberman, E. & Callaham, M. F. 1979. Induction of terminal differentiation in human promyelocytic leukemia cells by tumor-promoting agents. *Proc Natl Acad Sci U S A,* 76, 1293-7.

Hui, K., Gao, Y., Huang, J., Xu, S., Wang, B., Zeng, J., Fan, J., Wang, X., Yue, Y., Wu, S., Hsieh, J. T., He, D. & Wu, K. 2017. RASAL2, a RAS GTPase-activating protein, inhibits stemness and epithelial-mesenchymal transition via MAPK/SOX2 pathway in bladder cancer. *Cell Death Dis,* 8, e2600.

Hung, M. C. & Link, W. 2011. Protein localization in disease and therapy. *J Cell Sci,* 124, 3381-92.

Hunt, P., Zsebo, K. M., Hokom, M. M., Hornkohl, A., Birkett, N. C., Delcastillo, J. C. & Martin, F. 1992. Evidence That Stem-Cell Factor Is Involved in the Rebound Thrombocytosis That Follows 5-Fluorouracil Treatment. *Blood,* 80, 904-911.

Huo, X. F., Yu, J., Peng, H., Du, Z. W., Liu, X. L., Ma, Y. N., Zhang, X., Zhang, Y., Zhao, H. L. & Zhang, J. W. 2006. Differential expression changes in K562 cells during the hemin-induced erythroid differentiation and the phorbol myristate acetate (PMA)-induced megakaryocytic differentiation. *Mol Cell Biochem,* 292, 155-67.

Hussein, K., Bock, O., Theophile, K., Seegers, A., Arps, H., Basten, O., Grips, K. H., Franz-Werner, J., Busche, G. & Kreipe, H. 2008. Chronic myeloproliferative diseases with concurrent BCR-ABL junction and JAK2V617F mutation. *Leukemia,* 22, 1059-62.

Hutchins, B. I. & Kalil, K. 2008. Differential outgrowth of axons and their branches is regulated by localized calcium transients. *Journal of Neuroscience,* 28, 143-153.

Iborra, F. J. & Papadopoulos, P. 2017. Calreticulin in Essential Thrombocythemia: StressINg OUT the Megakaryocyte Nucleus. *Front Oncol,* 7, 103.

Ihle, J. N. & Gilliland, D. G. 2007. Jak2: normal function and role in hematopoietic disorders. *Curr Opin Genet Dev,* 17, 8-14.

Jacquel, A., Herrant, M., Defamie, V., Belhacene, N., Colosetti, P., Marchetti, S., Legros, L., Deckert, M., Mari, B., Cassuto, J. P., Hofman, P. & Auberger, P. 2006. A survey of the signaling pathways involved in megakaryocytic differentiation of the human K562 leukemia cell line by molecular and c-DNA array analysis. *Oncogene,* 25, 781-94.

James, C., Ugo, V., Le Couedic, J. P., Staerk, J., Delhommeau, F., Lacout, C., Garcon, L., Raslova, H., Berger, R., Bennaceur-Griscelli, A., Villeval, J. L., Constantinescu, S. N., Casadevall, N. & Vainchenker, W. 2005. A unique clonal JAK2 mutation leading to constitutive signalling causes polycythaemia vera. *Nature,* 434, 1144-8.

Jeong, J. H., Lee, H. T., Seo, J. Y., Seo, Y. H., Kim, K. H., Kim, M. J., Lee, J. H., Park, J., Hong, J. S., Park, P. W. & Ahn, J. Y. 2016. Screening PCR Versus Sanger Sequencing: Detection of CALR Mutations in Patients With Thrombocytosis. *Ann Lab Med,* 36, 291-9.

Jethra, G., Mishra, A. K., Pandey, P. S. & Chandrasekharan, H. 2012. Structure and function prediction of unknown wheat protein using LOMETS and I-TASSER. *Indian Journal of Agricultural Sciences,* 82, 867-874.

Johnson, S., Michalak, M., Opas, M. & Eggleton, P. 2001. The ins and outs of calreticulin: from the ER lumen to the extracellular space. *Trends Cell Biol,* 11, 122-9.

Junt, T., Schulze, H., Chen, Z., Massberg, S., Goerge, T., Krueger, A., Wagner, D. D., Graf, T., Italiano, J. E., Jr., Shivdasani, R. A. & Von Andrian, U. H. 2007. Dynamic visualization of thrombopoiesis within bone marrow. *Science,* 317, 1767-70.

Kalev-Zylinska, M. L., Green, T. N., Morel-Kopp, M. C., Sun, P. P., Park, Y. E., Lasham, A., During, M. J. & Ward, C. M. 2014. N-methyl-D-aspartate receptors amplify activation and aggregation of human platelets. *Thromb Res,* 133, 837-47.

Kamal, T., Green, T. N., Morel-Kopp, M. C., Ward, C. M., Mcgregor, A. L., Mcglashan, S. R., Bohlander, S. K., Browett, P. J., Teague, L., During, M. J., Skerry, T. M., Josefsson, E. C. & Kalev-Zylinska, M. L. 2015. Inhibition of glutamate regulated calcium entry into leukemic megakaryoblasts reduces cell proliferation and supports differentiation. *Cellular Signalling,* 27, 1860-1872.

Kang, C. D., Lee, B. K., Kim, K. W., Kim, C. M., Kim, S. H. & Chung, B. S. 1996. Signaling mechanism of PMA-induced differentiation of K562 cells. *Biochem Biophys Res Commun,* 221, 95-100.

Kang, C. D., Lee, B. K., Kim, K. W., Kim, C. M., Kim, S. H. & Chung, B. S. 1996. Signaling mechanism of PMA-induced differentiation of K562 cells. *Biochem Biophys Res Commun,* 221, 95-100.

Khan, S. & Vihinen, M. 2007. Spectrum of disease-causing mutations in protein secondary structures. *BMC Struct Biol,* 7, 56.

Kiladjian, J. J. 2012. The spectrum of JAK2-positive myeloproliferative neoplasms. *Hematology Am Soc Hematol Educ Program,* 2012, 561-6.

Kilpivaara, O. & Levine, R. L. 2008. JAK2 and MPL mutations in myeloproliferative neoplasms: discovery and science. *Leukemia,* 22, 1813-7.

Kisseleva, T., Bhattacharya, S., Braunstein, J. & Schindler, C. W. 2002. Signaling through the JAK/STAT pathway, recent advances and future challenges. *Gene,* 285, 1-24.

Klampfl, T., Gisslinger, H., Harutyunyan, A. S., Nivarthi, H., Rumi, E., Milosevic, J. D., Them, N. C., Berg, T., Gisslinger, B., Pietra, D., Chen, D., Vladimer, G. I., Bagienski, K., Milanesi, C., Casetti, I. C., Sant'antonio, E., Ferretti, V., Elena, C., Schischlik, F., Cleary, C., Six, M., Schalling, M., Schonegger, A., Bock, C., Malcovati, L., Pascutto, C., Superti-Furga, G., Cazzola, M. & Kralovics, R. 2013. Somatic mutations of calreticulin in myeloproliferative neoplasms. *N Engl J Med,* 369, 2379-90.

Klco, J. M., Vij, R., Kreisel, F. H., Hassan, A. & Frater, J. L. 2010. Molecular pathology of myeloproliferative neoplasms. *Am J Clin Pathol,* 133, 602-15.

Koeffler, H. P., Bareli, M. & Territo, M. C. 1981. Phorbol Ester Effect on Differentiation of Human Myeloid-Leukemia Cell-Lines Blocked at Different Stages of Maturation. *Cancer Research,* 41, 919-926.

Kollmann, K., Nangalia, J., Warsch, W., Quentmeier, H., Bench, A., Boyd, E., Scott, M., Drexler, H. G. & Green, A. R. 2015. MARIMO cells harbor a CALR mutation but are not dependent on JAK2/STAT5 signaling. *Leukemia,* 29, 494-7.

Kollmann, K., Warsch, W., Gonzalez-Arias, C., Nice, F. L., Avezov, E., Milburn, J., Li, J., Dimitropoulou, D., Biddie, S., Wang, M., Poynton, E., Colzani, M., Tijssen, M. R., Anand, S., Mcdermott, U., Huntly, B. & Green, T. 2016. A novel signalling screen demonstrates that CALR mutations activate essential MAPK signalling and facilitate megakaryocyte differentiation. *Leukemia*. 31: 934-944.

Kondo, M., Weissman, I. L. & Akashi, K. 1997. Identification of clonogenic common lymphoid progenitors in mouse bone marrow. *Cell,* 91, 661-72.

Kozlov, G., Pocanschi, C. L., Rosenauer, A., Bastos-Aristizabal, S., Gorelik, A., Williams, D. B. & Gehring, K. 2010. Structural basis of carbohydrate recognition by calreticulin. *J Biol Chem,* 285, 38612-20.

Kralovics, R., Passamonti, F., Buser, A. S., Teo, S. S., Tiedt, R., Passweg, J. R., Tichelli, A., Cazzola, M. & Skoda, R. C. 2005. A gain-of-function mutation of JAK2 in myeloproliferative disorders. *N Engl J Med,* 352, 1779-90.

Kwon, M. S., Park, C. S., Choi, K., Ahn, J., Kim, J. I., Eom, S. H., Kaufman, S. J. & Song, W. K. 2000. Calreticulin couples calcium release and calcium influx in integrin-mediated calcium signaling. *Mol Biol Cell,* 11, 1433-43.

Lacabaratz-Porret, C., Launay, S., Corvazier, E., Bredoux, R., Papp, B. & Enouf, J. 2000. Biogenesis of endoplasmic reticulum proteins involved in Ca2+ signalling during megakaryocytic differentiation: an in vitro study. *Biochem J,* 350, 723-34.

Lanner, J. T., Georgiou, D. K., Joshi, A. D. & Hamilton, S. L. 2010. Ryanodine receptors: structure, expression, molecular details, and function in calcium release. *Cold Spring Harb Perspect Biol,* 2, a003996.

Laskowski, R. A., Rullmannn, J. A., Macarthur, M. W., Kaptein, R. & Thornton, J. M. 1996. AQUA and PROCHECK-NMR: programs for checking the quality of protein structures solved by NMR. *J Biomol NMR,* 8, 477-86.

Lau, W. W. Y., Hannah, R., Green, A. R. & Gottgens, B. 2015. The JAK-STAT signaling pathway is differentially activated in CALR-positive compared with JAK2V617F-positive ET patients. *Blood,* 125, 1679-1681.

Leach, M. R., Cohen-Doyle, M. F., Thomas, D. Y. & Williams, D. B. 2002. Localization of the lectin, ERp57 binding, and polypeptide binding sites of calnexin and calreticulin. *J Biol Chem,* 277, 29686-97.

Lee, S., Zhou, G., Clark, T., Chen, J., Rowley, J. D. & Wang, S. M. 2001. The pattern of gene expression in human CD15+ myeloid progenitor cells. *Proc Natl Acad Sci U S A,* 98, 3340-5.

Levine, R. L., Wadleigh, M., Cools, J., Ebert, B. L., Wernig, G., Huntly, B. J. P., Boggon, T. J., Wlodarska, L., Clark, J. J., Moore, S., Adelsperger, J., Koo, S., Lee, J. C., Gabriel, S., Mercher, T., D'andrea, A., Frohling, S., Dohner, K., Marynen, P., Vandenberghe, P., Mesa, R. A., Tefferi, A., Griffin, J. D., Eck, M. J., Sellers, W. R., Meyerson, M., Golub, T. R., Lee, S. J. & Gilliland, D. G. 2005. Activating mutation in the tyrosine kinase JAK2 in polycythemia vera, essential thrombocythemia, and myeloid metaplasia with myelofibrosis. *Cancer Cell,* 7, 387-397.

Lim, C. P., Cao, X. 2006. Structure, function, and regulation of STAT proteins. *Mol Biosyst*, 11, 536-50.

Loghavi, S., Bueso-Ramos, C. E., Kanagal-Shamanna, R., Young Ok, C., Salim, A. A., Routbort, M. J., Mehrotra, M., Verstovsek, S., Medeiros, L. J., Luthra, R. & Patel, K. P. 2016. Myeloproliferative Neoplasms With Calreticulin Mutations Exhibit Distinctive Morphologic Features. *Am J Clin Pathol,* 145, 418-27.

Long, M. W. & Williams, N. 1981. Immature Megakaryocytes in the Mouse: Morphology and quantitation by acetylcholinesterase staining. *Blood,* 58, 1032-9.

Long, M. W., Heffner, C. H., Williams, J. L., Peters, C. & Prochownik, E. V. 1990. Regulation of megakaryocyte phenotype in human erythroleukemia cells. *J Clin Invest,* 85, 1072-84.

Lozzio, C. B. & Lozzio, B. B. 1975. Human chronic myelogenous leukemia cell-line with positive Philadelphia chromosome. *Blood,* 45, 321-34.

Lu, T. S., Yiao, S. Y., Lim, K., Jensen, R. V. & Hsiao, L. L. 2010. Interpretation of biological and mechanical variations between the Lowry versus Bradford method for protein quantification. *N Am J Med Sci,* 2, 325-8.

Lu, Y. C., Chen, C. N., Wang, B., Hsu, W. M., Chen, S. T., Chang, K. J., Chang, C. C. & Lee, H. 2011. Changes in tumor growth and metastatic capacities of J82 human bladder cancer cells suppressed by down-regulation of calreticulin expression. *Am J Pathol,* 179, 1425-33.

Lu, Y. C., Weng, W. C. & Lee, H. 2015. Functional roles of calreticulin in cancer biology. *Biomed Res Int,* 2015, 526524.

Luckhoff, A., Bohnert, M. & Busse, R. 1991. Effects of the calmodulin antagonists fendiline and calmidazolium on aggregation, secretion of ATP, and internal calcium in washed human platelets. *Naunyn Schmiedebergs Arch Pharmacol,* 343, 96-101.

Lytton, J., Westlin, M. & Hanley, M. R. 1991. Thapsigargin inhibits the sarcoplasmic or endoplasmic reticulum Ca-ATPase family of calcium pumps. *J Biol Chem,* 266, 17067-71.

Machlus, K. R., Thon, J. N. & Italiano, J. E., JR. 2014. Interpreting the developmental dance of the megakaryocyte: a review of the cellular and molecular processes mediating platelet formation. *Br J Haematol,* 165, 227-36.

Manochitra, K. & Parija, S. C. 2017. In-silico prediction and modeling of the Entamoeba histolytica proteins: Serine-rich Entamoeba histolytica protein and 29 kDa Cysteine-rich protease. *PeerJ,* 5, e3160.

Marty, C., Pecquet, C., Nivarthi, H., El-Khoury, M., Chachoua, I., Tulliez, M., Villeval, J. L., Raslova, H., Kralovics, R., Constantinescu, S. N., PLO, I. & VAINCHENKER, W. 2016.

Calreticulin mutants in mice induce an MPL-dependent thrombocytosis with frequent progression to myelofibrosis. *Blood,* 127, 1317-24.

Mcguffin, L. J., Bryson, K. & Jones, D. T. 2000. The PSIPRED protein structure prediction server. *Bioinformatics,* 16, 404-5.

Mehta, J., Wang, H., Iqbal, S. U. & Mesa, R. 2014. Epidemiology of myeloproliferative neoplasms in the United States. *Leuk Lymphoma,* 55, 595-600.

Mery, L., Mesaeli, N., Michalak, M., Opas, M., Lew, D. P. & Krause, K. H. 1996. Overexpression of calreticulin increases intracellular Ca2+ storage and decreases store-operated Ca2+ influx. *J Biol Chem,* 271, 9332-9.

Mesa, R. A., Li, C. Y., Ketterling, R. P., Schroeder, G. S., Knudson, R. A. & Tefferi, A. 2005. Leukemic transformation in myelofibrosis with myeloid metaplasia: a single-institution experience with 91 cases. *Blood,* 105, 973-7.

Mesa, R., Miller, C. B., Thyne, M., Mangan, J., Goldberger, S., Fazal, S., Ma, X. M., Wilson, W., Paranagama, D. C., Dubinski, D. G., Boyle, J. & Mascarenhas, J. O. 2016. Myeloproliferative neoplasms (MPNs) have a significant impact on patients' overall health and productivity: the MPN Landmark survey. *Bmc Cancer,* 16.

Mesaeli, N., Nakamura, K., Zvaritch, E., Dickie, P., Dziak, E., Krause, K. H., Opas, M., Maclennan, D. H. & Michalak, M. 1999. Calreticulin is essential for cardiac development. *Journal of Cell Biology,* 144, 857-868.

Methia, N., Louache, F., Vainchenker, W. & Wendling, F. 1993. Oligodeoxynucleotides antisense to the proto-oncogene c-mpl specifically inhibit in vitro megakaryocytopoiesis. *Blood,* 82, 1395-401.

Michalak, M., Groenendyk, J., Szabo, E., Gold, L. I. & Opas, M. 2009. Calreticulin, a multi-process calcium-buffering chaperone of the endoplasmic reticulum. *Biochem J,* 417, 651-66.

Migliaccio, A. R. & Uversky, V. N. 2017. Dissecting physical structure of calreticulin, an intrinsically disordered Ca2+-buffering chaperone from endoplasmic reticulum. *J Biomol Struct Dyn*, 1-20.

Mikoshiba, K. 2007. IP3 receptor/Ca2+ channel: from discovery to new signaling concepts. *J Neurochem,* 102, 1426-46.

Miller, B. A., Cheung, J. Y., Tillotson, D. L., Hope, S. M. & Scaduto, R. C. 1989. Erythropoietin Stimulates a Rise in Intracellular-Free Calcium-Concentration in Single Bfu-E Derived Erythroblasts at Specific Stages of Differentiation. *Blood,* 73, 1188-1194.

Miller, B. A., Scaduto, R. C., Jr., Tillotson, D. L., Botti, J. J. & Cheung, J. Y. 1988. Erythropoietin stimulates a rise in intracellular free calcium concentration in single early human erythroid precursors. *J Clin Invest,* 82, 309-15.

Molinari, M., Eriksson, K. K., Calanca, V., Galli, C., Cresswell, P., Michalak, M. & Helenius, A. 2004. Contrasting functions of calreticulin and calnexin in glycoprotein folding and ER quality control. *Mol Cell,* 13, 125-35.

Mondet, J., Park, J. H., Menard, A., Marzac, C., Carillo, S., Pourcelot, E., Girodon, F., Cabagnols, X., Lode, L., Socoro, N., Chauvet, M., Bulabois, C. E., Cony-Makhoul, P., Corm, S., Cahn, J. Y. & Mossuz, P. 2015. Endogenous megakaryocytic colonies underline association between megakaryocytes and calreticulin mutations in essential thrombocythemia. *Haematologica,* 100.

Mound, A., Vautrin-Glabik, A., Foulon, A., Botia, B., Hague, F., Parys, J. B., Ouadid-Ahidouch, H. & Rodat-Despoix, L. 2017. Downregulation of type 3 inositol (1,4,5)-trisphosphate

receptor decreases breast cancer cell migration through an oscillatory Ca(2+) signal. *Oncotarget,* 8, 72324-72341.

Nagata, Y., Nagahisa, H., Aida, Y., Okutomi, K., Nagasawa, T. & TODOKORO, K. 1995. Thrombopoietin induces megakaryocyte differentiation in hematopoietic progenitor FDC-P2 cells. *J Biol Chem,* 270, 19673-5.

Nakamura, K., Robertson, M., Liu, G., Dickie, P., Nakamura, K., Guo, J. Q., Duff, H. J., Opas, M., Kavanagh, K. & Michalak, M. 2001a. Complete heart block and sudden death in mice overexpressing calreticulin. *J Clin Invest,* 107, 1245-53.

Nakamura, K., Zuppini, A., Arnaudeau, S., Lynch, J., Ahsan, I., Krause, R., Papp, S., De Smedt, H., Parys, J. B., Muller-Esterl, W., Lew, D. P., Krause, K. H., Demaurex, N., Opas, M. & Michalak, M. 2001b. Functional specialization of calreticulin domains. *J Cell Biol,* 154, 961-72.

Nangalia, J., Massie, C. E., Baxter, E. J., Nice, F. L., Gundem, G., Wedge, D. C., Avezov, E., Li, J., Kollmann, K., Kent, D. G., Aziz, A., Godfrey, A. L., Hinton, J., Martincorena, I., Van Loo, P., Jones, A. V., Guglielmelli, P., Tarpey, P., Harding, H. P., Fitzpatrick, J. D., Goudie, C. T., Ortmann, C. A., Loughran, S. J., Raine, K., Jones, D. R., Butler, A. P., Teague, J. W., O'meara, S., Mclaren, S., Bianchi, M., Silber, Y., Dimitropoulou, D., Bloxham, D., Mudie, L., Maddison, M., Robinson, B., Keohane, C., Maclean, C., Hill, K., Orchard, K., Tauro, S., Du, M. Q., Greaves, M., Bowen, D., Huntly, B. J., Harrison, C. N., Cross, N. C., Ron, D., Vannucchi, A. M., Papaemmanuil, E., Campbell, P. J. & Green, A. R. 2013. Somatic CALR mutations in myeloproliferative neoplasms with nonmutated JAK2. *N Engl J Med,* 369, 2391-405.

Nanney, L. B., Woodrell, C. D., Greives, M. R., Cardwell, N. L., Pollins, A. C., Bancroft, T. A., Chesser, A., Michalak, M., Rahman, M., Siebert, J. W. & Gold, L. I. 2008. Calreticulin enhances porcine wound repair by diverse biological effects. *Am J Pathol,* 173, 610-30.

Norgaard Toft, K., Larsen, N., Steen Jorgensen, F., Hojrup, P., Houen, G. & Vestergaard, B. 2008. Small angle X-ray scattering study of calreticulin reveals conformational plasticity. *Biochim Biophys Acta,* 1784, 1265-70.

Nowell, P. C. 2007. Discovery of the Philadelphia chromosome: a personal perspective. *J Clin Invest,* 117, 2033-5.

Nurden, P., Debili, N., Vainchenker, W., Bobe, R., Bredoux, R., Corvazier, E., Combrie, R., Fressinaud, E., Meyer, D., Nurden, A. T. & Enouf, J. 2006. Impaired megakaryocytopoiesis in type 2B von Willebrand disease with severe thrombocytopenia. *Blood,* 108, 2587-95.

Oancea, E. & Meyer, T. 1998. Protein kinase C as a molecular machine for decoding calcium and diacylglycerol signals. *Cell,* 95, 307-318.

Obeid, M., Tesniere, A., Ghiringhelli, F., Fimia, G. M., Apetoh, L., Perfettini, J. L., Castedo, M., Mignot, G., Panaretakis, T., Casares, N., Metivier, D., Larochette, N., Van Endert, P., Ciccosanti, F., Piacentini, M., Zitvogel, L. & Kroemer, G. 2007. Calreticulin exposure dictates the immunogenicity of cancer cell death. *Nat Med,* 13, 54-61.

Ogawa, M. 1993. Differentiation and proliferation of hematopoietic stem cells. *Blood,* 81, 2844-53.

Ogino, S., Shima, K., Nosho, K., Irahara, N., Baba, Y., Wolpin, B. M., Giovannucci, E. L., Meyerhardt, J. A. & Fuchs, C. S. 2009. A cohort study of p27 localization in colon cancer, body mass index, and patient survival. *Cancer Epidemiol Biomarkers Prev,* 18, 1849-58.

Oldfield, C. J. & Dunker, A. K. 2014. Intrinsically disordered proteins and intrinsically disordered protein regions. *Annu Rev Biochem,* 83, 553-84.

Olson, K. R., Erdman, A. R., Woolf, A. D., Scharman, E. J., Christianson, G., Caravati, E. M., Wax, P. M., Booze, L. L., Manoguerra, A. S., Keyes, D. C., Chyka, P. A., & Troutman, W. G. 2005. Calcium channel blocker ingestion: an evidence-based consensus guideline for out-of-hospital management. *Clin Toxicol (Phila),* 43, 797-822.

Pang, S. F., Li, X. K., Zhang, Q., Yang, F. & Xu, P. 2009. Interference RNA (RNAi)-based silencing of endogenous thrombopoietin receptor (Mpl) in Dami cells resulted in decreased hNUDC-mediated megakaryocyte proliferation and differentiation. *Exp Cell Res,* 315, 3563-73.

Papayannopoulou, T., Nakamoto, B., Kurachi, S. & Nelson, R. 1987. Analysis of the erythroid phenotype of HEL cells: clonal variation and the effect of inducers. *Blood,* 70, 1764-72.

Pardanani, A. D., Levine, R. L., Lasho, T., Pikman, Y., Mesa, R. A., Wadleigh, M., Steensma, D. P., Elliott, M. A., Wolanskyj, A. P., Hogan, W. J., Mcclure, R. F., Litzow, M. R., Gilliland, D. G. & Tefferi, A. 2006. MPL515 mutations in myeloproliferative and other myeloid disorders: a study of 1182 patients. *Blood,* 108, 3472-6.

Paredes, R. M., Etzler, J. C., Watts, L. T., Zheng, W. & Lechleiter, J. D. 2008. Chemical calcium indicators. *Methods,* 46, 143-51.

Park, O. K., Schaefer, T. S. & Nathans, D. 1996. In vitro activation of Stat3 by epidermal growth factor receptor kinase. *Proc Natl Acad Sci U S A,* 93, 13704-8.

Patel, K. P., Newberry, K. J., Luthra, R., Jabbour, E., Pierce, S., Cortes, J., Singh, R., Mehrotra, M., Routbort, M. J., Luthra, M., Manshouri, T., Santos, F. P., Kantarjian, H. & Verstovsek, S. 2015. Correlation of mutation profile and response in patients with myelofibrosis treated with ruxolitinib. *Blood,* 126, 790-7.

PERIASAMY, M. & KALYANASUNDARAM, A. 2007. SERCA pump isoforms: Their role in calcium transport and disease. *Muscle & Nerve,* 35, 430-442.

Pietra, D., Rumi, E., Ferretti, V. V., Di Buduo, C. A., Milanesi, C., Cavalloni, C., Sant'antonio, E., Abbonante, V., Moccia, F., Casetti, I. C., Bellini, M., Renna, M. C., Roncoroni, E., Fugazza, E., Astori, C., Boveri, E., Rosti, V., Barosi, G., Balduini, A. & Cazzola, M. 2015. Differential clinical effects of different mutation subtypes in CALR-mutant myeloproliferative neoplasms. *Leukemia*, 30, 431-8.

Pikman, Y., Lee, B. H., Mercher, T., Mcdowell, E., Ebert, B. L., Gozo, M., Cuker, A., Wernig, G., Moore, S., Galinsky, I., Deangelo, D. J., Clark, J. J., Lee, S. J., Golub, T. R., Wadleigh, M., Gilliland, D. G. & Levine, R. L. 2006. MPLW515L is a novel somatic activating mutation in myelofibrosis with myeloid metaplasia. *PLoS Med,* 3, e270.

Pinto, M. C., Tonelli, F. M., Vieira, A. L., Kihara, A. H., Ulrich, H. & Resende, R. R. 2016. Studying complex system: calcium oscillations as attractor of cell differentiation. *Integr Biol (Camb),* 8, 130-48.

Prevarskaya, N., Ouadid-Ahidouch, H., Skryma, R. & Shuba, Y. 2014. Remodelling of Ca2+ transport in cancer: how it contributes to cancer hallmarks? *Philosophical Transactions of the Royal Society B-Biological Sciences,* 369.

Putney, J. W. & Bird, G. S. 2008. Cytoplasmic calcium oscillations and store-operated calcium influx. *J Physiol,* 586, 3055-9.

Quentmeier, H., Geffers, R., Jost, E., Macleod, R. A. F., Nagel, S., Rohrs, S., Romani, J., Scherr, M., Zaborski, M. & Drexler, H. G. 2008. SOCS2: inhibitor of JAK2V617F-mediated signal transduction. *Leukemia,* 22, 2169-2175.

Quintas-Cardama, A. & Cortes, J. 2009. Molecular biology of bcr-abl1-positive chronic myeloid leukemia. *Blood,* 113, 1619-30.

Quintas-Cardama, A., Vaddi, K., Liu, P., Manshouri, T., Li, J., Scherle, P. A., Caulder, E., Wen, X., Li, Y., Waeltz, P., Rupar, M., Burn, T., Lo, Y., Kelley, J., Covington, M., Shepard, S., Rodgers, J. D., Haley, P., Kantarjian, H., Fridman, J. S. & Verstovsek, S. 2010. Preclinical

characterization of the selective JAK1/2 inhibitor INCB018424: therapeutic implications for the treatment of myeloproliferative neoplasms. *Blood,* 115, 3109-17.

Racke, F. K., Wang, D., Zaidi, Z., Kelley, J., Visvader, J., Soh, J. W. & Goldfarb, A. N. 2001. A potential role for protein kinase C-epsilon in regulating megakaryocytic lineage commitment. *J Biol Chem,* 276, 522-8.

Rawlings, J. S., Rosler, K. M. & Harrison, D. A. 2004. The JAK/STAT signaling pathway. *J Cell Sci,* 117, 1281-3.

Roderick, H. L. & Cook, S. J. 2008. Ca2+ signalling checkpoints in cancer: remodelling Ca2+ for cancer cell proliferation and survival. *Nat Rev Cancer,* 8, 361-75.

Rotunno, G., Mannarelli, C., Guglielmelli, P., Pacilli, A., Pancrazzi, A., Pieri, L., Fanelli, T., Bosi, A., & Vannucchi, A. M. 2014. Impact of calreticulin mutations on clinical and hematological phenotype and outcome in essential thrombocythemia. *Blood,* 123, 1552-5.

Ru, Y. X., Dong, S. X., Liang, H. Y. & Zhao, S. X. 2016. Platelet production of megakaryocyte: A review with original observations on human in vivo cells and bone marrow. *Ultrastruct Pathol,* 40, 163-70.

Rumi, E. & Cazzola, M. 2017. Diagnosis, risk stratification, and response evaluation in classical myeloproliferative neoplasms. *Blood,* 129, 680-692.

Rumi, E., Pietra, D., Ferretti, V., Klampfl, T., Harutyunyan, A. S., Milosevic, J. D., Them, N. C., Berg, T., Elena, C., Casetti, I. C., Milanesi, C., Sant'antonio, E., Bellini, M., Fugazza, E., Renna, M. C., Boveri, E., Astori, C., Pascutto, C., Kralovics, R., & Cazzola, M. 2014. JAK2 or CALR mutation status defines subtypes of essential thrombocythemia with substantially different clinical course and outcomes. *Blood,* 123, 1544-51.

Sammels, E., Parys, J. B., Missiaen, L., De Smedt, H. & Bultynck, G. 2010. Intracellular Ca2+ storage in health and disease: a dynamic equilibrium. *Cell Calcium,* 47, 297-314.

Sanchez, S. & Ewton, A. 2006. Essential thrombocythemia: a review of diagnostic and pathologic features. *Arch Pathol Lab Med,* 130, 1144-50.

Schaefer, A., Magocsi, M. & Marquardt, H. 1997. Signalling mechanisms in erythropoiesis: the enigmatic role of calcium. *Cell Signal,* 9, 483-95.

Schindl, R., Muik, M., Fahrner, M., Derler, I., Fritsch, R., Bergsmann, J. & Romanin, C. 2009. Recent progress on STIM1 domains controlling Orai activation. *Cell Calcium,* 46, 227-32.

Schmittgen, T. D. & Livak, K. J. 2008. Analyzing real-time PCR data by the comparative C(T) method. *Nat Protoc,* 3, 1101-8.

Schonwasser, D. C., Marais, R. M., Marshall, C. J. & Parker, P. J. 1998. Activation of the mitogen-activated protein kinase/extracellular signal-regulated kinase pathway by conventional, novel, and atypical protein kinase C isotypes. *Mol Cell Biol,* 18, 790-8.

Schulze, H., Korpal, M., Hurov, J., Kim, S. W., Zhang, J., Cantley, L. C., Graf, T. & Shivdasani, R. A. 2006. Characterization of the megakaryocyte demarcation membrane system and its role in thrombopoiesis. *Blood,* 107, 3868-75.

Sell, S. 2005. Leukemia: stem cells, maturation arrest, and differentiation therapy. *Stem Cell Rev,* 1, 197-205.

Shaffer, K. L., Sharma, A., Snapp, E. L. & Hegde, R. S. 2005. Regulation of protein compartmentalization expands the diversity of protein function. *Dev Cell,* 9, 545-54.

Shide, K., Kameda, T., Yamaji, T., Sekine, M., Inada, N., Kamiunten, A., Akizuki, K., Nakamura, K., Hidaka, T., Kubuki, Y., Shimoda, H., Kitanaka, A., Honda, A., Sawaguchi, A., Abe, H.,

Miike, T., Iwakiri, H., Tahara, Y., Sueta, M., Hasuike, S., Yamamoto, S., Nagata, K. & Shimoda, K. 2017. Calreticulin mutant mice develop essential thrombocythemia that is ameliorated by the JAK inhibitor ruxolitinib. *Leukemia,* 31, 1136-1144.

Shivarov, V., Ivanova, M. & Tiu, R. V. 2014. Mutated calreticulin retains structurally disordered C terminus that cannot bind Ca(2+): some mechanistic and therapeutic implications. *Blood Cancer J,* 4, e185.

Singh, A., Chagtoo, M., Tiwari, S., George, N., Chakravarti, B., Khan, S., Lakshmi, S. & Godbole, M. M. 2017. Inhibition of Inositol 1, 4, 5-Trisphosphate Receptor Induce Breast Cancer Cell Death Through Deregulated Autophagy and Cellular Bioenergetics. *J Cell Biochem,* 118, 2333-2346.

Smithgall, T. E. 1998. Signal transduction pathways regulating hematopoietic differentiation. *Pharmacol Rev,* 50, 1-19.

Smyth, J. T., Hwang, S. Y., Tomita, T., Dehaven, W. I., Mercer, J. C. & Putney, J. W. 2010. Activation and regulation of store-operated calcium entry. *J Cell Mol Med,* 14, 2337-49.

Sonkin, D., Palmer, M., Rong, X., Horrigan, K., Regnier, C. H., Fanton, C., Holash, J., Pinzon-Ortiz, M., Squires, M., Sirulnik, A., Radimerski, T., Schlegel, R., Morrissey, M. & Cao, Z. A. 2015. The identification and characterization of a STAT5 gene signature in hematologic malignancies. *Cancer Biomark,* 15, 79-87.

Sonnichsen, B., Fullekrug, J., Van, P. N., Diekmann, W., Robinson, D. G. & Mieskes, G. 1994. Retention and Retrieval - Both Mechanisms Cooperate to Maintain Calreticulin in the Endoplasmic-Reticulum. *Journal of Cell Science,* 107, 2705-2717.

Sormanni, P., Camilloni, C., Fariselli, P. & Vendruscolo, M. 2015. The s2D method: simultaneous sequence-based prediction of the statistical populations of ordered and disordered regions in proteins. *J Mol Biol,* 427, 982-96.

Stathopulos, P. B., Zheng, L., Li, G. Y., Plevin, M. J. & Ikura, M. 2008. Structural and mechanistic insights into STIM1-mediated initiation of store-operated calcium entry. *Cell,* 135, 110-122.

Stokes, L., Gordon, J. & Grafton, G. 2004. Non-voltage-gated L-type Ca2+ channels in human T cells: pharmacology and molecular characterization of the major alpha pore-forming and auxiliary beta-subunits. *J Biol Chem,* 279, 19566-73.

Suh, H. C., Leeanansaksiri, W., Ji, M., Klarmann, K. D., Renn, K., Gooya, J., Smith, D., Mcniece, I., Lugthart, S., Valk, P. J., Delwel, R. & Keller, J. R. 2008. Id1 immortalizes hematopoietic progenitors in vitro and promotes a myeloproliferative disease in vivo. *Oncogene,* 27, 5612-23.

Sun, S., Liu, Y. M., Lipsky, S. & Cho, M. 2007. Physical manipulation of calcium oscillations facilitates osteodifferentiation of human mesenchymal stem cells. *Faseb Journal,* 21, 1472-1480.

Syme, R. & Gluck, S. 2001. Effects of cytokines on the culture and differentiation of dendritic cells in vitro. *J Hematother Stem Cell Res,* 10, 43-51.

Szabo, E., Qiu, Y., Baksh, S., Michalak, M. & Opas, M. 2008. Calreticulin inhibits commitment to adipocyte differentiation. *J Cell Biol,* 182, 103-16.

Tabilio, A., Pelicci, P. G., Vinci, G., Mannoni, P., Civin, C. I., Vainchenker, W., Testa, U., Lipinski, M., Rochant, H. & Breton-Gorius, J. 1983. Myeloid and megakaryocytic properties of K-562 cell lines. *Cancer Res,* 43, 4569-74.

Takahashi, A., Camacho, P., Lechleiter, J. D. & Herman, B. 1999. Measurement of intracellular calcium. *Physiol Rev,* 79, 1089-125.

Tan, F., Ghosh, S., Mbeunkui, F., Thomas, R., Weiner, J. A. & Ofori-Acquah, S. F. 2010. Essential role for ALCAM gene silencing in megakaryocytic differentiation of K562 cells. *BMC Mol Biol,* 11, 91.

Tefferi, A. & Nagorney, D. M. 2000. Myelofibrosis with myeloid metaplasia - Reply. *New England Journal of Medicine,* 343, 659-660.

Tefferi, A. & Vardiman, J. W. 2008. Classification and diagnosis of myeloproliferative neoplasms: the 2008 World Health Organization criteria and point-of-care diagnostic algorithms. *Leukemia,* 22, 14-22.

Tefferi, A. 2010. Novel mutations and their functional and clinical relevance in myeloproliferative neoplasms: JAK2, MPL, TET2, ASXL1, CBL, IDH and IKZF1. *Leukemia,* 24, 1128-1138.

Tefferi, A. 2016a. Myeloproliferative neoplasms: A decade of discoveries and treatment advances. *Am J Hematol,* 91, 50-8.

Tefferi, A. 2016b. Primary myelofibrosis: 2017 update on diagnosis, risk-stratification, and management. *Am J Hematol,* 91, 1262-1271.

Tsien, R. Y. 1981. A Non-Disruptive Technique for Loading Calcium Buffers and Indicators into Cells. *Nature,* 290, 527-528.

Tufi, R., Panaretakis, T., Bianchi, K., Criollo, A., Fazi, B., Di Sano, F., Tesniere, A., Kepp, O., Paterlini-Brechot, P., Zitvogel, L., Piacentini, M., Szabadkai, G. & Kroemer, G. 2008. Reduction of endoplasmic reticulum Ca2+ levels favors plasma membrane surface exposure of calreticulin. *Cell Death Differ,* 15, 274-82.

Ueda, Y., Hirai, S., Osada, S., Suzuki, A., Mizuno, K. & Ohno, S. 1996. Protein kinase C activates the MEK-ERK pathway in a manner independent of Ras and dependent on Raf. *J Biol Chem,* 271, 23512-9.

Uhlen, P., Laestadius, A., Jahnukainen, T., Soderblom, T., Backhed, F., Celsi, G., Brismar, H., Normark, S., Aperia, A. & Richter-Dahlfors, A. 2000. Alpha-haemolysin of uropathogenic E. coli induces Ca2+ oscillations in renal epithelial cells. *Nature,* 405, 694-7.

Uversky, V. N., Dave, V., Iakoucheva, L. M., Malaney, P., Metallo, S. J., Pathak, R. R. & Joerger, A. C. 2014. Pathological unfoldomics of uncontrolled chaos: intrinsically disordered proteins and human diseases. *Chem Rev,* 114, 6844-79.

Van Der Lee, R., Buljan, M., Lang, B., Weatheritt, R. J., Daughdrill, G. W., Dunker, A. K., Fuxreiter, M., Gough, J., Gsponer, J., Jones, D. T., Kim, P. M., Kriwacki, R. W., Oldfield, C. J., Pappu, R. V., Tompa, P., Uversky, V. N., Wright, P. E. & Babu, M. M. 2014. Classification of intrinsically disordered regions and proteins. *Chem Rev,* 114, 6589-631.

Vanguilder, H. D., Vrana, K. E. & Freeman, W. M. 2008. Twenty-five years of quantitative PCR for gene expression analysis. *Biotechniques,* 44, 619-26.

Vannucchi, A. M., Antonioli, E., Guglielmelli, P., Pancrazzi, A., Guerini, V., Barosi, G., Ruggeri, M., Specchia, G., Lo-Coco, F., Delaini, F., Villani, L., Finotto, S., Ammatuna, E., Alterini, R., Carrai, V., Capaccioli, G., Di Lollo, S., Liso, V., Rambaldi, A., Bosi, A. & Barbui, T. 2008. Characteristics and clinical correlates of MPL 515W>L/K mutation in essential thrombocythemia. *Blood,* 112, 844-7.

Varricchio, L., Falchi, M., Dall'Ora, M., De Benedittis, C., Ruggeri, A., Uversky, V. N., & Migliaccio, A. R. 2017. Calreticulin: Challenges Posed by the Intrinsically Disordered Nature of Calreticulin to the Study of Its Function. *Frontiers in Cell and Developmental Biology*, 5, 96.

Vyklicky, V., Korinek, M., Smejkalova, T., Balik, A., Krausova, B., Kaniakova, M., Lichnerova, K., Cerny, J., Krusek, J., Dittert, I., Horak, M. & Vyklicky, L. 2014. Structure, function, and pharmacology of NMDA receptor channels. *Physiol Res,* 63 Suppl 1, S191-203.

Wang, H. T., Yang, B., Hu, B., Chi, X. H., Luo, L. L., Yang, H. Q., Lang, X. L., Geng, J., Qiao, C. X., Li, Y., Wu, X. X., Zhu, H. L., Lv, M. & Lu, X. C. 2016. The effect of amifostine on differentiation of the human megakaryoblastic Dami cell line. *Cancer Med,* 5, 2012-21.

Ways, D. K., Dodd, R. C. & Earp, H. S. 1987. Dissimilar effects of phorbol ester and diacylglycerol derivative on protein kinase activity in the monoblastoid U937 cell. *Cancer Res,* 47, 3344-50.

Wemeau, M., Kepp, O., Tesniere, A., Panaretakis, T., Flament, C., De Botton, S., Zitvogel, L., Kroemer, G. & Chaput, N. 2010. Calreticulin exposure on malignant blasts predicts a cellular anticancer immune response in patients with acute myeloid leukemia. *Cell Death Dis,* 1, e104.

Wen, J., Huang, Y. C., Xiu, H. H., Shan, Z. M. & Xu, K. Q. 2016. Altered expression of stromal interaction molecule (STIM)-calcium release-activated calcium channel protein (ORAI) and inositol 1,4,5-trisphosphate receptors (IP3Rs) in cancer: will they become a new battlefield for oncotherapy?. *Chin J Cancer,* 35, 32.

Wen, Q., Goldenson, B. & Crispino, J. D. 2011. Normal and malignant megakaryopoiesis. *Expert Rev Mol Med,* 13, e32.

West, A. E., Griffith, E. C. & Greenberg, M. E. 2002. Regulation of transcription factors by neuronal activity. *Nat Rev Neurosci,* 3, 921-31.

Wierenga, A. T. J., Vellenga, E. & Schuringa, J. J. 2008. Maximal STAT5-Induced Proliferation and Self-Renewal at Intermediate STAT5 Activity Levels. *Molecular and Cellular Biology,* 28, 6668-6680.

Wiersma, V. R., Michalak, M., Abdullah, T. M., Bremer, E. & Eggleton, P. 2015. Mechanisms of Translocation of ER Chaperones to the Cell Surface and Immunomodulatory Roles in Cancer and Autoimmunity. *Front Oncol,* 5, 7.

Wijeyesakere, S. J., Bedi, S. K., Huynh, D. & Raghavan, M. 2016. The C-Terminal Acidic Region of Calreticulin Mediates Phosphatidylserine Binding and Apoptotic Cell Phagocytosis. *J Immunol*.

Wilkins, B. S., Erber, W. N., Bareford, D., Buck, G., Wheatley, K., East, C. L., Paul, B., Harrison, C. N., Green, A. R. & Campbell, P. J. 2008. Bone marrow pathology in essential thrombocythemia: interobserver reliability and utility for identifying disease subtypes. *Blood,* 111, 60-70.

Williams, R. M., Obradovi, Z., Mathura, V., Braun, W., Garner, E. C., Young, J., Takayama, S., Brown, C. J. & Dunker, A. K. 2001. The protein non-folding problem: amino acid determinants of intrinsic order and disorder. *Pac Symp Biocomput*, 89-100.

Wolanskyj, A. P., Schwager, S. M., Mcclure, R. F., Larson, D. R. & Tefferi, A. 2006. Essential thrombocythemia beyond the first decade: life expectancy, long-term complication rates, and prognostic factors. *Mayo Clin Proc,* 81, 159-66.

Wright, P. E. & Dyson, H. J. 1999. Intrinsically unstructured proteins: re-assessing the protein structure-function paradigm. *J Mol Biol,* 293, 321-31.

Wright, P. E. & Dyson, H. J. 2009. Linking folding and binding. *Curr Opin Struct Biol,* 19, 31-8.

Xia, W., Chen, J. S., Zhou, X., Sun, P. R., Lee, D. F., Liao, Y., Zhou, B. P. & Hung, M. C. 2004. Phosphorylation/cytoplasmic localization of p21Cip1/WAF1 is associated with HER2/neu overexpression and provides a novel combination predictor for poor prognosis in breast cancer patients. *Clin Cancer Res,* 10, 3815-24.

Xue, B., Dunbrack, R. L., Williams, R. W., Dunker, A. K. & Uversky, V. N. 2010. PONDR-FIT: a meta-predictor of intrinsically disordered amino acids. *Biochim Biophys Acta,* 1804, 996-1010.

Yan, J., Dunker, A. K., Uversky, V. N. & Kurgan, L. 2016. Molecular recognition features (MoRFs) in three domains of life. *Mol Biosyst,* 12, 697-710.

Yang, J., Yan, R., Roy, A., Xu, D., Poisson, J. & Zhang, Y. 2015. The I-TASSER Suite: protein structure and function prediction. *Nat Methods,* 12, 7-8.

Yang, S. N. & Berggren, P. O. 2006. The role of voltage-gated calcium channels in pancreatic beta-cell physiology and pathophysiology. *Endocr Rev,* 27, 621-76.

Yang, Z. R., Thomson, R., Mcneil, P. & Esnouf, R. M. 2005. RONN: the bio-basis function neural network technique applied to the detection of natively disordered regions in proteins. *Bioinformatics,* 21, 3369-76.

Yoshida, H., Kondo, M., Ichihashi, T., Hashimoto, N., Inazawa, J., Ohno, R. & Naoe, T. 1998. A novel myeloid cell line, Marimo, derived from therapy-related acute myeloid leukemia during treatment of essential thrombocythemia: consistent chromosomal abnormalities and temporary C-MYC gene amplification. *Cancer Genet Cytogenet,* 100, 21-4.

Yu, M. & Cantor, A. B. 2012. Megakaryopoiesis and thrombopoiesis: an update on cytokines and lineage surface markers. *Methods Mol Biol,* 788, 291-303.

Zhang, D., Cho, E. & Wong, J. 2007. A critical role for the co-repressor N-CoR in erythroid differentiation and heme synthesis. *Cell Res,* 17, 804-14.

Zimmet, J. & Ravid, K. 2000. Polyploidy: occurrence in nature, mechanisms, and significance for the megakaryocyte-platelet system. *Exp Hematol,* 28, 3-16.
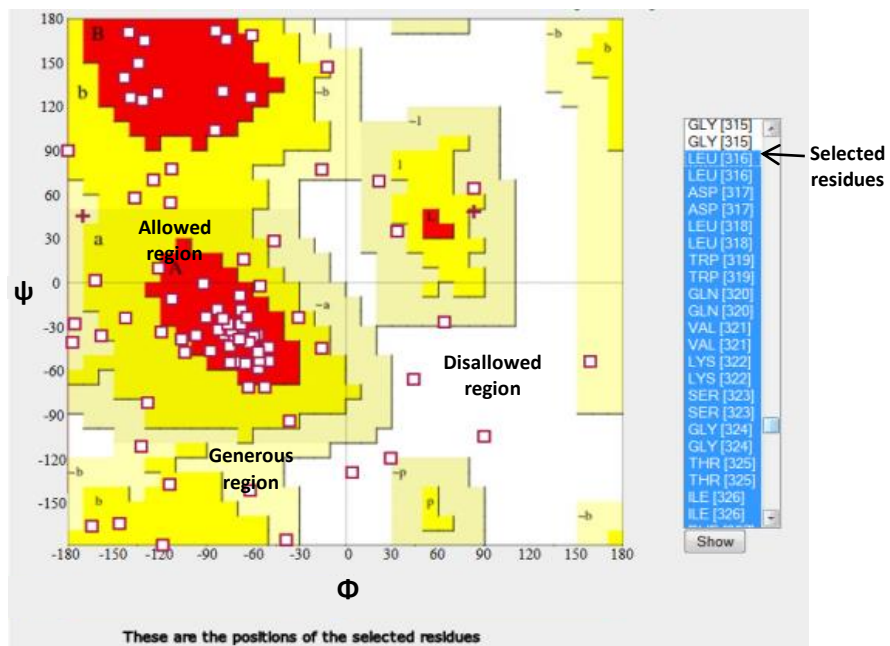
Appendices

1. Ramachandran plots

Best predicted I-TASSER structural models of CALR wt, CALR type 1 and CALR type 2 mutants were validated using PROCHECK server. Analysis was performed in the C-terminal domain of these proteins and therefore, residues were selected from 316 to the end of the amino acid chain. Then, the percentage of residues within the allowed, generous and disallowed regions was calculated. The following images display the obtained Ramachandran plots of each C-terminal domain of the predicted structural models.

A. CALR wt C-terminal domain Ramachandran plot (residues number 316-417)

These are the positions of the selected residues
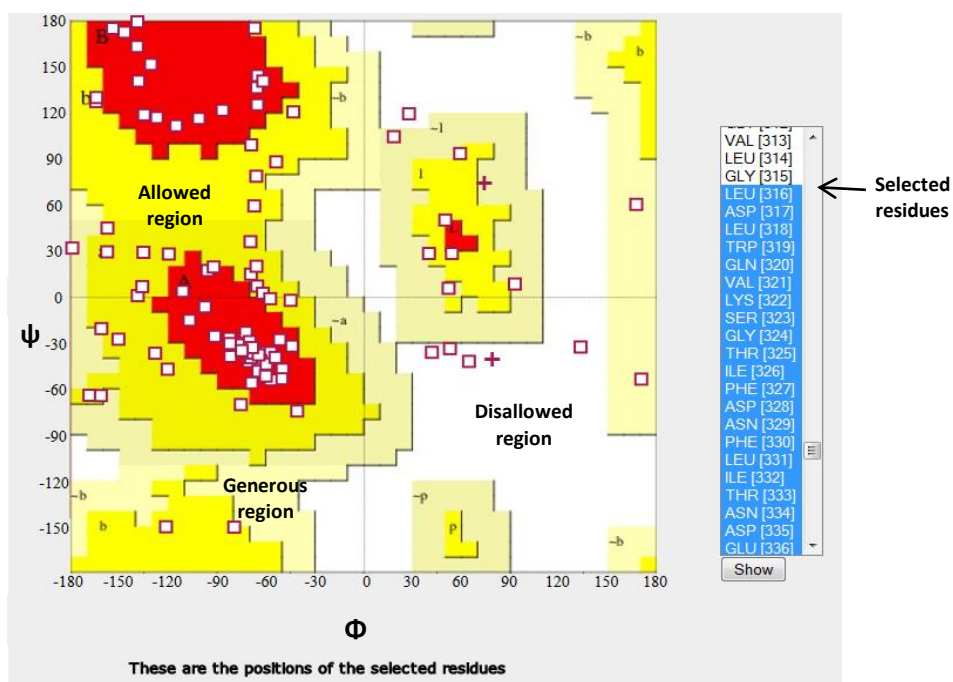
B. CALR type 1 mutant C-terminal domain Ramachandran plot (residues number 316-410)

These are the positions of the selected residues

C. CALR type 2 mutant C-terminal domain Ramachandran plot of CALR type2 mutant predicted model (residues number 316-428)


These are the positions of the selected residues
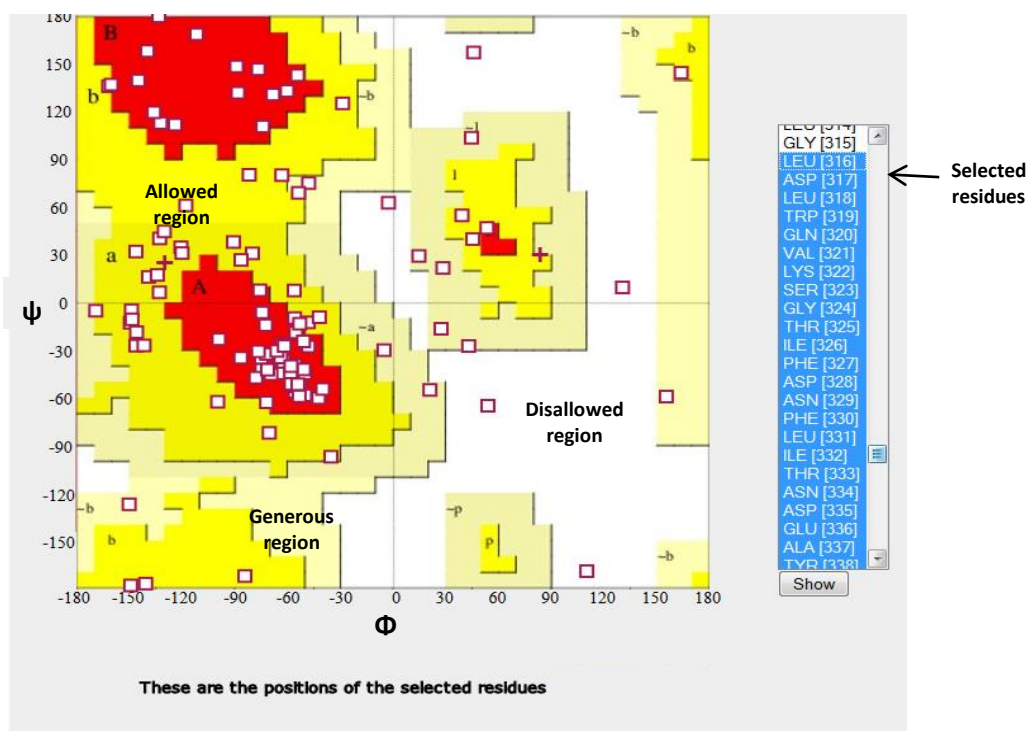
2. qRT-PCR Melting curves

During qRT-PCR analysis, melting curves were performed in order to corroborate the amplification of a single DNA product and eliminate the possibility of false positives and primer dimer signal. Following images show examples of the obtained melting curves of each primer reaction used during this study:

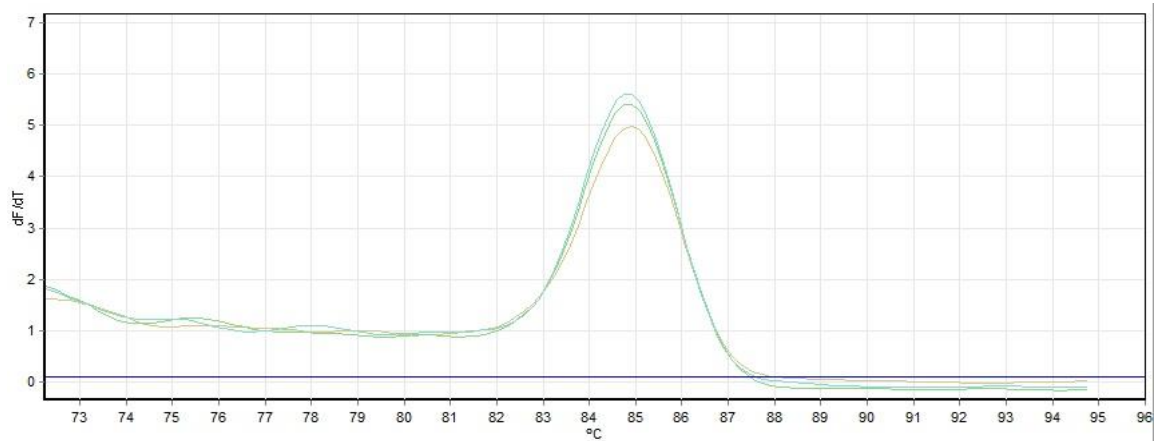A. **GAPDH**: Obtained melting curve during *GAPDH* amplification.
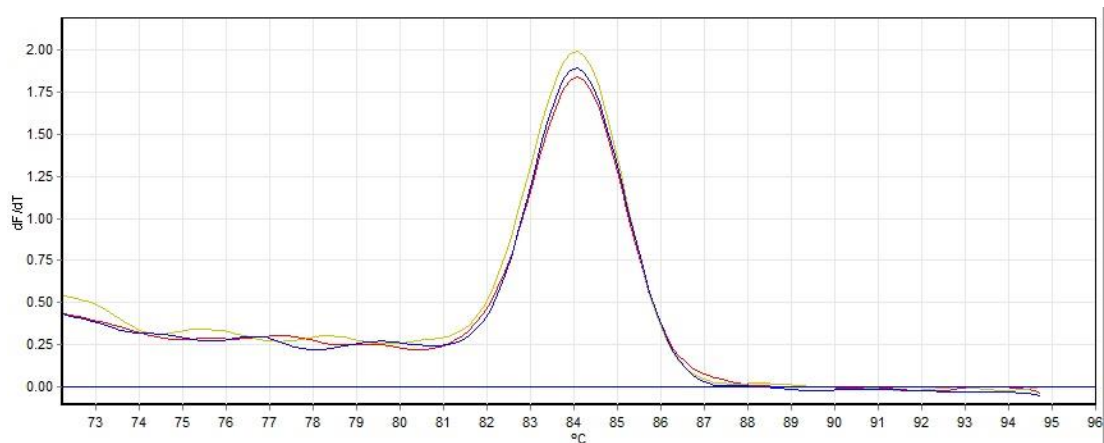
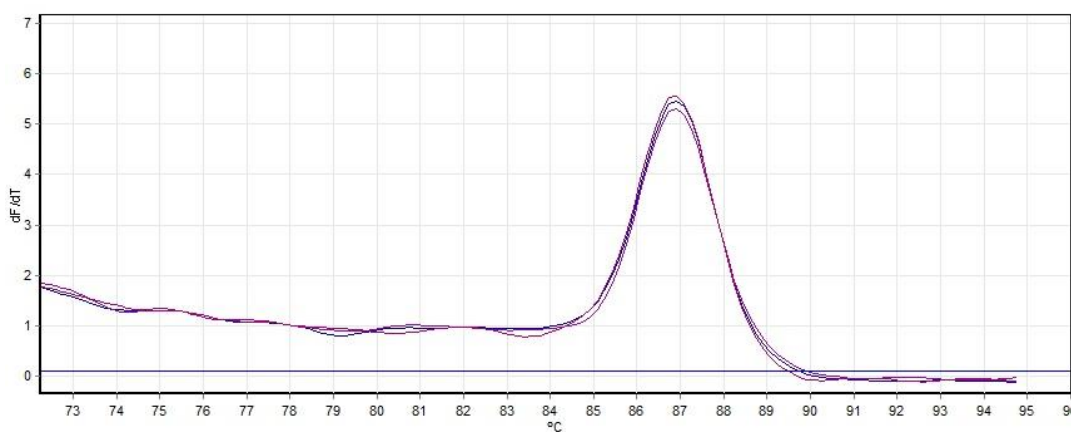B. **PIM1:** Obtained melting curve during *PIM1* amplification
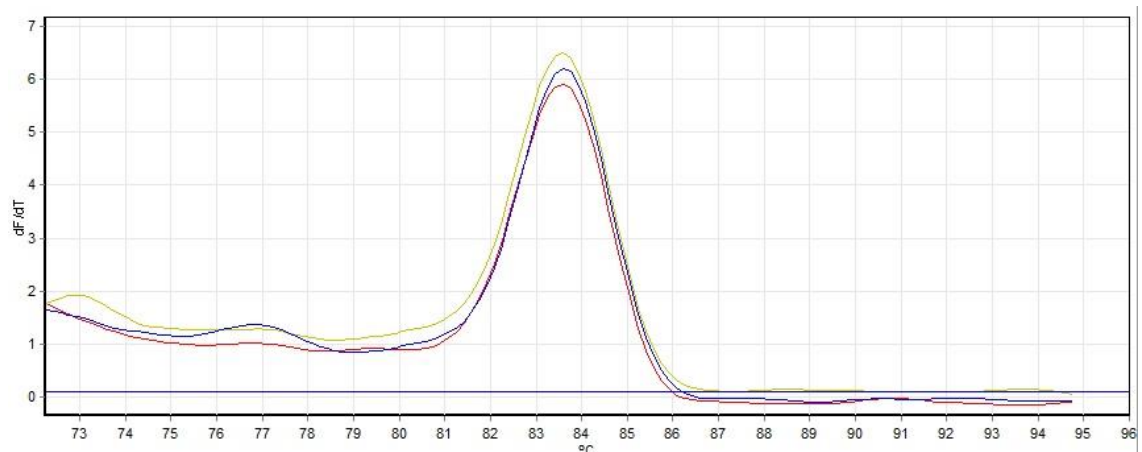
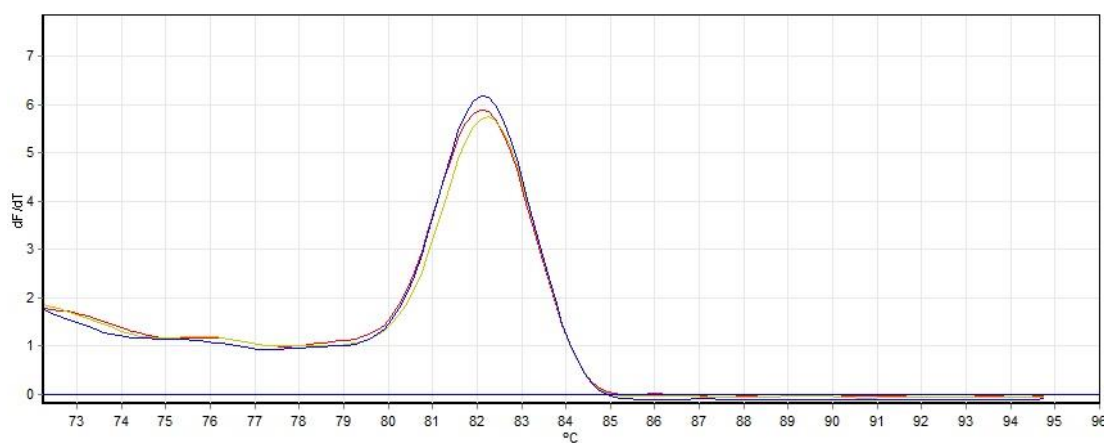**C. ID1:** Obtained melting curve during *ID1* amplification
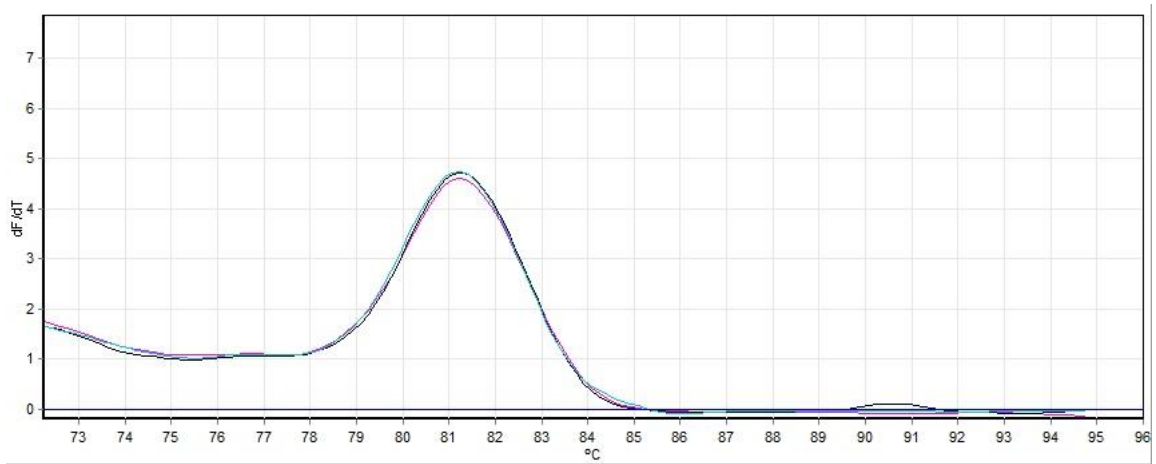
D. SOCS2: Obtained melting curve during *SOCS2* amplification

**E. CISH:** Obtained melting curve during *CISH* amplification

F. cMPL: Obtained melting curve during *cMPL* amplification

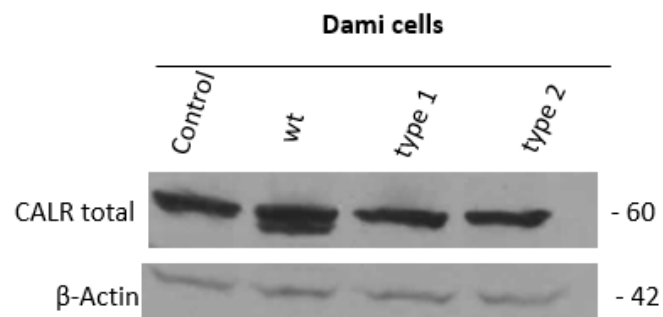## 3. Control assays of DAMI clones overexpressing *CALR* wt, type 1 and type 2 mutants.

DAMI cells used in this study were transduced to overexpress *CALR* wt, type 1 and type 2 mutants. GFP empty vector was used as a control to test the efficiency of transduction. Therefore, GFP expression within these cells was assed by flow cytometry and results showed expression of GFP within the whole DAMI population.

A. GFP fluorescence in DAMI control cells used in this study.

DAMI GFP negative cells   DAMI GFP cells
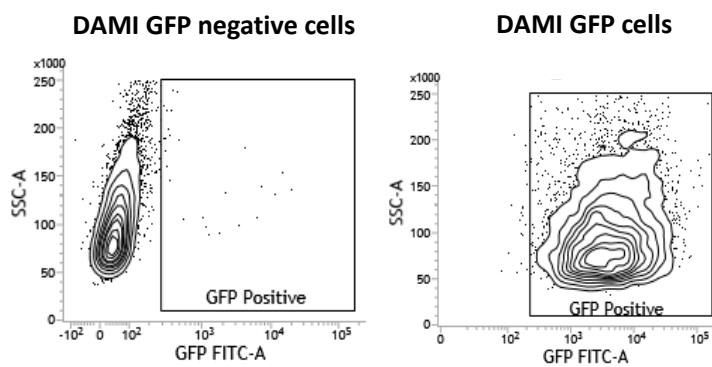
Moreover, quantification of CALR protein amount in DAMI clones was assed by western blot analysis. Following images show examples of the obtained blots:

B. Clones 1.

C. Clones 2.